The effect of chemokines on brain endothelial cell function

Ana Carolina Estevao

Thesis submitted in fulfilment of the requirement for the degree of Doctor of Philosophy

University College London

Institute of Ophthalmology

Supervisor: John Greenwood

Declaration

I, Ana Carolina Branco Estevao, confirm that the work presented in this thesis is my own. Where information has been derived from other sources, I confirm that this has been indicated in the thesis.

Acknowledgments

I would like to express my gratitude to my primary supervisor, Professor John Greenwood whose knowledge, understanding and wittiness made this experience extremely enriching. I am still to learn his enviable public speech and networking skills.

A very special thanks goes to my secondary supervisor, Professor Patric Turowski who supported me and was always available to discuss ideas with. Thank you for endless hours of discussion, your motivation and encouragement were essential, I would also like to acknowledge Professor Steve Moss and Professor Karl Matter who gave an invaluable intellectual input to my project and helped me look at research questions differently.

Thank you to my Examination Committee, for taking the time to read yet another thesis and allowing me to discuss my work with you.

To the Greenwood lab members, past and present, a sincere thank you! Your constant support, patience and openness to share your time and knowledge with me have made this work possible. I could have not imagined a better group of people to share these four years with. A special thanks to Chantelle Bowers who has offered her sharp critical approach and her immense patience.

I would like to thank my friends and family who always believed in me and kept me sane. A special thanks to my grandparents Frederico and Madalena, whose support was essential throughout these four years.

Abstract

The blood-brain barrier (BBB) and the blood-retinal barrier (BRB) are two closely related tight endothelial cell barriers that control the movement of molecules and cells between the blood and the central nervous system (CNS). This feature is partly due to the presence of tight intercellular junctions between opposing endothelial cells (ECs) that limit the diffusion of molecules and restrict the passage of immune cells. This latter phenomenon is the primary driver for the observed immune privilege of the brain and retina. The breakdown of these barriers is a feature of many disorders of the CNS including Multiple Sclerosis, Alzheimer's disease, and stroke. At a molecular level, the breakdown of the BBB and BRB involves disengagement of intercellular junctions and a consequent increase in barrier permeability. Increased entry of macromolecules and/or immune cells through the BBB in pathological states have been extensively described in the literature. These events can be mediated by a paracellular route or a transcellular route of entry.

Leukocyte migration from the blood, across the vascular wall and to the underlying tissue, occurs both in inflammation and immunosurveilance. The multi-step paradigm that explains this process, involves a series of interactions between leukocytes and endothelial cells with the involvement of chemokines. Chemokines were originally discovered as mediators of immune cell chemoattraction to sites of injury or inflammation. Immune cells are known to express receptors for chemokines and their behavior can be governed by receptor engagement with the various chemokine ligands. ECs express chemokine receptors raising the possibility that these cells can respond following exposure to chemokines.

Since chemokines are heavily involved in inflammatory processes, we have investigated the role of the chemokines CCL4, CXCL8 and CXCL10 on BBB endothelial cell function. We observed that the chemokines studied induced signaling events in human umbilical vein endothelial cells (HUVEC) and in an immortalised human brain endothelial cell line (hCMEC/D3). All chemokine treatments resulted in phosphorylation of the MAPKs and CCL4 resulted in a significant translocation of these proteins to the nucleus of hCMEC/D3. The distribution of junctional proteins ZO-1 and VE-cadherin were altered in response to chemokine treatments. VE-cadherin total protein was not affected by chemokines but there was internalization of the protein following treatments. There was evidence that the cytoskeleton, in the form of stress fibers, was also modulated by these chemokines. In hCMEC/D3 treatment with the chemokines CCL4 and CXCL10 resulted in an increased transendothelial cell monolayer permeability and an increase in the rate of migration of CD4+ T lymphocytes across the monolayer. *In vivo* there was also evidence that CCL4 induced increased permeability in the BBB. Taken together, these results indicate that that these chemokines may contribute to the opening of the BBB and the pathogenesis of neuroinflammatory diseases.

Table of Figures

Table of Contents

Table of Tables

Abbreviations

AC- alternating current

AJ – Adherens junctions

ANOVA - one-way analysis of variance

APC – Antigen-presenting cell

ATP- adenosine triphosphate

BBB- Blood-Brain Barrier

BCEC- Brain Capillary endothelial cells

BRB- Blood-retinal Barrier

Ca2+- calcium

$CaCl_2$ - Calcium chloride

CAMs - cell adhesion molecules

CCL4/MIP-1β - Macrophage inflammatory protein-1β

CNS- central nervous system

CO_2- carbon dioxide

CXCL10/IP-10 - Interferon γ-inducible protein 10

CXCL8/IL-8 – interleukin 8

MS - Multiple sclerosis

DARC- Duffy antigen receptor for chemokines

DC- direct current

DPBS - Dulbecco's Phosphate-buffered saline

EAE – experimental autoimmune encephalitis

EAU – experimental autoimmune uveitis

EC – endothelial cell

ECIS- electric cell-substrate impedance sensing

ERK 1/2- extracellular regulated kinase 1/2

ERK 3/4- extracellular regulated kinase 3/4

ERK 5- extracellular regulated kinase 5

ERK 7/8- extracellular regulated kinase 7/8

FBS - Foetal Bovine Serum

FFA - Fundus fluorescein angiography

GAGs - glycosaminoglycans

GAPs - GTPase-activating proteins

GDP - guanosine diphosphate

GFAP - glial fibrillary acidic protein

GPCR- G-protein coupled receptor

GTP - guanosine triphosphate

hCMEC/D3 - human immortalised brain microvascular endothelial cells

HDMEC- human dermal microvascular endothelial cells

HEPES - (4-(2-hydroxyethyl)-1-piperazineethanesulfonic acid)

HIV- human immunodeficiency virus

HSP27- heat shock protein 27

HSC70 - Heat shock cognate 71 kDa protein

HUVEC - Human Umbilical Vein Endothelial Cell

ICAM-1 - Intercellular Adhesion Molecule 1

IFN-γ- Interferon gamma

IL-1β- interleukin 1 beta

IL-6- interleukin-6

IP_3- Inositol triphosphate

JAM - junctional adhesion molecule

JNK- c-Jun N-terminal kinase

KCl - Potassium chloride

KH_2PO_4 - Monopotassium phosphate

LFA-1- Lymphocyte function-associated antigen 1

LPA- Lysophosphatidic acid

LPS- Lipopolysaccharides

Mac-1- Macrophage-1 antigen

MAPK - mitogen-activated protein kinase

MS- multiple sclerosis

NaCl – Sodium chloride

NAD+- Nicotinamide adenine dinucleotide

$NaHCO_3$ - Sodium bicarbonate

NK- natural killer

NLK- Nemo-like kinase

P/S - Penicillin Streptomycin

PAF- platelet-activating factor

PCR – polymerase chain reaction

PECAM-1- Platelet and Endothelial Cell Adhesion Molecule 1

PFA - Paraformaldehyde

PI3K- phosphoinositide 3-kinase

PLC - phospholipase C

PSLG-1- Selectin P ligand 1

qPCR – quantitative polymerase chain reaction

ROS - reactive oxygen species

RT-PCR- reverse transcription polymerase chain reaction

Ser- serine

SO_4 – Sulphate

TBS - Tris-buffered saline

TEER- transendothelial electrical resistance

Thr- threonine

TJ- tight junctions

TNFα – tumour necrosis factor alpha

Tyr – tyrosine

VCAM-1 - vascular cell-adhesion molecule 1

VE-cadherin- vascular endothelial cadherin

VEGF- vascular endothelial growth factor

VLA-4- Very Late Antigen-4

ZO-1- zonula occludens-1

ZO-2- zonula occludens-2

1. General introduction

1.1 Inflammation

The term inflammation originates from the Latin word *inflammare* and was first described by Aulus Cornelius Celsus. *Inflammare* was defined by four cardinal signs: *rubor et tumour cum calore et dolore* (redness and swelling with heat and pain). The term was redefined two centuries later by Galen (AD 129–199), as a beneficial response to injury. In the 19th century, Rudolf Virchow added the fifth cardinal sign: *functio laesa* (loss of function in inflamed tissues) and postulated that inflammation consists of various processes (Nathan, 2002, Heidland et al., 2006).

Modern developments, mostly due to the advent of microscopy and cell biology laboratory techniques, have shown that inflammation is the result of complex processes involving diverse cell populations, chemical mediators and spanning various organs (Scott, 2004). The cellular and vascular components of inflammation will be explored in the following subchapters.

Inflammation can be categorised as acute or chronic. In the acute phase there are vascular changes and accumulation of soluble factors, fluid and immune cells. During the chronic phase there is the development of humoral and cellular immune responses at the site of injury (Feghali and Wright, 1997). Inflammation is beneficial if tightly regulated, otherwise a prolonged inflammatory milieu has been shown to cause damage to healthy tissues. In pathological conditions like ischemia, stroke, sepsis, multiple sclerosis (MS), arthritis, atherosclerosis and tumorigenesis, inflammatory mediators are released and

the intercellular space is altered, allowing the passage of macromolecules, plasma and immune cells that otherwise would have been severely restricted (Lucas et al., 2006).

1.2 The Immune System

The immune system consists of an organised network of cells and molecules that defend the host against infectious agents. The response orchestrated by these cells and molecules is called immunity and it can be classified in two categories: innate immunity and adaptive immunity. The type of response depends on the specific reaction of the organism to a shift in homeostasis. In innate immune responses, the response to an infectious agent occurs to the same degree as a previous response whereas in an adaptive immune response it is improved and refined with repeated exposure (adaptive immunity). Certain components, such as lymphocytes, complement proteins and cytokines, are known to overlap these two separate responses, indicating the interdependency of these processes (**Figure 1**)(Janeway, 2001).

Pathogens and harmful substances in the environment put the homeostasis of the host under threat. The immune system has surveillance mechanisms in place to sort between pathogens and the self that rely primarily on the recognition of the structure of pathogens and the host cells. These mechanisms are essential to eliminate the threat without compromising the host (Chaplin, 2010).

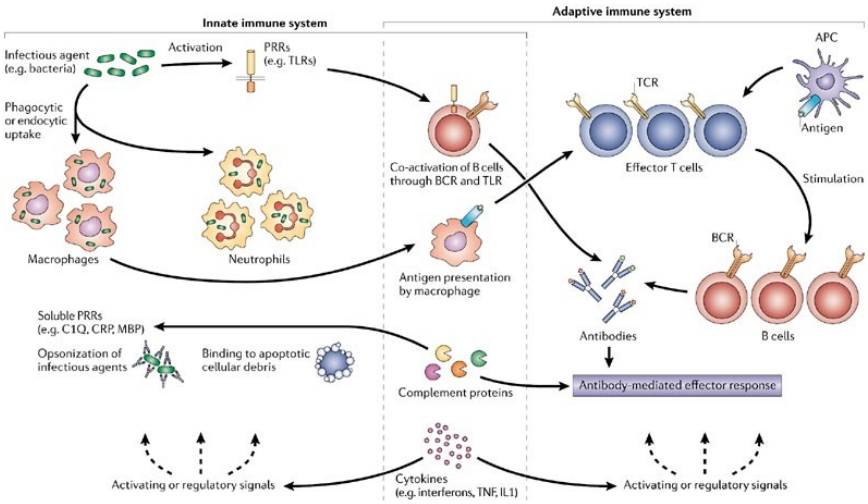

Figure 1 Immune cells and molecules in innate and adaptive immunity and the dependency of the adaptive immunity in components of the innate immunity (Gregersen and Behrens, 2006). PRRs - Pattern recognition receptors, TCR – T-cell receptor, BCR – B cell receptor, TLR – toll-like receptor, APC- antigen presenting cell.

1.2.1 Innate and Adaptive Immunity

The elements of innate immunity comprise physical, chemical and microbial barriers and the immune system. The barriers include epithelial and endothelial cells that express cell-junction molecules, a mucus layer that surrounds the epithelium in the respiratory, gastro-intestinal and genitourinary tracts and cilia that moves the mucus where pathogens and contaminants are trapped. The immune system in innate immunity is comprised of neutrophils, macrophages, monocytes, complement, cytokines and acute phase proteins. The recognition of the threat is rapid and relies on the host's germ line, recognizing patterns that are absent in the host (Janeway, 2001).

An essential immune cell for the innate response, the macrophage, recognises cell surface proteins of pathogens, engulfing and eliminating them. Activated macrophages and other cells release specialised cytokines and chemokines that chemoattract

neutrophils and monocytes from the circulation to the site of infection. Molecules present in biological fluids or released by immune cells such as cytokines, chemokines, lipid mediators and enzymes bind to molecules on the surface of pathogens, initiating the innate immune response (**Figure 2**).

This cascade of events induces the release of peptides involved in further inflammatory processes. Innate immunity profiles the type of adaptive response by modulating antigen presentation and T cell activity and ultimately regulating lymphocyte activity and trafficking. The complement cascade triggered by proteins on the surface of pathogens results in local inflammation and phagocytosis (Janeway et al., 2001 1999).

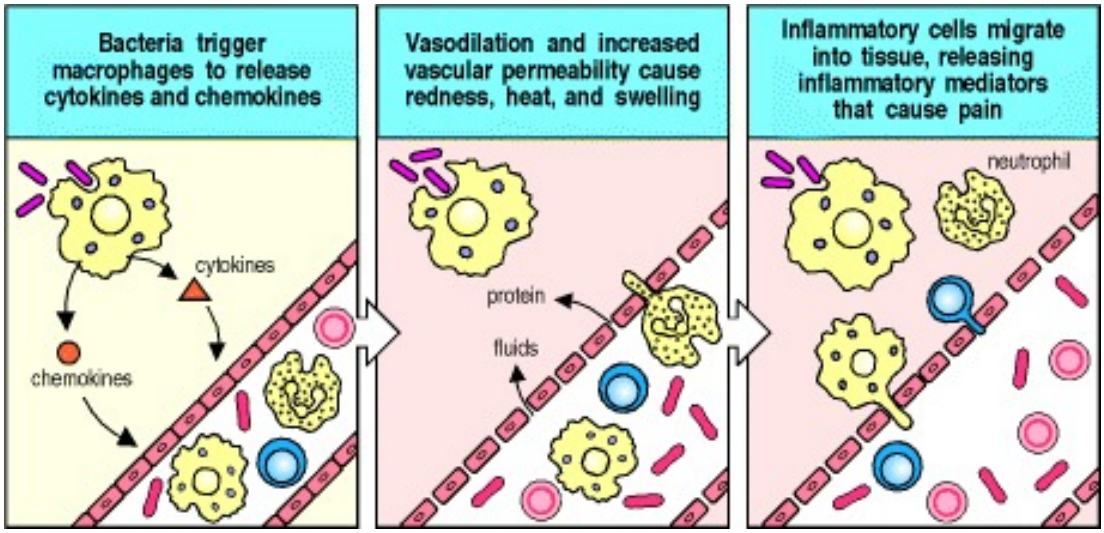

Figure 2 The inflammatory response to bacteria (Janeway, 2001).

The adaptive response, which depends on the rearrangement of genes to generate antigen-binding molecules, is essentially composed of immune cells that are specific for a certain pathogen or toxin. The generation of antigen receptors from germline-encoded genes allows the production of a vast array of antigen receptors, specific to an antibody, also known as immunoglobulins. This type of response, led primarily by the lymphocytes (antigen-specific B and T cells), allows increased protection against pathogens (Janeway, 2001).

Antigen-presenting cells (APCs) (dendritic cells, macrophages, Langerhans cells and B cells) present the antigen to lymphocytes compelling them to respond. The subtype of T cell activated and the resulting response depends in part on the milieu in which the APC encountered the antigen. The activation of a T cell results in cytokine release and activates macrophages. B cells, by interacting with T cells, produce antibodies against the specific antigen (**Figure 3**). These cells persist in a dormant state and can be re-activated when a specific antigen is presented, this feature is known as 'immune memory' (Chaplin, 2010 1999).

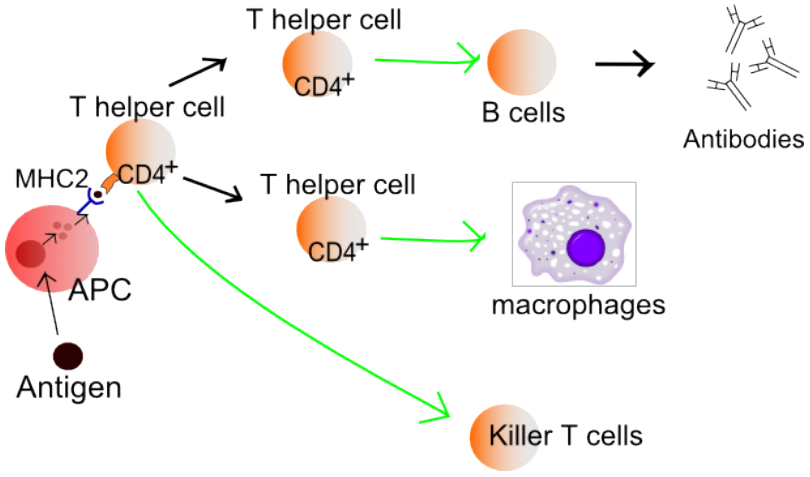

Figure 3 Lymphocyte activation (Häggström, 2014).

Lymphocytes are generated in the foetal liver and bone marrow and are released into the circulation. B lymphocytes mature in the bone marrow whilst T lymphocytes need to reach the thymus to achieve maturity. Lymphocytes are trafficked between the vasculature, the tissues and the secondary lymphoid organs, which include the lymph nodes, the spleen and the Peyer's patches (Miyasaka and Tanaka, 2004). This process, known as immune surveillance, is responsible for the maturation of lymphocytes into different subsets that then migrate into the tissues and sites of inflammation monitoring the body for potential threats (Butcher and Picker, 1996). T cells direct other immune cells, orchestrating the immune response. The innate and adaptive responses are mutually dependent: components of the innate immune system are involved in the

activation of antigen-specific cells, which recruit elements of the adaptive immune system to aid in the elimination of harmful pathogens (Chaplin, 2010).

The success of the immune system in combating infection relies mostly on the properties of T cells and their ability to recognise and eliminate threat without damaging the self. Self-tolerance, the ability of the immune system to respond to threats without damaging itself, is expressed in many parts of the innate and adaptive immune system. This tolerance mechanism can fail and the host's immune cells react against the self, leading to autoimmune diseases such as multiple sclerosis, psoriasis, rheumatoid arthritis and inflammatory bowel disease among others (Chaplin, 2010 2001). In autoimmune diseases T cells can mediate immune responses that are harmful for the host. One of the hallmarks is the dysregulation of leukocyte extravasation into tissues causing dysfunction of an organ or system (Xu et al., 2003, Norman and Hickey, 2005)

1.3 The blood vascular system

Vertebrates have closed blood systems where, apart from injury, blood remains within the vessels or chambers that collect and distribute the blood throughout the body. In vertebrates the endothelial cells that line the vascular wall possess intercellular junctions and present polarity: a luminal side, facing the lumen and an apical side facing the surrounding tissue, also called basoapical polarity (Monahan-Earley et al., 2013).

The human blood vascular system consists of a network of vessels, sinuses (the liver, spleen, and bone marrow) and pumping organs (the heart) that circulates blood around the tissues of the body (Monahan-Earley et al., 2013). Arteries and veins, the largest calibre vessels, are surrounded by connective tissue and smooth muscle cells, and are lined by endothelial cells (ECs), separated from the outer layers by a basal lamina. The distribution of connective tissue and muscle cells depends on the function and location

of the blood vessels. The capillaries and sinusoids, the smallest calibre vessels, consist of a single layer of ECs, basal lamina and pericytes that invest the vessels (Alberts et al., 2002).

Arterioles are lined by ECs and smooth muscle cells that provide contractile properties to the microvessel, dilating and contracting, thus, regulating blood flow. The contraction of the smooth muscle cells is controlled by metabolic and humoral factors. The exchange of solutes takes place in the capillary and postcapillary vessels that form the capillary beds. The capillary beds are formed by ECs and can have associated cells in the outer layers (pericytes, fibroblasts, smooth muscle cells) and have high basal permeability. The two levels of vasculature, macrovasculature and microvasculature are responsible for the delivery of nutrients and O_2 and removal of waste in the body. The macrovasculature, veins and arteries distribute the blood to and from the organs, whilst the microvasculature, composed of arterioles, capillaries, and venules, are responsible for localised nutrient and gas exchange (**Figure 4**)(Yuan and Rigor, 2010). The lymphatic system collects, recycles and then returns the interstitial fluid to the blood vessels (Alberts et al., 2002, Monahan-Earley et al., 2013).

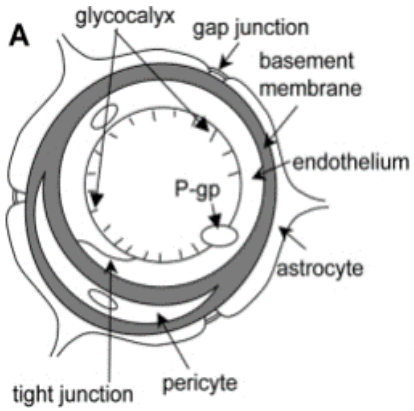

Figure 4 Schematic representation of the blood-brain barrier microvasculature with ECs embedded in a basement membrane and glycocalyx (Ueno, 2009).

1.3.1 Microvasculature

The microvessel wall is composed of ECs arranged side by side, forming a monolayer. This structure forms the vessel's lumen, and is the barrier that is responsible for the selective permeability of the vessel. The surfaces of the ECs facing the lumen (luminal/apical side) are covered in glycocalyx, a glycan bound to the endothelium by a network of glycoproteins and polysaccharides (Reitsma et al., 2007). The opposing surface, facing the basolateral side (abluminal) is attached to the basal membrane via focal adhesions and transmembrane integrins (Yuan and Rigor, 2010).

The endothelium has selective permeability and controls the transport of molecules to and from the circulation, forming a barrier. This barrier integrity is vital for EC structure and functionality. In non-pathogenic conditions, the endothelium maintains homeostasis by regulating vascular tone, blood flow, and non-thrombogenic balance. These small calibre vessels express adhesion molecules involved in capture, adhesion and migration of leukocytes into the sites of inflammation. It is in the microvasculature, specifically at the level of the post-capillary and collecting venules where transendothelial leukocyte migration occurs (**Figure 5**) (Luscinskas et al., 2002).

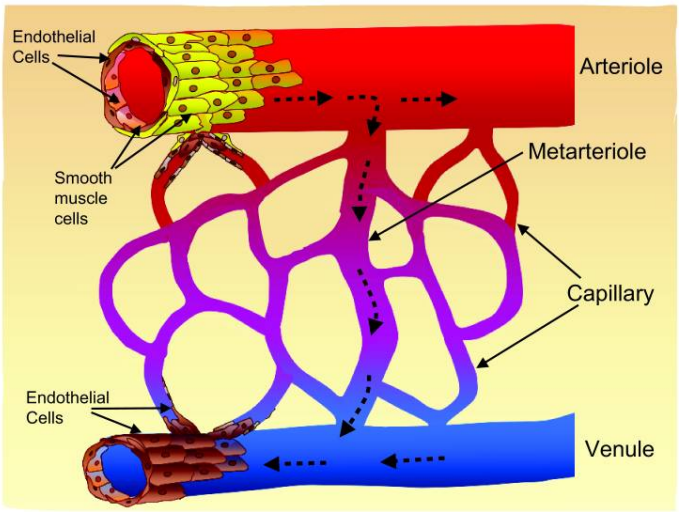

Figure 5 Schematic representation of a microvascular bed: arteriole, capillary and venule (Yuan and Rigor, 2010).

Intercellular junctions allow the passage of macromolecules from bi-directionally between the extracellular and the intracellular environment. There is homeostatic passage of molecules, ions and cells that is regulated by mechanisms of the endothelium. Vesicular transcytosis involves endocytosis of vesicles at the luminal membrane, followed by transcytosis across the cell and, eventually, exocytosis at the basolateral side of the membrane. The process can be achieved by a single vesicle that shuttles macromolecules or by clusters of vesiculo-vacuolar organelles that form a channel across the interior of the endothelial cell. Endo- and exocytosis are mediated by

caveolae that create invaginations in the cellular membrane. Leukocytes may also be transported via transcytosis, by envelopment by endocytic vesicles. Caveolae contain caveolin-1, which has been shown to be associated with EC barrier properties, as the absence of the protein increases paracellular permeability. Another mechanism for transcellular passage of fluid is through water channel aquaporins. Integral membrane proteins that transport water across the cell membrane (Yuan and Rigor, 2010).

1.3.2 Intercellular junctions in ECs

The paracellular pathway, under pathophysiological conditions is the main pathway of leakage of blood components and macromolecules across the microvasculature. In some organs, the endothelial cells are discontinued by fenestrations, allowing the passage of these substances. In the base of endothelial barriers, the physical integrity of the barrier is achieved by molecular junctions that connect adjacent ECs. There are three groups into which junctions can be categorised according to functional and structural properties: tight junctions, adherens junctions and gap junctions (

Figure 6).

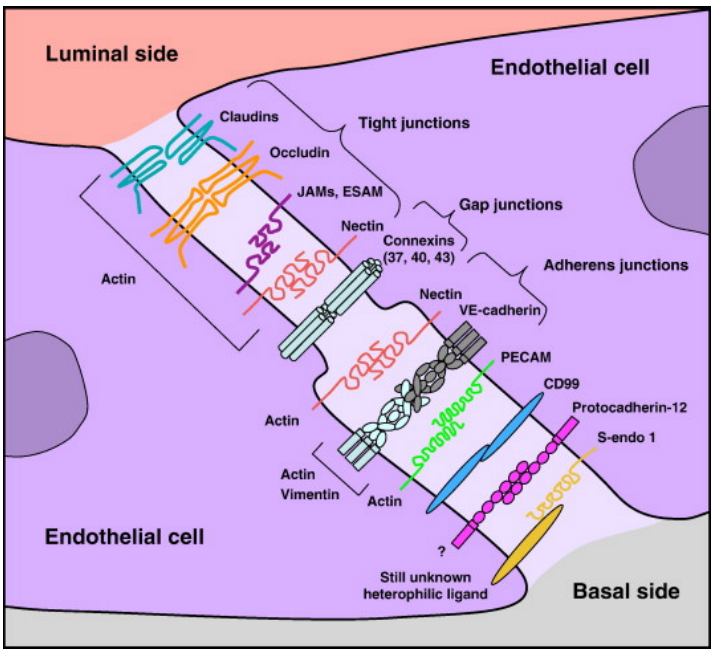

Figure 6 Proteins in the different types of junction in ECs (Wallez and Huber, 2008)

Tight Junctions

The continuous intercellular barriers between epithelial, vascular ECs and mesothelial cells, which function to separate tissues and create a selective movement of solutes, are called tight junctions (Van De Wetering et al.) (Van De Wetering et al.). TJs form a semi-permeable barrier to water, ions and other hydrophyllic solutes. Other functions include signalling and molecule trafficking and gate keeping function; providing a separation of the apical and basal plasma membrane compartments (Anderson and Van Itallie, 2009). Tight junctions act as a fence, restricting diffusion of proteins and lipids across the plasma membrane and maintaining cell polarity (Gonzalez-Mariscal et al., 2008).

TJs are formed by closely opposed interconnected plasma membranes of adjacent cells and can be made up from a group of over 40 proteins, the majority of which are part of the claudin family, with claudin-5 being the most important in ECs. Associated to TJs, other transmembrane proteins have been identified: occludin, tricellulin, junctional adhesion molecules (JAMs), and associated scaffold proteins (

Figure 7).

Claudins are cell transmembrane proteins that are found in epithelial and ECs TJs. They form the backbone of the paracellular barriers and pores which regulate cell permeability by selecting against molecular size and charge. These two characteristics make them the determinants of TJ barrier function (Gunzel and Yu, 2013).

Occludins associate with zonula occludens-1 (ZO-1) and zonula occludens-2 (ZO-2), and are thought to be important for signal transmission within the junctions and barrier function (Anderson and Van Itallie, 2009). This protein links the TJ to the cytoskeleton, increasing stability. ZO-1 is found not only in TJ but also adherens junctions (AJ) and gap junctions. Thus, ZO-1 dissociation from the TJ complex has been directly linked to permeability (Hawkins and Davis, 2005)

JAMs belong to the immunoglobulin superfamily and function as cell–cell adhesion molecules. These proteins interact with integrins αLβ2 (Lymphocyte function-associated antigen 1, LFA-1), α4β1 (Very Late Antigen-4, VLA-4) and αMβ2 (Macrophage-1 antigen, Mac-1), present on immune cells and orchestrate leukocyte transendothelial migration (

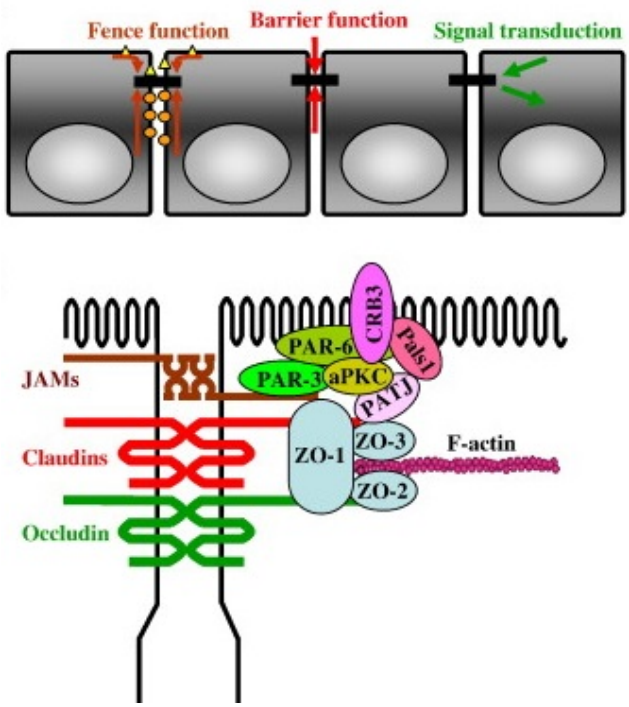

Figure 7) (Anderson and Van Itallie, 2009 2008, Wallez and Huber, 2008).

Figure 7 Schematic representation of tight junctions and associated junctional proteins (Chiba et al., 2008).

Adherens junctions

Tight junctions are part of a junctional complex that includes adherens junctions (AJ), and this complex is responsible for the biochemical barrier function of the BBB (Huber et al., 2001). Adherens junctions mediate adhesion between ECs and are involved in the modulation of tight junction permeability. Adherens junctions are formed by transmembrane cadherins that anchor their cytoplasmic tails to catenins. These

junctions are deeply involved in the maintenance of the vascular barrier, controlling the permeability of circulating immune cells (Gavard, 2009).

The adherens junction complex is composed of a cadherin-catenin complex (VE-cadherin bound to β-catenin, plakoglobin, and α-catenin) and associated proteins (such as p120) (**Figure 8**)(Stamatovic et al., 2006). The best described transmembrane protein in the EC AJ is vascular endothelial (VE-) cadherin, essential to the maintenance of vessel integrity (M. Corada et al., 1999). In endothelial cells, VE-cadherin is anchored to the actin cytoskeleton via catenins and vinculin (Lampugnani et al., 1995). An important function of VE-cadherin is the regulation of the physiological paracellular passage of macromolecules through the barrier (Fukuhara et al., 2005, Gavard and Gutkind, 2006). VE-cadherin is known to control vascular permeability and leukocyte transmigration (Gotsch et al., 1997, Gavard, 2014). VE-cadherin binds to β-catenin and plakoglobin that ultimately bind to the actin cytoskeleton stabilizing the AJ complex (Hawkins and Davis, 2005).

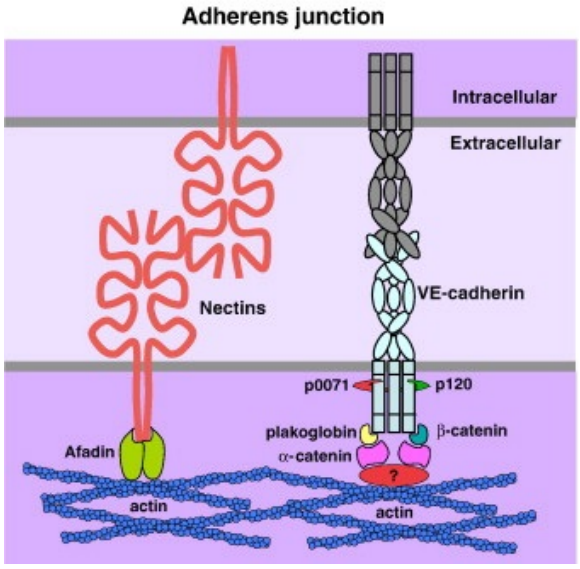

Figure 8 Adherens junctions and associated proteins (Wallez and Huber, 2008)

Gap Junctions

Gap junctions form aqueous channels between the cytoplasm of adjacent ECs, allowing direct diffusion of molecules and ions. These channels are formed by connexins and result from the connection of two hemichannels (one from each connecting EC). The channels allow the passage of molecules up to 1000 daltons (such as Ca^{2+} and IP_3) between the cytoplasm of adjacent cells. Independent hemichannels can also release ATP and NAD+ (**Figure 9**). In ECs, the most abundant connexin is Cx40, although other connexins are also expressed and are closely associated with vasodilation and blood pressure. It has been suggested that monocytes and macrophages also express connexin channels that regulate adhesion (Lampe and Lau, 2000, Goodenough and Paul, 2009).

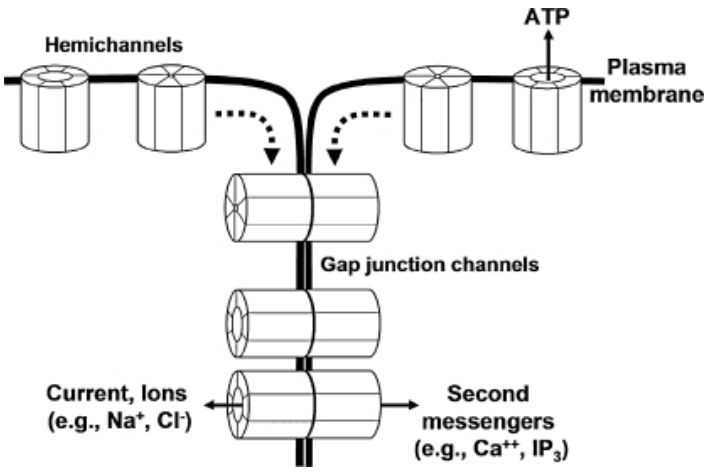

Figure 9 Gap junction channels and hemichannels (Figueroa and Duling, 2009)

The EC junctions described above, tight, adherens and gap junctions, are essential for the maintenance of blood vessel integrity and the passage of ions and solutes. In inflammation, these junctions are also involved in critical response of the immune system: the delivery of leukocytes to the site of injury. This process, which culminates in leukocyte transendothelial migration (TEM) or diapedesis, involves the passage of leukocytes through (transcellular pathway) or between ECs (paracellular pathway) (Muller, 2011).

1.4 Chemokines in inflammation

Chemokines are low molecular weight (8-17 kDa) cytokines, classically known to be secreted in response to pro-inflammatory stimuli. They signal through GPCR's on the cell membrane and can be important in directing leukocytes to specific sites of injury (**Figure 10**) (Speyer C., 2011). Other than inflammation, chemokines are involved in biological processes, including development, response to viral infections, osteoporosis, tumourigenesis and metastasis (Lazennec and Richmond, 2010).

Chemokines are classified into subfamilies according to the presence of conserved cysteine residues in the amino acid sequence. There are four chemokine subfamilies: CC, CXC, CX3C and XC. The CXC subfamily has an amino acid located between the two cysteines and is composed of 17 members. The two smaller families with only one chemokine each are the CX3C (three amino acids between the two cysteines) and the fourth subfamily, that includes two molecules with only two cysteine residues (XC chemokines). The CXC subfamily can be subdivided according to the ELR motif, present in classically angiogenic chemokines (CXCL1, 2, 3, 5, 6, 7 and 8) and absent in angiostatic chemokines (all other CXCL- chemokines, except CXCL12) (Lazennec and Richmond, 2010)

The CC subfamily with two adjacent cysteine residues is composed of 28 chemokines.

Functionally, chemokines are classified as homeostatic or inflammatory. Homeostatic chemokines are constitutively expressed and have pivotal role in organogenesis and angiogenesis.

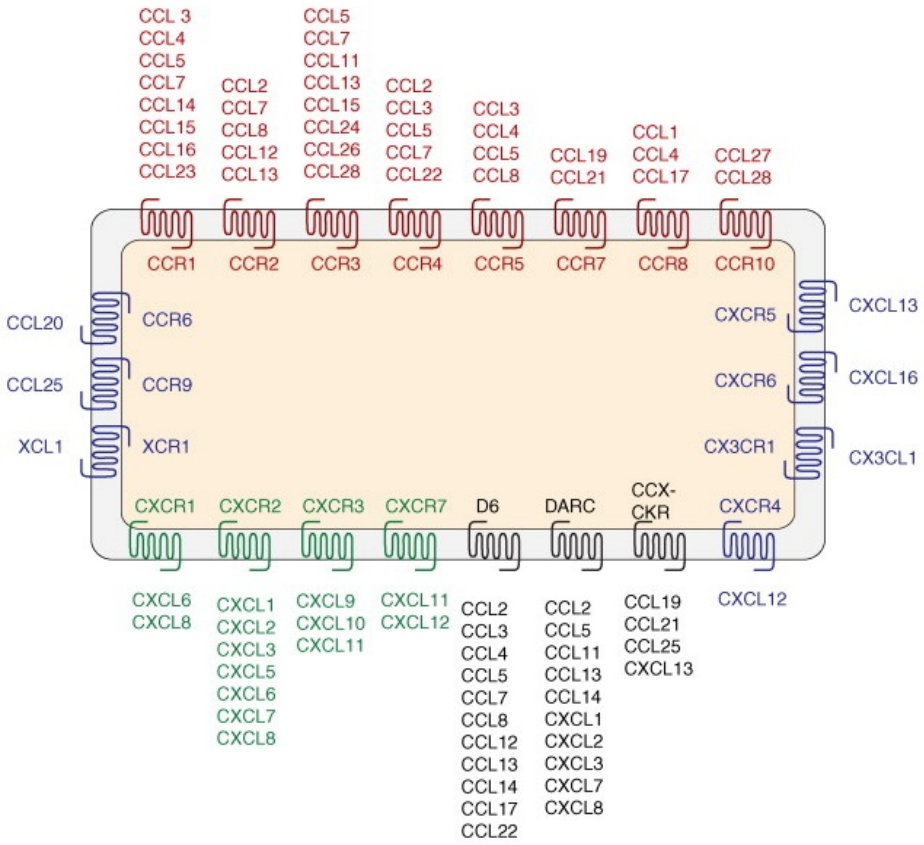

Figure 10 Schematic representation of chemokines and their receptors (Lazennec and Richmond, 2010).

They are also important for immune system regulation, including leukocyte trafficking to the sites of injury. Despite these two distinct chemokine classifications, there is an overlap of function, as many chemokines classified as homeostatic can have inflammatory functions and *vice versa* (Bosisio et al., 2014). Epithelial and ECs, in addition to producing chemokines, also express chemokine receptors for an array of

chemokines, including inflammatory chemokines (Hillyer P., 2003). Accordingly, chemokines are known to activate ECs through their chemokine receptors (Hillyer and Male, 2005). This suggests that ECs have a role in the vascular response in inflammation and can contribute to the development of inflammatory disorders (Murdoch and Finn, 2000). Activation of ECs by chemokines can be divided into two types: type I activation or stimulation, rapid responses that are not dependent of gene expression, and mediated by GPCRs and chemokines; and type II activation that is dependent on gene expression (Pober and Sessa, 2007).

Chemokines (and their receptors) are also involved in many of the steps required for leukocyte transmigration. Chemokines expressed by leukocytes create adhesive interactions between leukocytes and EC, resulting in activation of signalling pathways; including the Mitogen-activated protein kinases (MAPK) pathway (Takeshita and Ransohoff, 2012). This process will be described in a different subchapter below.

1.4.1 Chemokine signalling: GPCRs

Chemokine signalling is triggered by binding to G-protein coupled receptors (GPCRs). Structurally GPCRs consist of a seven transmembrane single polypeptide that is embedded in the cell's plasma membrane. The extracellular loops of the receptor form part the structure that the agonist (ligand) molecules bind. The ligands bind to the transmembrane segments or the amino terminus and extracellular sequences linking the transmembrane domains (peptide hormones and proteins) causing a conformational change (Kobilka and Deupi, 2007). Ligand binding to a G protein leads to the activation of an array of signalling pathways associated with chemotaxis, including MAP kinases, PLC, phosphoinositide 3-kinase (PI3K), RAS and Rho GTPase isoforms (Lazennec and Richmond, 2010).

GPCR receptors are the largest and most diverse group of cell surface receptors in eukaryotes, and are targets for 30-50% of modern drugs, functioning in processes as diverse as: neurotransmission, hormone action, platelet aggregation, and leukocyte chemotaxis. The architecture of GPCRs has been highly conserved over the course of evolution and across different species. Humans have nearly one thousand GPCRs, and each respond to a specific ligand group. GPCRs are promiscuous: each chemokine binds to more than one receptor and one receptor binds to several different chemokines. Additionally, chemokines can bind to silent receptors that lack a signalling function but can regulate inflammatory and immune reactions, such as decoy receptors and scavenger receptors. Decoy receptors include Duffy antigen receptor for chemokines (DARC), D6 and CCX-CKR. DARC and D6 are mainly expressed by the endothelium (although erythrocytes also express DARC and leukocyte express D6). CCX-CKR is expressed by an array of tissues and leukocytes. Scavenger receptors remove chemokines from the extracellular environment and by controlling chemokine availability modulate leukocyte migration (Mantovani et al., 2006).

1.4.2 Chemokine signalling and MAPK

Upon chemokine binding to GPCR's a number of downstream signalling pathways can be triggered. One of these is the MAPK signalling pathway and one of the key downstream intracellular signalling components are the mitogen-activated protein kinases (MAPKs) (Naor et al., 2000). MAPK are a family of enzymes which are regulated by phosphorylation cascades and are involved in numerous cellular functions *in vivo*, including cell differentiation, inflammation and cell death (Kyriakis and Avruch, 2012). There are seven families of MAPKs: extracellular regulated kinase 1/2 (ERK1/2), extracellular regulated kinase 3/4 (ERK3/4), extracellular regulated kinase 5 (ERK5), extracellular regulated kinase 7/8 (ERK7/8), P38 kinase, Nemo-like kinase (NLK) and the c-Jun N-terminal kinase (JNK) group. In most instances dual phosphorylation of a

threonine and tyrosine residues are required for full MAPK activation (Broom et al., 2009).

ERK 1 and ERK 2 MAPK are activated by growth factors, cytokines, stress stimuli, GPCR ligands and other factors. They are ubiquitously and abundantly expressed throughout mammalian cells, and are activated through Tyr and Thr phosphorylation at two closely spaced residues in their activation loop (Raman et al., 2007) (Pearson et al., 2001). Once stimulated ERK phosphorylates more than 250 different substrates and the functional outputs include, amongst other outcomes, early gene and protein expression resulting in proliferation and migration (Seger and Krebs, 1995).

The P38 MAPK was discovered as a tyrosine phospho-protein in LPS treated macrophages. P38 is activated by dual phosphorylation on Thr180 and Tyr182 residues by agents such as cytokines, hormones, GPCRs, osmotic and heat shock, and stress inducing agents (Pearson et al., 2001, Kaminska, 2005). The main functional outcome of P38 activation is the production of inflammatory mediators that initiate leukocyte activation and recruitment and related gene expression. Therapeutic inhibition of P38 has been explored in various diseases and has been shown to be beneficial in rheumatoid arthritis, inflammatory bowel disease, brain and systemic inflammation (Kaminska, 2005).

Chemokine/EC interactions have been described in a number of diseases. For example, in rheumatoid arthritis, chemokine expression and presentation by ECs mediates neutrophil migration into the tissues as well as promoting neovascularization, leading to dysregulated inflammation and injury (Speyer C., 2011). In the context of HIV infection, where brain capillary ECs are target for HIV, it has been demonstrated that CXCR4 and other CC receptors are co-factors with CD4 for infection (Moses et al., 1993). In addition, processes such as proliferation, migration and differentiation of vascular cells in

angiogenesis have also been shown to be modulated by chemokines through their receptors in ECs (Speyer C., 2011).

In inflammation, leukocyte capture and transmigration requires chemokines to be immobilised on the EC luminal surface. In fact, many chemokines are produced by the tissue, they need to be transported to the luminal space where they can interact with circulating leukocytes. This process has been described for many chemokines, including CCL5, CCL19 and CXCL8 and entails the biding the chemokine to the abluminal surface of the endothelium, transport via a caveolae system (vesicles) to the luminal surface of ECs (Middleton et al., 1997, Baekkevold et al., 2001). The multi-step process of leukocyte transendothelial migration will be detailed in a different section (Leukocyte transendothelial migration-1.5.4).

1.4.3 CXC Family of Chemokines: CXCL8

CXCL8 (interleukin (IL)-8) is a chemokine produced by macrophages, monocytes, epithelial cells and ECs, amongst others in response to infection or injury. In ECs, CXCL8 is stored in the Weibel-Palade bodies, secretory organelles that are specific to ECs and contain proteins involved in inflammation, angiogenesis, and tissue repair (Valentijn et al., 2011). The expression of CXCL8 in a non-pathological state is extremely low but increases rapidly in response to pro-inflammatory cytokine stimulation, such as TNFα and interleukin (IL)-1β (Liu et al., 2016).

CXCL8 binds to the cell membrane receptors CXCR1 and CXCR2, two closely related GPCRs, mediating immune response such as chemotaxis of granulocytes to the sites of infection (Kohidai and Csaba, 1998). CXCR1 is selective only for CXCL8 and CXCL6 whilst CXCR2 binds to an array of CXC chemokines (Mancardi et al., 2003). CXCR1 and CXCR2 are expressed by a number of cells including neutrophils, monocytes, CD8+ T

cells, NK cells and ECs (Russo et al., 2014). Mast cells and keratinocytes also produce and respond to CXCL8. (Omatsu et al., 2014). CXCL8 has been shown to cause the formation of filapodia-like protrusions in ECs following receptor activation, where they interact with polimorphonuclear cells (PMN) by presenting chemokines. CXCL8 is also involved in neutrophil adhesion, cell adhesion and angiogenesis (Koch Ae, 1992, Wolff et al., 1998, Strieter et al., 2005, Goczalik et al., 2008).

Signalling through the CXCL8 receptors CXCR1 and CXCR2 activates the Rho and Rac signalling pathways, leading to cytoskeletal rearrangement and it has been suggested contribute to the increased vascular permeability observed in acute inflammation and during the angiogenic response (Schraufstatter et al., 2001 2001). CXCL8 has been shown to induce the phosphorylation of the vascular endothelial growth factor receptor (VEGFR-2) in ECs, regulating the permeability of the endothelial barrier and phosphorylating VE-cadherin and occludin, opening tight and AJ (Petreaca et al., 2007, Chen et al., 2009). In other recent publications, CXCL8-induced permeability has been suggested to involve downregulation of TJ protein expression (occludin, ZO-1 and claudin-5) in a dose and time dependent manner (Yu et al., 2013, Sun et al., 2016). Consistent with this, CXCL8 and its receptors have been shown to be involved in inflammatory and autoimmune pathologies including atherosclerosis, inflammatory bowel disease, ischemia, multiple sclerosis and rheumatoid arthritis (Goczalik et al., 2008).

1.4.4 CXC Family of Chemokines: CXCL10

Another widely studied CXC chemokine is CXCL10 (previously known as interferon gamma-induced protein 10, IP-10), secreted by monocytes, ECs and fibroblasts and other cell types. CXCL10 shows sequence homology with a family of proteins with chemotactic and mitogenic roles which are associated with proliferation and

inflammation. CXCL10 has “homing” functions, attracting macrophages, dendritic cells, NK cells and activated T lymphocytes towards the sites of inflammation. Studies have shown a role of CXCL10 in chemoattracting activated T cells and their adhesion to ECs, angiogenesis in infectious and inflammatory diseases and tumour supressing activity (Liu et al., 2011). Moreover, CXCL10 is proposed to also be involved in angiogenesis, as well as infection control and in the generation and function of T cells (Luster et al., 1985 1985, Dufour et al., 2002).

CXCL10 induces its effects by signalling through the cell surface chemokine receptor CXCR3 (Luster et al., 1985 1985, Dufour et al., 2002). CXCR3 has 41% homology with CXCR1 and CXCR2 and it is involved in the recruitment of T cells but not granulocytes (Murdoch and Finn, 2000, Mancardi et al., 2003). CXCL10 signalling through CXCR3 has been reported to be responsible for angiogenesis and tumour supressing activity. A recent study reports that endothelial and epithelial cells can express an additional unidentified CXCL10 receptor that is neither CXCR3 nor a glycosaminoglycan and is able to transduce signal that might mediate the angiostatic effect of CXCL10 (Soejima and Rollins, 2001).

In the context of neuroinflammation, CXCL10 expression is upregulated in early multiple sclerosis and in EAE (experimental autoimmune encephalomyelitis) (Mckimmie and Michlmayr, 2014). In support of this hypothesis, in MS patients a correlation between high levels of the chemokines CXCL9 and CXCL10 and increased BBB permeability and leukocyte infiltration has been suggested (Cramer et al., 2015). Furthermore, in post viral infection in mouse neurons, CXCL10 has been reported to be produced. In this context, this is seen as an initial step in an inflammatory cascade that leads to immune cell infiltration, decrease of junctional protein expression, and increase in BBB permeability (Chai et al., 2015). In a separate study, CXCL10 has been shown to induce a rapid transmigration of activated $CD4^{+}$T cells across a HUVEC monolayer in the presence of

shear stress (Manes et al., 2007). Moreover, in HUVEC where CXCR3 has been knocked down, CXCL10 treated cells showed less of an increase in permeability in comparison to wild type cells (Zhu et al., 2016). These studies implicate a role for CXCL10 in neuroinflammatory conditions and potentially for affecting BBB function.

1.4.5 CC Family of Chemokines: CCL4

The chemokine CCL4 (also known as macrophage inflammatory protein-1 beta, MIP-1β) was first identified as a heparin-binding protein in macrophages stimulated with LPS. Other cells have since been identified that are also capable of producing CCL4 such as human brain microvascular ECs that synthesise CCL4 in response to LPS, TNF-α, IFN-γ, or IL-1β (Menten et al., 2002). Once secreted, MIP-1 proteins (a family of which CCL4 is part of), may then bind to their GPCR receptors and initiate signalling pathways. For example, in immune cells MIP-1 proteins can induce degranulation, TEM of monocytes, dendritic and natural killer (NK) cells, and the synthesis of inflammatory mediators (Maurer and Von Stebut, 2004).

A major receptor for CCL4 is CCR5, which can also bind CCL3, CCL5 and CCL8, and which shares some homology with CCR1 (55%), -3 (49%) and -4 (48%). Other CCL4 receptors have also been suggested including CCR1 (Lu et al., 2003), CCR3 (Manousou et al., 2010) and CCR8 (Fox et al., 2006).

In the immune system CCR5 is expressed by monocytes, macrophages, $CD4^+$ and $CD8^+$ T cells and the THP-1 monocyte cell line and is implicated as a co-receptor in association with CD4 for the entry into cells of the human immunodeficiency virus (Arthur et al.); (Murdoch and Finn, 2000). CCL4 induces adhesion and migration of T cells and promotes leukocyte chemotaxis and transmigration through human brain endothelial cells (Quandt and Dorovini-Zis, 2004). Indeed, the chemokine has been shown to

activate ECs, inducing an increase in expression of E-selectin on the cell surface, which is consistent with it enhancing leukocyte migration (Menten et al., 2002).

CCL2, which is structurally similar to CCL4, and a chemoattractant for T cells and monocytes has been shown be expressed by BCEC and to play a role in leukocyte recruitment across the BBB and the BRB (Harkness et al., 2003).

1.5 Immune System Barriers

1.5.1 Blood-Brain Barrier

The maintenance of a distinct CNS environment is possible due to the existence of a physical barrier that separates the neural microenvironment and the circulating blood, restricting the transport of toxic or harmful substances from the blood into the brain. This barrier, the blood-brain barrier (BBB), is formed by brain capillary ECs (BCEC) that line

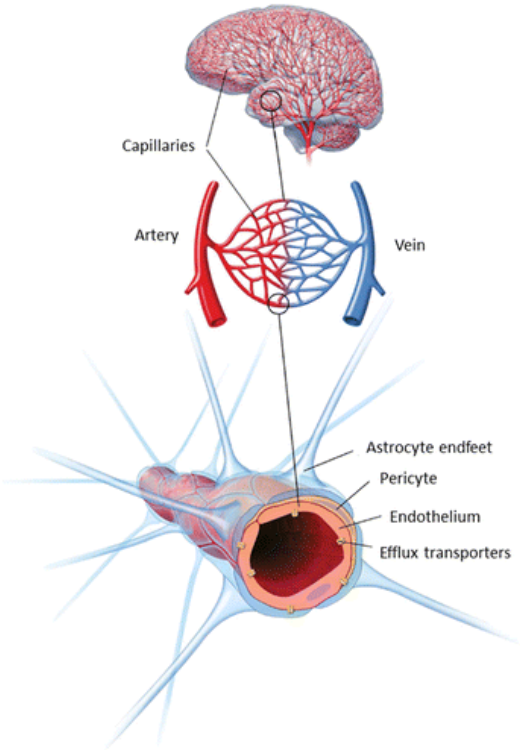

Figure 11 The neurovascular unit (Helms et al., 2016)

the capillary walls, forming an interface between the CNS and the circulation. The BCEC and the surrounding accompanying cell types (astrocytes, pericytes, neurons, microglia) constitute the neurovascular unit (**Figure 11**) (Hawkins and Davis, 2005).

The most important components of the neurovascular unit are the BCEC that have numerous characteristics in common with ECs found throughout the body: expression of glycoproteins, adhesion molecules and integrin receptors. BCECs also have specific characteristics that distinguish them from ECs found in other vascular sites; these include a lower number of caveolae, circumferential TJs between the cells, and higher mitochondrial density (Abbott et al., 2010).

The TJs of the BBB are the major defining components that determine the selective permeability to macromolecules, drugs and other soluble elements that otherwise would penetrate the CNS. The existence of TJs, and the high electrical resistance, means that most molecules must cross the BBB by the transcellular route, rather than crossing paracellulary. The release of soluble barrier-inducing factors by neighbouring cell types, such as astrocytes, pericytes and neurons also contributes to the high electrical resistance found at the BBB (Abbott et al., 2010). Other elements, the expression of homophilic transmembranar claudin proteins (claudin 3 and 5) and occludin (ZO-1-3, cingulin) are responsible for the paracellular occlusion and the IgSF JAMs may also influence the TJ and ultimately the BBB function (Abbott et al., 2006).

In addition to TJs the EC of the BBB also express AJs. These junctions are composed of the transmembrane cadherin VE-cadherin, which is very abundant in BCECs, and is linked to the cytoskeleton through association with catenins. The disruption of AJ has been shown to cause BBB loss of integrity (Abbott et al., 2010).

To overcome the impenetrable nature of the BBB, there are several transport processes for transferring essential hydrophilic molecules across the BBB including the SLC solute carriers (such as glucose transporters 1 and 2, organic anion and anion/cation families, etc.), transcytosis receptor-mediated carriers (such as the transferrin receptor) and non-specific adsorptive-mediated transcytosis. Transcytosis provides the main form of transport of macromolecules such as proteins and peptides through vesicles that can enter the CNS this way. The binding of these macromolecules to an extracellular receptor triggers a signalling event, forms a transcytosis vesicle and transports the macromolecule through the BCEC (Abbott et al., 2010, Wilhelm et al., 2011). There are also transport systems for lipid soluble xenobiotics, the ABC efflux transporters, that prevent the entry of harmful lipid soluble molecules into the brain.

Engulfed in the basal matrix, pericytes cover intermittently 22-32% of the capillaries in the CNS (Takeshita and Ransohoff, 2012). Pericytes are involved in regulating EC proliferation, angiogenesis and inflammation. Pericyte deficiency has been shown to induce increased BBB permeability (Armulik et al., 2010). Another cell responsible for the BBB essential properties, including TJ integrity in the neurovascular unit, is the astrocyte. Endfeet of astrocytes are in contact with the basement membrane and release regulatory factors such as TGF-β, GDNF, bFGF and IL-6. Neural cells can regulate the expression of BBB-related enzymes and activated microglia, in the perivascular space, and are also important in the immunological role of the BBB (Wilhelm et al., 2011).

Traditionally the CNS has been described as an immune-privileged organ isolated from systemic immune responses and surveillance, and where the immune system has little influence. The CNS lacks classical antigen-presenting cells (instead, has microglia and astrocytes), MHC I and MHC II expression on cells of the parenchyma which, taken together, only allow a limited immune activity in the CNS (Abbott et al., 2010).

The notion that immune surveillance is absent in the CNS has been challenged in recent years, and it is known that in pathological conditions such as ischemia, viral infections or inflammatory diseases (such as multiple sclerosis) there is invasion of immune cells into the CNS. This response involves other essential processes such as glial activation, oedema, complement activation, synthesis of proteins and mediators and major histocompatibility complex and adhesion molecules expression (Lucas et al., 2006).

There is evidence of immunological reactions in the CNS that are similar to immune reactions in other organs, suggesting the existence of a drainage network. The meninges are immunological sites within the CNS with a network of vessels that run along the perisinual space that allow CNS immune surveillance. The specialized network of vessels have characteristics of lymphatic vessels carrying immune cells, fluid and macromolecules that are involved in immune surveillance. In addition to this function, the CNS lymphatic system also clears waste from the brain parenchyma into the CSF, also called the “glymphatic system”. The clearance of macromolecules is drained via the nasal mucosa into cervical lymph nodes, via de cribriform plate (Weller et al., 2010, Raper et al., 2016). In fact, the role of this drainage into the cervical nodes in T cell mediated immune reactions has been shown in EAE, where the removal of the nodes in rodents resulted in 40% reduction in inflammation in the brain (Phillips et al., 1999).

To overcome the impenetrable BBB there are several transport processes for transferring essential hydrophilic molecules across the BBB including the SLC solute carriers (such as glucose transporters 1 and 2, organic anion and anion/cation families, etc.), transcytosis receptor-mediated carriers (such as the transferrin receptor) and non-specific adsorptive-mediated transcytosis. Transcytosis provides the main form of transport of macromolecules such as proteins and peptides through vesicles that can enter the CNS this way. The binding of these macromolecules to an extracellular receptor triggers a signalling event, forms a transcytosis vesicle and transports the

macromolecule through the BCEC (Wilhelm et al., 2011, Abbott et al., 2010a). There are also transport systems for lipid soluble xenobiotics, the ABC efflux transporters that prevent the entry of harmful lipid soluble molecules into the brain.

The traffic of substances between organs and the removal of drugs and harmful compounds, the degradation of hormones and prostanoids is governed by proteins involved in drug transport and metabolism at the BBB. These proteins, such as drug transporters and drug metabolizing enzymes have beneficial effects on the maintenance of the homeostasis of the BBB (by removing or metabolizing harmful compounds) but can also have a detrimental effect, by keeping therapeutic drugs from entering the brain or drug metabolizing enzymes for metabolites (in the case of drugs or carcinogens). It is still largely unknown whether the transporters and enzymes work in coordination in the BBB or exactly how they are regulated (Kapitulnik, 2011).

Transport proteins in the BBB allow the passage of beneficial substances such as glucose, amino acids and precursors of neurotransmitters whilst preventing the entry of toxic substances, such as metabolites which could cause damage to the brain. In disease, if the properties of the BBB are compromised, there could be an increased risk of exposure if the brain to neurotoxic compounds and a dysregulated removal of CNS-proteins, such as amyloid that could promote neurodegeneration (Kapitulnik, 2011).

BBB dysfunction has been described in a number of conditions such as multiple sclerosis, ischemia, hypoxia, Parkinson's and Alzheimer's diseases. Transient or mild TJ disruption, and in some cases, microglial activation have been shown to be an early sign of CNS dysfunction (Abbott et al., 2010).

Additionally to the BBB, there are other non-endothelial barriers in the CNS, the blood–cerebrospinal fluid barrier (BCSFB) formed by epithelial cells and the choroid plexus and

the arachnoid barrier that is formed by a tight epithelial layer with TJs (Abbott et al., 2010).

1.5.2 Blood-Retinal Barrier

The blood-ocular barriers are formed of two main components that work in equilibrium: the blood-aqueous barrier and the blood-retinal barrier (BRB). The two components are responsible for the fluid, ionic and macromolecular balance within the eye, regulating and restricting the entrance of substances and solutes by a complex network of cells, proteins and signalling events. Similar to the BBB in the CNS, the BRB allows the eye to be a privileged immune site where the penetration of immune cells occurs at a much lower rate in very tightly regulated conditions (Xu et al., 2003).

The BRB is comprised of an outer and an inner BRB, which create a separation between the ocular vascular beds and the retinal tissues. The inner compartment is formed by retinal ECs interconnected by TJs. This layer rests on the basal lamina covered by the processes of astrocytes, Muller cells and pericytes. These cells regulate the microenvironment of the BRB by sending signals to the ECs. The outer compartment is formed by a layer of retinal pigment epithelial cells (RPE) bound laterally by TJs, resting upon Bruch's membrane. The outer compartment is essential to regulate the exchange of nutrients and elimination of waste from the photoreceptors to the circulation (Cunha-Vaz et al., 2011).

The endothelial cells of retinal capillaries have a small number of vesicles for endocytosis or transcytosis. This transport system has been suggested to be mediated by caveolae or a vesico-tubular system. This small number of vesicles contributes to the barrier integrity and a disruption in the iBRB has been associated with an increase in endocytosis and endothelial changes (Kaur et al., 2008).

Changes in the permeability of retinal ECs is the primary process contributing to changes in BRB function. In particular, matrix metalloproteinases produced by Muller cells have been shown to lead to proteolytic degradation of occludin and PEDF, also produced by Muller cells results in an increased production of VEGF resulting in increased retinal permeability (Kaur et al., 2008).

These changes are a result of a multi-factorial process, mediated by various factors including growth factors, cytokines, inflammation and loss of pericytes. Furthermore, structural changes of the glycocalyx and the basal lamina, along with functional changes in pericytes and astrocytes promote leakage of the BRB. The increase in transport of plasma proteins subsequently leads to macular oedema (Ingeborg et al., 2013). Indeed, inner BRB dysfunction contributes to the most frequent retinal diseases; namely diabetic retinopathy and age-related macular degeneration (Schenkel et al.) (Cunha-Vaz et al., 2011).

The two structures, the inner BRB and the BBB are both composed of tight junctions between endothelial cells. They share common features, offering selective separations between the circulation and an immune privileged organ (the brain or the retina). The BRB is not an absolute barrier, allowing the passage of molecules from the retina to the circulation and *vice versa*, comparably to what has been described in the BBB. Both structures present uptake mechanisms for amino acids and glucose but present other characteristics that are distinct such as differential pericyte attachment and astrocyte coverage (Gardner et al., 1999, Campbell and Humphries, 2012).

1.5.3 Hyperpermeability of the BBB and BRB

In the normal endothelium, there is a regulated level of permeability but under pathological conditions, the endothelium can become hyperpermeable. The pathological

increase of BBB permeability, leakage or hyperpermeability, is a consequence of pathologies such as infection, ischemic stroke or traumatic brain injury. In acute and chronic inflammation, the permeability of the vascular barriers in immune-privileged sites can be altered. The consequences of this pathological change in tissue permeability include fluid extravasation, oedema and ultimately tissue dysfunction (Michiels, 2003). There are other events that disturb BBB function. Namely hypoxia, a feature of ischemic stroke and traumatic brain injury, leads to BBB TJ opening and increased permeability. Moreover, there is evidence that hypoxic stress may also increase permeability via the transcellular route, independent of TJs (Cipolla et al., 2004).

The maintenance of haemostasis in the CNS greatly depends on the integrity of the intercellular junctions in BCECs. Increased permeability at the BBB level can be the result of AJs being compromised, but the main players are TJs, that are responsible for low paracellular permeability and the high electrical resistance of the BBB (Hawkins and Davis, 2005).

Inflammatory mediators, such as cytokines, and the chemokine CCL2 are known to be involved in BBB disruption by interacting with junctional proteins (Stamatovic et al., 2003, Abbott et al., 2010). Pro-inflammatory molecules such as histamine, thrombin, cytokines and the vascular endothelial growth factor (VEGF) are known to induce endothelial permeability (Michiels, 2003). In chronic hyperpermeability, as a result of the lasting effect of a permeability inducing agent, there is a structural change or damage of existing vessels e.g. in rheumatoid arthritis, psoriasis, cellular immunity, or even angiogenesis, where new vessels grow that are abnormal, as found in proliferative diabetic retinopathy and cancer (Nagy et al., 2008). A well known example of this is the inflammatory events of MS and its experimental counterpart EAE (Hawkins and Davis, 2005).

Another EC component, the actin cytoskeleton, is essential for the barrier properties of the BBB. In quiescent conditions, actin forms a cortical rim in ECs, that interacts with intercellular and cell-matrix complexes. In non-muscle cells, β and γ actin polymerise and form F-actin, essential for actin structures within the cells (Prasain and Stevens, 2009). Adherens junctions are anchored to F-actin, a characteristic essential for the regulation of barrier function (Navarro et al., 1995). Stress fibres are essential for cell contraction and influence the rate and dimension of the gaps that cells create at their borders (Cramer et al., 1997).

In the BBB leakage triggers astrocyte activation and the production of glial fibrillary acidic protein (GFAP) and recently it has been shown that Muller cells, in the retina, also produce this protein in hypoxic conditions. Similarly, VEGF has been reported in both the BBB and the BRB as a marker of hypoxia, contributing to disruption of the barriers and ultimately, leakage (Kaur, 2008).

Pathological increase of permeability in the BBB and BRB may result in unregulated entry of not only macromolecules but also immune cells. The section below details the physiological and pathological mechanisms of entry of leukocytes into the BBB and BRB.

1.5.4 Leukocyte transendothelial migration

The extravasation of leukocytes is part of many pathological and non-pathological processes, such as immune surveillance, leukocyte recruitment in inflammatory responses and homing and mobilization of hematopoietic cells (Van Buul and Hordijk, 2004).

The capture of circulating leukocytes by the vascular endothelium has been studied extensively and the basic principles governing this process delineated. This process, the “multistep paradigm”, consists of, in summary; the process of tethering and rolling of

leukocytes on the endothelium facilitated by selectins, activation of integrins followed by arrest and transmigration of the leukocytes through ECs, following a paracellular or transcellular route (Springer, 1994). This process may be specific to the disease, the organ and the type of leukocyte involved in the migration (Norman and Hickey, 2005).

The first stage of leukocyte recruitment involves the capture of circulating cells. Selectins are a family of transmembranar proteins with a cytoplasmic domain, involved in signal transduction, and an extracellular domain responsible for leukocyte/endothelium interactions. Endothelial (E)-selectin is expressed in response to cytokines such as IL-1, TNF-α and lipopolysaccharide (LPS), and like platelet (P)-selectin, binds to Selectin P ligand (PSGL-1), as well as E-selectin ligand 1 and CD44 on the leukocyte surface. These interactions slow the velocity of leukocytes though rapid make and break connections resulting in the process of leukocyte rolling along the EC surface. The interaction between selectins, leukocytes and the endothelium is reversible, and allows communication between leukocytes and the endothelium through, amongst other mediators, chemokines on the endothelial surface (Granger and Senchenkova, 2010).

The slowing down of leukocyte through selectin interactions enables tissue derived chemokines, sequestered on glycosaminoglycans (GAGs) on the EC luminal surface, to be presented to the rolling leukocytes (Zlotnik and Yoshie, 2000). Chemokines, produced by immune and non-immune cells, also create a gradient from the site of injury/disease, chemoattracting circulating cells and providing directionality. Chemokines are then able to bind to their G-protein coupled receptors (GPCRs) on the leukocyte where they initiate signalling pathways that alter the function of leukocyte integrins that mediate part of the adhesion cascade (Murdoch and Finn, 2000).

Integrins are a group of transmembrane signalling glycoproteins that possess various phosphorylation and protein binding sites that transduce and activate signalling

pathways. In leukocytes, integrins are responsible for firm adhesion and arrest of immune cells through binding to immunoglobulin superfamily cell adhesion molecules (ICAMs) on the EC. In non-activated leukocytes these integrins exist in a low affinity/low avidity state but following capture by selectins, the immobilised chemokines are able to engage with their GPCRs that results in the integrins changing their binding state to a high affinity configuration. Moreover, induced clustering of integrins leads to higher avidity binding (Granger and Senchenkova, 2010).

The signalling cascade from GPCR to integrin activation can be divided in key stages: phospholipase C (PLC) signalling, small GTPases activation and integrin conformational change. The conformational change and integrin activation then initiates additional signalling responses such as the outside-in integrin signalling (Ley et al., 2007). The leukocytes are able to bind to the EC CAMs with sufficient strength to initiate arrest and to resist shear flow (Springer, 1994, Massena and Philipson, 2012).

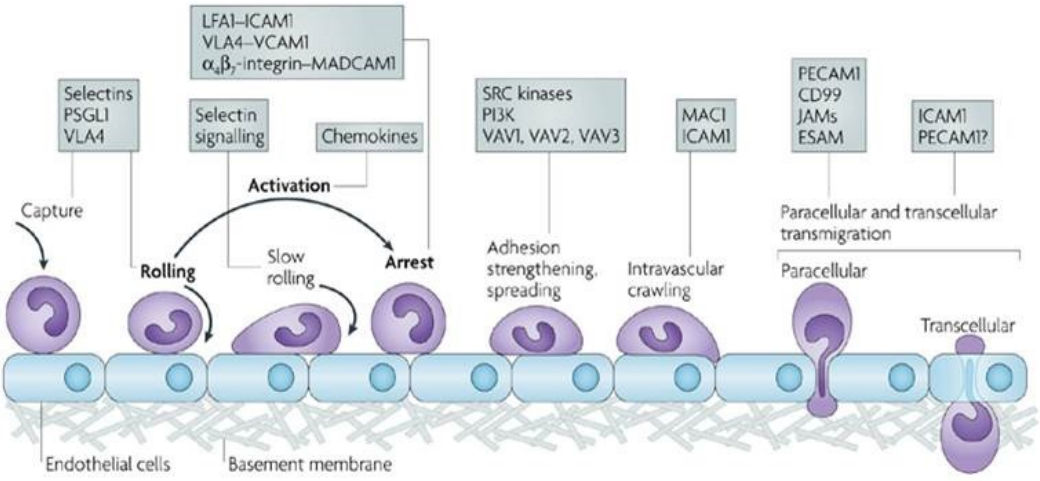

Figure 12 The multistep paradigm (Ley et al., 2007).

The immunoglobulin superfamily CAMs on ECs, in particular ICAM-1, ICAM-2 and VCAM-1, are necessary for the subsequent arrest of leukocytes through binding to leukocyte integrins. Under normal conditions the expression of these CAMs is low or absent but upon activation of the EC by cytokines, such as TNFα and IL-1β, gene expression is induced/up-regulated leading to enhanced protein expression (Massena and Philipson, 2012).

Monocytes and ECs also secrete chemokines, such as CCL2, acting on T lymphocytes and monocytes, and CXCL8, that act on neutrophils. This then allows the leukocyte integrins to bind to CAM counter-receptors on the EC (Xiao et al., 2014).

Through leukocyte engagement to CAMs, there is active involvement of the EC through activation of outside-in signalling cascades initiated. This is believed to result in pore formation or cell junction disengagement that allows leukocytes to migrate through a transcellular, or paracellular route respectively. Once in the sub-endothelial space leukocytes migrate through gaps between pericytes and the endothelial basement membrane, (in regions of low protein concentration in the extracellular matrix), mediated by integrins and proteases (**Figure 12**) (Ley et al., 2007).

Leukocyte TEM is also only possible with the rearrangement of the leukocyte's cytoskeleton and actin polymerisation, with the leukocyte becoming polarised and migrating along the luminal surface of the vessels (Springer, 1994, Carman et al., 2007, Nourshargh et al., 2010).

Paracellular pathway

The paracellular pathway is thought to be the preferential pathway for leukocyte transmigration in most organs except in the brain and retina where specialised vessels form the BBB and BRB respectively. In paracellular migration there is a disruption of the

junctions between adjacent cells through the binding to and activation of EC adhesion receptors (Luscinskas et al., 2002, Weber et al., 2007 2007). These receptors, such as PECAM-1, ICAM, CD99 and the JAMs, activate Rho- and Rac- dependent pathways which result in junctional destabilisation (Van De Wetering et al., 2003, Etienne-Manneville, 2012). PECAM-1 is a cellular adhesion molecule and receptor, expressed in blood and vascular cells, regulating leukocyte trafficking (Privratsky and Newman, 2014). CD99, expressed in hematopoietic cells and EC junctions, facilitating diapedesis. Therefore, diapedesis via the paracellular migration pathway is highly dependent on PECAM-1 and CD99 (Schenkel et al., 2002). ICAM-1 mediates leukocyte-endothelial interactions via integrins and has crucial role in leukocyte adhesion and rolling. It also initiates outside-in signalling, facilitates diapedesis and regulates the permeability of microvessels in basal and pathological conditions (Sumagin et al., 2008) (Dragoni et al., 2017). ICAM-1 signalling, in particular, has been implicated in T-cell migration across brain ECs (Greenwood et al., 2003).

Transcellular pathway

There is growing evidence in the literature that the preferred route for the passage of leukocytes though the EC of the central nervous system (CNS) and neuroretina is via the transcellular pathway (Muller, 2011, Takeshita and Ransohoff, 2012). For example, using an experimental model of autoimmune uveoretinitis (EAU) in the rat and detailed ultrastructural analysis it was suggested that leukocyte migration occurs via the transcellular route (Greenwood et al., 1994). In the context of bacterial meningitis, migration of neutrophils into the CNS has also been shown to occur via the same route (Wewer et al., 2011).

According to recent findings, transcellular migration starts with the extension of leukocytic membrane protrusions, or invadossome-like protrusions by the path of least

resistance into the underlying EC (Carman and Springer, 2004). This causes the deforming the nuclear lamina and actin of the EC, compromising the barrier and allowing the leukocyte to transmigrate transcellularly. This process of finding the path of least resistance has been coined as *tenertaxis* (Martinelli et al., 2014).

1.6 Leukocyte migration in the BBB and BRB

Under normal physiological conditions, there is very limited recruitment of lymphocytes into the CNS. In contrast, in pathological conditions where the BBB is compromised, circulating activated T lymphocytes can readily access the CNS (Hickey et al., 1991).

The mechanisms for recruitment of lymphocytes into the BBB and BRB have common features to the mechanisms seen elsewhere. Each step of the already described multi-step paradigm involves the expression of CAMs (ICAM-1, V-CAM-1, PECAM-1) by BCEC interacting circulating leukocytes that express their ligands (such as αLβ2 (LFA-1) and α4β1 (VLA-4)) (Larochelle et al., 2011). ICAM-1, in particular, is essential during adhesion of ECs to leukocytes and has been shown to be increased in various inflammatory conditions (Greenwood et al., 2002) (Turowski et al., 2005). On the brain EC surface, ICAM-1 is crucial in adhesion and rolling and is counteracted by PECAM-1 that regulates activation in brain ECs (Couty et al., 2007 2233).

Resting T cells have a limited ability to enter the brain but studies have shown that freshly activated T cells are able to transmigrate through the BBB (Hickey, 2001). In the BBB, tethering and rolling of $CD8^+$ and $CD4^+$T lymphocytes is dependent on expression of E- and P-selectin and their ligands. Signalling through GPCRs mediate integrin activation which consequently leads to leukocyte firm arrest to the CNS microvasculature. Transendothelial migration of T-cells has been shown to be mediated by G-protein signalling in brain ECs (Adamson et al., 2002)

The migration of leukocytes through the BBB increases permeability, increasing further leukocyte infiltration. Tighter junctions and low F-actin regions in the BBB show higher levels of transcellular migration (Martinelli et al., 2014). In EAE, ICAM-1 and VCAM-1 have been shown to be upregulated in microvascular ECs of the CNS, with the expression of the latter in the human cerebral EC still being contentious (Steffen et al., 1996, Chaudhary et al., 2006). In EAU, infiltration of the inner retinal vessels by leukocytes is associated with dysfunction of endothelial cells, breakdown of tight junctions and ultimately of the inner BRB. This phenomenon has been shown to be mediated by TNF and IL-1β, reactive oxygen and nitrogen species. Cuffing with accumulation of exudates around pericytes and glia has been observed both in EAU and EAE (in the form of perivascular cuffs). In the BRB, after crossing the inner barrier T cells interact with APCs (perivascular macrophages), driving the inflammatory process further (Shechter et al., 2013)

Interestingly, in the retina, PSGL-1–E- or P-selectin are involved in T cell recruitment. Although the inflamed brain, in EAE and MS, expresses an array of chemokines and lymphocytes express receptors for those chemokines, the exact mechanism of chemokine signalling in BCEC is yet to be elucidated (Engelhardt and Ransohoff, 2005)

There is some evidence that points towards the involvement of cells such as microglia and other APCs in the inflammatory response in the iBRB. Recent studies point towards a proinflammatory signal by these cells leads to the progression of inflammation, whilst negative signals could result in resolution of inflammation in the retina (Crane, 2008 #2284). There is currently limited knowledge of leukocyte migration inthe retina and further studies elucidate this processes would be a great contribution to the field.

1.7 Aims and hypothesis

In the past decades, research has shown the pivotal role of chemokines on immune cells, and how they direct leukocytes to the sites of inflammation. A number of components of ECs have been identified in regulating EC barrier permeability and mediating leukocyte transmigration.

In the context of the regulation of EC function and leukocyte TEM in the BBB, the role of CCL4, CXCL8 and CXCL10, and their receptor expression in ECs, remains poorly investigated. It is of interest to determine these mechanisms and how leukocyte migration across the BBB's endothelium is influenced by chemokines and their receptors expressed by BCEC.

We hypothesised that the downstream effect of CCL4, CXCL8 and CXCL10 on brain endothelial cells could affect the BBB properties, translating into changes in junctional proteins, permeability and leukocyte migration.

2. Materials and Methods

Equipment, general and tissue culture reagents used in this thesis in Appendix I.

2.1 Cell Lines

2.1.1 Human umbilical vein endothelial cells (HUVEC)

HUVEC were obtained commercially from Lonza (Wokingham, UK). Cells were cultured in EGM-2 medium supplemented with EGM-2 B BulletKit™ (VEGF, IGF, bFGF, hydrocortisone, ascorbate, gentamycin and 2.5% foetal bovine serum (FBS)) as indicated by the manufacturer. Plates/flasks were coated with gelatin (0.5% in ddH_2O). Upon dissociation using TrypLE™ Cell Dissociation Reagent, a trypsin alternative, cells were seeded at $8x10^4$ - $1x10^5$ cells/mL in gelatin coated cell culture plates/flasks and media was changed every other day. They were grown in a humidified atmosphere at 37 °C in 5% carbon dioxide (CO_2) and up to 75-90% confluence and used between passage 2 and 5.

2.1.2 Human brain microvascular endothelial cells (hCMEC/D3)

The immortalised cell line hCMEC/D3 was donated by Pierre Couraud (Institut Cochin) at P26 and used as a Blood-Brain Barrier model (Weksler et al., 2013).

HCMEC/D3 were maintained in growth media at 37 °C in 5% CO_2. Cells were cultured in EGM™-2 Basal Medium supplemented with FBS, Penicillin Streptomycin (P/S) (1%),

hydrocortisone (1 mg/mL), ascorbic acid (2.5 mg/mL), lipid concentrate, HEPES and bFGF (10 µg/mL).

Cells were seeded at $8x10^4$ to $1x10^5$ cells/mL in collagen I (1:60 in DPBS) coated cell culture plates/flasks and media was changed every other day following a DPBS wash. Cultures were grown to 75-90% confluence before passaging and were used between passage 26 and 35.

The immortalised cell line presents an endothelial and BBB phenotype, retaining immunological and permeability characteristics of the cells of origin (**Figure 13**).

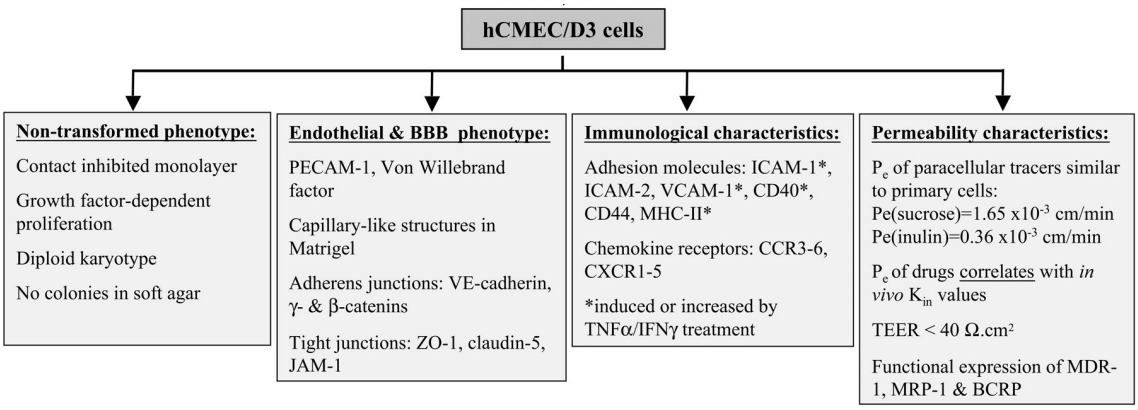

Figure 13 Diagram representing the main properties of hCMEC/D3 (Weksler et al., 2005).

2.1.3 T cell culture

Peripheral whole blood samples were obtained from healthy volunteers. 30 mL of blood was divided in three falcon tubes and diluted in equal volumes of PBS. 9 mL Ficoll® Plaque Premium were added to new falcon tubes and the diluted blood samples were slowly added creating two separated layers. Samples were centrifuged at 1500 rpm for 35 minutes. The peripheral blood mononuclear cell layer was removed, resuspended in 40 mL of PBS and spun at 1200 rpm for 10 minutes. The pellets were pooled into the same falcon, resuspended in 14 mL of PBS and spun again at 1200 rpm for 10 min. The

resulting pellet was resuspended in 160 µL of buffer (0.5% Bovine Serum Albumin in PBS (PBSA)) and 40 µL of CD4 Microbeads and incubated at 4^0C for 15 minutes. Samples were diluted in 4 mL of buffer and centrifuged at 1200 rpm for 10 min. The magnet was washed in buffer before the pellet was resuspended in 500 µL and passed through a filtration column. Then, 3 mL of buffer was added three times to the column and the collecting tube was replaced. Finally, 5 mL of buffer was added to the column and was flushed using the plunger supplied with the column. The resulting suspension was centrifuged at 1200 rpm for 10 min, resuspended in 1 mL of medium and counted. $CD4^+$T cells were resuspended at a density of 500,000 cells/mL and transferred into a T25 flask. 25 ng/mL of IL-2 was added to the final suspension. IL-2 has been extensively used for maintenance and expansion of T lymphocytes *in vitro* (Smith, 1988).

2.2 Molecular Biology Methods

2.2.1 Sodium dodecyl sulphate-polyacrylamide gel electrophoresis (SDS-PAGE) and Western blotting

Cells were lysed in 80 µL (12-well plates) or 160 µL (6-well plates) of lysis buffer (4% SDS, 10% 2-mecaptoethanol, 20% glycerol, 0.004% bromophenol blue 0.125 M Tris HCl) with 5% 2-mecaptoethanol to reduce disulphide bridge formation. Samples were collected and denatured at 100^0C for 5 min and centrifuged at 4^0C for 10 min at 13.1 g and frozen at -20^0C until further use. Alternatively, cells were lysed in RIPA buffer with protease and phosphatase inhibitors, centrifuged for 5 min at 13.1 g. 20 µL of supernatant was then collected and mixed with 80 µL of sample buffer containing DTT, boiled for 5 min and centrifuged again before loading. 8-18 µL of sample was loaded on 8-10% resolving/ 5% stacking SDS-PAGE gels or 4-12% NuPAGE™ Novex pre-cast

gels and run in NuPAGE™ MOPS running buffer for 90 min at 160 V. The reagents used for SDS-PAGE and the consequent Western blot are shown in Table 1.

Table 1 Products used for SDS-PAGE and Western blotting

Product	Manufacturer
Amersham Protran 0.45 NC nitrocellulose membrane	GE Healthcare Life Sciences (Little Chalfont, UK)
Bovine Serum Albumin (BSA), lyophilised	First Link UK (Wolverhampton, UK)
ECL Prime Western Blotting Detection Reagent	GE Healthcare Life Sciences (Little Chalfont, UK)
ECL Western Blotting Detection Reagent	GE Healthcare Life Sciences (Little Chalfont, UK)
NuPAGE® MOPS SDS Running Buffer (20X)	Fisher Scientific - UK (Loughborough, UK)
NuPAGE™ Novex™ 4-12% Bis-Tris Midi Protein Gels	Fisher Scientific (Loughborough, UK)
RIPA Lysis Buffer, 10X	Milipore (Watford,UK)
Tris-Glycine Electroblotting Buffer (10X)	National Diagnostics (Nottingham, UK)
Ponceau S solution BioReagent, suitable for electrophoresis, 0.1 %	Sigma (Poole, UK)

2.2.2 Western Blotting

Proteins were resolved and transferred to nitrocellulose membranes in transfer buffer (900 mL Tris-Glycine Electroblotting Buffer, 100 mL methanol, 100 mL H_2O), 12 V overnight at 4^0C. Transfer success was assessed using Ponceau S (5% in acetic acid) and then membranes were incubated with 5% BSA in TBST (0.05 M Tris and 0.15 M sodium chloride, pH 7.6) at room temperature. Incubation with primary antibodies (Table 2) was carried out overnight at 4^0C or for 1-3 h at room temperature, as per optimised conditions. Membranes were then incubated with a species-specific secondary antibody

(Table 3) conjugated with horseradish peroxidase for 1 h at room temperature and then visualised by enhanced chemiluminescence detection with GE Healthcare Amersham ECL Western Blotting Detection Reagent (Little Chalfont, UK), using the Prime alternative when a more sensitive detection method was needed. Membranes were incubated simultaneously but separately. If necessary, membranes were stripped in mild stripping buffer (2% (w/v) SDS, 0.0625 M Tris pH 6.8, 0.008% (v/v) β-mecaptoethanol) and re-probed.

The signal intensities of the bands were then normalised to the housekeeping protein – HSC70. The antibody anti-HSC70 (Heat shock cognate 71 kDa protein) was used as a loading control since its expression remains constant and it has been used extensively as a housekeeping protein in the literature (Plenchette et al., 2004, Zhu et al., 2005). Another factor that lead us to select this protein, was due to its clonality, allowing us to have a loading control in the same membrane as the antibody of interest – without the need to strip and reprobe the membrane, which has been shown to lead to loss of protein or incomplete removal of the previous antibody used (Yeung and Stanley, 2009). We found that the amount of protein obtained from HUVEC and hCMEC/D3 lysates obtained was constant through the experiments, and any variation seen in the immunoblots is a result of technical issues during the loading of the SDS-PAGE gels.

Table 2 Primary antibodies used in western blotting

Primary Antibody	Dilution	Species raised in	Manufacturer
P-P44/43 MAPK (T202/Y204)	1:5,000	Rabbit	Cell Signalling Technology (Hitchin, UK)
P44/42 MAPK (ERK 1/2)	1:5,000	Rabbit	Cell Signalling Technology (Hitchin, UK)

P-P38 MAPK (T180/Y182)	1:3,000	Rabbit	Cell Signalling Technology (Hitchin, UK)
P38 MAPK	1:3,000	Rabbit	Cell Signalling Technology (Hitchin, UK)
GAPH (1D4)	1:20,000	Mouse	Novus Biologicals (Abingdon, UK)
CXCR1	1:1,000	Rabbit	Abcam (Cambridge, UK)
CXCR2	1:1,000	Rabbit	Abcam (Cambridge, UK)
CXCR3	1:1,000	Rabbit	Abcam (Cambridge, UK)
CCR5	1:1,000	Mouse	Abcam (Cambridge, UK)
HSC70	1:10,000	Mouse	Sigma (Poole, UK)
P--Tyrosine (P-Tyr-102)	1:1,000	Mouse	Cell Signalling Technology (Hitchin, UK)
P-Threonine (P-Thr-Polyclonal)	1:1,000	Rabbit	Cell Signalling Technology (Hitchin, UK)
P-Serine Antibody Q5	1:1,000	Mouse	Qiagen (Manchester, UK)

Table 3 Secondary antibodies used in Western Blotting

Secondary Antibody	Dilution	Species raised in	Manufacturer
Polyclonal Goat anti-mouse immunoglobulins HRP	1:10,000	Mouse	Dako (Cambridge, UK)
Polyclonal Goat anti-rabbit immunoglobulins HRP	1:10,000	Rabbit	Dako (Cambridge, UK)

2.2.3 Immunofluorescence (IF)

The additional reagents were used for IF. Antibodies in the section above were also included in IF experiments, details provided below:

Table 4 General materials used for hCMEC/D3 staining

Product	Manufacturer
Fluorescent mounting media	DAKO (CA, USA)
Coverslips	VWR (Lutterworth, UK)
Formalin (3.7% formaldehyde, 1xPBS)	VWR (Lutterworth, UK)

Table 5 Primary antibodies and manufacturers.

Primary Antibody	Dilution	Species raised in	Manufacturer
Dynabeads sheep anti-rat IgG		rat	Life Technologies (Loughborough, UK)
Collagen IV goat anti-mouse	1:200	mouse	Millipore (Watford, UK)
Anti-Human VE-Cadherin Monoclonal Antibody	1:200	mouse	R&D Systems (Abingdon, UK)
VE-cadherin Antibody (C-19)	1:200	Goat	Santa Cruz Biotechnology (Wembley, UK)
P-P44/43 MAPK (T202/Y204)	1:500	Rabbit	Cell Signalling Technology (Hitchin, UK)
P-P38 MAPK (T180/Y182)	1:3,000	Rabbit	Cell Signalling Technology (Hitchin, UK)
ZO-1	1:50	Rabbit	Thermofisher (Wilmington, USA)

Table 6 Secondary antibodies from Fisher Scientific (Loughborough, UK).

Host/Isotype	Dilution	Target Species	Conjugate Wavelength
Goat IgG	1:300	Donkey	488
Goat IgG	1:300	Donkey	594
Goat IgG	1:300	Donkey	647
Rabbit IgG	1:300	Donkey	488
Rabbit IgG	1:300	Donkey	568
Rabbit IgG	1:300	Donkey	594
Rabbit IgG	1:300	Donkey	647
Rabbit IgG	1:300	Goat	488
Rabbit IgG	1:300	Goat	555
Rabbit IgG	1:300	Goat	647
Rat IgG	1:300	Donkey	488
Rat IgG	1:300	Donkey	594
Rat IgG	1:300	Goat	594
Rat IgG	1:300	Donkey	488
Mouse IgG	1:300	Goat	Cy5
Mouse IgG	1:300	Goat	594

HCMEC/D3 were grown to confluency on collagen I coated 35 mm^2 Petri dishes. Treatments were performed at pre-determined timepoints. Control samples were produced by adding the same volume of the diluent of chemokines, 0.1%PBSA, as the volume of diluent with chemokines that was added to the treatment wells/dishes. Treatment start times were staggered in order for all the wells/dishes to finish at the same time. Once the treatment period was concluded, the dishes were placed on ice, and the media with or without treatments was aspirated and replaced with ice-cold DPBS. DPBS

was replaced with 4% formalin for 15 min and then replaced by blocking buffer (1x PBS, BSA (0.5%), sodium azide (0.05%)). Cells were then permeabilised with ice-cold acetone for 5 min. Acetone was diluted in DPBS before being diluted in blocking buffer and poured off. Blocking was performed for 1 h at room temperature. The edges of the dishes were dried off, creating a circular central area in the dish with 100 µL of antibodies were added. Primary antibody incubation was performed in an incubator at 37^0C for 30 min; followed by three blocking buffer washes and secondary antibody incubations for 30 min at 37^0C. Nuclei of cells were visualised by the addition of 1 µg/mL Hoechst 33258 (bis-benzminide) or DAPI in the secondary antibody staining solution. Dishes were then washed in blocking buffer, twice in PBS and finally in distilled H_2O, before being mounted with a coverslip over the circumscribed stained area, using DAKO fluorescence mounting media. The dishes were stored at 4^0C and imaged using the Zeiss LSM 710 confocal microscope within 4 days of staining.

For multiple antibody staining, where one of the antibodies targeted an extracellular protein, permeabilisation was needed after the first primary antibody incubation. Initial primary antibody incubation was performed on ice for 30 min and the dishes were then washed in blocking buffer followed by permeabilisation in ice-cold methanol or 4% PFA. Dishes were then incubated in blocking buffer for 1 h at room temperature followed by primary antibody incubation at room temperature for 2 h. A central area in the dish for the incubations was created as described above. Following blocking buffer washes, dishes were incubated with secondary antibodies for 30 min in an incubator. Following washing with blocking buffer, DPBS and water, dishes were mounted and imaged as described above.

Distribution of the MAP kinases P-ERK and P-P38 in hCMEC/D3 following chemokine treatments

To determine whether we could observe phosphorylation of the MAP kinases of interest *in situ* using IF, hCMEC/D3 were grown to confluence in 35 mm collagen-coated petri-dishes, serum-starved overnight and treated with chemokines for the same timepoints as the previous protein expression time course. Following treatments, hCMEC/D3 were labelled with antibodies against P-ERK and P-P38.

The nuclei of the samples were scanned using the following method: the first slice taken where the nucleus was at its smallest detectable diameter. The scan was carried on through the sample and subsequent slices where gradually larger diameters of the nucleus were obtained until the nucleus diameters decreased and disappeared from the field of view. This was performed in the 405 nm channel that corresponds to the nuclear stain, DAPI/Hoechst. Both the 405 nm (nuclear stain) and the 488 nm (phospho protein) channels were switched on and the pre-set Z-stack slices were obtained for both channels simultaneously (**Figure 14**). The number and thickness of slices remained constant throughout samples. The slice were the nucleus was the largest (usually the middle slice) was then recorded and that same slice was extracted for both channels. For each slice, threshold levels determined (also constant for each technical repeat) and mean pixel area and a ratio to control image was calculated. This method intends to

capture only the signal from the nuclear portion of the sample. Nevertheless, perinuclear stain could have been included in the images obtained.

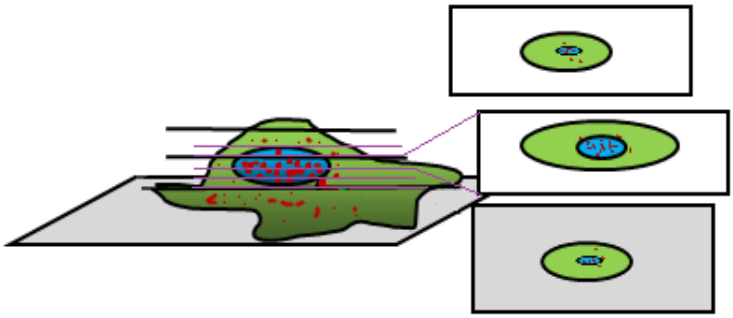

Figure 14 Graphic representation of method to obtain the nuclear portion (DAPI/Hoechst) of the hCMEC/D3 samples on petri dishes (Hartley, 2018).

ZO-1 expression following chemokine treatments

HCMEC/D3 were grown to confluency in collagen-coated Petri dishes, serum-starved overnight and treated with CCL4, CXCL8 or CXCL10 for 10 and 60 min. Following immunofluorescent antibody staining of ZO-1, dishes were imaged using confocal microscopy. Z stacks generated from confocal imaging and at least 3 10x fields from the same dish were imaged and the number pixels in the channel of ZO-1 (red pixels) and channel of DAPI (blue pixels) in each image were averaged on Image J. A ratio between the number of pixels corresponding to ZO-1 and DAPI in each image was then calculated. For junctional quantification, cytoplasmic and nuclear ZO-1 staining was manually masked using Image J, allowing the measurement of the area of junctional ZO-1 (**Figure 15**). A ratio for each image was then calculated using the mean area of junctional ZO-1 (red pixels) and DAPI (blue pixels).

VE-cadherin distribution following CCL4, CXCL8 and CXCL10 treatment

HCMEC/D3 were grown to confluency in collagen-coated Petri dishes, serum-starved overnight, and treated with CCL4, CXCL8 or CXCL10 for 5, 10 and 60 min. Following immunofluorescent antibody staining of VE-cadherin, dishes were imaged using confocal microscopy. The channels were thresholded, the number of pixels in the VE-cadherin channel (green channel) and the DAPI channel (blue channel) were quantified and a ratio normalised to control was calculated.

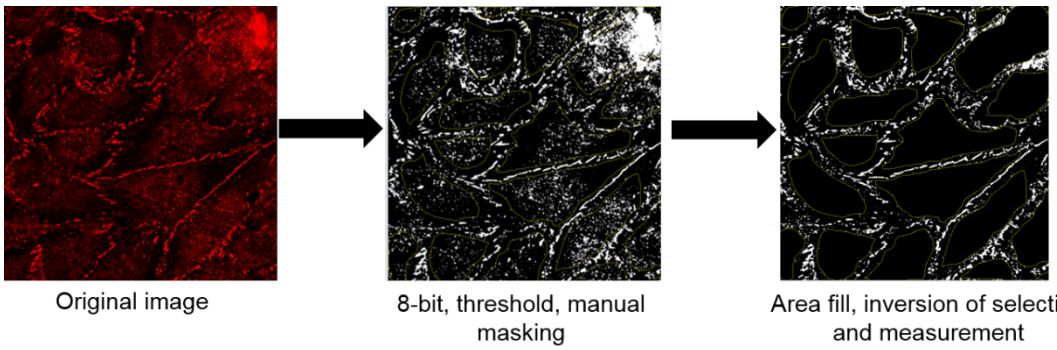

Figure 15 Example of ZO-1 masking method allowing the measurement of the area of junctional ZO-1. For junctional quantification, cytoplasmic and nuclear ZO-1 staining was manually masked using Image J, each channel thresholded and pixel number measured.

Quantification of VE-cadherin protein expression in hCMEC/D3 following chemokine treatments

HCMEC/D3 were grown to confluence, overnight serum-starved and treatment with chemokines were carried out for 5, 10 and 60 min. Cells were then harvested, lysed and SDS-PAGE followed by immunoblotting. The SDS-PAGE gel was run to its full length and transferred to a membrane in order to detect all possible sizes of VE-cadherin fragments (considering the possibility of protein cleavage).

Quantification of plasma membrane VE-cadherin using IF in chemokine treated hCMEC/D3 (with EGTA)

The following protocol was created to allow exclusive staining of extracellular portion of the protein and, using EGTA, to expose (unmask) the membranar/extracellular epitope completely. A buffer containing EGTA was used to open the adherens junctions in the EC monolayers and allow the anti-VE-cadherin antibody to access its extracellular epitope (Tamura et al., 1998) (Nagar et al., 1996).

HCMEC/D3 were grown to confluency in collagen-coated Petri dishes, serum-starved overnight and treated with chemokines for 5, 10, 30 and 60 min. Following PBS washes, live cell staining was performed. Cells were incubated with an anti-VE-cadherin antibody recognizing an extracellular epitope of VE-cadherin, in an EGTA containing buffer for 30 min. This was done at 4^0C to prevent internalisation. Following fixation in PFA and permeabilisation, respective secondary antibody was then added and cells were counterstained with DAPI prior to mounting (**Figure 16**).

A

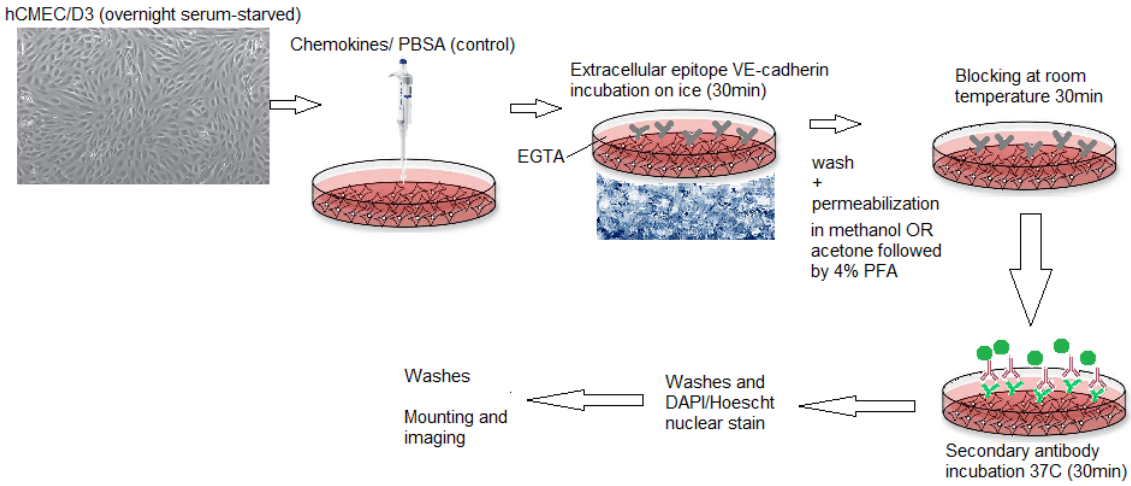

B

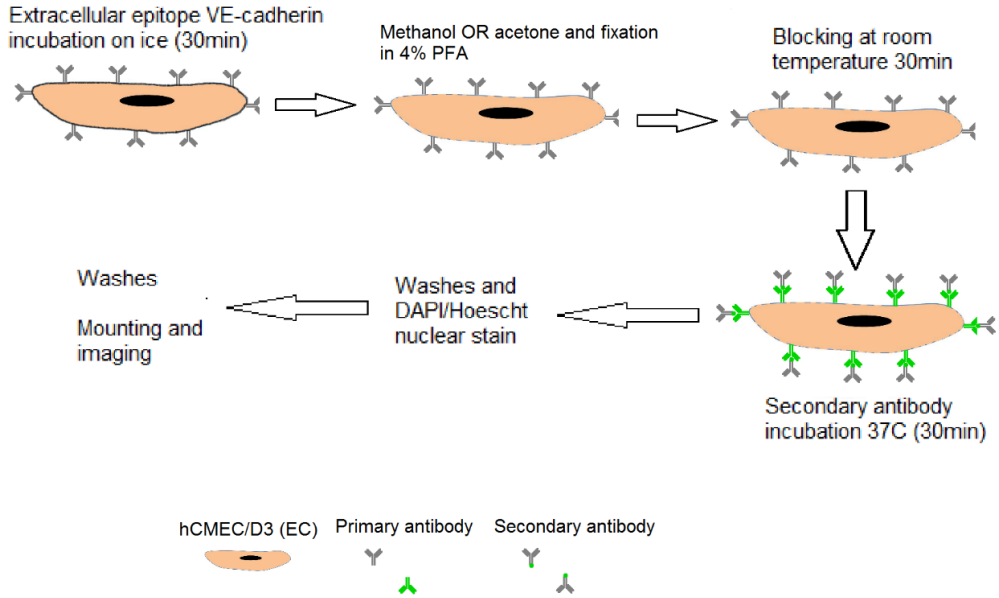

Figure 16 Protocol used for quantification of VE-cadherin expression using IF. (A) Protocol overview. (B) No B on figure! Single cell IF staining details. HCMEC/D3 were grown to confluency in collage-coated Petri dishes, serum-starved overnight and treated with chemokines for 5, 10, 30 and 60 min. Following PBS washes, live cell staining was performed. Cells were incubated with an anti-VE-cadherin antibody recognizing an extracellular epitope of VE-cadherin, in an EGTA containing buffer. This was done at 4ºC to prevent internalisation. Following fixation in PFA and permeabilisation, respective secondary antibody was then added and cells were counterstained with DAPI prior to mounting.

Z stacks were generated from confocal imaging and at least 3 fields from the same dish were imaged. The resulting images were thresholded and the pixel area of the VE-cadherin (green channel) and DAPI (blue channel) were calculated and a ratio of both channels for each image was generated. The statistical difference between control and treatment was calculated.

Expression of plasma membrane and total cell VE-cadherin following chemokine treatments

HCMEC/D3 were grown to confluency in collage-coated Petri dishes, serum-starved overnight and treated with chemokines for 5, 10, 30 and 60 min. Following PBS washes, cells were incubated with an anti-VE-cadherin antibody recognizing an extracellular epitope of VE-cadherin, in an EGTA containing blocking/washing buffer at 4^0C, as the previous experiment. Following fixation in PFA and permeabilisation, cells were incubated with an antibody recognizing an intracellular epitope of VE-cadherin for 30 min at 37^0C. Respective secondary antibodies were then added and cells were counterstained with DAPI prior to mounting (**Figure 17**).

Three separate fields from the same dish were imaged. The experiment was repeated thrice. Maximum projection Z stacks were generated from confocal imaging and the ratio of thresholded extracellular VE-cadherin (green) and total VE-cadherin (red) pixels were calculated and normalised to DAPI (blue).

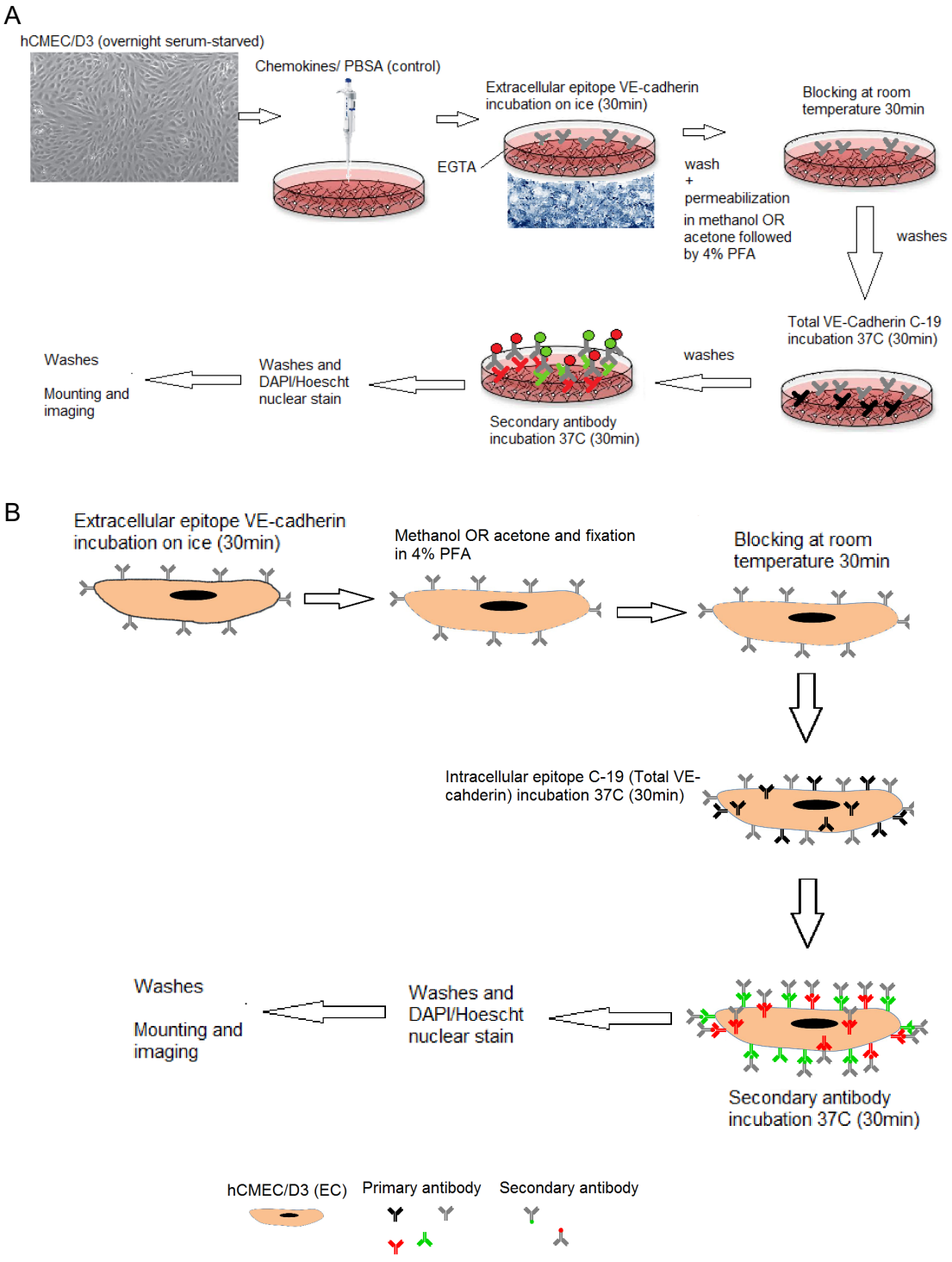

Figure 17 Protocol used for quantification of extracellular and total VE-cadherin expression using IF. (A) Protocol overview. (B) Single cell IF staining details. HCMEC/D3 were grown to confluency in collage-coated Petri dishes, serum-starved overnight and treated with chemokines for 5, 10, 30 and 60 min. Following PBS washes, cells were incubated with an anti-VE-cadherin antibody recognizing an extracellular epitope of VE-cadherin, in an EGTA containing blocking/washing buffer at 4ºC, as the previous experiment. Following fixation in PFA and permeabilisation, cells were incubated with an antibody recognizing an intracellular epitope of VE-cadherin. Respective secondary antibodies were then added and cells were counterstained with DAPI prior to mounting

Two different analyses were carried out. First, the signal of the two VE-cadherin antibodies was compared for each timepoint and chemokine treatment. Ratios for DAPI and VE-cadherin were calculated and shown as a ratio of control. Secondly, the co-localization coefficient was calculated using the JACoP plugin on image J, allowing the determination of the ratio of extracellular (plasma membrane) VE-cadherin (green) that co-localised with total (plasma membrane plus internal) VE-cadherin (red). Using this method we were able to asses if there was an increase in intracellular VE-cadherin following treatments.

Filamentous actin response in chemokine treated EC

In order to determine if chemokines induced actin remodelling in hCMEC/D3, phalloidin conjugated to a fluorescent dye was added to control and chemokine treated ECs. This protein binds directly to filamentous actin (F-actin). Confluent, overnight serum-starved hCMEC/D3 grown in Petri dishes were treated with CCL4, CXCL8 or CXCL10 for the appropriate lengths of time. Following fixation and fluorescent staining, dishes were mounted with a coverslip and imaged using confocal microscopy. Mean area of three fields of three independent images were analysed and an average +/- SEM of phalloidin area/DAPI, normalized to control was calculated

2.2.4 Permeability coefficient (Pe): Determination of permeability coefficients from FITC/RITC-dextran flux studies

The permeability coefficient (Pe) allows comparison of multiple experiments since it is independent of the experimental design but corrected for the transport surface area, the duration of the experiment and the applied concentration of tracer (Artursson, 1990).

HCMEC/D3 were grown to confluency in collagen-coated transwell filters and serum-starved overnight. The appropriate FITC or RITC-dextran tracer was added to the upper chamber (transwell filter) and samples from the bottom chamber were taken at set intervals of time. Method to calculate the permeability coefficient described below (Weksler et al., 2005, Perriere et al., 2007):

Measurements taken: lux measurements (-blank, i.e. value of PBS or HBSS) over time, including a filter control without cells and the specific fluorescence of the dextran dilution (i.e. totals in the top well).

1 - Each sample measurement was multiplied to give the total fluorescence in the well: measured 50 µL aliquots and total volume in the bottom well was 1.5 mL (1500 µL), so each fluorescent value was multiplied by 30. The volume withdrawn at each timepoint was taken into account into the bottom well volume: Total units n (at time n) = value n (in 50 µL at time n) * 30 + value n-1 (in 50 µL at time n-1).

2 - The specific fluorescence of each dextran dilution was determined for each well: 5 µL were removed at the start of the experiment (fluorescence in 5 µL of the top well was multiplied by 200 to give units/mL.

3- Each value obtained in step 1 was divided by its corresponding specific fluorescence value (determined in step 2). This yielded the values of cleared volume (in mL) for each well at each time point.

The values were plotted for each condition (including filters without cells) against time (in minutes) and the slope before and after additions was calculated (in mL/min). This was then adjusted to the surface area (1 cm^2 for a 12mm filter). The final result is then expressed in cm/min (1ml = 1 cm3). Formula: 1/P (cells+filter) = 1/P (cells) + 1/P (filter), so Pc = (Pcf * Pf)/ (Pf – Pcf) in cm/min.

2.2.5 Paracellular permeability of 4, 70 and 250 kDa FITC/RITC dextrans

The immortalised hCMEC/D3 cells were grown on type I collagen coated 12-mm transwell filters with 0.4 µm pore size (Corning). Cells were cultured for 3-4 days to confluence and starved in EBM-2 overnight. Fluorescein isothiocyanate-dextran (FITC)-dextran of 4 or 250 kDa, or Rhodamine B isothiocyanate (RITC)-dextran of 70 kDa was added at 1 mg/mL to the apical side of the transwell filters. 50 µl samples were aspirated from the basal chamber (and replaced by EBM-2) at 15 min intervals and samples were removed to t=180 min. Fluorescence of samples was measured in a Tecan Safire Fluorescence Reader, plotted against time and permeability changes were determined from linear slope changes (Hudson et al., 2014). Statistical analysis was done using a two tailed Student's t-test. Analysis performed using GraphPad Prism version 5.00 for Windows (GraphPad Software, San Diego CA USA).

2.2.6 T-lymphocyte endothelial transmigration

HCMEC/D3 were cultured in 96-well plates and grown to confluence (3-4 days post passage). Additions were performed in a tissue culture hood at room temperature followed by incubation in a tissue culture incubator (37^0C and 5% CO_2).

In set up A, chemokines (CCL4 and CXCL8 at 1 µg/mL or CXCL10 at 0.5 µg/mL) were added to T cells and incubated for 30min. T cells were then centrifuged, resuspended in HBSS and counted. A total of 50,000 T cells (in 100 µL) were added to hCMEC/D3 and incubated for 30min. Lymphocytes were left to adhere and migrate for 30 min in an incubator at 37^0C and non-adherent T lymphocytes were gently washed off using warm HBSS.

For set up B, T cells were added to hCMEC/D3 and chemokines were simultaneously added to the wells. For 30 min, lymphocytes incubated with activated hCMEC/D3 at 37^0C. Finally, non-adherent T lymphocytes were gently washed off using warm HBSS.

In set up C, chemokines were incubated with hCMEC/D3 for 10min, and after this time they were rinsed using HBSS. T cells resuspended in HBSS were added to the wells for 30min. Lymphocytes were left to adhere and migrate for 30 min in an incubator and non-adherent T lymphocytes were removed using HBSS at 37^0C.

Finally, in set up D, chemokines were added to hCMEC/D3 for 30min, washed off, and T cells resuspended in HBSS were added to the wells. Lymphocytes were left to adhere and migrate for 30 min in an incubator and T lymphocytes that did not adhered were gently washed off using HBSS at 37^0C.

Imaging: Plates were then mounted on a phase contrast microscope (Zeiss 200 M) with a CO_2 and temperature-controlled chamber. Images of a 672 μm x 512 μm frame were taken every 10 seconds, up to 30 frames. Percentage of transmigrated adherent T lymphocytes was determined by counting the flattened lymphocytes under ECs divided by total number of adherent T lymphocytes with migrating potential (that show movement over the 30 frames) and multiplying by 100. Mean migration rates and standard mean errors were calculated from at least three independent experiments. Experimental set up and criteria for transmigrated lymphocytes can be seen in the figure below (**Figure 18**).

Statistical analysis was carried out using a two-tailed Student's t-test. Analysis performed using GraphPad Prism version 5.00 for Windows (GraphPad Software, San Diego CA USA).

2.2.7 Transendothelial electrical resistance (TEER) in hCMEC/D3

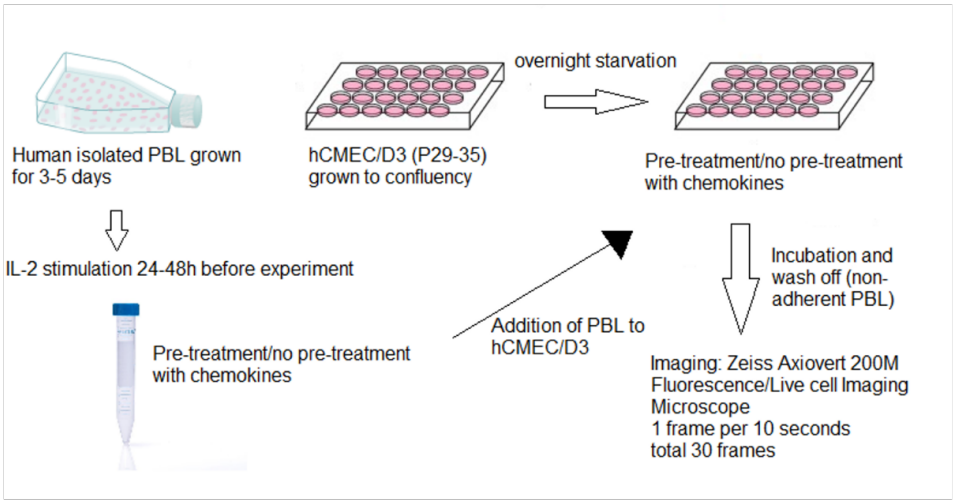

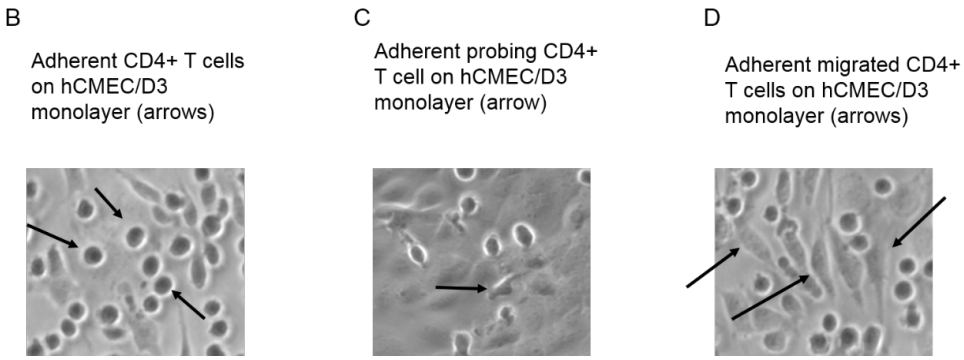

Figure 18 A – Human PBL (CD4+) were freshly isolated and cultured for 3-5 days prior to use. HCMEC/D3 were grown to confluence on collagen-coated 96-well plates. 24-48h before the start of the experiment, hCMEC/D3 were serum-starved. PBL or hCMEC/D3 were pre-treated with chemokines or 0.1% PBSA prior to PBL addition to hCMEC/D3. Following incubation, non-adherent PBL were washed off and wells were imaged using a Zeiss Axiovert 200M, capturing 1 frame every 10 seconds for a total of 30 frames. B – representative image of adherent CD4+ cells (inside red rectangle, round-shaped) on hCMEC/D3 (spindly cells on background). C- Representative image of an adherent CD4+ cell (red rectangle) probing the hCMEC/D3 monolayer. D- Representative image of 4 migrated CD4+ cells (red rectangle) on an hCMEC/D3 monolayer.

TEER was assessed by impedance spectroscopy using cells grown on gold electrodes (8-well 8W1E) and measured using ECIS (4,000 Hz; Applied Biophysics). TEER values of empty collagen IV/fibronectin-coated wells containing hCMEC/D3-conditioned medium were subtracted to determine monolayer TEER. Following overnight serum-starvation compounds diluted in 20-50µL of conditioned media were added to the pre-

determined wells. During additions, data collection was paused and resumed once additions were completed (less than 60 seconds pause).

hCMEC/D3 were grown to confluency, previously assessed to be 3-4 days post plating (plated at $6x10^4$ cells/cm^2), serum-starved and treated with CCL4, CXCL8 and CXCL10 in triplicate (3 wells per condition). The ECIS system produces a data set containing TEER measurements for each well at determined intervals (60 seconds in our experiments) that can be extracted as a Microsoft Office Excel file. TEER readings were taken throughout and the change in TEER was expressed in $\Omega.cm^2$. Exact time point of additions was equalled to zero (0) and all other time readings were expressed as a negative value (barrier establishment, before additions) or as a positive value (after additions). The TEER reading immediately before additions was expressed as one (1) and increases or decreases in TEER were expressed as a ratio of 1. Readings of wells with cells were normalised to empty wells coated with collagen. TEER was plotted against time and a One-way ANOVA and a Dunnet's post-test were used for statistical analysis.

2.3 In vivo work

2.3.1 *In vivo* permeability measurements in pial microvessels

The method used in this study, and its theoretical basis, has been described previously (Easton and Fraser, 1994, Easton et al., 1997). The experiments were performed on Wistar rats (25-30 days) within guidelines set by The Animals (Scientific Procedures) Act 1986. The rats were anesthetised by intraperitoneal injection of 60 mg/kg body weight sodium pentobarbital diluted in water, and maintained by supplemental injection if necessary. The dura and arachnoid was removed, thus exposing the microcirculation of

the surface of the brain and leaving it free of any diffusion barrier towards the superfusing solution (artificial cerebrospinal fluid: 110.5 MM sodium chloride (NaCl), 4.7 mM potassium chloride (KCl), 2.5 mM Calcium chloride ($CaCl_2$), 1.1 mM monopotassium phosphate (KH_2PO_4), 1.25 mg sulphate $(SO)_4$, 25 mM sodium bicarbonate ($NaHCO_3$) and 15 mM HEPES, pH 7.4, maintained at 37°C). Sulforhodamine B was added to the brain microcirculation into the carotid artery, and viewed under 540/25 nm illumination. The signal was captured through a microscope coupled to an image-intensifier camera (Hamamatsu). Video microscopy (1 frame per 2s) recorded the time-dependent loss of dye in a single vessel, occluded by a glass probe. All experiments were performed within 2 h from the start of the procedure, when the preparation is stable without noticeable change in baseline permeability (Sarker et al., 2000). A baseline recording was established for 20-60 s. To obtain measurements, the flow of superfusing solution was stopped so that a pool was formed between the brain and the microscope's water immersion lens. Dye was injected into the circulation and the probe was placed over the vessel to be analysed. Remaining dye in the circulation was removed by the blood flow. For the abluminal additions, the compounds were applied to the pool on the brain surface. For luminal additions, the carotid artery was injected with the compound mixed with the dye. Image analysis and densitometry was performed using ImageJ 1.45s (NIH). At the end of the experiment animals were culled by an overdose of the anaesthetic.

The mean pixel intensity was measured for each vessel tested for each frame/2 seconds and plotted against time. Data was normalised to diameter of the vessel according to pre-set graticule that correlates vessel diameter in a 20x Olympus field (used for the experiment) with 10µm grid (**Figure 19**). Mean pixel intensity before and after addition

and corresponding SEM were calculated and a paired t-test was used to compare differences between the two time sets (before and after additions).

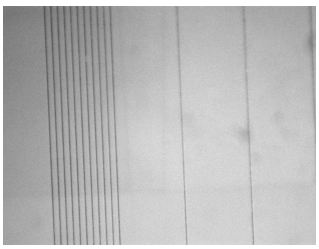

Figure 19 – Graticule 20x Olympus microscope (16-bit) provided by Professor Patric Turowski. Each far left line corresponds to a 10μm diameter vessel.

2.3.2 Intravitreal injections and fundus fluorescein angiography (Suffredini et al.)

Adult C57BL/6 animals were anaesthetised using an intra-peritoneal injection of Ketamine (60 mg/Kg) and Domitor® (10 mg/Kg). For intravitreal injections, 1 μL of CCL4 (at 1 mg/mL diluted in 0.1% PBSA) to give a final dose of 1 μg per eye. Control animals received 1 μL of vehicle. FFA was carried out 10 min following CCL4 injections using a Micron III: pupils were dilated with 1% tropicamide, eyes kept moist with Viscotears®, and light fundus images acquired followed by green fluorescence images at 1.5 and 7 min following subcutaneous injection of 2% fluorescein.

3. General EC activation and signalling by chemokines

3.1 Introduction

Chemokines, expressed by an array of immune and non-immune cells, including ECs, have been shown to have a role in the inflammatory process. The engagement of chemokines with their GPCR receptors results in a change in cell behaviour, including migration, proliferation, and activation of inflammatory responses. In inflammatory responses, chemokines are closely involved in engaging leukocytes and promoting their chemotaxis and migration to the site of injury (Speyer and Ward, 2011). Leukocyte engagement and recruitment across the BBB is known to be tightly regulated, although the involvement of chemokines in this process remains largely unknown. Alterations in the properties of the BBB, where barrier function is compromised, have been found in various neurological conditions such as stroke, trauma and neurodegenerative diseases (Barzo et al., 1997, Kortekaas et al., 2005, Zlokovic, 2005, Bell et al., 2010, Iadecola, 2010).

The effect of chemokines on ECs has been explored, but the contributions of CCL4, CXCL8 and CXCL10 in inflammatory conditions that affect the BBB remain poorly understood. Amongst the CXC chemokines, CXCL8 and CXCL10 have been selected due to their involvement in CNS pathologies. CXCL8 has been implicated in multiple sclerosis, ischemic brain injury and traumatic brain injury, among other non-CNS inflammatory conditions (Semple et al., 2010, Ha et al., 2017) (Subileau et al., 2009). The chemokine CXCL10 has equally been implicated in multiple sclerosis in addition to Parkinson's disease, HIV-associated dementia, and Alzheimer's disease (Subileau et

al., 2009, Mckimmie and Michlmayr, 2014). Additionally, the CC chemokine, CCL4, has been shown to be elevated in patients with pneumococcal meningitis, and induces BBB disruption in an animal model of the same disease (Geeta et al., 2013). In an *in vivo* model, CCL4 has also been shown to increase T cell adhesion to cerebral endothelial cells (Quandt and Dorovini-Zis, 2004). During TEM, the expression of CCL4 and CXCL8 was also found to be upregulated in hCMEC/D3, following ICAM-1 crosslinking (Dragoni et al., 2017).

When chemokines bind to their GPCRs, they initiate a cascade of intracellular events, including signal transduction. MAPK have been shown to play a role in regulating these signalling events in a number of different cells (Arbabi et al., 1999). Signalling events linked to MAPK have been implicated in the pathogenesis of cancer and neurodegenerative diseases such as Alzheimer's disease, Parkinson's disease and amyotrophic lateral sclerosis (Kim and Choi, 2015). Protein phosphorylation is one of the most common post-translational modifications. The amino acids tyrosine, serine or threonine can be phosphorylated in this manner and result in the activation or inhibition of signalling pathways. MAP kinases are known to be phosphorylated in these residues, resulting in the modification of downstream signalling effects (Ardito et al., 2017).

MAP kinases are Ser/Thr protein kinases that are activated by stimuli such as stress and growth factors. The inflammatory status of the endothelium is known to be influenced by the balance of MAP kinase expression and activation (Hoefen and Berk, 2002). ERK1/2 MAP kinases are related protein-serine/threonine kinases that take part in the Ras-Raf-MEK-ERK signalling cascade. Their activation depends on the phosphorylation of residues at Tyr204/187 and then Thr202/185, and results in numerous cell processes including cell adhesion, migration, proliferation, and transcription (Roskoski, 2012). P38, classically involved in stress responses and inflammation, is activated by phosphorylation at Thr180 and Tyr182 (Tudor et al., 2009).

3.2 Aims

The aim of this initial part of the study was to investigate whether the chemokines CCL4, CXCL8 and CXCL10 activate ECs. Firstly, the expression of the chemokine receptors was explored in two types of human ECs; HUVEC and hCMEC/D3, primary peripheral macrovascular and immortalised brain microvascular cells respectively. Secondly, the phosphorylation of tyrosine, serine and threonine residues was investigated in response to chemokine treatments, to determine if the chemokines were able to induce signalling events within the ECs. Finally, concentration and time-dependent activation of MAP kinases in HUVEC and hCMEC/D3 was assessed, with different chemokines and MAP kinase activation. In particular, we focused on two MAPK, P-ERK 1/2 and P-P38. Further, the distribution of these phospho-proteins in the ECs was explored to determine if chemokine treatment induced an increase in nuclear P-ERK and P-P38.

3.3 Results

3.3.1 ECs expression of receptors for CCL4, CXCL8 and CXCL10

We initially set out to determine whether specific chemokine receptors for CCL4, CXCL8 and CXCL10 were expressed on two distinct macrovascular and microvascular EC types: HUVEC and hCMEC/D3, respectively.

The two cell lines hCMEC/D3 and HUVEC were chosen as they represent two well characterised vascular beds. HUVECs are primary human umbilical vein cells that retain many of the characteristics of ECs *in vivo* (Jimenez et al., 2013). The immortalised human brain EC line hCMEC/D3, has been successfully used as a BBB model for various diseases as it maintains many of the characteristics displayed by primary brain EC lines

(Tai et al., 2010, Freese et al., 2014, Page et al., 2016, Ma et al., 2017) resulting in its use in over 800 publications. HCMEC/D3 express adhesion proteins like ICAM-1 and VCAM-1, and functional chemokine and cytokine receptors such as TNFR1 and 2, IFNGR1, CXCR1-5 and CCR3-6 (Vu et al., 2009, Weksler et al., 2013).We investigated the classic receptors for the chemokines of interest, namely the receptors for CXCL8 (CXCR1 and CXCR2), CXCL10 (CXCR3) and CCL4 (CCR5). Following western blot analysis, we observed protein expression at the predicted molecular weights, which suggested that these receptors were expressed by HUVEC and hCMEC/D3 (**Figure 20**).

3.3.2 Phosphorylation of tyrosine, serine and threonine residues following chemokine treatments

Proteins expressed in eukaryotic cells carry thousands of sites which can be phosphorylated. These phosphorylation sites are involved in cellular function or activation (Cohen, 2002). For example, threonine residue phosphorylation has been shown to be implicated in cell signalling, activation and in various physiological functions of the cardiovascular system (Sugimoto et al., 2007, Ilan, 2000 #865, Dimmeler, 1999 #864). Furthermore, serine residues are also frequently phosphorylated as part of cell signalling processes in eukaryotes, and are involved in signalling transduction events (Manning et al., 2002). Equally, albeit less abundant (only around 0.1% of phosphorylated sites are tyrosine phosphorylated), tyrosine phosphorylation is a key event that initiates many signalling pathways (Hunter, 2000a). This reversible phosphorylation is known to control many cellular processes including cellular signalling, differentiation, and growth (Cohen, 2000). Growth factor binding to receptors, results to phosphorylation on tyrosine residues (Pasantes-Morales and Franco, 2002) (Ahn et al., 1992). In capillary ECs, tyrosine phosphorylation plays a role in proliferation and angiogenesis (Hayashi et al., 1997).

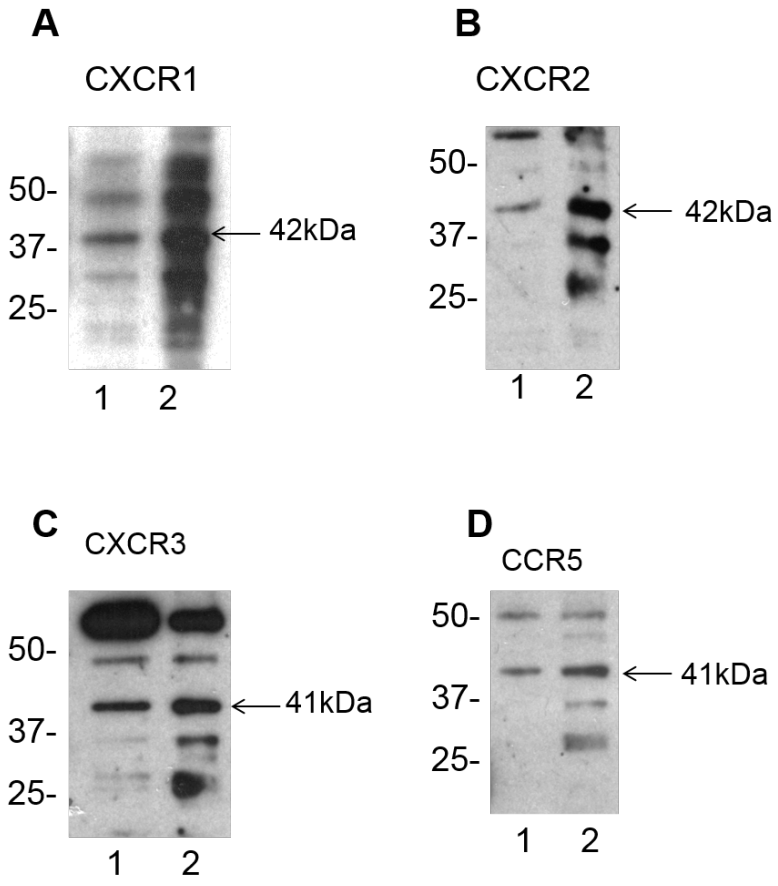

Figure 20 Chemokine receptor expression on HUVEC and hCMEC/D3. Both HUVEC (lane 1) and hCMEC/D3 (lane 2) express the chemokine receptors: A- CXCR1; B- CXCR2, C- CXCR3; D- CCR5. Shown on the left of each immunoblot is the relative molecular mass (in kDa) of marker proteins run in parallel. Arrows indicate the band that matches the predicted weight of the protein in question.

To investigate the ability of CCL4, CXCL8 and CXCL10 to induce intracellular responses in our ECs of choice, we investigated the phosphorylation of tyrosine, serine and threonine residues in lysates of chemokine treated EC. Additionally, an aim of this experiment was to ascertain that the cells responded to the chemokine concentrations chosen. HSC70, a housekeeping protein of 70 kDa, was used as an internal loading control for western blotting throughout (Daugaard et al., 2007).

Chemokine treatments result in phosphorylation of tyrosine residues

Phosphorylation of tyrosine residues was investigated followed treatment with CCL4, CXCL8 and CXCL10 in HUVEC and hCMEC/D3. In HUVEC there was a negligible effect on phosphorylation (**Figure 21**A-C). In hCMEC/D3 however, CXCL8, CXCL10 and CCL4 induced an evident phosphorylation of tyrosine residues at several molecular weights, mainly in the regions of 100-250 kDa (CXCL8), 25-37 and 150-250 kDa regions (CXCL10) and 25-37 and 50-75 kDa (CCL4) (**Figure 21**D-F). Overall, hCMEC/D3 showed a more obvious response in tyrosine residue phosphorylation than HUVEC.

Chemokine treatments result in phosphorylation of serine residues

The effect on phosphorylation of serine residues in chemokine treated HUVEC was modest, seen exclusively at the 38 kDa region in CXCL8 treated samples, and at the 37-50 and the 100-15 kDa in the immunoblot of CCL4 treated HUVEC (**Figure 22**A-C). CXCL8, CXCL10 and CCL4 induced an evident phosphorylation of serine residues at different molecular weights in hCMEC/D3 (**Figure 22**D-F), mainly in the region of 100-150 kDa and 150-250 kDa at the 10, 30 and 60 min timepoints. In accordance with the previous results in tyrosine phosphorylation, hCMEC/D3 presented a more evident response in serine phosphorylation than HUVEC.

Chemokine treatments result in phosphorylation of threonine residues

Chemokine treatments of HUVEC resulted in modest levels of phosphorylation of threonine residues. The region of 37-50 kDa shows some evidence of phosphorylation, in the CXCL8 and CCL4 treated immunoblots (**Figure 23**A-C). In hCMEC/D3, chemokines induced the phosphorylation of threonine residues mostly at the 25-37 and 100-250 kDa in CXCL8 and CCL4 treated samples (**Figure 23**D-F). In agreement with tyrosine and serine phosphorylation, hCMEC/D3 showed more threonine phosphorylation when compared to HUVEC.

These data demonstrate that chemokines are able to elicit signalling events in both HUVEC and hCMEC/D3 cells and that former are less responsive than the latter. Despite the potential clues that these phosphorylation events can offer regarding the response of EC to chemokine treatment, it would be purely speculative to attempt to identify which proteins would have been phosphorylated at the specific sites seen in the immunoblots. Further investigation of specific signalling proteins was necessary.

Overall, the response of HUVECs to chemokine treatments was not as evident as the response of hCMEC/D3. It appeared that the receptor expression was higher in hCMEC/D3 than in HUVEC and therefore the increased level in phosphorylation might correlate with this. These concentrations of chemokines and time-points tested were used as a good starting point and were taken forward to the following experiment.

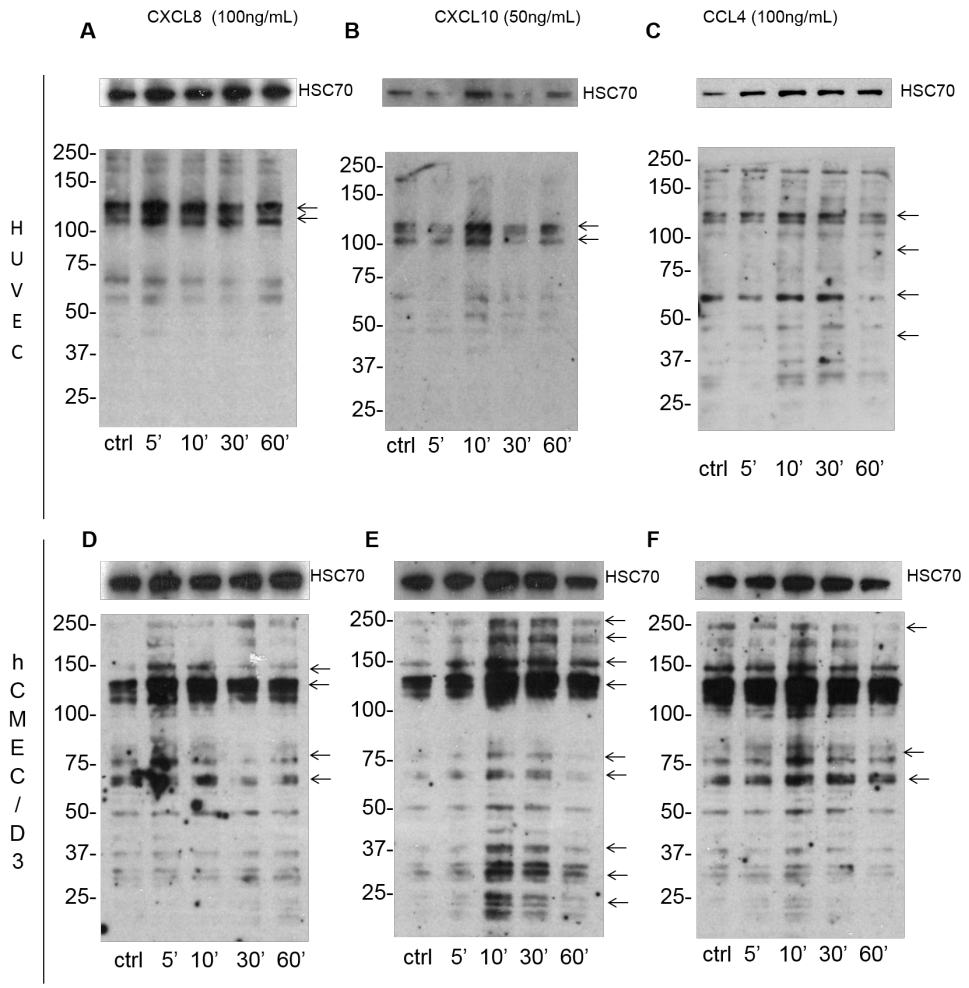

G

	HUVEC		
Ratio (P-Tyr/HSC70)	CXCL8	CXCL10	CCL4
Control	1.08	1.40	0.72
5	0.98	1.28	0.91
10	0.95	1.66	0.97
30	1.51	1.84	0.82
60	1.30	1.46	0.81
Region of the blot	120kDa	110kDa	120kDa

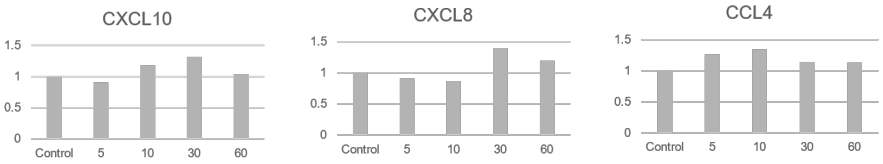

H

	hCMEC/D3		
Ratio (P-Tyr/HSC70)	CXCL8	CXCL10	CCL4
Control	0.64	0.71	0.41
5	0.93	0.86	0.47
10	0.92	0.95	0.61
30	0.72	0.97	0.61
60	0.72	1.26	0.76
Region of the blot	120kDa	150kDa	60kDa

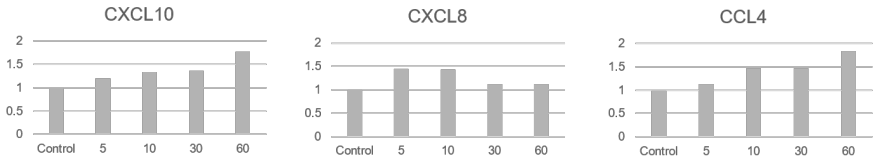

Figure 21 Expression of phosphorylated tyrosine residues on HUVEC (A-C) and hCMEC/D3 (D-F) in response to chemokines for 5, 10, 30 and 60 min. (A and D) CXCL8 (100 ng/mL), (B and E) CXCL10 (50 ng/mL) and (C and F) CCL4 (100 ng/mL). HSC70 used as an internal loading control for each immunoblot. Arrows indicate potential hyper phosphorylation of tyrosine residues. G and H – Ratios of P-tyr/HSC70 of selected bands.

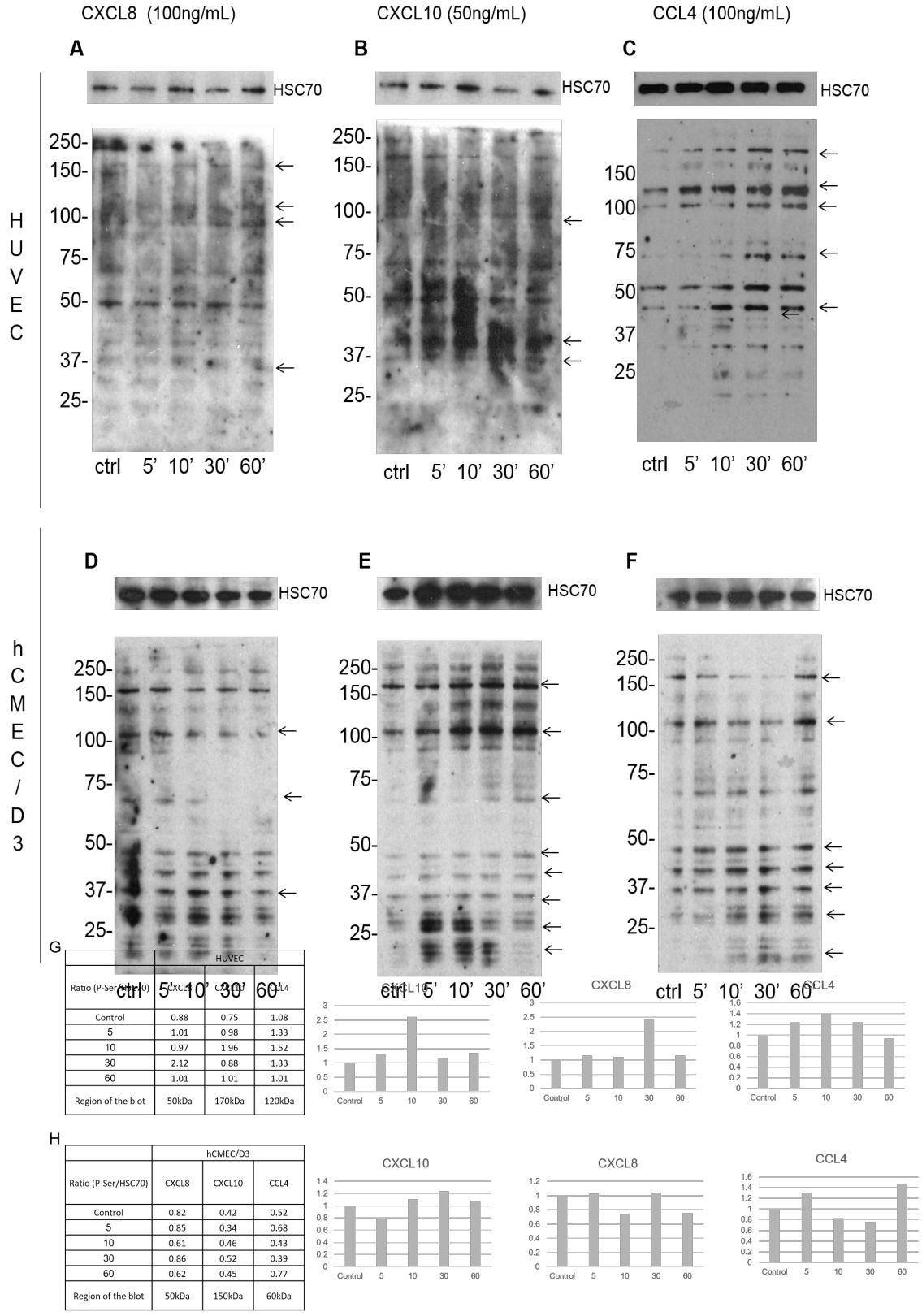

Figure 22 Expression of phosphorylated serine residues on HUVEC (A-C) and hCMEC/D3 (D-F) in response to chemokines for 5, 10, 30 and 60 min. (A and D) CXCL8 (100 ng/mL), (B and E) CXCL10 (50 ng/mL) and (C and F) CCL4 (100 ng/mL). HSC70 used as an internal loading control for each immunoblot. Arrows indicate potential hyper phosphorylation of serine residues. G and H – Ratios of P-tyr/HSC70 of selected bands.

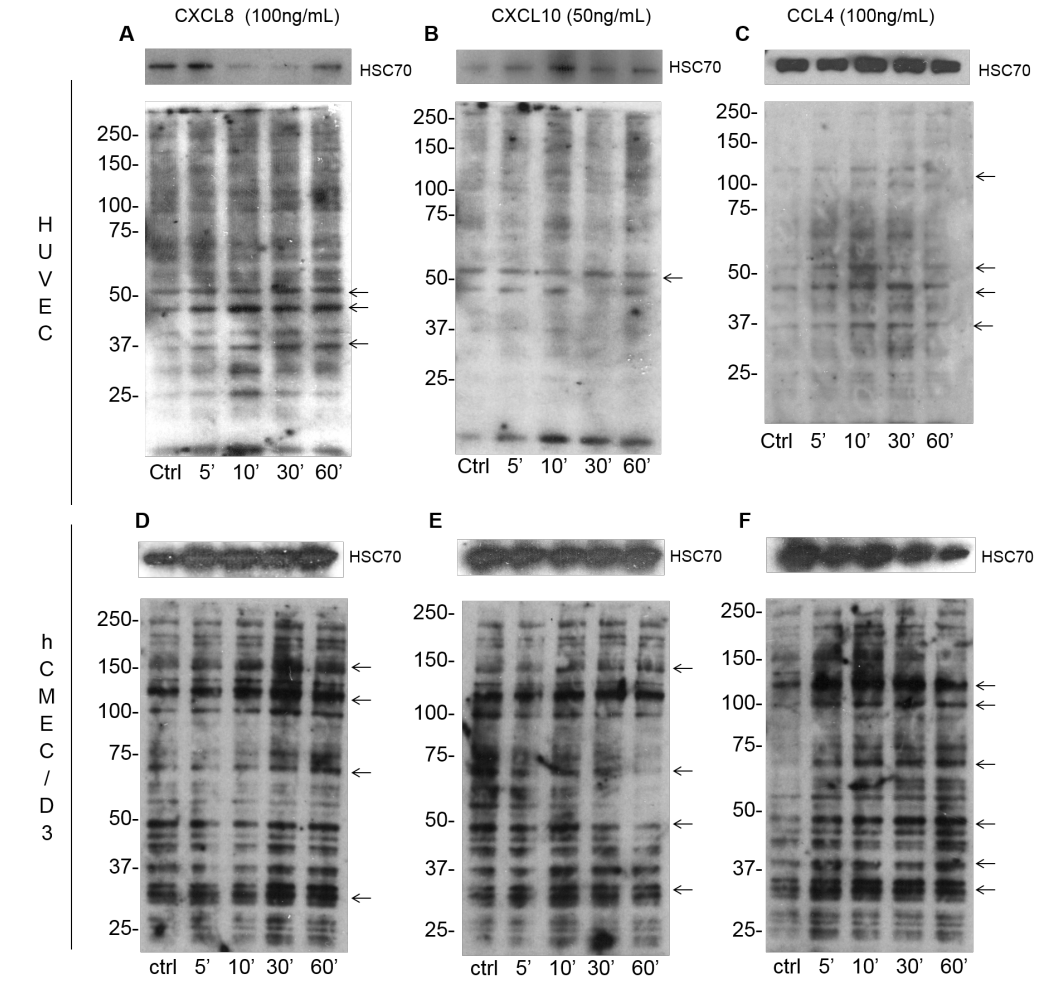

G

	HUVEC		
Ratio (P-Thr/HSC70)	CXCL8	CXCL10	CCL4
Control	1.22	0.69	0.30
5	0.90	1.85	0.83
10	1.25	2.18	0.75
30	1.02	1.42	0.46
60	1.31	1.41	0.45
Region of the blot	47kDa	55kDa	43kDa

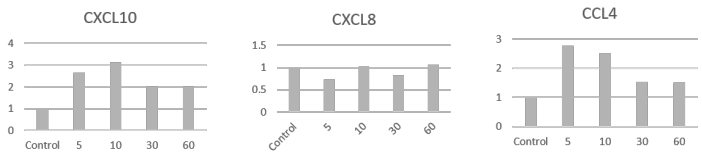

H

	hCMEC/D3		
Ratio (P-Thr/HSC70)	CXCL8	CXCL10	CCL4
Control	0.89	0.73	0.32
5	0.65	0.65	0.87
10	0.73	1.15	0.67
30	0.70	0.56	1.01
60	0.74	0.25	1.25
Region of the blot	47kDa	47kDa	60kDa

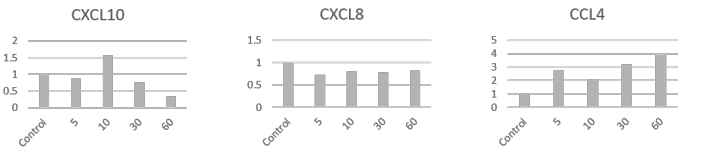

Figure 23 Expression of phosphorylated threonine residues on HUVEC (A-C) and hCMEC/D3 (D-F) in response to chemokines for 5, 10, 30 and 60 min. (A and D) CXCL8 (100 ng/mL), (B and E) CXCL10 (50 ng/mL) and (C and F) CCL4 (100 ng/mL). HSC70 used as an internal loading control for each immunoblot. Arrows indicate potential hyper phosphorylation of threonine residues. G and H – Ratios of P-thr/HSC70 of selected bands.

3.3.3 MAPK activation in EC

We have shown previously that our chemokines of interest induce phosphorylation of threonine and tyrosine residues in hCMEC/D3. Having established that the chemokines CCL4, CXCL8 and CXCL10 are capable of initiating signalling events in ECs, we next investigated whether they could activate MAPK, whereby we tested the phosphorylation of two main kinases, ERK and P38. ERK and P38 can phosphorylate and activate downstream proteins, amplifying signalling pathways (Roux and Blenis, 2004).

ERK 1/2, the most widely studied ERK MAPK, has been associated with numerous proteins and signalling outcomes, including their contribution in inflammation (Broom et al., 2009). The expression of P38 is also of interest since it is known to be upregulated in response to stress and inflammatory stimuli. There is increasing evidence that the protein acts as an important mediator in liver, kidney, lung and brain inflammation (Cuenda and Rousseau, 2007, Yang et al., 2014).

Activation of the MAP kinases ERK1/2 and P38 was determined in confluent HUVEC and hCMEC/D3 which were made quiescent by overnight serum-starvation. We have determined that the concentrations of CXCL8 and CXCL10 used in the phosphorylation experiments yield good results and therefore that concentration was used. A lower concentration for each chemokine was also tested, to determine if an effect was also obtained at a more physiological concentration. CCL4, was used at a concentration previously assessed by a previous researcher in our lab, to result in a maximum response in hCMEC/D3 (results not shown). Lysates generated were analysed for MAP kinase activation by immunoblotting using specific anti-phospho antibodies against ERK1/2 and P38.

ERK1/2 and P38 phosphorylation following CCL4 treatment

Treatment of hCMEC/D3 with CCL4 induced a significant phosphorylation of ERK 1/2 at 5 and 10 min following treatment (**Figure 24**-1). At the subsequent timepoints there was a time-dependent decrease in the levels of phospho ERK 1/2 and at 60 min post treatment the level of the phospho protein was near control levels. We also observed in hCMEC/D3, a time-dependent increase in the levels of phospho P38 but with a different temporal profile, reaching a nearly 3-fold average increase by 60 min, although variability between replicates deemed the phosphorylation of P38 following CCL4 treatments non-significant (**Figure 24**-3).

In HUVEC, CCL4 failed to induce significant phosphorylation of ERK 1/2 (**Figure 24**-2). The levels of phospho-P38 following treatment were not significantly altered remaining near control levels throughout the time course tested (**Figure 24**-4).

It must be noted that the antibody used to detect P-ERK produced two clear bands at 43 and 44kDa as expected allowing more precise quantification than the antibody used to detect P-P38. In the cases where P-P38 was detected, there was a technical need to expose the film for longer, resulting in overexposed housekeeping signal (HSC70). The concentration used for CCL4 (100ng/mL) was pre-determined in our lab by another researcher as the optimal concentration for hCMEC/D3 response. According to the manufacturer's guidelines, the recombinant peptide has a biological activity range of 5.0-20.0 ng/mL and using it at a 5x higher concentration, the effects seen might be overestimated when compared to physiological effects of the chemokine.

ERK1/2 and P38 phosphorylation following CXCL8 treatment

Treatment of hCMEC/D3 with 100 ng/mL of CXCL8 resulted in strong phosphorylation of ERK 1/2 at 5 min post treatment (**Figure 25**-1). Thereafter there was a decrease in

phosphorylation levels, with phosphorylation back to control levels at 60 min. CXCL8 also induced P38 phosphorylation to significant levels at the higher concentration at the 10 and 30 min timepoint (**Figure 25**-3).

Unlike hCMEC/D3, the effect of CXCL8 in HUVEC resulted in a slight but insignificant increase in the phosphorylation of ERK 1/2 and P38. Whilst not significant, the mean phosphorylation of P38 at the highest concentration tested, 100 ng/mL, was consistently raised throughout the time course (**Figure 25**-2 and 4).

ERK1/2 and P38 phosphorylation following CXCL10 treatment

Whilst there was a modest increase in phospho ERK 1/2 following 50 ng/mL treatment at 5 min (**Figure 26**-3), CXCL10 treatments of hCMEC/D3 did not induce significant phosphorylation of ERK 1/2 or P38 at any of the concentrations or timepoints studied (**Figure 26**-1 and 3).

Similarly, treatments of HUVEC with CXCL10 did not result in a significant increase in the levels of ERK phosphorylation (**Figure 26**-2 and 4). CXCL10 at 50 ng/mL resulted in significant P38 phosphorylation at 60 min in HUVEC but not at any other timepoints in that time course (**Figure 26**-4).

Up until this point, the results obtained with hCMEC/D3 were more robust than the results seen with HUVEC. Since hCMEC/D3 represent an accessible alternative to using primary cells, and due to their microvascular brain endothelial origin, this cell line was selected from this point on as the sole model of investigation to be used throughout the project. An expanded analysis of the differences between HUVEC and hCMEC/D3 can be found in the discussion section of this chapter.

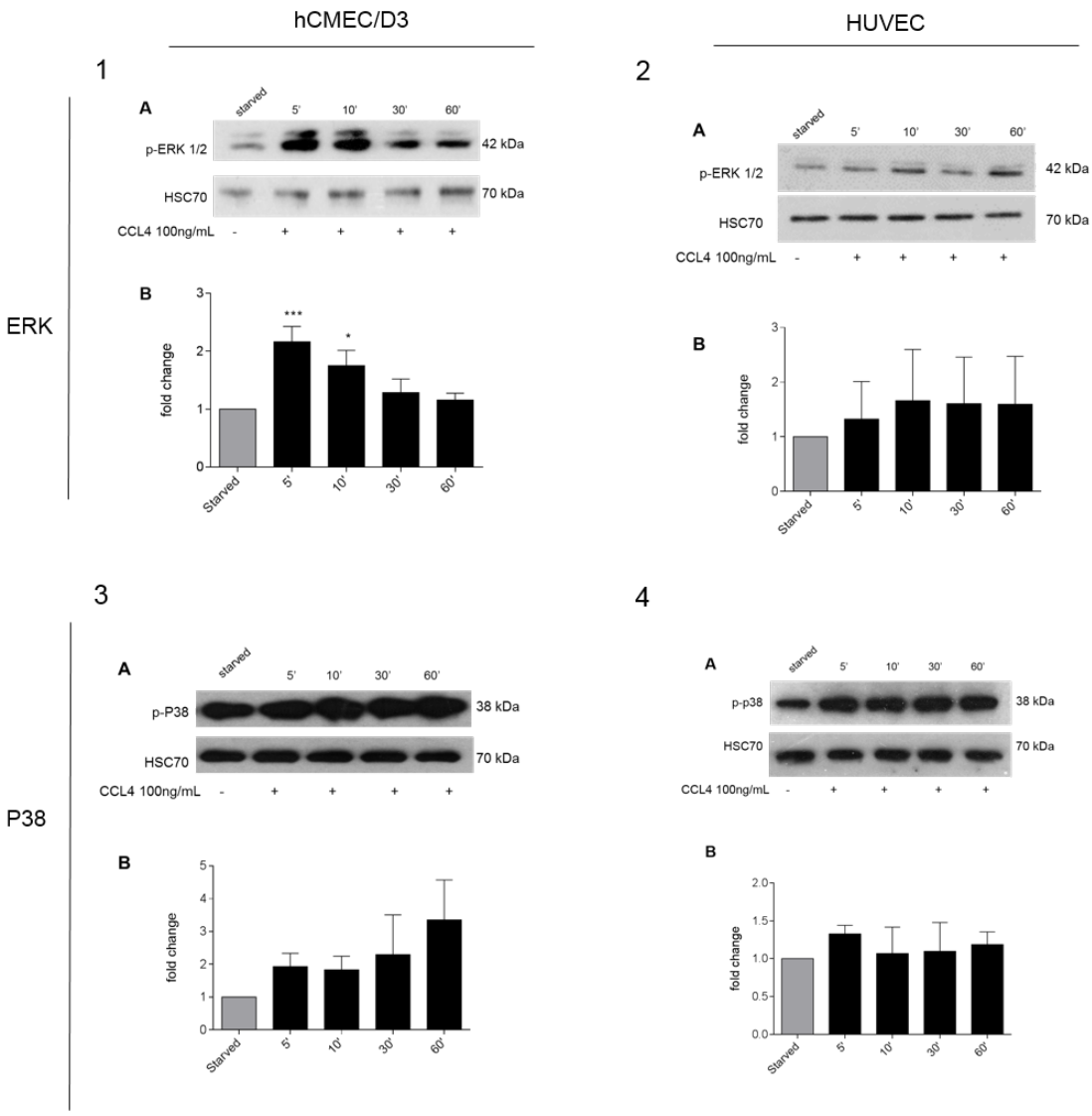

Figure 24 CCL4 treatment of hCMEC/D3 and HUVEC (A) HUVEC and hCMEC/D3 were grown to confluency, serum-starved and treated with CCL4 at 100 ng/mL for 5, 10, 30 and 60 minutes. Lysates were prepared and phosphorylation of ERK and P38 were analysed by immunoblots as described in Material and Methods. (B) Densitometric quantifications were derived from at least 3 independent analyses, where the phospho-protein was normalized to the housekeeping protein. HSC70 was used as an internal loading control. Results are expressed as average means +/- SEM. Statistical analysis was performed using a One-way ANOVA and a Dunnet post hoc test for statistical analysis of mean value variances. *, P<0.05; ***, P≤0.001.

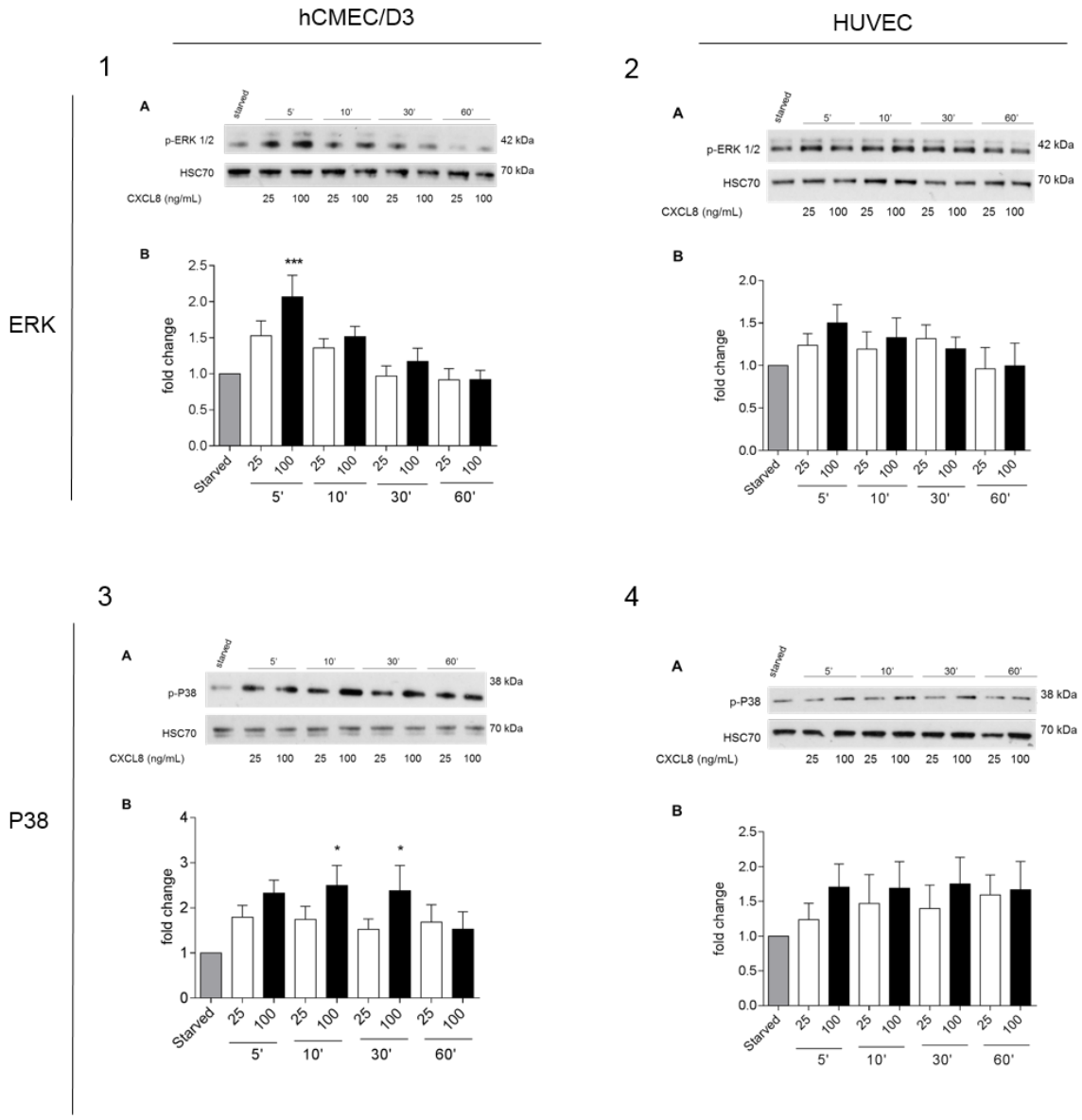

Figure 25 CXCL8 treatment of hCMEC/D3 and HUVEC. (A) HUVEC and hCMEC/D3 were grown to confluency, serum-starved and treated with CXCL8 at 25 and 100 ng/mL for 5, 10, 30 and 60 minutes. Lysates were prepared and phosphorylation of ERK and P38 were analysed by immunoblots as described in Material and Methods. (B) Densitometric quantifications were derived from at least 3 independent analyses, where the phospho-protein was normalized to the housekeeping protein. HSC70 was used as an internal loading control. Results are expressed as average means +/- SEM. Statistical analysis was performed using a One-way ANOVA and a Dunnet post hoc test for statistical analysis of mean value variances. *, P<0.05; ***, P≤0.001

ERK1/2 and P38 phosphorylation following chemokine treatments for 1 and 3 min

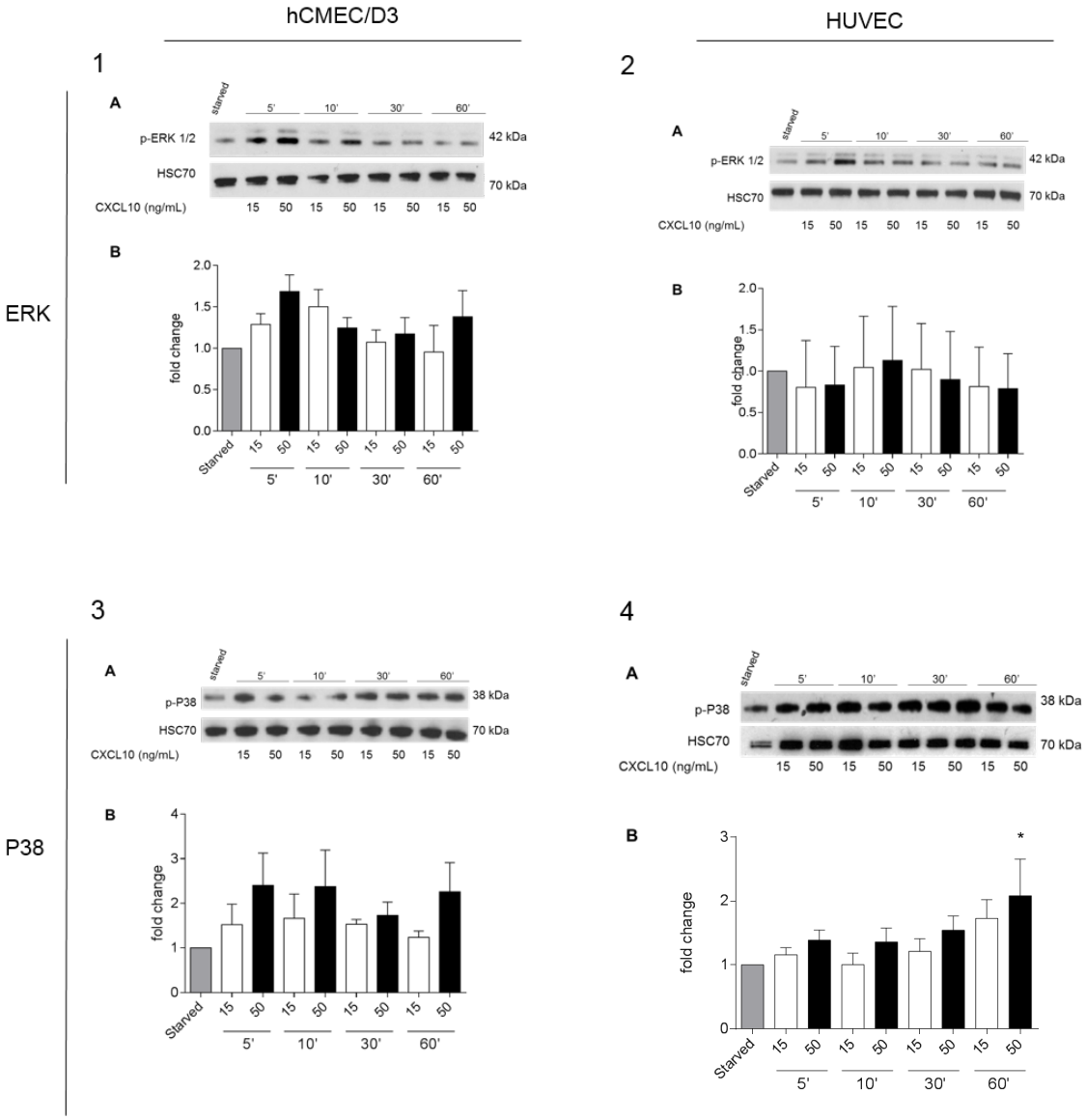

Figure 26 CXCL10 treatment of hCMEC/D3 and HUVEC (A) HUVEC and hCMEC/D3 were grown to confluency, serum-starved and treated with CXCL10 at 15 and 50 ng/mL for 5, 10, 30 and 60 minutes. Lysates were prepared and phosphorylation of ERK and P38 were analysed by immunoblots as described in Material and Methods. (B) Densitometric quantifications were derived from at least 3 independent analyses, where the phospho-protein was normalized to the housekeeping protein. HSC70 was used as an internal loading control. Results are expressed as average means +/- SEM. Statistical analysis was performed using a One-way ANOVA and a Dunnet post hoc test for statistical analysis of mean value variances. *, P<0.05

Overall, hCMEC/D3 showed a more consistent response to chemokine treatment than HUVEC, where statistical significance was rarely achieved. This confirmed that HUVEC did not respond to the chemokines tested, as the phosphoblots suggested.

Since we observed a generalised increase in the phosphorylation levels of ERK 1/2 and P38 following treatments at the 5 min timepoint in hCMEC/D3, we next investigated earlier timepoints to establish how rapidly the activation occurred. Cells were chemokine-treated for 1 and 3 min, prior to cell lysis, SDS-PAGE and Western blot.

Phosphorylation of ERK 1/2 and P38 was significantly increased following CXCL8 and CCL4 treatments at 100 ng/mL in hCMEC/D3 at certain timepoints (**Figure 25**). These effects were particularly obvious for P-ERK at 5 min post CXCL8 and CCL4 treatments, and so earlier timepoints were investigated.

Both CCL4 and CXCL8 treatment induced a strong phosphorylation of ERK 1/2 by 3 min post treatment (**Figure 27**-2A, 2C). In contrast, CXCL10 did not induce a statistically significant increase in P-ERK at these early timepoints (**Figure 27**-2E).

For P38, none of the chemokines tested caused a significant change in the phosphorylation levels of the protein (**Figure 27**-B, D and F).

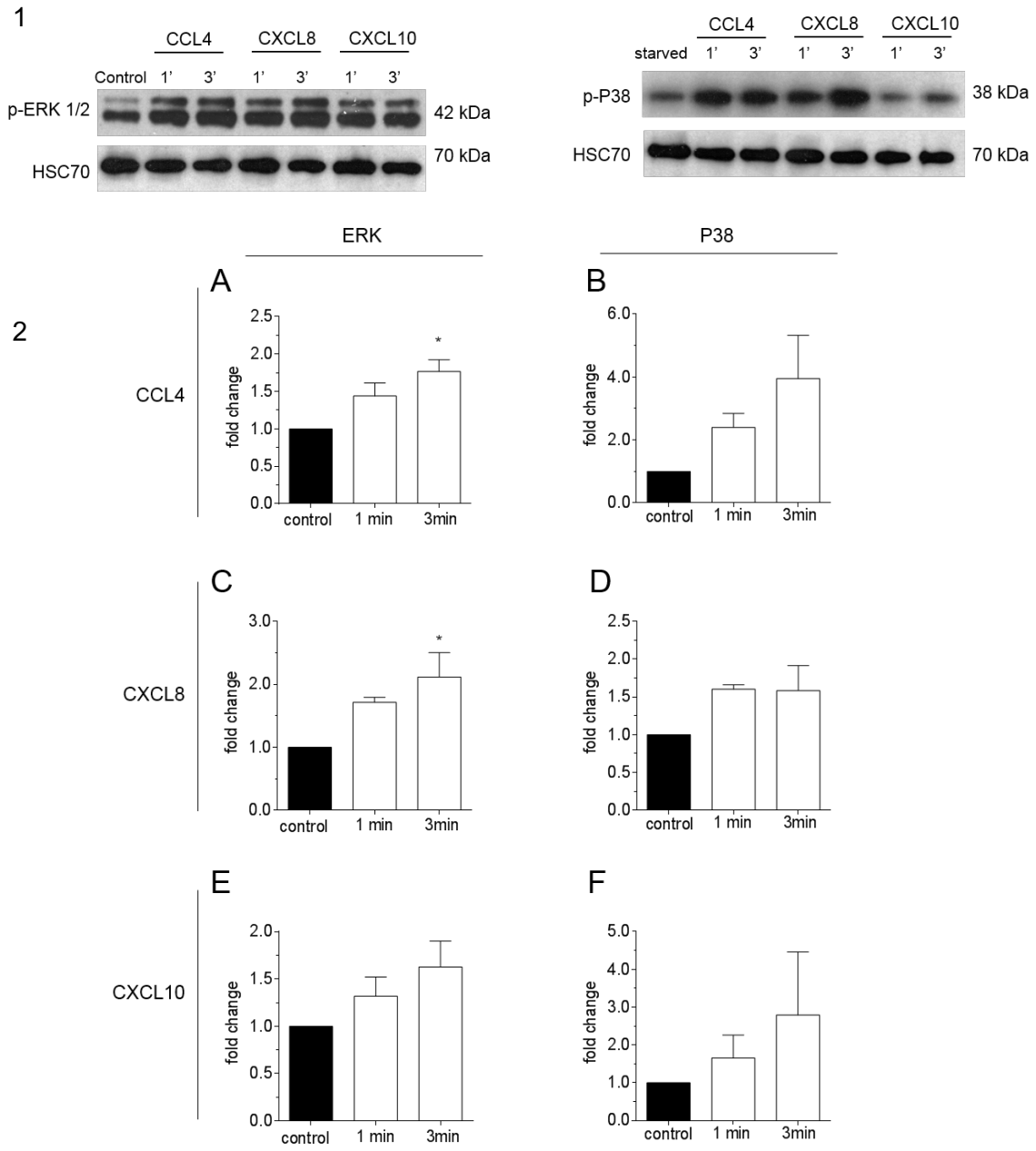

Figure 27 CCL4, CXCL8 and CXCL10 treatment of hCMEC/D3 for 1 and 3 min. 1- hCMEC/D3 were grown to confluency, serum-starved and treated with either CCL4 at 100 ng/mL, CXCL8 at 100 ng/mL or CXCL10 at 50 ng/mL for 1 and 3 min. Lysates were prepared and phosphorylation of ERK and P38 were analysed by immunoblots as described in Material and Methods. HSC70 was used as an internal loading control. 2- Densitometric quantifications were derived from at least 3 independent analyses, where the phospho-protein was normalized to the housekeeping protein. Statistical analysis was performed using a One-way ANOVA and a Dunnet post-test for statistical analysis of mean value variances. *, $P<0.05$

3.3.4 Distribution of phosphorylated ERK and P38 in hCMEC/D3 following chemokine treatments

Once we established that ERK, and possibly P38, were activated in response to chemokines, we investigated the subcellular localization of these phospho-proteins.

Distribution of phosphorylated ERK and P38 following CCL4 treatment

Treatment of hCMEC/D3 with CCL4 resulted in changes in the distribution pattern of P-ERK in the cell. In control samples low levels of P-ERK were detectable exhibiting a punctate appearance throughout the cell. Following treatment with CCL4, there was a visible increase in the P-ERK signal that appeared to cluster preferentially in the nuclear region but also in the perinuclear region. Some cytoplasmic staining could be seen at 30 and 60 min post treatment (**Figure 28**-A). Quantification of pixel intensity within the nuclear region confirmed the increase with changes in signal intensity becoming significant at 30 min post treatment where there is a 2.3 fold increase in nuclear P-ERK (**Figure 28**-B). When comparing the ratio of staining in the nuclear and cytosolic compartment, a significant increase in nuclear staining was also observed at 30 min, suggesting that the increase in phospho-protein was due to its nuclear localization (**Figure 28**-C). Phospho P38 distribution also changed in response to CCL4 treatments, with strong signal at 5 and 10min post treatment. Interestingly, the pattern of signalling at 30 min was distinct from previous timepoints, with low P-P38 signal through the cells (**Figure 29**-A). In addition to an apparent increase in overall intensity the pattern of staining of the nuclear P-P38 fraction also increased 5 min post treatment (1.7 fold increase) but not at the subsequent timepoints (**Figure 29**-B). When analysing the increase in P-P38 in the nuclear and cytosolic compartments, a significant nuclear increase could be observed, indicating a rapid significant increase of the phospho protein at 5min post CCL4 treatment (**Figure 29**-C).

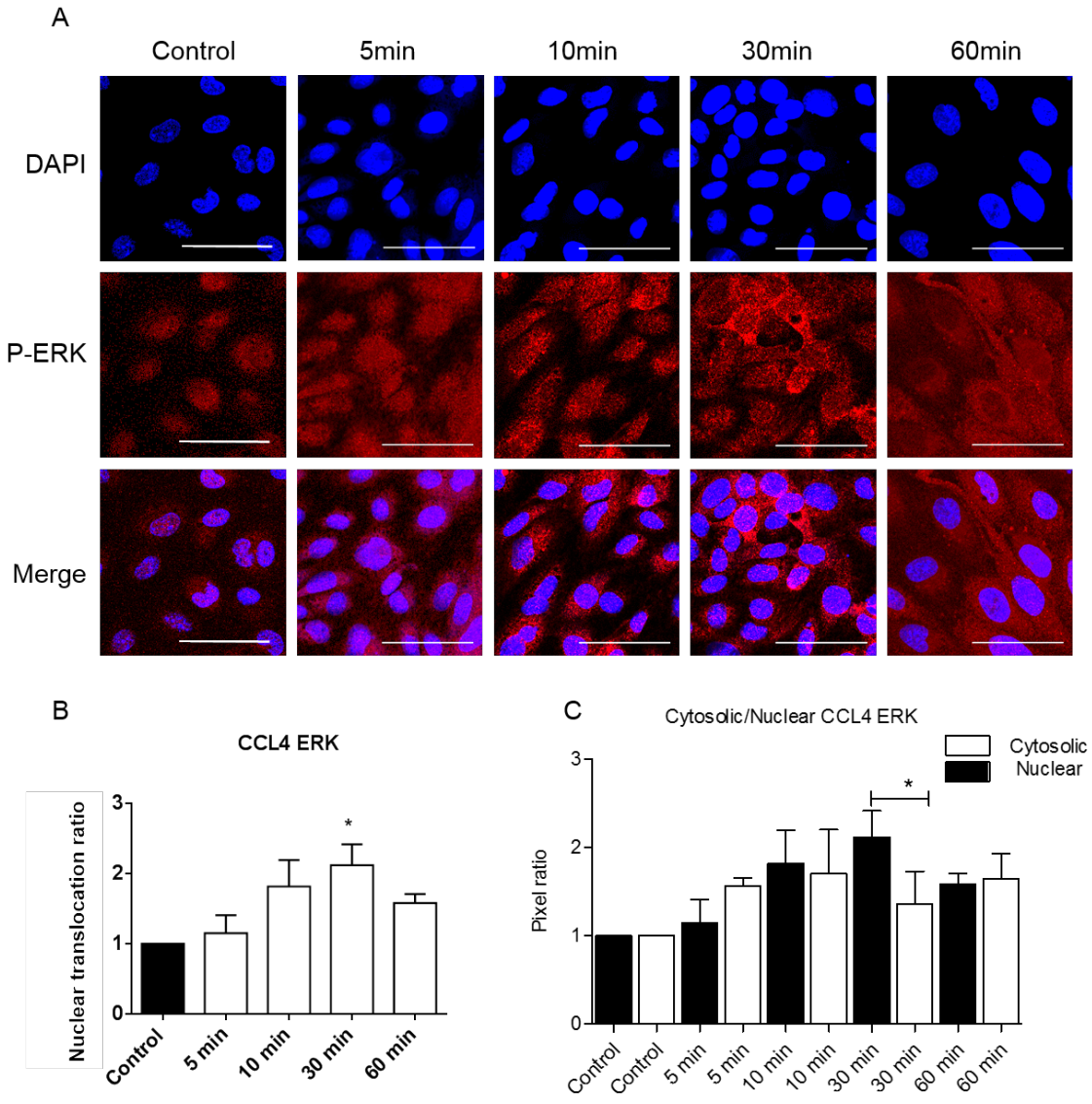

Figure 28 Distribution of p-ERK in hCMEC/D3 following CCL4 (100 ng/mL) treatment. (A) Confocal microscopy images (B) analysis of nuclear distribution of P-ERK following treatments for n=3 independent experiment. Images were taken on Zeiss LSM700. Scale bar 50µm. Images processed using Image J for mean pixel intensity of P-ERK co-localizing with nucleus. (C) Cytosolic/nuclear phospho-protein quantification, normalised to control. Results are expressed as average means +/- SEM. Statistical analysis was performed using a One-way ANOVA and a Dunnet post hoc test for statistical analysis of mean value variances. *, $P < 0.05$.

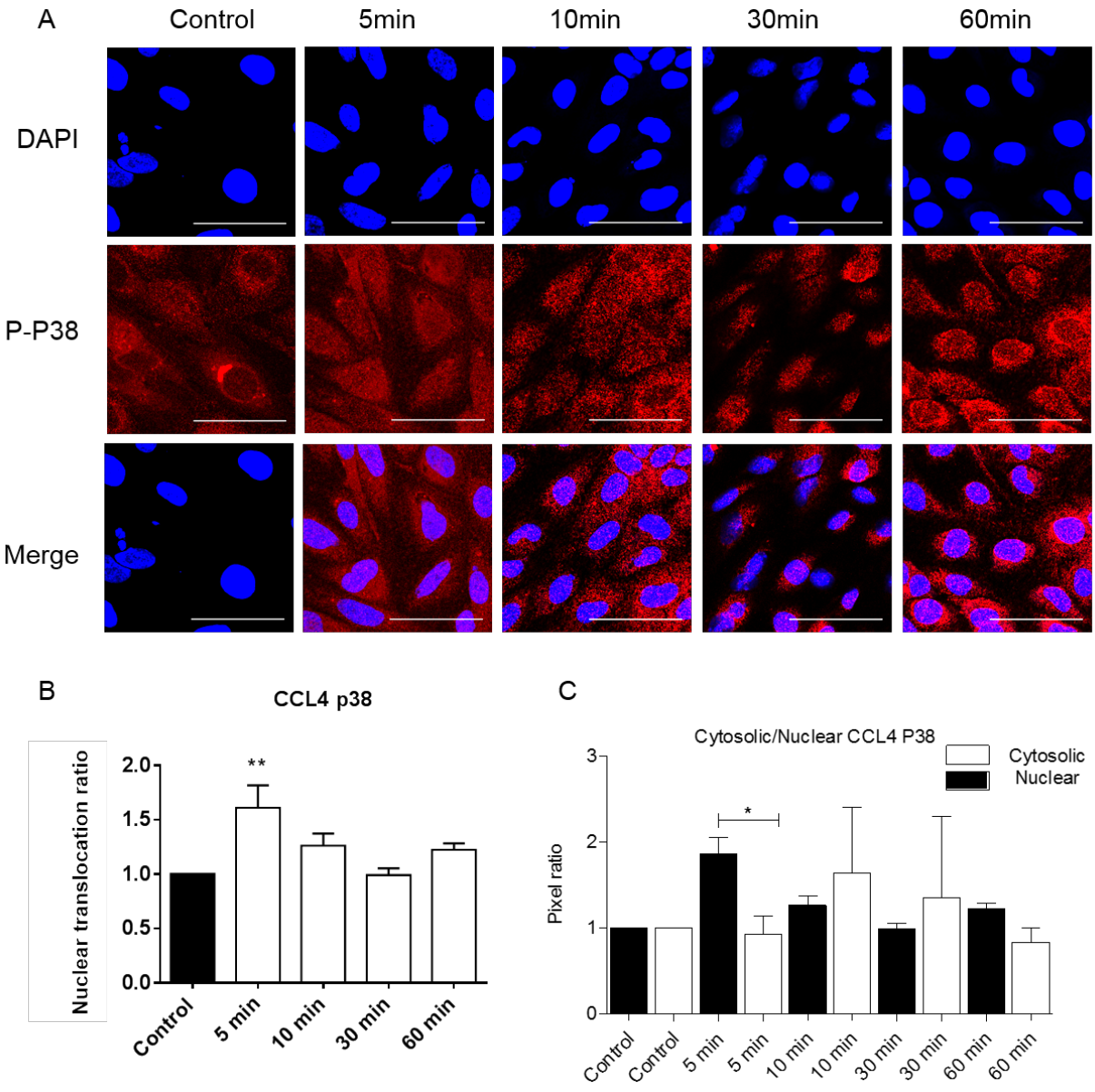

Figure 29 Distribution of P-P38 in hCMEC/D3 following CCL4 treatment (100ng/mL). (A) Confocal microscopy images (B) analysis of nuclear distribution of P-ERK following treatments for n=3 independent experiment. Images were taken on Zeiss LSM700. Scale bar 50µm. Images processed using Image J for mean pixel intensity of P-ERK co-localizing with nucleus. (C) Cytosolic/nuclear phospho-protein quantification, normalised to control. Results are expressed as average means +/- SEM. Statistical analysis was performed using a One-way ANOVA and a Dunnet post hoc test for statistical analysis of mean value variances. *, $P < 0.05$; **, $P < 0.01$.

Distribution of phosphorylated ERK and P38 following CXCL8 treatments

In control cells, the expression of P-ERK 1/2 was generally low with occasional cells expressing variable amounts of the protein. Following CXCL8 treatment, no visible change in the staining pattern of P-ERK was observed (**Figure 30**-A) and when the nuclear portion was quantitated the distribution of the phospho-protein in the nucleus was not significantly different from control levels (**Figure 30**-B). Despite a trend of increase of P-ERK 1/2 in the cytosolic compartment, the results found when comparing cytosol/nucleus were not significant (**Figure 30-C).**

Phospho P38 expression in the nucleus is comparable with the pattern seen in the previous figure. The staining pattern of P-P38 was clustered in the nucleus and perinuclear region in control and 5 min treatment samples. At the following timepoints staining included the nuclear, perinuclear and cytoplasmic areas (**Figure 31**-A). There was no visible change in the nuclear distribution of P-P38 post CXCL8 treatment, and there were no significant differences at any of the timepoints tested (**Figure 31**-B). Equally, upon analysis of the distribution of the protein within the cells, there was no evidence of an increase either in the nucleus or the cytosol (**Figure 31**-C).

Distribution of phosphorylated ERK and P38 following CXCL10 treatments

In control cells there was a low expression of P-ERK that remained at control levels post CXCL10 treatment. Upon treatment, P-ERK seemed to concentrate in the nuclear area and perinuclear area, with very low signal at 30 and 60 min post treatment (**Figure 32**-A). The levels of nuclear P-ERK were nearly undetectable, with some cells showing a visible staining pattern at 5 and 10 min post treatment. Upon statistical analysis, any changes in nuclear signal were found to be not significant (**Figure 32**-B). Upon analysis of the ratio of distribution of P-ERK in the nuclear and the cytosolic compartments, there

was a significant increase in the phospho-protein in the cytosol 60 min post treatment (**Figure 32-C)**.

The staining pattern for P-P38 was comparable in control and all timepoints tested, with nuclear and cytoplasmic staining across timepoints. Phospho P38 nuclear distribution in CXCL10 treated hCMEC/D3 was not statistically different from control (**Figure 33**-A). Despite an apparent decrease at 5 and 10 min followed by a recovery in the signal pattern, upon statistical analysis, these results were not significant (**Figure 33**-B). Despite a trend of increase in cytosolic P-P38 following CXCL10 treatment at 10, 30 and 60 min timepoints, upon analysis this was not significant (**Figure 33-C**).

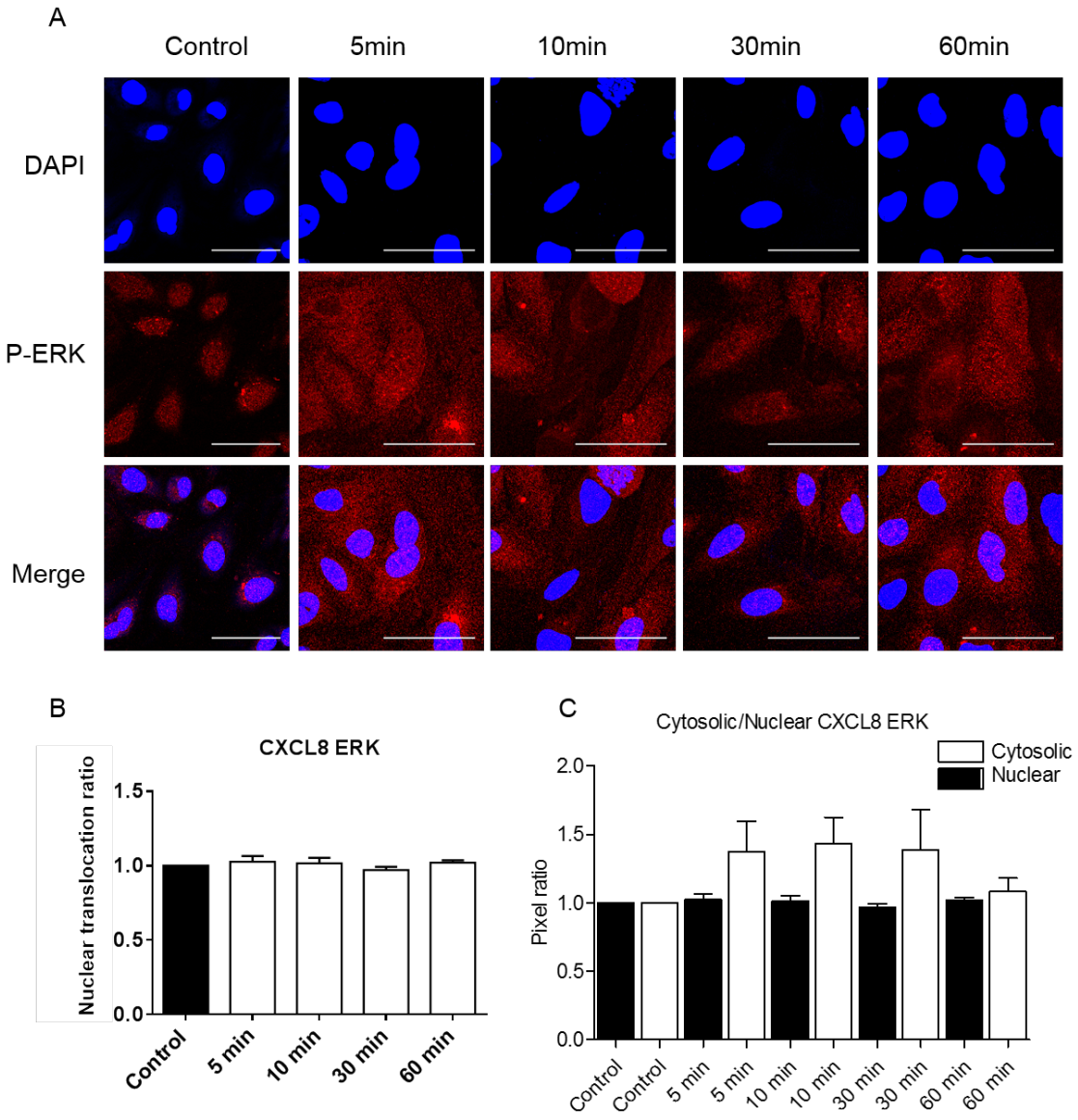

Figure 30 Distribution of p-ERK in hCMEC/D3 following CXCL8 (100ng/mL) treatment. (A) Confocal microscopy images (B) analysis of nuclear distribution of P-ERK following treatments for n=3 independent experiment. Images were taken on Zeiss LSM700. Scale bar 50µm. Images processed using Image J for mean pixel intensity of P-ERK co-localizing with nucleus. (C) Cytosolic/nuclear phospho-protein quantification, normalised to control. Results are expressed as average means +/- SEM. Statistical analysis was performed using a One-way ANOVA and a Dunnet post hoc test for statistical analysis of mean value variances. Data not significant.

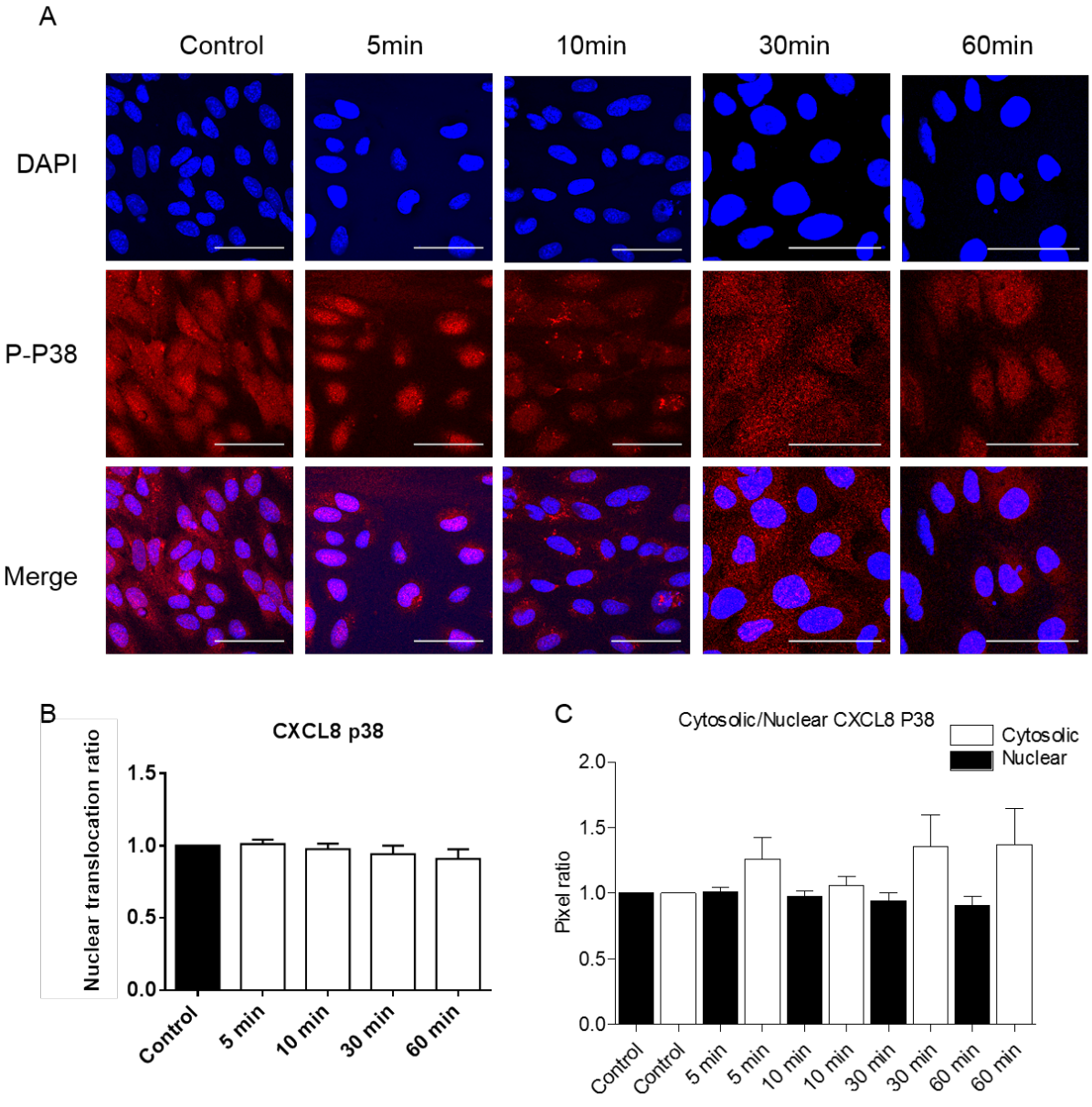

Figure 31 Distribution of P-P38 in hCMEC/D3 following CXCL8 (100ng/mL) treatment. (A) Confocal microscopy images (B) analysis of nuclear distribution of P-ERK following treatments for n=3 independent experiment. Images were taken on Zeiss LSM700. Scale bar 50µm. Images processed using Image J for mean pixel intensity of P-ERK co-localizing with nucleus. (C) Cytosolic/nuclear phospho-protein quantification, normalised to control. Results are expressed as average means +/- SEM. Statistical analysis was performed using a One-way ANOVA and a Dunnet post hoc test for statistical analysis of mean value variances. Data not significant.

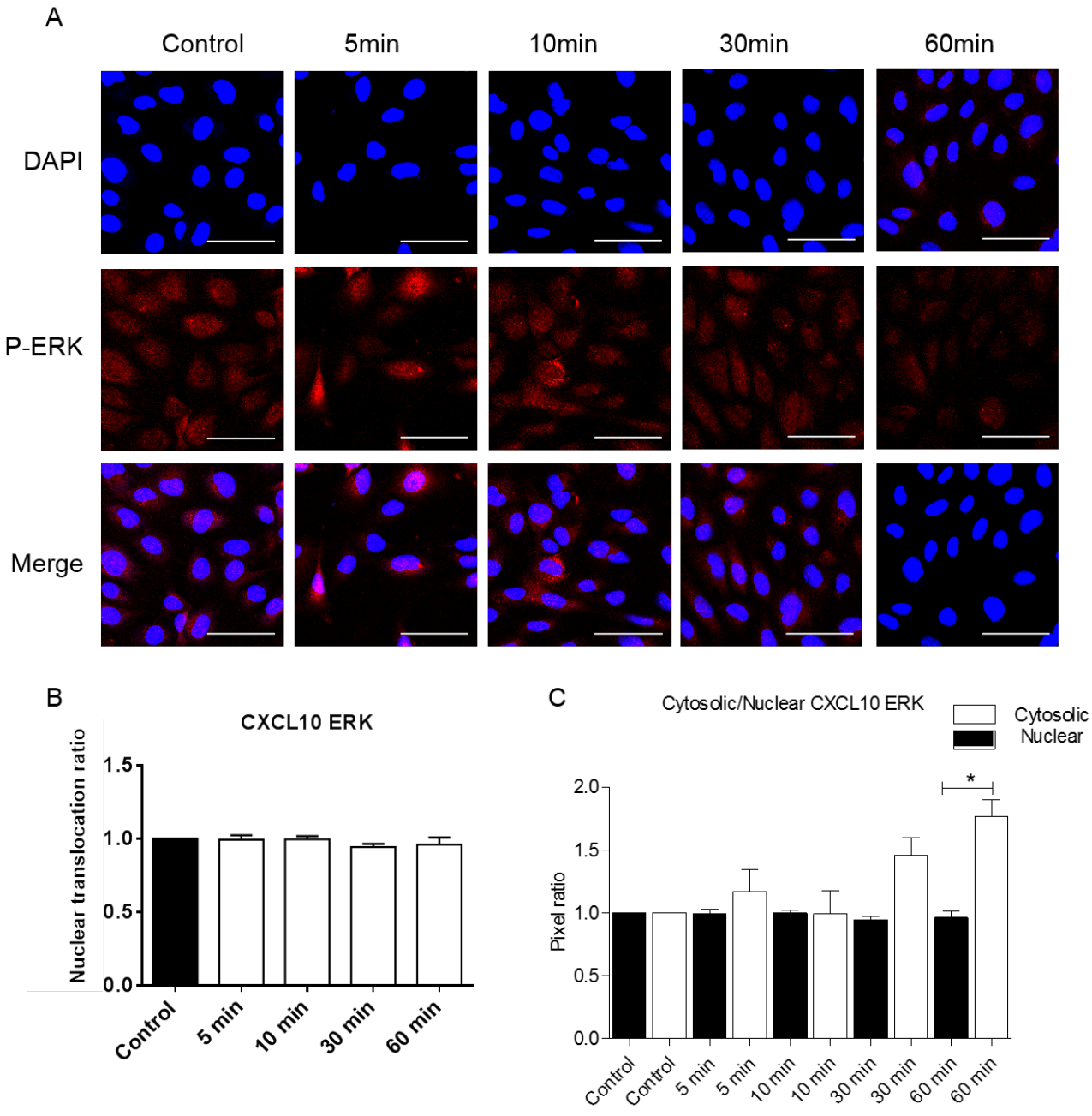

Figure 32 Distribution of p-ERK in hCMEC/D3 following CXCL10 (50ng/mL) treatment. (A) Confocal microscopy images (B) analysis of nuclear distribution of P-ERK following treatments for n=3 independent experiment. Images were taken on Zeiss LSM700. Scale bar 50µm. Images processed using Image J for mean pixel intensity of P-ERK co-localizing with nucleus. (C) Cytosolic/nuclear phospho-protein quantification, normalised to control. Results are expressed as average means +/- SEM. Statistical analysis was performed using a One-way ANOVA and a Dunnet post hoc test for statistical analysis of mean value variances. *, $P < 0.05$

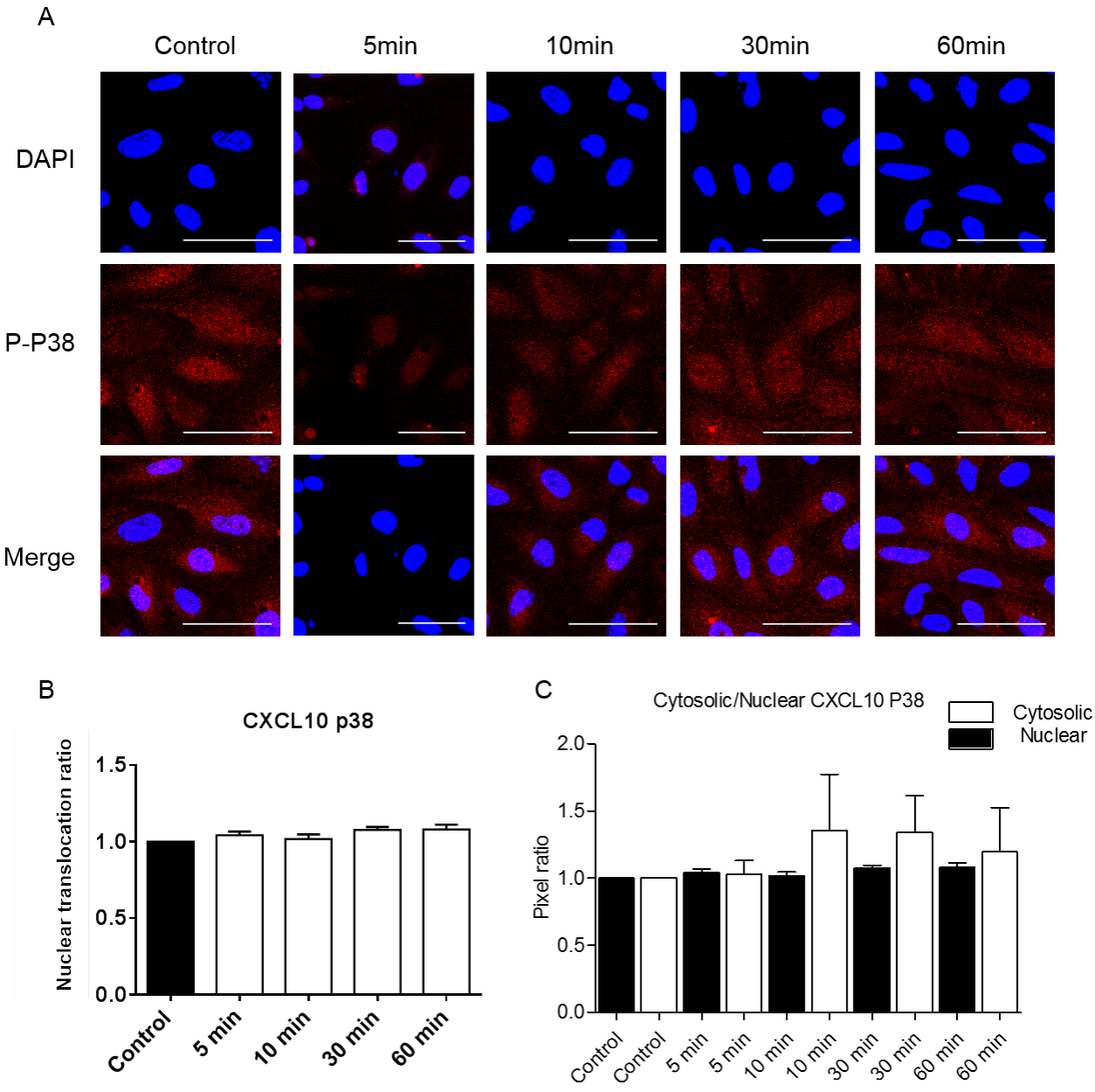

Figure 33 Distribution of P-P38 in hCMEC/D3 following CXCL10 (50ng/mL) treatment. (A) Confocal microscopy images (B) analysis of nuclear distribution of P-ERK following treatments for n=3 independent experiment. Images were taken on Zeiss LSM700. Scale bar 50µm. Images processed using Image J for mean pixel intensity of P-ERK co-localizing with nucleus. (C) Cytosolic/nuclear phospho-protein quantification, normalised to control. Results are expressed as average means +/- SEM. Statistical analysis was performed using a One-way ANOVA and a Dunnet post hoc test for statistical analysis of mean value variances. Data not significant.

3.4 Discussion

We initially tested the expression of the classically described receptors for CCL4, CXCL8 and CXCL10, namely CCR5, CXCR1 and CXCR2, and CXCR3 respectively. The results obtained with both cell lines tested, HUVEC and hCMEC/D3, confirmed previous reports in the literature that demonstrate expression of CXCL8, CXCL10 and CCL4 receptors in these cells (Salcedo R., 2000, Li et al., 2003, Howland et al., 2015). Aside from the bands that appeared at the correct molecular weight, we also found multiple bands with the antibodies used against CXCR1-3 and CCR5. Despite several attempts to optimise the technique, multiple bands were consistently found indicating potential non-specific binding or cross reactivity to other proteins. Glycosylation can have great impact in a protein's structure and function (including determination of downstream signalling pathways) and should be considered in the results showed in this chapter. In fact, glycosylation of CXCR2, a receptor for CXCL8, is required for neutrophil responsiveness in inflammation (Ludwig et al., 2000). The receptor CCR2 has also shown to be regulation by glycosylation (Petti et al., 2018).

Whilst band excision and mass spec analysis could have been undertaken it was decided that since the aim of this experiment was to confirm reports in the literature that hCMEC/D3 and HUVEC express these receptors and a response to the respective chemokines was consequently verified, no further investigation was done. Despite these results, it is known that the chemokine receptors are promiscuous, making it impossible to exclude the involvement of other receptors and chemokines in the possible effects of receptor engagement (Mantovani, 1999).

Having established that our two ECs of choice express receptors for these chemokines, this allowed us to extrapolate from previously reported effects of the chemokines on other cell types to guide our experimental design. For example CCR5, a receptor for CCL4,

has been shown to regulate macrophage recruitment in the context of adipose tissue inflammation (Kitade et al., 2012). CXCL8 receptors, CXCR1 and CXCR2 have been strongly implicated in inflammation and tumourigenesis, and their blockade shown to limit inflammatory processes (Ginestier et al., 2010, Marsh and Flemming, 2011). Equally, the receptors are known to be mediators of neutrophil migration (Smith et al., 2004, Chapman et al., 2007, Jamieson et al., 2012). Antibody blockage of CXCR3 has been shown to diminish T cell recruitment to sites of inflammation (Xie et al., 2003). Lastly, a CXCL10 receptor, CXCR3 has been implicated in the development of autoimmune diseases, rheumatoid arthritis and lupus erythematosus (Zeremski et al., 2008, Lacotte et al., 2009).

Taken together, the expression of these receptors in HUVEC and hCMEC/D3 suggest that CCL4, CXCL8 and CXCL10 may trigger signalling pathways relevant to inflammation and immune cell recruitment. Once we had established that HUVEC and hCMEC/D3 expressed the necessary chemokine receptors, we then tested the chemokines' abilities to activate key signalling events through the induction of phosphorylation in tyrosine, serine and threonine residues. Since there were infinite phosphorylation sites that may be phosphorylated, we initially looked at global phosphorylation on these residues to establish the principle that these chemokines can elicit responses in ECs.

Our results showed that there was an increase in phosphorylation of mainly tyrosine and threonine residues in response to CCL4, CXCL8 and CXCL10. Unfortunately, the commercially available antibodies result in immunoblots that do not allow clear identification of the exact phosphorylation site. Nevertheless, these results demonstrate that these chemokines are capable of eliciting protein phosphorylation and hence the potential to activate signalling pathways in these ECs. Several reports in the literature have shown that both chemokine receptors and intracellular proteins can have their tyrosine, serine and threonine residues phosphorylated, indicating a downstream effect

in cell function (Mueller et al., 1995, Oppermann et al., 1999, Li et al., 2006, Barberis et al., 2009, Millard et al., 2014).

Overall we have shown a signalling response to our chemokines of interest in the timeframe and dosage tested. Having demonstrated that proteins were phosphorylated in response to our chemokines of interest we then looked for candidate proteins to investigate further. Two such proteins were ERK1/2 and P38 as increased phosphorylation was observed in bands that corresponded to the molecular weight of these kinases. Due to the lack of time and since the focus of the projected was not to dissect specific signalling pathway, we did not investigate the protein JNK. Time allowing, the phosphorylation of this protein could have provided insights into regulation of leukocyte and inflammatory gene expression (Dragoni et al., 2017).

We then focused on MAPK kinases and catalytic kinases that regulate numerous functions in eukaryotic cells (Hunter, 2000b). The upstream protein MEK1/2 catalyses the phosphorylation of ERK1/2 at tyrosine 204/187 and then at threonine 202/185 (Chuderland and Seger, 2005). Another major MAP kinase, P38 is activated by phosphorylation of tyrosine 182 and threonine 180 (Mittelstadt et al., 2005).

There is evidence in the literature that shows that chemokines are able to induce MAPK signalling. *In vitro*, it has been shown that CCL3, a CCL4 related protein, induces migration of neutrophils via CCR5-dependent activation of ERK 1/2 (Luciano Ottonelloa, 2005). Similarly, CCL4 has been shown to induce chemotaxis of macrophages through activation of class IA PI3K, and the proline-rich tyrosine kinase Pyk2 upstream of ERK (Cheung et al., 2009). In our experiments CCL4 was also able to induce a strong transient phosphorylation of ERK in hCMEC/D3. This strong effect in phosphorylation was also seen as early as 3 min following treatment, indicating an immediate effect in triggering intracellular signalling. ERK has been shown to be present in both the

cytoplasm and nucleus and upon activation to be rapidly translocated to the nucleus (Chen et al., 1992).

Our experiments showed a comparable pattern to the activation seen with the immunoblots, with partial but significant nuclear translocation of P-ERK after 30 min of CCL4 treatment. CCL4 did not significantly alter levels of P-P38 in both cell types tested at any of the timepoints studied but there was significant nuclear translocation of P-P38 at 5 min post treatment. Similar to ERK, P38 has been reported in the nucleus and the cytoplasm of resting cells, translocating to the nucleus upon activation. We observed a significant increase in nuclear P-P38 at 5 min post treatment, albeit modest, when compared to P-ERK. The nuclear translocation of P-P38 could potentially result in the activation of inflammatory-related genes (Gong et al., 2010).

The chemokine CXCL8 has been shown to induce activation of the MAPK signalling cascade, with downstream phosphorylation of ERK1/2 in neutrophils, endothelial and cancer cell lines (Waugh and Wilson, 2008). The effects of CXCL8 in ECs, namely survival, proliferation and regulation of angiogenesis, are consistent with the effects of downstream of MAPK signalling (Li et al., 2003). In our experiments, CXCL8 activated both ERK 1/2 and P38 within 30 min of treatment in hCMEC/D3, but not in HUVEC. As seen with CCL4 treatments, ERK phosphorylation following CXCL8 treatment was highly significant at 5 min post treatment. In this case, CXCL8 did not induce significant phosphorylation at the earlier 1 or 3 min timepoints. When investigating nuclear distribution, there was no significant increase of nuclear P-ERK or P-P38, suggesting that potential targets of the phospho-protein may be in the cytoplasm.

ERK is localised mainly in the cytoplasm, bound to anchoring proteins and upon activation can be shuttled to other locations in the cell, including the nucleus (Chuderland and Seger, 2005). Upon stimulation, ERK 1/2 phosphorylates substrates in several

cellular compartments, resulting in proliferation, differentiation, and stress response among others (Yoon and Seger, 2006). In the cytoplasm, activated ERK can activate cytosolic substrates that signal to additional cytoplasmic and nuclear targets or phosphorylate cytoskeletal elements (Yoon and Seger, 2006). Phosphorylated ERK in the cytoplasm has been linked to senescence and anti-apoptotic functions. In the nucleus P-ERK can activate transcription factors, which result in the downstream induction of genes coding for growth factors, cytokines and adhesion molecules (**Figure 34**) (Zhao et al., 2006).

The kinase P38 mediates stress signalling by phosphorylation of Thr180 and Tyr182 upstream of MAP kinase 3/6 (Kyriakis and Avruch, 2001). P38 is highly activated by pro-inflammatory stimuli and has an important function of stabilising the 3' UTR of certain RNA's during the inflammatory response. Adenosine/uridine rich elements (AREs) are well-characterised regulatory elements in these UTRs of cytokines, growth factors and proto-oncogene mRNAs. Chemokines and chemokine receptors mRNA's have rich 3' UTR and are prone to regulation through this process, altering the stability of the mRNAs (Tebo et al., 2003). AREs from CXCL8, for instance, mediate regulation of mRNA stability by the P38 pathway (Mahtani et al., 2001). In another study, the mechanism that regulates the stability of CXCL2 mRNA was elucidated, with P38 pathway involved in this process (Numahata et al., 2003). Therefore, P38-mediated regulation of chemokine mRNA stability or translation, could be a mechanism of regulation of the inflammatory response (Clark et al., 2003).

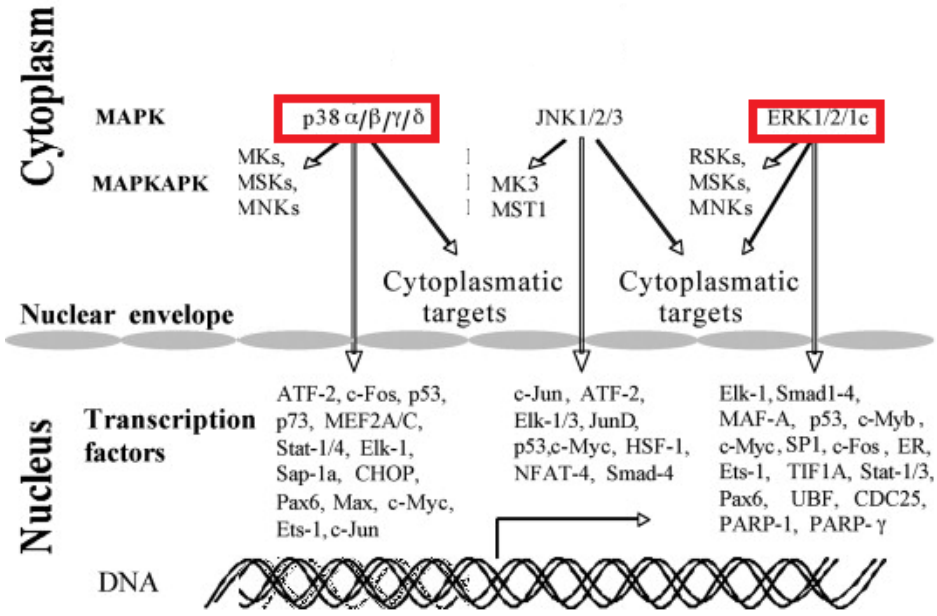

Figure 34 Schematic representation of the MAPK cascades and their nuclear targets (adapted from (Plotnikov, 2011 #2193).

Another non-nuclear effect of the P38 pathway is the regulation of actin dynamics, through the phosphorylation of the heat shock protein 27 (HSP27). This function could

indicate the non-nuclear role of P38 in the cytoskeleton of ECs in agonist induced rearrangement of the cytoskeleton in stress conditions (Guay et al., 1997). The P38 pathway, when activated by VEGF through the phosphorylation of HSP27, mediates cell migration and actin reorganization, indicating a possible function in angiogenesis (Rousseau et al., 1997).

The MAPK ERK and P38 have been shown to be activated by CXCL10/CXCR3 in human airway epithelial cells and human pneumocytes, inducing chemotaxis (Shahabuddin et al., 2006, Liu et al., 2011). This evidence suggests that CXCL10 could also have an effect on MAPK signalling in ECs, a structurally similar cell type to epithelial cells. However, CXCL10 treatments resulted in only a modest increase in phosphorylation of the MAP kinases tested, failing to reach statistical significance with the exception of one time point. Thus, there was significant P38 phosphorylation at 60 min post treatment in HUVEC but since this cell type showed limited response to the other chemokines, this was considered to be a likely false positive result and so was not investigated further. Consistent with these immunoblot results, immunofluorescence did not indicate nuclear translocation of P-ERK or P-P38 following CXCL10 treatments, suggesting that CXCL10 does not elicit a strong response in these cells in its inactive form (Ben-Levy et al., 1998). P38 translocates upon stimulation, depending on the nature of the stimulus (Chen et al., 1992). Accordingly, cytosolic P38, once phosphorylated, is translocated to the nucleus, allowing it to access its nuclear substrates. When stimulation ceases, dephosphorylated P38 is transported back to the cytosol until further stimulation (Gong et al., 2010).

Given our results, where CCL4 induced nuclear translocation of P-ERK, one can hypothesise that the phospho protein is, in part, translocated to the nucleus where it can activate transcription factors. It is important to note, however, that following chemokine treatment both P38 and P-ERK were also present in the cytoplasm, suggesting these proteins could be activating both nuclear and cytosolic pathways. Interestingly, it was

also found that following CXCL10 treatments, there was a significant increase in cytosolic P-ERK but not nuclear, suggesting a cytosolic target for the phospho-protein.

The effect of chemokines on MAPK phosphorylation were observed mostly in hCMEC/D3 and not HUVEC, indicating a heterogeneity in response between the two sources of vascular endothelium. EC heterogeneity is apparent not only between different organs but evident in sections of a vascular tree (Kumar et al., 1987, Hewett, 2016). The molecular expression and signalling profiles of micro and macrovessels are distinct, resulting in specific functional outcomes (Lokeshwar and Selzer, 2000, Rocha and Adams, 2009). Here we are also comparing a specialised microvascular endothelium from the brain with a large vein endothelium from the umbilical vein.

In order to generate a model that fully mimics the properties of the BBB, complex culture systems with different cell types and flow would be necessary. This adds to the complexity of the system, adding variables to the experimental set up. Primary or low passage brain ECs, that retain genotypic and phenotypic properties of the *in vivo* BBB would be ideal but the low yield of cells obtained from rodents and ethical limitations of human brain ECs hinder this possibility (He et al., 2014). Primary cells, such as HUVEC used in some experiments in this chapter, resemble cells found in a living human since they have not accumulated mutations during passage in tissue culture or immortalization. They are genetically more diverse, offering a more representing microenvironment to test compounds (Hare et al., 2016). HUVEC, however, originate from large calibre vessels (umbilical cord) and are not from cerebral origin, restricting their suitability for BBB studies.

On the other hand, immortalised cell lines offer other advantages. They are easier to manipulate in culture and are able to divide up to high passage numbers. However, these cells are distinct from the same cell type *in vivo*: they accumulate mutations during

passage, altering their phenotype, and their innate and senescence pathways may overlap. One must consider the dysregulation of signalling pathways as a consequence of the immortalisation process (Hare et al., 2016).

After weighing up the pros and cons of both cells lines, and following the results obtained initially with both cells, it was decided to abandon the HUVEC primary cell line, since, despite some use as an *in vitro* model of the BBB, the response to chemokines was not consistent.

There is some inconsistency in the protein expression and nuclear translocation results for all chemokines. Whilst there was no significant P38 phosphorylation in western blots there was significant nuclear localisation of the protein at 5 min. Following CXCL8 treatments, there was significant P38 phosphorylation on western blot but no significant nuclear translocation. Despite the attempt to assure absolute comparability between the two experiments, it is important to note that PFA fixation can alter epitopes in cells, masking epitopes, making them less available for IF staining. On the other hand, the changes seen in protein expression on western blot were quite modest and due to the enzymatic nature of ECL (the resulting signal is non-linear) there can be under or over estimations of the resulting signal. In conclusion, the two experiments do not completely align but taken together show MAPK phosphorylation induced by chemokine treatments in hCMEC/D3.

Our results show a clear effect of CCL4, CXCL8 and CXCL10 on brain EC activation (Table 7). Following these findings, our next step was to establish what the functional outcome of chemokine signalling in brain ECs might be, starting with the investigation of their effect on tight and adherens junctions and the actin cytoskeleton.

Table 7 Summary of chapter 3 – Key findings in hCMEC/D3

Experiment	CCL4	CXCL8	CXCL10
P-ERK expression	+++ (3', 5', 10')	+++ (5'), + (3')	-
P-P38 expression	-	+ (10', 30')	+ (1')
P-ERK nuclear localization	+ (30')	-	-
P-P38 nuclear localization	++ (5')	-	-

.

4. Effects of chemokines on EC junctional proteins

4.1 Introduction

Pro-inflammatory agents, such as chemokines, can disturb the organization of junctions in endothelial cells (Gonzalez-Mariscal et al., 2008, Wallez and Huber, 2008). Studies have shown that chemokines increased permeability and disrupted the tight junctions of human vascular endothelium cells of non-cerebral origin (Lee et al., 2006). Of special interest, the chemokine CXCL8 has been shown to downregulate the expression of tight junction proteins in ECs in a time-dependant manner (Yu et al., 2013). In brain endothelial cells, recent work has exposed the effect of the chemokine CCL2 in tight junction disorganization, including ZO-1 distribution, and consequent increase in BBB permeability (Dimitrijevic et al., 2006, Luissint et al., 2012). There is strong evidence that tight junctions' proteins can be modulated by chemokines and that MAPK signalling, protein phosphorylation and cytoskeleton rearrangement could be involved in the process (Shahabuddin et al., 2006, (Hudson et al., 2014).

The tight junction proteins, occludin and ZO-1, can be phosphorylated and dephosphorylated on Ser, Thr and Tyr residues. In the previous chapter we demonstrated that chemokines can lead to the phosphorylation of numerous tyrosine, serine and threonine residues in proteins expressed in hCMEC/D3. Reports in the literature have shown that the phosphorylation of tyrosine residues in tight junction proteins results in the loss of barrier properties, in the form of reduced occludin expression, decreased transendothelial resistance, and increased endothelial permeability (Wachtel et al., 1999).

Moreover, we have shown that chemokine signalling results in downstream ERK and P38 phosphorylation. The MAPK kinases, including ERK1/2 and P38 have been shown to be involved in modulating the expression and distribution of TJ proteins, including ZO-1. It is known that by regulating activity within cells, MAPK kinases co-modulate tight junction protein phosphorylation and regulate paracellular transport (Gonzalez-Mariscal et al., 2008). In corneal epithelial cells, for example, activation of ERK 1/2 resulted in changes in ZO-1 distribution and an increase in paracellular permeability (Wang et al., 2004). In another study, using lung endothelial cells, activated P38/MAPK, resulted in microtubule depolymerisation and hyperpermeability (Li et al., 2015).

Another junctional protein of interest, VE-cadherin, can be redistributed by pro-inflammatory mediators, resulting in junction destabilization and perturbation of the endothelial cell barrier (Esser et al., 1998). VEGF induces a transient phosphorylation of VE–cadherin, β-catenin and plakoglobin, increasing vascular paracellular permeability. Other factors such as histamine, tumour necrosis factor (TNF)-α, platelet-activating factor (PAF), neutrophils and integrin activation can also lead to the phosphorylation of VE-cadherin (Wallez and Huber, 2008 2003). This evidence on the pivotal role of VE-cadherin reiterates its importance in the maintenance of an endothelial barrier. In the context of leukocyte migration, VE-cadherin is phosphorylated and transiently leaves the junctions at specific sites of migration, leading to barrier breakdown (Aragon-Sanabria et al., 2017). It has been shown that ICAM-1 mediated VE-cadherin phosphorylation is essential to transendothelial lymphocyte migration (Turowski et al., 2008).

In tight junctions of epithelial cells, pro-inflammatory agents, including cytokines, have been shown to alter the actin cytoskeleton, induce F-actin stress fibres and ultimately increase barrier permeability (Prasain and Stevens, 2009, Ivanov et al., 2010). Adherens junctions, upon TNF stimulation, connect stress fibres between cells and the disruption

of the actin rim and the formation of stress fibres increases paracellular transport (Prasain and Stevens, 2009) (Millan et al., 2010). The actin cytoskeleton was therefore explored as a possible target for the downstream effects of chemokines on ECs.

Since these BBB structural proteins can be challenged in neuroinflammation, resulting in barrier disruption, increased vascular permeability and leukocyte migration, the question of whether pro-inflammatory chemokines can modify BBB ECs junctional proteins and cytoskeleton requires further examination. Clarifying the role of chemokines in regulating the BBB would provide new insights into the mechanism and yield potential neuroprotective strategies in neuroinflammatory diseases.

4.2 Aims

In the previous chapter, we demonstrated that ECs express receptors for CCL4, CXCL8 and CXCL10, and that chemokine treatment of ECs induces rapid signalling events. Amongst the tyrosine, serine and threonine proteins tested that could be phosphorylated by chemokines, we selected the MAPK family to investigate further. Since the MAPK ERK 1/2 and P38 were strongly phosphorylated in our experimental conditions and due to their involvement in protein expression, stress responses and inflammation, the effect of chemokines in endothelial junctional proteins was investigated. The aim of this section of the study was to test whether CCL4, CXCL8 and CXCL10 could alter the expression and distribution of proteins associated with the tight and adherens junction proteins, ZO-1 and VE-cadherin, respectively. Finally, we investigated the effect of chemokines on filamentous actin in the form of stress fibres to assess the effect of our chemokines of interest on the ECs cytoskeleton.

4.3 Results

4.3.1 ZO-1 expression following chemokine treatments

To gain insight into the effect of CCL4, CXCL8 and CXCL10 on ZO-1 expression, hCMEC/D3 cells were treated for up to 60 minutes and the distribution of ZO-1 was analysed following immunofluorescence quantification. Ratios were calculated by thresholding images within each experimental repeat, measuring the pixel area for each channel/DAPI, and expressing it as a percentage of the control.

In the control samples, ZO-1 staining was almost entirely in the membrane area, centred in paracellular areas typical for a junction protein. However, after treatment its expression became strongly cytoplasmic and specifically, perinuclear (**Figure 35**-**Error! Reference source not found.**).

CCL4 treatment of hCMEC/D3 resulted in a strong cytoplasmic and perinuclear expression of ZO-1 at 10 and 60 min (**Figure 35**-A). Upon pixel count of 10x fields of several experimental repeats, there was no significant change in the overall amount of ZO-1 (**Figure 35**-B). In contrast, junctional ZO-1 decreased in response to CCL4 treatment, with a significant decrease at 10 min and decreasing further at 60 min post treatment (**Figure 35**-C).

Unlike the pattern observed with CCL4, CXCL8 treatment resulted in a more junctional pattern of staining (**Figure 36**-A). Following pixel count of 10x fields of several experimental repeats, there was no significant change in the overall amount of ZO-1, although there was a visible upward trend in ZO-1 expression (**Figure 36**-B). There was, however, a significant decrease of junctional ZO-1 at 10 min post treatment but at 60 min, this decrease was not significant (**Figure 36**-C).

CXCL10 treatment resulted in a staining pattern, with a strong signal in the cytoplasm and junctions (**Error! Reference source not found.**-A). Upon pixel count of 10x fields of several experimental repeats, there was no significant change in the overall amount of ZO-1 (**Error! Reference source not found.**-B). Following analysis of junctional ZO-1, there was a significant reduction in signal at both timepoints studied, 10 and 60 min following treatments (**Error! Reference source not found.**-C).

In this case, inflammatory mediators, such as histamine, INF-γ or VEGF could have been used as a positive control to compare the extent of the effect chemokines on ZO-1 junctional distribution (Gardner et al., 1996, Youakim and Ahdieh, 1999, Wang et al., 2001).

In summary, none of the chemokine treatments appear to significantly alter the total ZO-1 protein expression but altered the location of the protein, causing it to translocate from the plasma membrane to the cytoplasm.

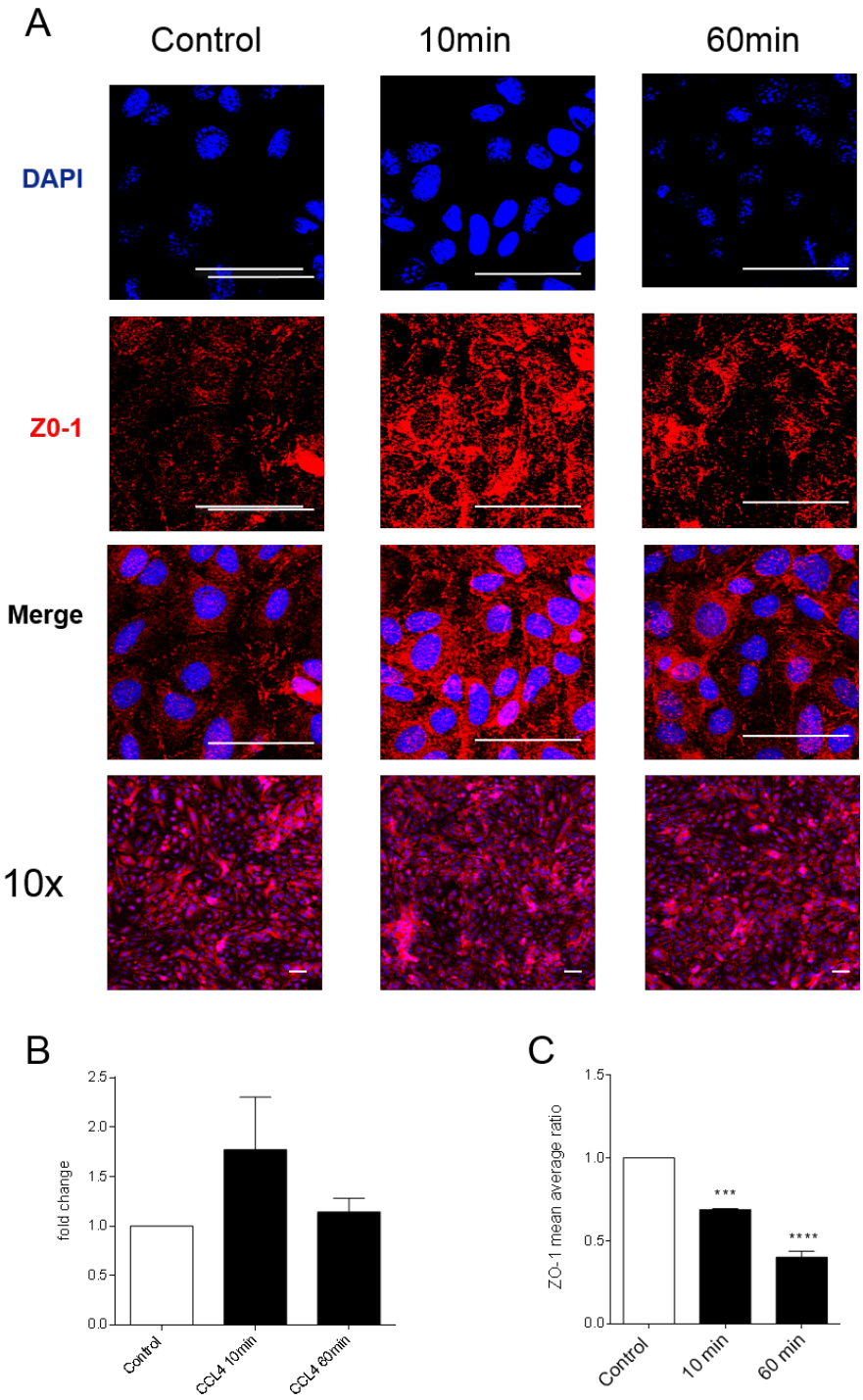

Figure 35 ZO-1 junctional expression following CCL4 treatments for 10 and 60 min. Confluent hCMEC/D3 were treated with CCL4 (100ng/mL) for the above mentioned timepoints, fixed and stained for IHC as detailed in Material and Methods. (A) Representative confocal images: Z stacks were taken on Zeiss LSM 700 using a 63x and a 10x objective. (B) ZO-1 quantification: Ratio of ZO-1 (red pixels)/ DAPI (blue pixels) in the 10x fields was calculated using Image J (C) ZO-1 junctional distribution: average mean area of junctional ZO-1, normalized to DAPI. Statistical analysis performed using a One-way ANOVA and Dunnet post hoc test. Means +/- SEM. ***, P<0.001, Scale bar: 50µm. Representative image of n=3.

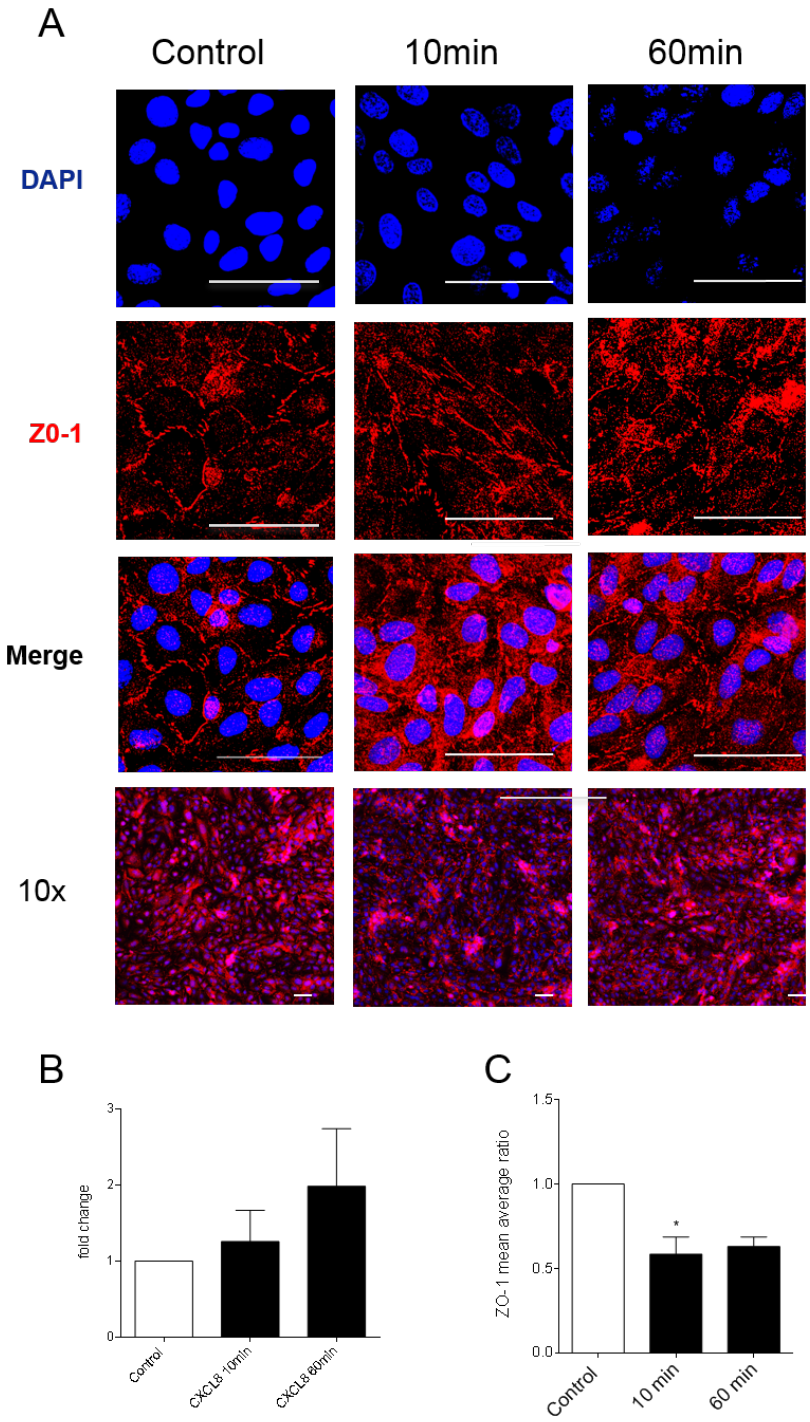

Figure 36 ZO-1 junctional expression following CXCL8 treatments for 10 and 60 min. Confluent hCMEC/D3 were treated with CXCL8 (100ng/mL) for the above mentioned timepoints, fixed and stained for IHC as detailed in Material and Methods. (A) Representative confocal images: Z stacks were taken on Zeiss LSM 700 using a 63x and a 10x objective. (B) ZO-1 quantification: Ratio of ZO-1 (red pixels)/ DAPI (blue pixels) in the 10x fields was calculated using Image J (C) ZO-1 junctional distribution: average mean area of junctional ZO-1, normalized to DAPI. Statistical analysis performed using a One-way ANOVA and Dunnet post hoc test. Means +/- SEM. *, $P<0.05$, Scale bar: 50µm. Representative image of n=3.

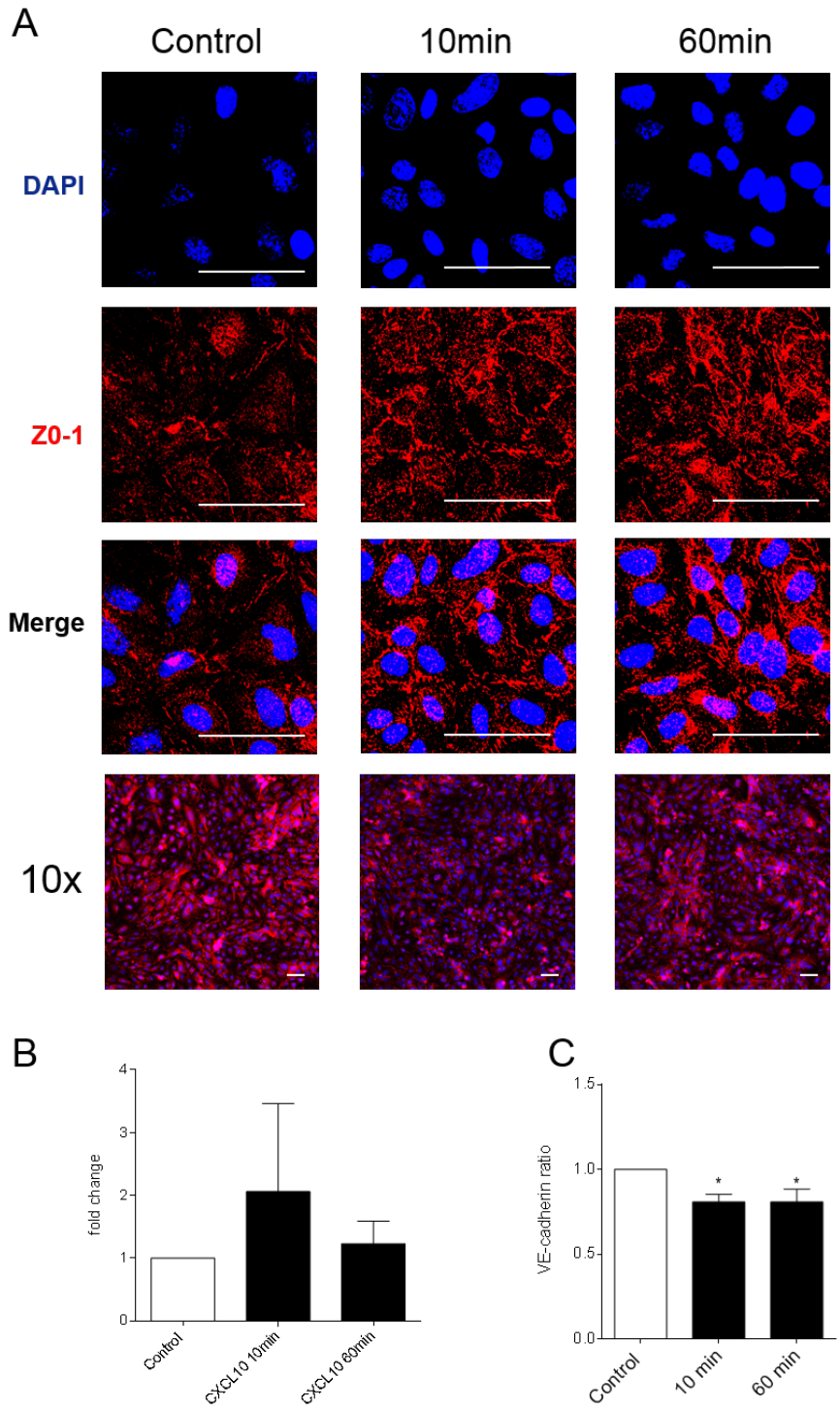

Figure 37 ZO-1 junctional expression following CXCL10 treatments for 10 and 60 min. Confluent hCMEC/D3 were treated with CXCL10 (50ng/mL) for the above mentioned timepoints, fixed and stained for IHC as detailed in Material and Methods. (A) Representative confocal images: Z stacks were taken on Zeiss LSM 700 using a 63x and a 10x objective. (B) ZO-1 quantification: Ratio of ZO-1 (red pixels)/ DAPI (blue pixels) in the 10x fields was calculated using Image J (C) ZO-1 junctional distribution: average mean area of junctional ZO-1, normalized to DAPI. Statistical analysis performed using a One-way ANOVA and Dunnet post hoc test. Means +/- SEM. *, $P<0.05$, Scale bar: 50µm. Representative image of n=3.

4.3.2 VE-cadherin distribution following CCL4, CXCL8 and CXCL10 treatment

The distribution of VE-cadherin can be altered by pro-inflammatory stimuli, including thrombin, inducing increased endothelial permeability (Mark J. Lim et al., 2001, Flemming et al., 2015). To investigate the effects of CCL4, CXCL8 and CXCL10 in VE-cadherin expression and junctional distribution, hCMEC/D3 were treated with chemokines at determined timepoints followed by immunofluorescent staining and imaging.

CCL4 treatment of hCMEC/D3 resulted in a reduction in total VE-cadherin staining. The pattern of staining suggests interrupted expression at the membrane with intermittent patches of VE-cadherin at all timepoints tested and especially evident at 10 and 60 min post treatment. This pattern was also seen in the 10x fields, where a strong VE-cadherin signal was observed in the control sample, in contrast to the treated cells where VE-cadherin was less evident (**Figure 39**-A). Upon statistical analysis, at 60 min post CCL4 treatment, there was a 56% reduction in the VE-cadherin signal compared to control (**Figure 39**-B).

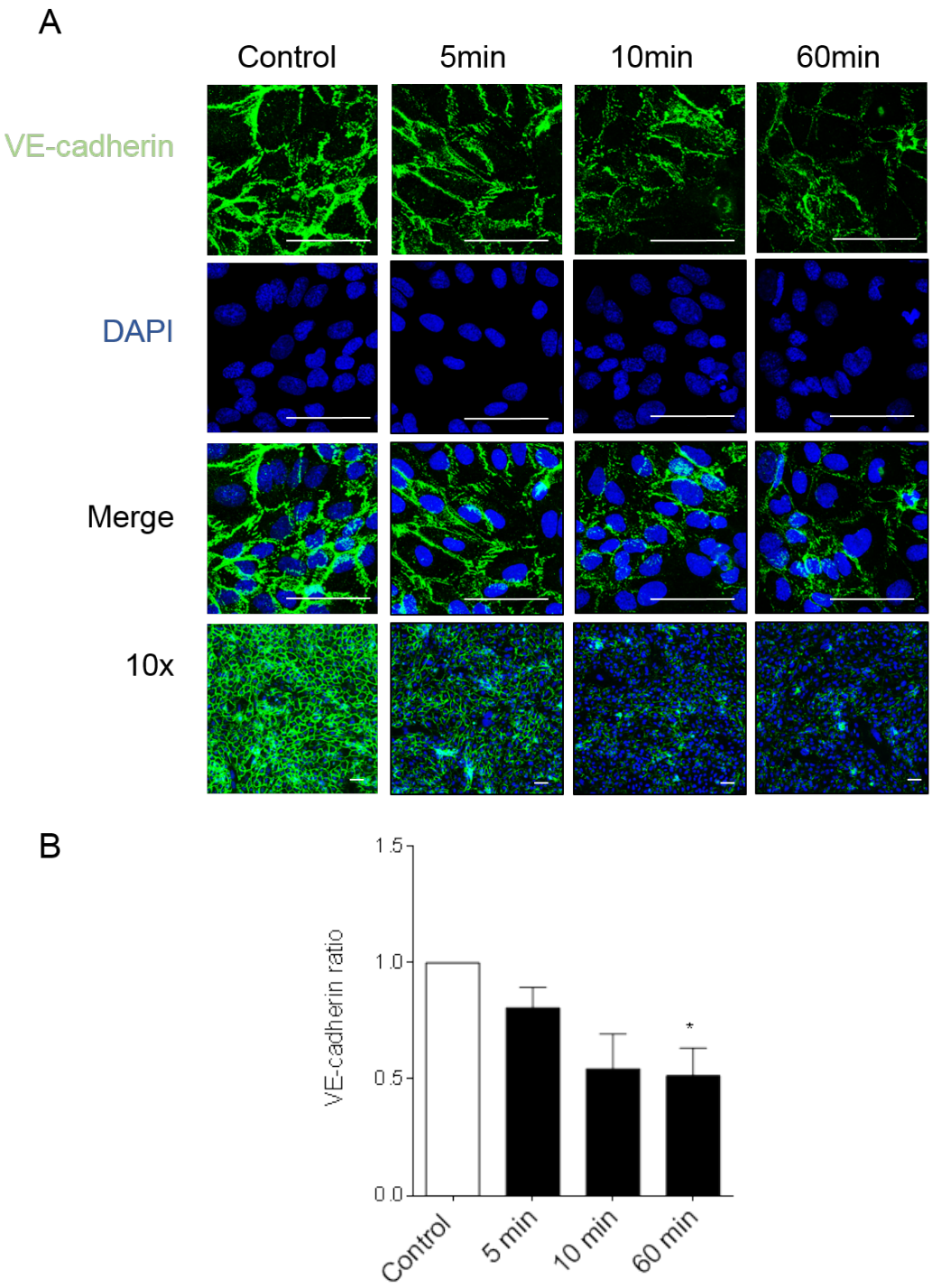

Figure 38 VE-cadherin staining following CCL4 treatments. HCMEC/D3 were treated with CCL4 (100ng/mL) for 5, 10 and 60 min, fixed and stained as described in Material and Methods. (A) Confocal images of 63x and 10x objectives. Z stacks were taken on Zeiss LSM700 using a 63x and a 10x objective. Scale bar: 50µm. Representative image of n≥3. (B) Analysis of the 63x fields. Mean area average +/- SEM of VE-cadherin stain, normalized to control. Statistical analysis performed using a One-way ANOVA and Dunnet post hoc test. Means +/- SEM. *, P<0.05.

CXCL8 treatment of hCMEC/D3 results in a loss of VE-cadherin staining

CXCL8 treatments resulted in a striking loss of VE-cadherin staining throughout the timepoints tested, but especially obvious at 5min post treatment. Similar to the effects seen with CCL4 treatments, the pattern of VE-cadherin became intermittently interrupted in comparison to control, where a more continuous pattern of VE-cadherin was seen at junctions.

Upon analysis of the 10x fields, a dramatic reduction in VE-cadherin is seen at 5 min and 10 min and a less evident loss is seen at 60 min post treatment with CXCL8. The strong VE-cadherin signal in the control is mostly lost at 5 min and gradually regained in the subsequent timepoints. Interestingly, at 60 min the pattern of staining has a more continuous linear display across the junctions than the other treatment timepoints (**Figure 40**-A).

Following statistical analysis, there was a significant reduction of VE-cadherin signal in all timepoints tested. At 5 min and 10 min there was a dramatic loss of signal (18% and 67% of control, respectively), and a gradual recovery at the 60 min timepoint (73% of control) (**Figure 40**-B).

CXCL10 treatment of hCMEC/D3 results in a loss of VE-cadherin staining

CXCL10 treatment resulted in a biphasic decrease in VE-cadherin staining. At 5 min post treatment there was a dramatic reduction in the VE-cadherin signal (38% of control) that recovered by 10 min to near control levels. However, by 60 min there was a similar loss of signal to that observed at 5 min (43% of control) (**Figure 41**-A). Interestingly, the pattern of staining following treatments appears less intermittent than the pattern observed following treatments with CXCL8. In the 10x fields, a strong VE-cadherin signal can be seen in the control sample and a marked reduction is visible post treatments.

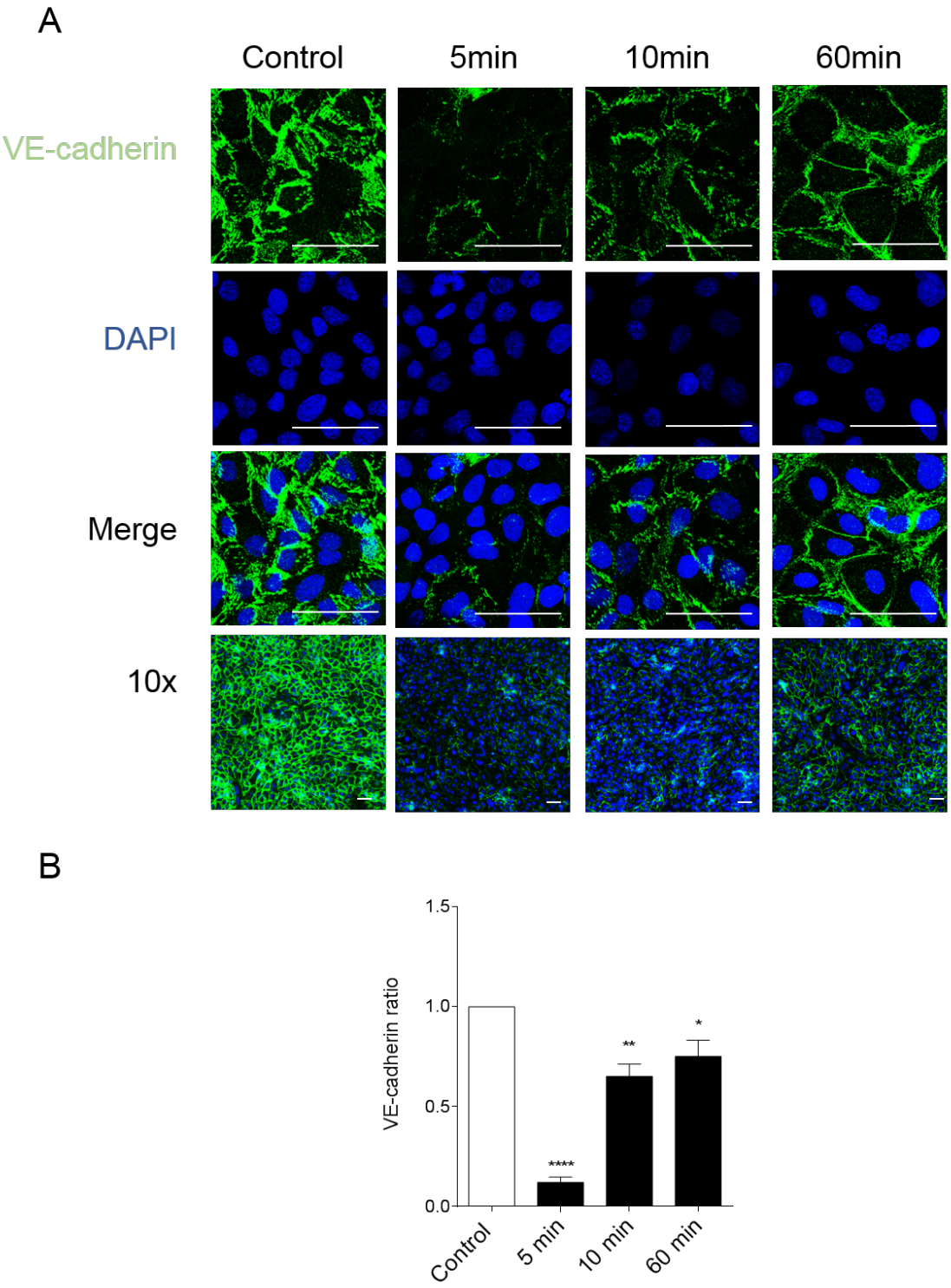

Figure 39 VE-cadherin staining following CXCL8 treatments. HCMEC/D3 were treated with CXCL8 (100ng/mL) for 5, 10 and 60 min, fixed and stained as described in Material and Methods. (A) Confocal images of 63x and 10x objectives. Z stacks were taken on Zeiss LSM700 using a 63x and a 10x objective. Scale bar: 50µm. Representative image of n≥3. (B) Analysis of the 63x fields. Mean area average +/- SEM of VE-cadherin stain, normalized to control. Statistical analysis performed using a One-way ANOVA and Dunnet post hoc test. *, P<0.05; **, 0.001<P<0.01; ****, P<0.0001.

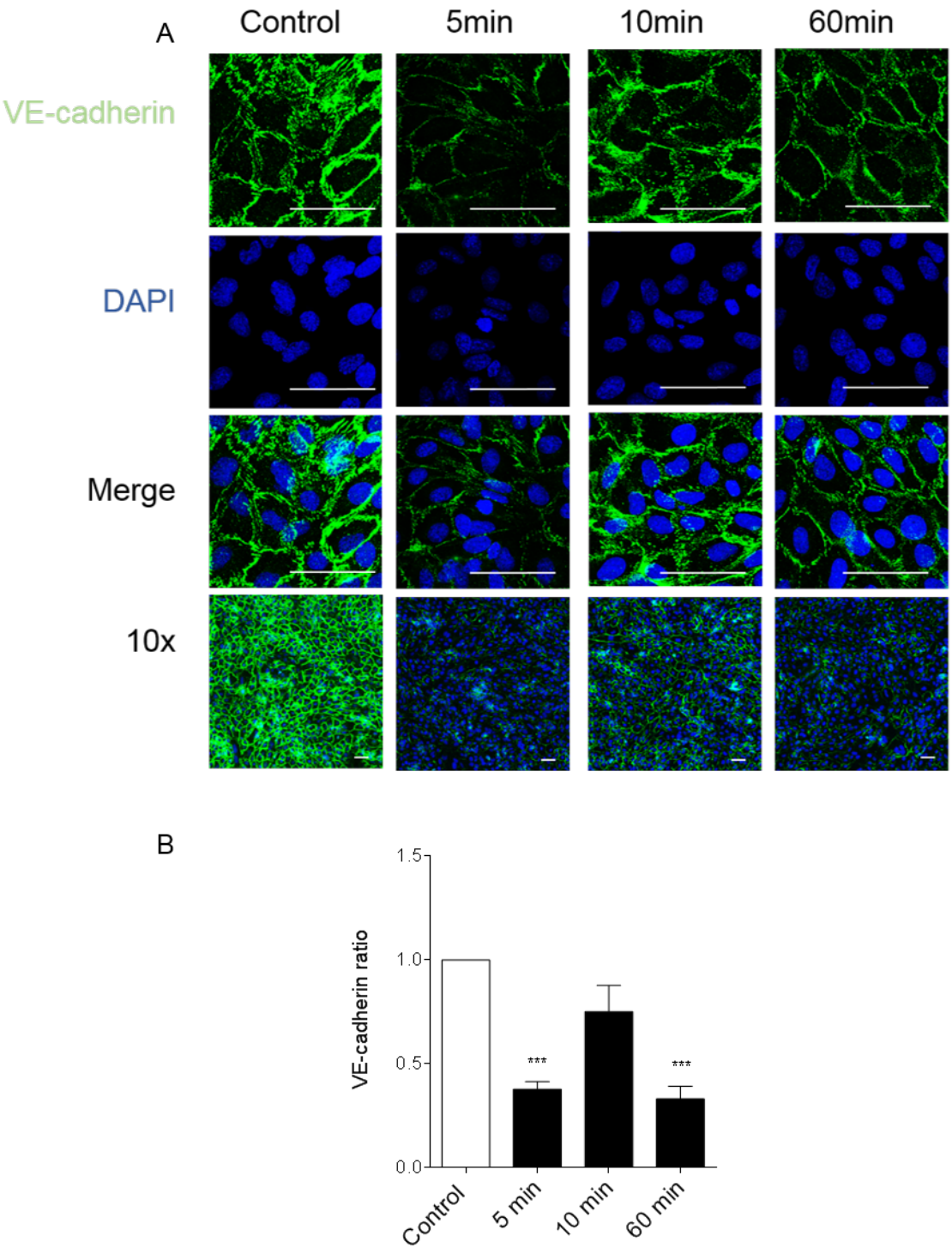

Figure 40 VE-cadherin staining following CXCL10 treatments. HCMEC/D3 were treated with CXCL10 (50ng/mL) for 5, 10 and 60 min, fixed and stained as described in Material and Methods. (A) Confocal images of 63x and 10x objectives. Z stacks were taken on Zeiss LSM700 using a 63x and a 10x objective. Scale bar: 50µm. Representative image of n≥3. (B) Analysis of the 63x fields. Mean area average +/- SEM of VE-cadherin stain, normalized to control. Statistical analysis performed using a One-way ANOVA and Dunnet post hoc test. ***, P<0.001.

4.3.3 Quantification of VE-cadherin protein expression in hCMEC/D3 following chemokine treatments

The previous experiments demonstrated that chemokine treatments resulted in a loss of signal of VE-cadherin. This loss was seen at the junctions and there was no evidence of signal translocation to the cytoplasm. This suggests that either the junctional VE-cadherin was being shed or that upon internalisation the epitope that the antibody recognised became masked.

In order to address this reduction in VE-cadherin signal and to determine if there was a loss in the overall amount of protein, or if the protein was being shed, changes in total protein expression as a result of chemokine treatments for 5, 10 and 60 min were investigated by western blot analysis (**Figure 42**). HCMEC/D3 were treated with each chemokine for the same time points as the previous experiment and an immunoblots were produced. An antibody that recognizes an external epitope of the VE-cadherin protein (R&D Systems, see Material and Methods, Immunofluorescence (IF)) was used in this experiment.

CCL4 treatment did not result in a significant decrease in VE-cadherin expression (**Figure 42**-A). Equally, CXCL8 treatment resulted in a non-significant change in protein expression (**Figure 42**-B). Moreover, stimulation with CXCL10 also did not result in changes in the overall protein expression at the timepoints studied (**Figure 42**-C).These data suggest that over the time-frame of our experiments protein loss was not the cause of the observed reduction in staining; there was no evidence of protein shedding (fragments above <25kDa).

Overall, the levels of total VE-cadherin remained unchanged following chemokine treatments (Figure 42). An alternative hypothesis is that there could have been VE-

cadherin cleavage of the portion where the antibody's epitope is located. To address this possibility, an additional western blot was run with the proteins present in the supernatant of the treated cultures but no VE-cadherin signal was obtained in the resulting immunoblot (not shown). This does not exclude the possibility that certain VE-cadherin fragments, that did not contain the epitope the antibody recognises, could have been cleaved in the tissue culture supernatant.

4.3.4 Quantification of VE-cadherin using IF in chemokine treated hCMEC/D3

Since the overall amount of protein in the cell did not significantly change within the 60 min time course, we hypothesised that the VE-cadherin epitope that the antibody recognizes is being masked or internalised due to the effect of the chemokines. In order to determine the effect of chemokine treatment on changes in VE-cadherin distribution in hCMEC/D3 (**Figure 39**-**Figure 41**), an alternative staining protocol using a buffer containing EGTA for live-cell staining was devised. The calcium chelator in the staining buffer, EGTA, depletes the extracellular calcium, opening junctional complex, allowing the VE-cadherin antibody we used to reach the external VE-cadherin epitope in the adherens junctions (Stuart et al., 1994). Note that cells were only permeabilised after staining and fixation, limiting the live-cell staining to the external portion of the VE-cadherin in hCMEC/D3.

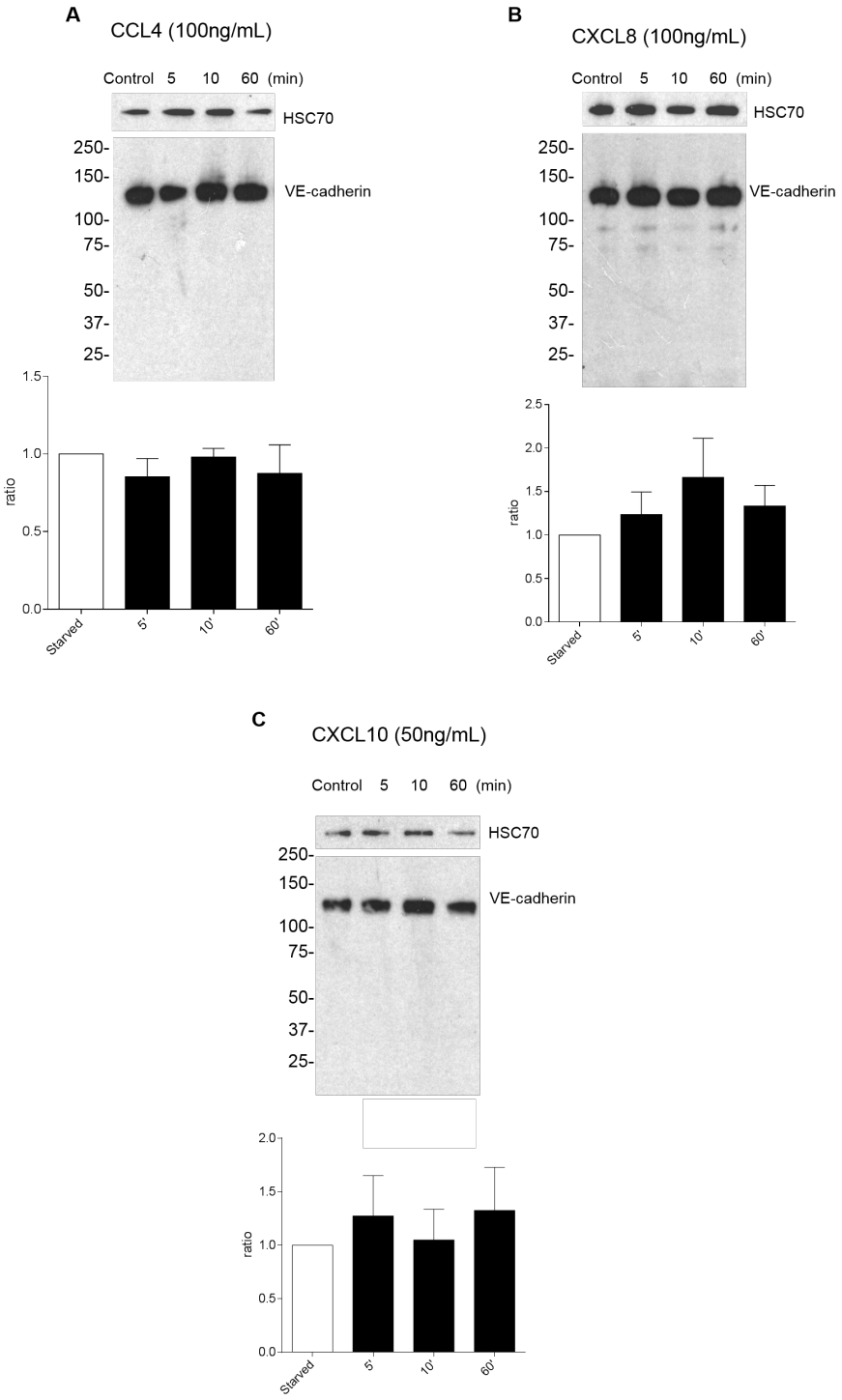

Figure 41 VE-cadherin protein expression following chemokine treatments. (A) CCL4 (100ng/mL), (B) CXCL8 (100ng/mL), (C) CXCL10 (50ng/mL). HCMEC/D3 were grown to confluency, serum-starved and treated with chemokines for 5, 10 and 60 min. Lysates were prepared and analysed by immunoblotting as described in Material and Methods. Densitometry quantification of 4 experiments, represented as a fold increase changes in VE-cadherin in relation to control +/-SEM. Variances of mean values were statistically analysed by One-way ANOVA with Dunnet's post hoc test. Data statistically not significant. $P<0.05$

Using this approach, stimulation of hCMEC/D3 with CCL4 resulted in a significant decrease in VE-cadherin staining at 10 (0.8-fold), 30 (0.7-fold) and 60 (0.7-fold) min when compared to control VE-cadherin levels. This decrease was especially significant at 30 and 60 min post treatment (**Figure 43**). These observations reflect the same pattern that was found with CCL4 (**Figure 39**) where no EGTA epitope unmasking was used but the loss of signal followed the same pattern, suggesting that CCL4 treatment does not lead to epitope masking.

The treatment of hCMEC/D3 with CXCL8 resulted in a significant reduction in VE-cadherin expression at 5 and 60 min (0.7 and 0.6-fold respectively) (**Figure 44**). These results are in line with what was observed in **Figure 40** where a pronounced effect of CXCL8 in VE-cadherin staining was observed.

Stimulation of hCMEC/D3 with CXCL10 also resulted in significant reduction in VE-cadherin staining at 5 and 30 min post stimulation (decrease of 0.6-fold at both timepoints) (**Figure 45**). These results are similar to those reported in **Figure 41**.

Overall, a stronger decrease of VE-Cadherin expression at the junctions was observed with the first protocol used but this effect is still significant when using EGTA. Therefore, it appears that CCL4, CXCL8 and CXCL10 treatments result in a true reduction of junctional VE-cadherin signal, even when the epitope is exposed using EGTA.

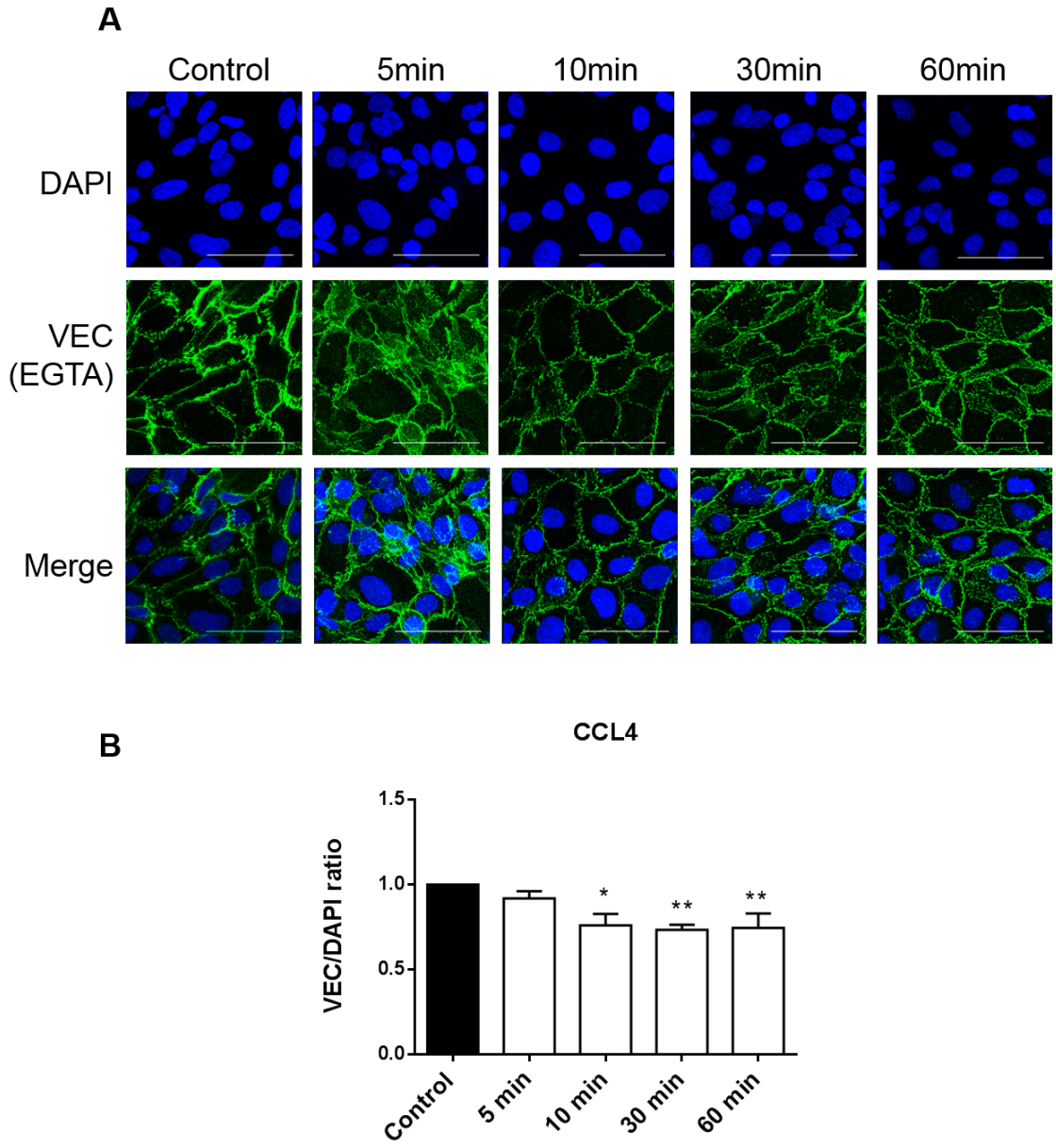

Figure 42 VE-cadherin expression following CCL4 treatments for 5, 10, 30 and 60 min. Confluent hCMEC/D3 were treated with CCL4 (100ng/mL) for the above mentioned timepoints, stained for the extracellular epitope, as detailed in Material and Methods. Z stacks were taken on Zeiss LSM 700 using a 63x objective. The ratio of extracellular VE-cadherin/DAPI was calculated using Image J. Statistical analysis performed using a One-way ANOVA and Dunnet post hoc test. *, P≤0.05; **, 0.001<P<0.01. Scale bar: 50µm. Representative image of n≥3.

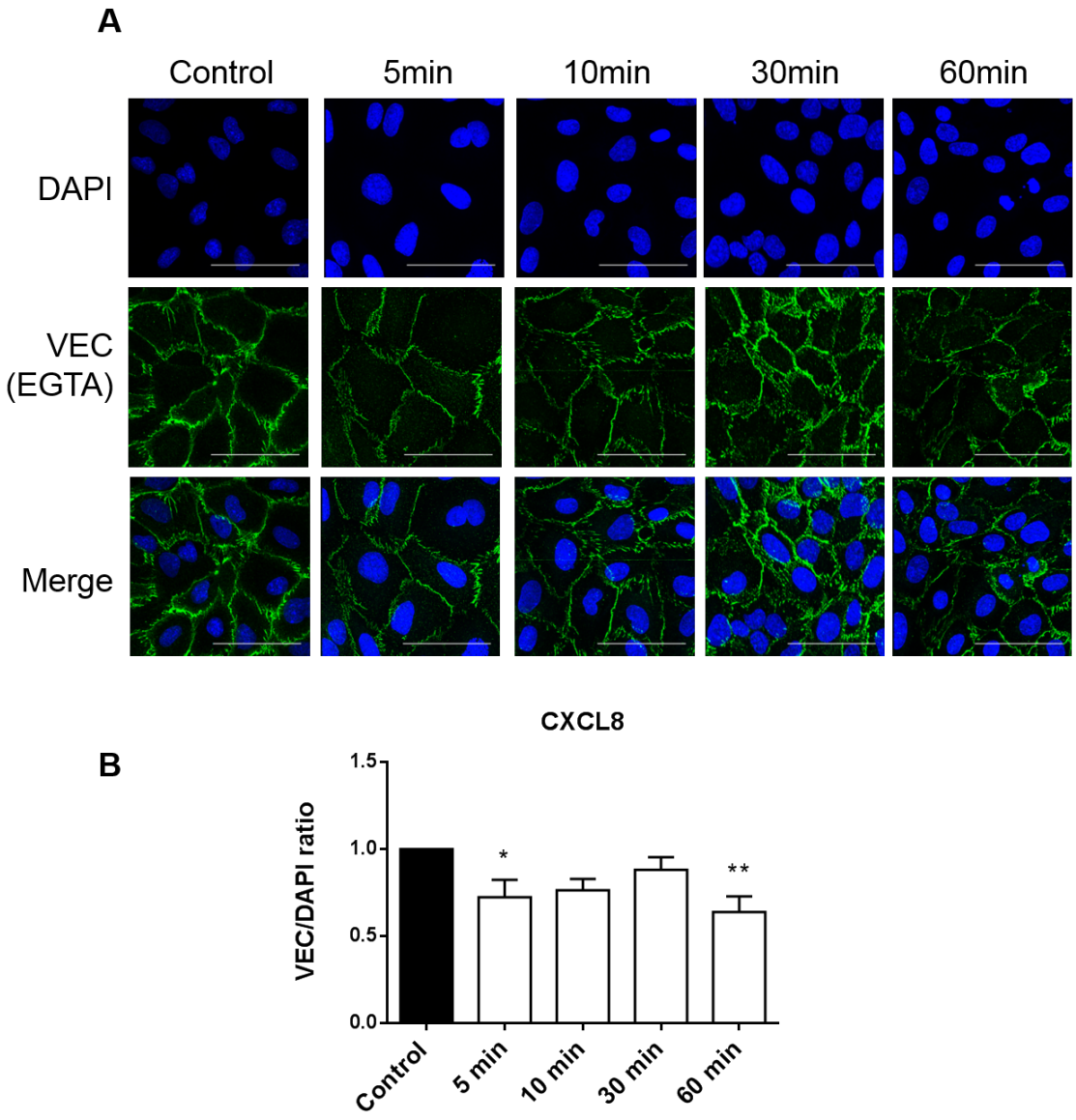

Figure 43 VE-cadherin expression following CXCL8 treatments for 5, 10, 30 and 60 min. Confluent hCMEC/D3 were treated with CXCL8 (100ng/mL) for the above mentioned timepoints, stained for the extracellular epitope, as detailed in Material and Methods. Z stacks were taken on Zeiss LSM 700 using a 63x objective. The ratio of extracellular VE-cadherin/DAPI was calculated using Image J. Statistical analysis performed using a One-way ANOVA and Dunnet post hoc test. *, P≤0.05; **, 0.001<P<0.01. Scale bar: 50µm. Representative image of n≥3.

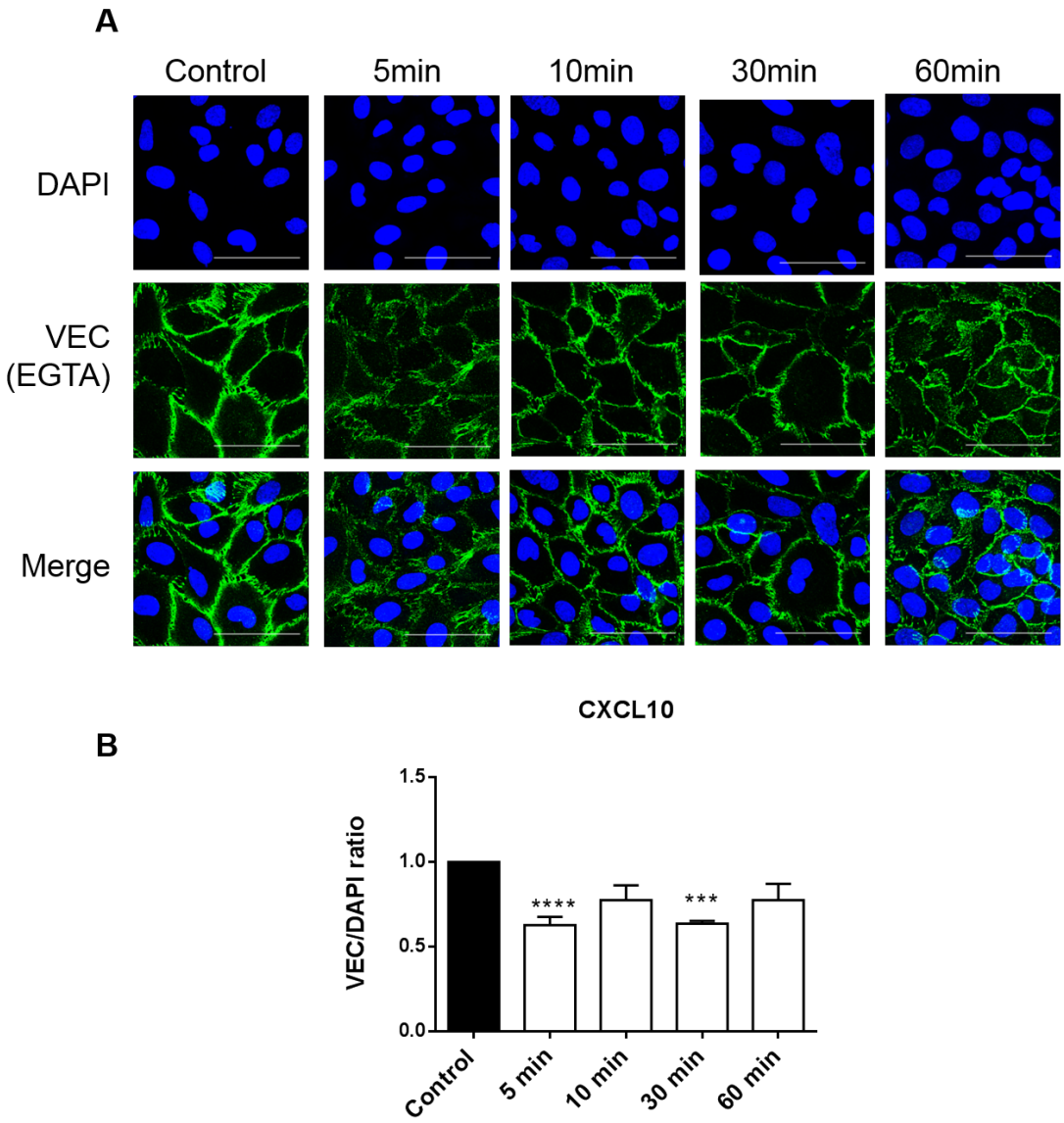

Figure 44 VE-cadherin expression following CXCL10 treatments for 5, 10, 30 and 60 min. Confluent hCMEC/D3 were treated with CXCL10 (50ng/mL) for the above mentioned timepoints, stained for the extracellular epitope, as detailed in Material and Methods. Z stacks were taken on Zeiss LSM 700 using a 63x objective. The ratio of extracellular VE-cadherin/DAPI was calculated using Image J. Statistical analysis performed using a One-way ANOVA and Dunnet post hoc test. ***, P ≤ 0.001 Scale bar: 50µm. Representative image of n≥3.

4.3.5 Expression of extracellular and total VE-cadherin following chemokine treatments

Pro-inflammatory stimuli, including the chemokine CXCL8 have been implicated in VE-cadherin internalisation and a subsequent effect on endothelial permeability (Gavard, 2014). The previous results suggest that CCL4 and CXCL10 treatment of hCMEC/D3 also induce a significant reduction in junctional VE-cadherin immunostaining, even when the epitope is exposed using EGTA.

Since there was no change in the overall amount of protein, we investigated changes in the immunofluorescent signal of the extracellular portion of VE-cadherin versus the total VE-cadherin in brain ECs following chemokine treatments. Two VE-cadherin antibodies were used in this experiment: the first to stain the “plasma membrane” VE-cadherin (R&D systems antibody in Materials and Methods), the antibody used in the previous experiments that recognizes an “extracellular” epitope and the second, an antibody that recognizes an intracellular epitope, that we used to stain total cellular VE-cadherin (Santa Cruz Biotechnology, antibody in Materials and Methods) in permeablised cells. The staining method for the first antibody (live-cell staining on ice) ensured that we only stained plasma membrane and not internalised VE-cadherin. The second antibody, is an antibody that recognizes an intracellular epitope, staining for extracellular and intracellular VE-cadherin in fixed and permeabilised cells – staining all VE-cadherin molecules in the ECs. It is important to point out that under these conditions this second antibody stains both “plasma membrane” and “intracellular” VE-cadherin. Please refer to Page 71 for full protocol details.

We hypothesised that following chemokine treatments there was internalisation of VE-cadherin or, possibly, that there were changes in the availability of the epitopes recognized by the antibodies used, causing significant differences in the

immunofluorescent signal. Note that the staining shown in the previous section (**Figure 43**-**Figure 45**) would be comparable with the "plasma membrane" epitope (green channel), since both protocols live-cell staining of hCMEC/D3 in EGTA enriched buffer prior to fixation. For all chemokines tested, there was a visible difference (quantification not shown) in the signal of both antibodies at control levels. This could indicate an overall difference in the availability of the epitopes or affinity of the antibody at baseline. The pixel quantification was calculated and expressed as a ratio for both antibodies. This allowed the statistical analysis of the two antibody signals following treatments, taking into account the differences seen at control levels.

Expression of extracellular and total VE-cadherin in CCL4 treated hCMEC/D3

Treatment of hCMEC/D3 with CCL4 resulted in a significant difference in signal at 30 and 60, when comparing the total protein and the extracellular portion epitopes (**Figure 46**-A). Note that the extracellular epitope antibody (green) is the same as used previously. This difference in signal between two antibodies that recognize the same protein, could indicate a difference in the availability of the epitope following treatments or an increase in intracellular signal. Despite the use of EGTA in the live-cell staining, the signal of the extracellular epitope of VE-cadherin (membranar VE-cadherin) was significantly lower than the total VE-cadherin, supporting the hypothesis that there is a loss of VE-cadherin at the junctions following CCL4 treatment and an increase of total VE-cadherin, possibly to the intracellular compartment. Upon analysis of co-localization of signal, there was a significant decrease in the percentage of overlap of the two VE-cadherin channels. A reduction in the extracellular VE-cadherin is visible whilst the total VE-cadherin shows additional staining bordering/overlapping the junctions (yellow shade at the junctions and red signal in cytoplasm). This suggests an internalisation of the molecule, or alternatively, an increase in affinity to the antibody that binds to the intracellular epitope (**Figure 46**-B).

Expression of extracellular and total VE-cadherin in CXCL8 treated hCMEC/D3

Treatment of hCMEC/D3 with CXCL8 resulted in a significant difference in staining levels of the extracellular and total VE-cadherin at 5 and 60 min, following a pattern that is in line with our previous results. There is an increase in total VE-cadherin but not membranar protein, suggesting that this increase is due to increased internal VE-cadherin (**Figure 47**- A).

The overlap of signal of the two antibodies against VE-cadherin was then calculated. Interestingly, there was a decrease in the overlap of the two channels at 5 and 30 min post treatment but not at 10 or 60 min post treatment (**Figure 47**-B).

Expression of extracellular and total VE-cadherin in CXCL10 treated hCMEC/D3

CXCL10 treatments resulted in an increase in the membrane to total VE-cadherin ratio at all timepoints tested. There was an increase in total protein with a marked decrease of membranar VE-cadherin at early timepoints – suggesting, once more a shift towards VE-cadherin internalisation. The increase was significantly different to the total VE-cadherin signal (**Figure 48**-A). At 30 and 60 min following treatments, there was a significant decrease in the co-localization in the channels of the two VE-cadherin antibodies. This result suggests that an increase in intracellular VE-cadherin at these timepoints (**Figure 48**-B).

In summary, there was significant difference in the total/membranar VE-cadherin for all chemokines studied and an increase in intracellular VE-cadherin signal following chemokine treatments. Taken together, these results suggest an internalisation of VE-cadherin upon treatment with these chemokines.

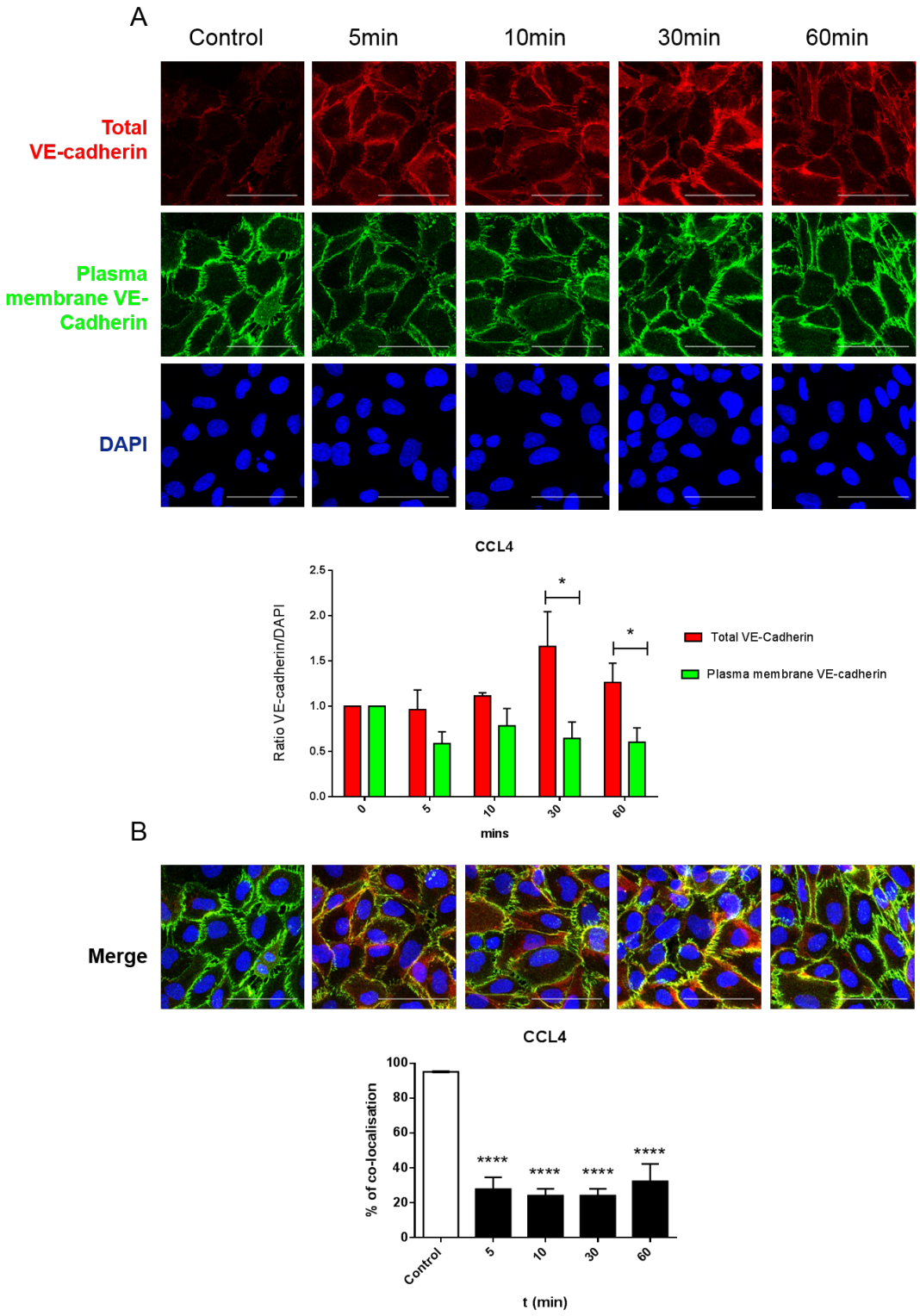

Figure 45 VE-cadherin distribution (intracellular epitope and extracellular epitope) following CCL4 treatments. Z stacks were taken on Zeiss LSM700 using a 63x and a 10x objective. (A) Pixel count of both VE-cadherin antibodies, normalised to DAPI. Student t test comparing the two channels per timepoint (B) JACoP plugin on image J was used to calculate the coefficient between the red/green channels for pixel co-localization between the two channels in 10x images. Statistical analysis performed using a One-way ANOVA and Dunnet post hoc test. *, P≤0.05, ****, P<0.0001. Scale bar: 50µm. Representative image of n≥3.

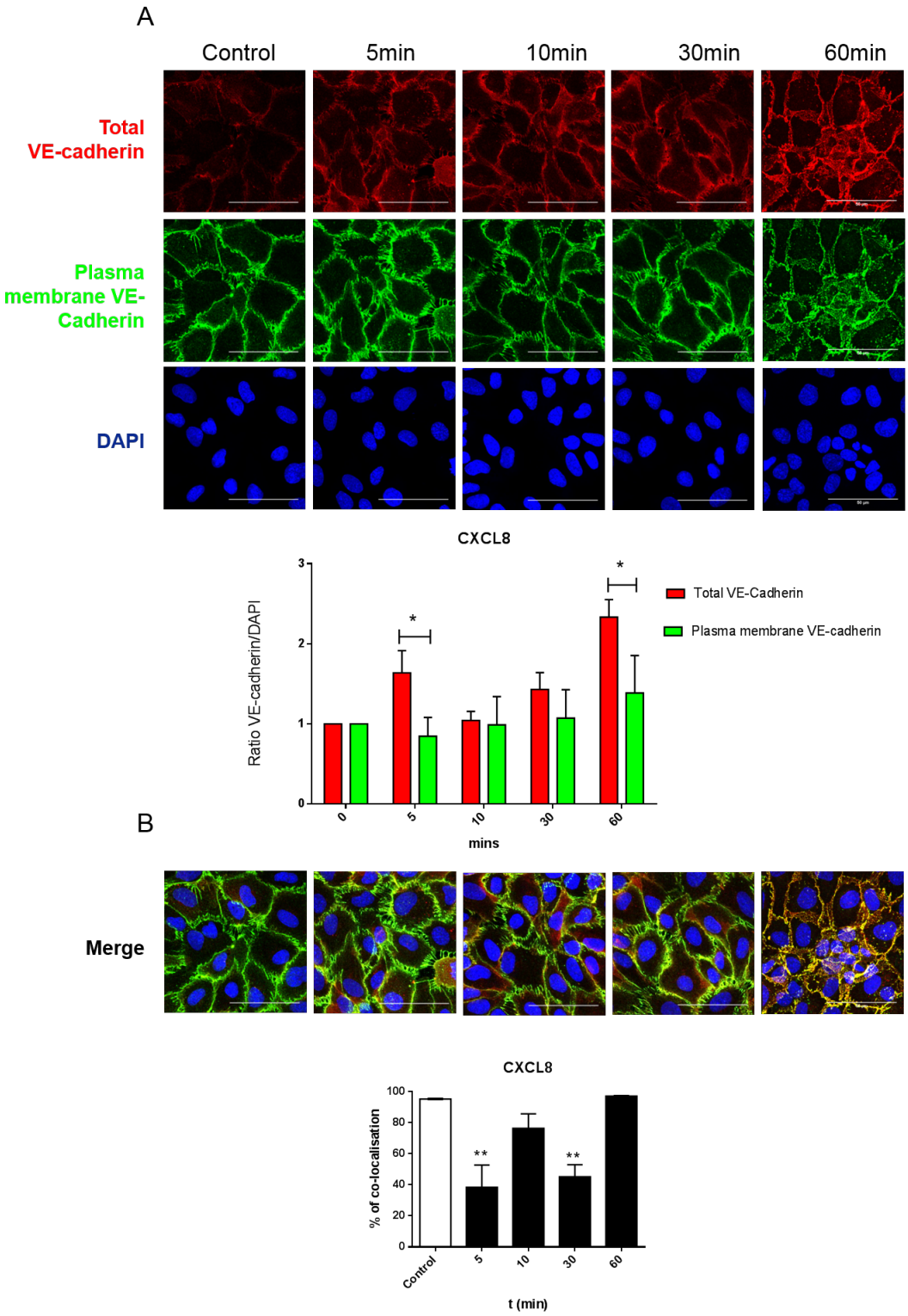

Figure 46 VE-cadherin distribution (intracellular epitope and extracellular epitope) following CXCL8 treatments. (A) Pixel count of both VE-cadherin antibodies, normalised to DAPI. Student t test comparing the two channels per timepoint (B) JACoP plugin on image J was used to calculate the coefficient between the red/green channels for pixel co-localization between the two channels in 10x images. Statistical analysis performed using a One-way ANOVA and Dunnet post hoc test. *, P≤0.05, Scale bar: 50µm. Representative image of n≥3.

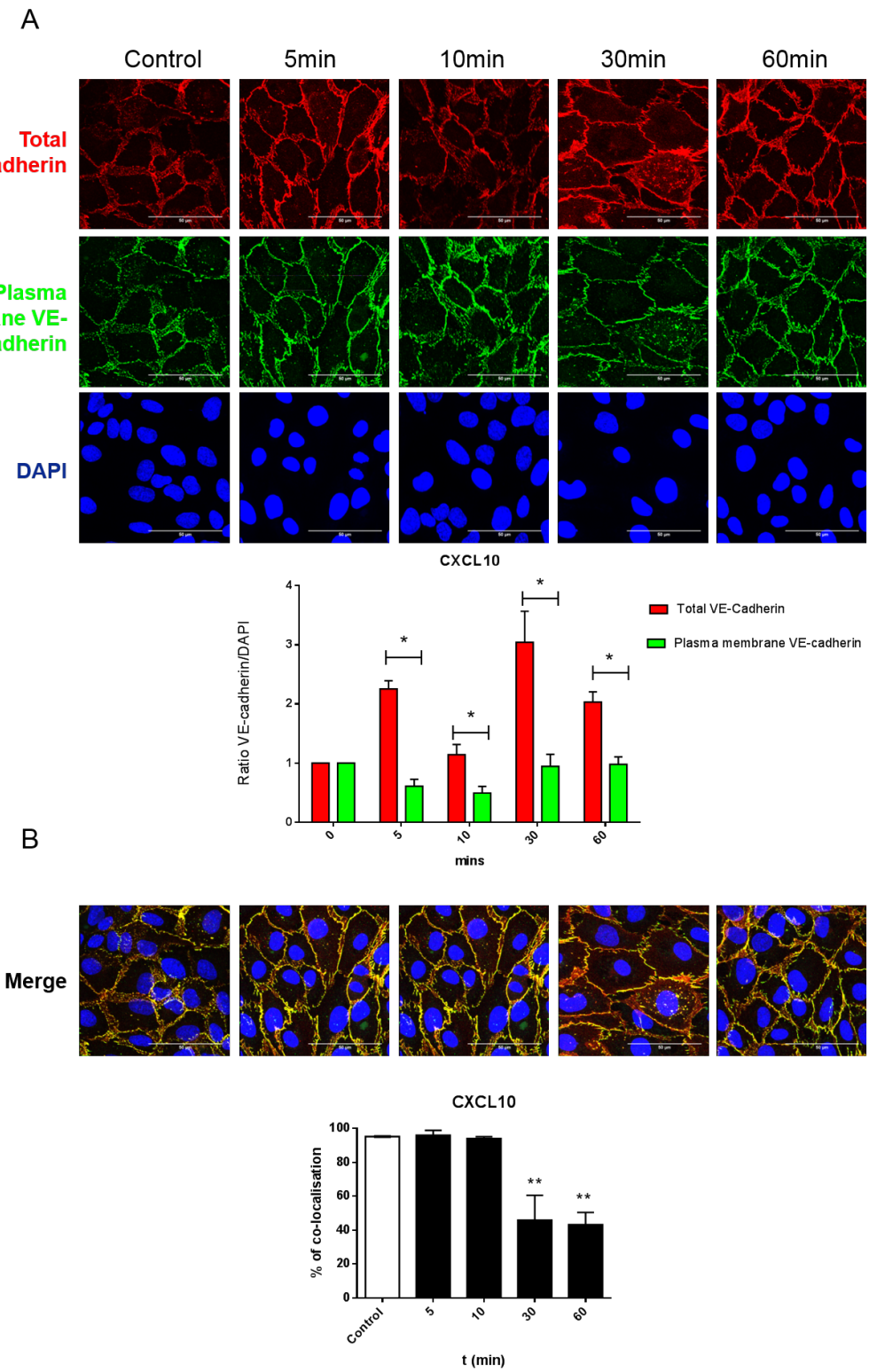

Figure 47 VE-cadherin distribution (intracellular epitope and extracellular epitope) following CXCL10 treatments. (A) Pixel count of both VE-cadherin antibodies, normalised to DAPI. Student t test comparing the two channels per timepoint (B) JACoP plugin on image J was used to calculate the coefficient between the red/green channels for pixel co-localization between the two channels in 10x images. Statistical analysis performed using a One-way ANOVA and Dunnet post hoc test. *, P≤0.05, **, 0.001<P<0.01. Scale bar: 50µm. Representative image of n≥3.

4.3.6 Filamentous actin response in chemokine treated EC

VE-cadherin is anchored to the cytoskeleton via catenins and vinculin (Hirase et al., 1997). A recent report has shown that VE-cadherin, upon stimulation by thrombin, increasingly associates with the cytoskeleton, resulting in increased permeability (Huveneers et al., 2012). Since there was an obvious effect of chemokines on VE-cadherin distribution, we investigated possible downstream effects on the cytoskeleton.

In CCL4 treated hCMEC/D3, there was a significant induction of stress fibres at 5, 10 and 30 min following chemokine treatment. However, the amount of stress fibres returned to near control levels by 60 min (**Figure 49**-A). Upon examination of the 10x images, it becomes obvious that there was formation of stress fibres at 5, 10 and 30 min post treatment (**Figure 49**-B).

Following CXCL8 treatments, there was a different response to that observed with CCL4 treatments. Activation of actin stress fibres increased after 5 min, became significant at 10 min post treatment and returned to control levels after 30 min (**Figure 50**-A). In the 10x fields a trend of an increase at 5 and 10 min in F-actin signal was observed (**Figure 50**-B).

Similarly to CCL4, CXCL10 treatments rapidly induced stress fibres at 5 and 10 min post treatment returning to control levels at the subsequent timepoints (**Figure 51**-A). Upon statistical analysis, the increase at 5 and 10 minutes was significant. When observing the 10x fields there seems to be a higher level of F-at all treatment timepoints than control (**Figure 51**-B).

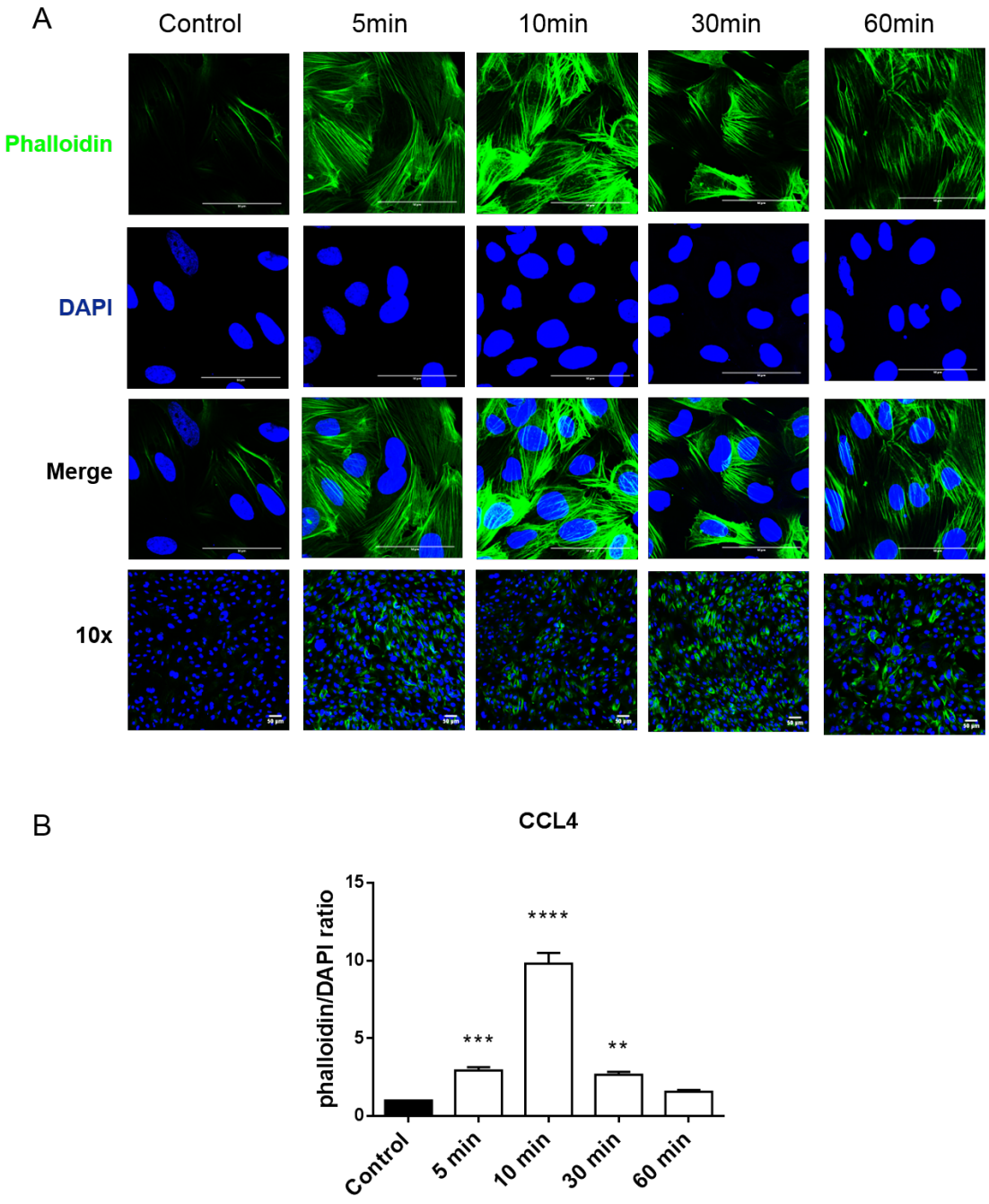

Figure 48 F-actin distribution following CCL4 treatments for 5, 10, 30 and 60 min. Confluent hCMEC/D3 were treated with CCL4 (100ng/mL) for the above mentioned timepoints, fixed and stained for IHC as detailed in Material and Methods. (A) Representative images were taken on Zeiss LSM 700 using a 63x and a 10x objective (B) 63x images analysis. Mean area average +/- SEM of phalloidin area/DAPI, normalized to control. Statistical analysis performed using a One-way ANOVA and Dunnet post hoc test. **, 0.001<P<0.01; ***, P<0.001; ****, P<0.0001.

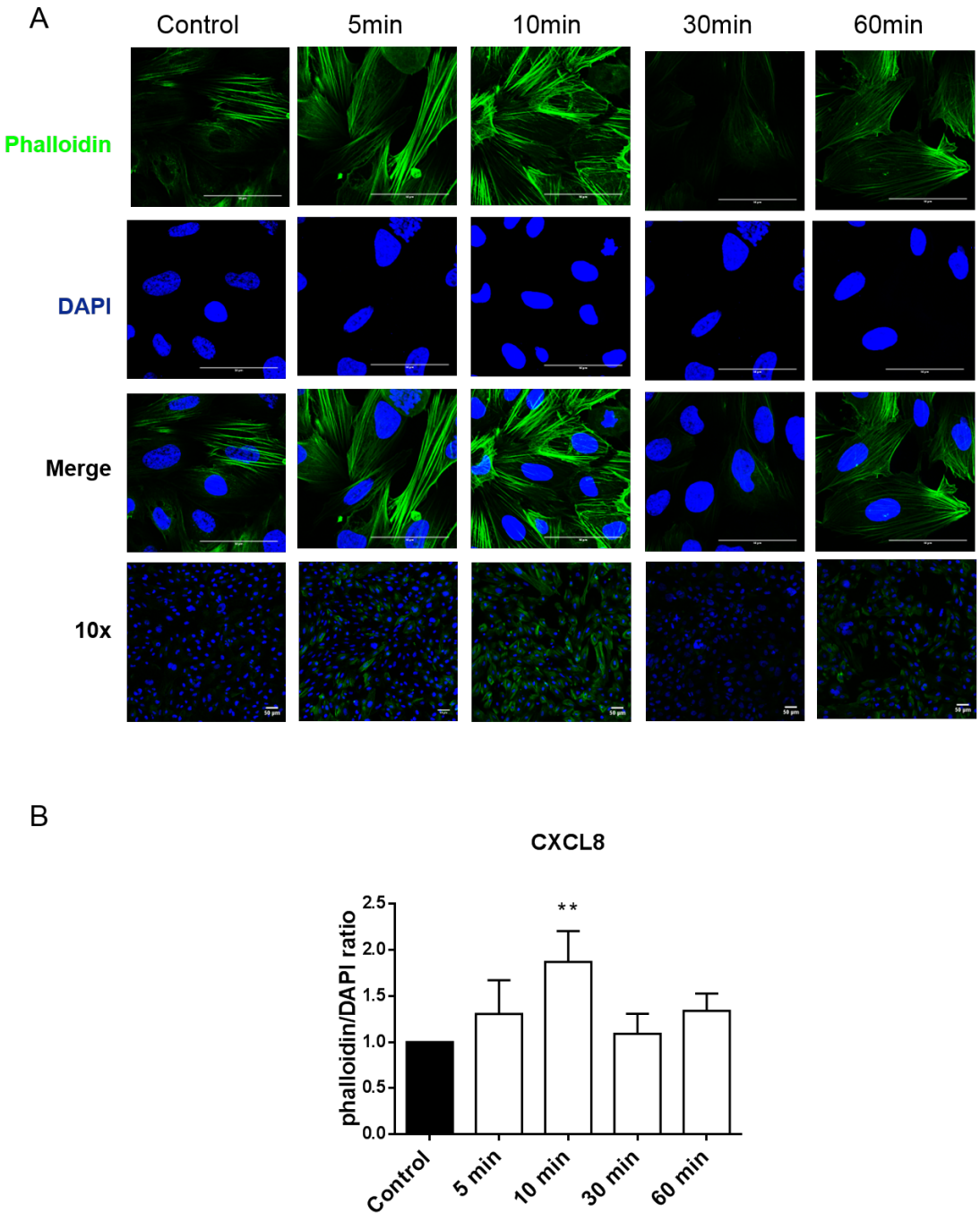

Figure 49 F-actin distribution following CXCL8 treatments for 5, 10, 30 and 60 min. Confluent hCMEC/D3 were treated with CXCL8 (100ng/mL) for the above mentioned timepoints, fixed and stained for IHC as detailed in Material and Methods (A) representative images were taken on Zeiss LSM 700 using a 63x and a 10x objective. (B) 63x images analysis. Mean area average +/- SEM of phalloidin area/DAPI, normalized to control. Statistical analysis performed using a One-way ANOVA and Dunnet post hoc test. **, 0.001<P<0.01.

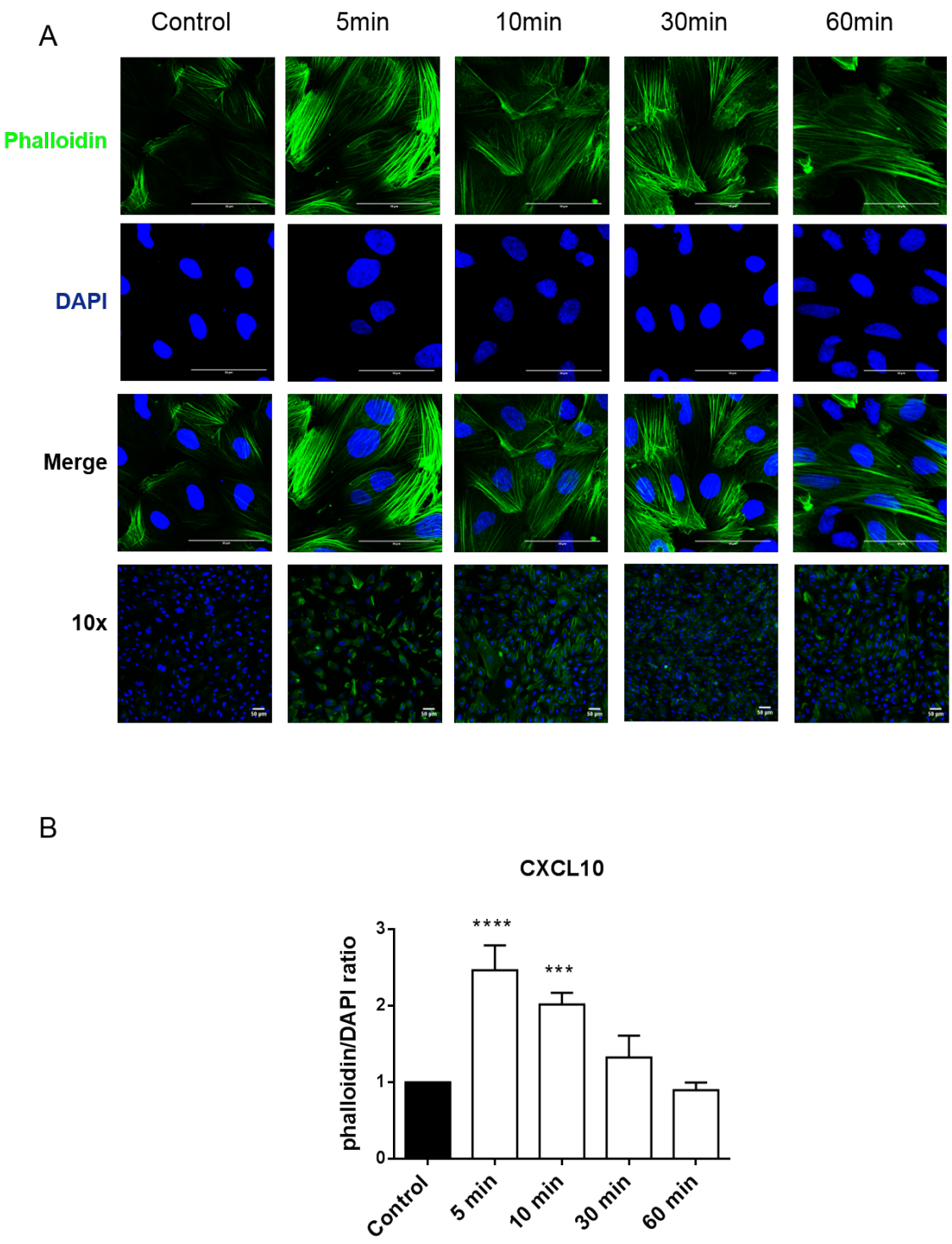

Figure 50 F-actin distribution following CXCL10 treatments for 5, 10, 30 and 60 min. Confluent hCMEC/D3 were treated with CXCL10 (50ng/mL) for the above mentioned timepoints, fixed and stained for IHC as detailed in Material and Methods (A) representative images were taken on Zeiss LSM 700 using a 63x and a 10x objective. (B) Mean area average +/- SEM of phalloidin area/DAPI, normalized to control. Statistical analysis performed using a One-way ANOVA and Dunnet post hoc test. ***, P<0.001; ****, P<0.0001.

4.4 Discussion

Changes in tight junction protein expression and distribution are associated with increased vascular permeability and leukocyte extravasation (Wallez and Huber, 2008). The zona occludens proteins (ZO-1, ZO-2 and ZO-3) are markers of tight junctions as well as being components of adherens junctions (Staddon et al., 1995). We started by investigating changes in ZO-1 to gain insight into tight junction destabilization by our chemokines of interest. From our experiments, we could conclude that total ZO-1 expression was unaffected by chemokine treatments, however, the staining pattern was not uniform throughout the culture and there was cytoplasmic staining. This pattern has been reported before in hCMEC/D3 (Biemans et al., 2017). There were slight variations in the level of ZO-1 in the staining analysed, but these were not significant (**Figure 35-Error! Reference source not found.**). Possibly, by looking at the total protein levels, using a protein quantification method such as western blot, there could be a more accurate calculation of the changes in ZO-1 expression since the entirety of the sample could have been considered. Another option to gain insight in the effect of chemokines on ZO-1 would be to test for its phosphorylation at the timepoints studied.

When investigating specifically junctional distribution of ZO-1 there was, interestingly, a strong reduction in signal in the junctions following chemokine treatments. This was particularly evident following CCL4 and CXCL10 treatments. There is precedent for this with other vasoactive molecules such as histamine where a 20% reduction in ZO-1 protein expression has been reported 1h post treatment (Gardner et al., 1996). Our results, therefore, suggest that the chemokines studies are able to induce mobilization of ZO-1 from the junctions and consequently could destabilise the barrier function of brain ECs. This is in line to reports in the literature: it has been previously been reported that CKLF1, a C-C chemokine, is involved in BBB disruption and downregulation of ZO-

1 expression (Kong et al., 2016). This is also consistent with reports that the chemokine CCL2 induces loss of ZO-1, and opening of tight junction in BCEC (Stamatovic et al., 2003, Stamatovic et al., 2009).

The main role of the junctional protein VE-cadherin is to maintain vascular integrity, actin cytoskeleton remodelling and signalling, so we then investigated the effect of our chemokines in this protein (Harris and Nelson, 2010). The loss in VE-cadherin that we initially observed in the junctions supports the hypothesis that our chemokines are able to indirectly destabilise adherens junctions of brain ECs. This is of particular interest as, besides its structural role, VE-cadherin is also involved in leukocyte migration and vascular permeability (Gotsch et al., 1997) (Monica Corada et al., 1999).

Upon protein expression analysis, there was no evidence that there was a change in the total amount of VE-cadherin or any protein cleavage following chemokine treatments (**Figure 42**). Thus, over the time-frame of our experiments protein loss was not the cause of the observed reduction in VE-cadherin staining in our immunocytochemical assays. This does not rule out the possibility that over extended time periods these particular chemokines have an effect on total protein expression. Nevertheless, over the duration of treatments studied it was clear that there is a shift in VE-cadherin distribution within the cells.

We are confident that the changes in junctional VE-cadherin distribution we observed are not due to antibody-induced internalisation of VE-cadherin or to changes in epitope accessibility as the conditions we used (non-permeabilisation at 4^{o}C and in the presence of EGTA) would minimise such artefacts. Subsequently, the data strongly indicated a change in cellular distribution of existing VE-cadherin upon chemokine stimulation. The principle of VE-cadherin internalisation from the junction is not new. Studies have reported that VE-cadherin can be internalised following stimulation with variety of

inflammatory agents. A recent study revealed VEGF-induced VE-cadherin endocytosis within 30 min of treatment, which is one of the timepoints we studied when treated hCMEC/D3 with our chemokines of interest (Gavard and Gutkind, 2006). Another recent publication demonstrated a faster internalisation of VE-cadherin within 5 min of anti-ICAM-1 cross-linking in ECs (Dragoni et al., 2017). In response to LPS and TNFα, two pro-inflammatory agents, VE-cadherin breakdown and loss of barrier properties has been shown within hours in ECs (Flemming et al., 2015). Similarly, VE-cadherin has been shown to undergo endocytosis 24h following stimulation with IL-2, a cytokine involved in immunity (Kim et al., 2014). There is plenty of evidence of VE-cadherin internalisation in an inflammatory mileau, comparable to what we created in our experimental conditions when adding chemokines to ECs, supporting the possibility that VE-cadherin was internalised.

We then tested whether there was a change in VE-cadherin signal using two different VE-cadherin antibodies and, in the same experiment, analysed the co-localisation of the resulting signal. The changes we identified in co-localization of the extracellular and intracellular epitopes of the VE-cadherin antibodies following chemokine treatments strongly suggest an internalization of VE-cadherin. For all the chemokines studied, there was an increase, compared to control, of the total VE-cadherin that did not co-localise with extracellular VE-cadherin (**Figure 46**-**Figure 48**). Alongside these results, there was a decrease in the signal of membranar (junctional) VE-cadherin following treatments, and an increase in the total VE-cadherin signal. All these results point towards the disappearance of VE-cadherin from junctions and an increase in internalised protein.

Many pro-inflammatory mediators, such as thrombin, histamine and VEGF are also pro-permeability mediators (Gavard, 2014). VE-cadherin redistribution from junctions in hyperpermeable areas was seen following TNFα and IFNγ administration in rats (Wong et al., 1999). Therefore, chemokine treatments of hCMEC/D3 could induce VE-cadherin

internalisation, consistent with not only the loss of VE-cadherin at junctions but also the loss of junctional ZO-1. A potential functional outcome of this is an increase in vascular permeability.

The actin microfilament system is linked to junctional proteins including VE- and E-cadherin, occludin and ZO proteins (Stamatovic et al., 2008). In quiescent cells, actin interacts with cell-cell and cell-matrix complexes, contributing to the maintenance of the endothelial barrier. VE-cadherin and the cytoskeleton association can be increased with the addition of receptor-mediated pathways (such as thrombin, a strong inflammatory mediator) or non-receptor mediated mechanisms, such as EGTA that breaks the cadherin-cadherin bonds by removing extracellular calcium (M. J. Lim et al., 2001). Pro-inflammatory agents are known to disturb the cortical actin and increase endothelial permeability (Prasain and Stevens, 2009). The actin microfilament is also involved in actin stress fibre formation in ECs resulting in an increase in BBB permeability (Wong et al., 1983, Shiu et al., 2007). Another permeability inducing agent, thrombin, has also shown to induce shape changes and gap formation in ECs, due to reorganization of actin microfilaments (Laposata et al., 1983). In our experiments, there was a significant induction of stress fibres in chemokine treated hCMEC/D3 (**Figure 49**-**Figure 51**). This was especially evident in CCL4 and CXCL10 treated cells (**Figure 50**-**Figure 51**) where the observed stress fibre formation could be involved in VE-cadherin internalisation and decrease in junctional ZO-1 expression.

CCL4, CXCL8 and CXCL10 treatments of hCMEC/D3 have shown to alter ZO-1 and VE-cadherin membranar distribution but not protein expression, with strong evidence of VE-cadherin internalisation. These events coincide with stress fibre induction (Table 8). Bringing the ZO-1, VE-cadherin and cytoskeleton results together, they are supportive of increased paracellular permeability. In epithelial cells, ZO-1 disruption and stress fibre formation resulted in increased paracellular permeability (Youakim and Ahdieh, 1999).

The results obtained in hCMEC/D3 could ultimately translate into functional outcomes in barrier function, both at level of paracellular permeability and passage of macromolecules or cells.

Table 8 Summary of chapter 4 – Key findings in hCMEC/D3

	Experiment	CCL4	CXCL8	CXCL10	Observations
Chapter 4	ZO-1 expression	-	-	-	No changes in ZO-1 expression in IF.
	ZO-1 distribution	+++ (10', 60')	+ (10')	+ (10', 60')	
	VE-cadherin distribution	+ (60')	+++ (5'), +/++ (10', 60')	+++ (5', 60')	
	VE-cadherin distribution (EGTA)	+ (5'), ++ (30', 60')	+ (5'), ++(60')	+++ (5', 30')	Expected to follow pattern above.
	VE-cadherin protein expression	-	-	-	No shedding or cleavage (>25 kDa).
	VE-cadherin membranar/total ratio	+ (30', 60')	+ (5', 60')	+ (5', 10', 30', 60')	
	VE-cadherin internalisation	++++ (5', 10', 30', 60')	++ (5', 30')	++ (30', 60')	
	F-actin - stress fibres induction	+++ (5', 30'), ++++ (10')	++ (10')	++++ (5'), +++(10')	

5. Effects of chemokines on barrier function

5.1 Introduction

The hallmarks of BBB dysfunction, increased vascular permeability and, in the case of inflammatory conditions, increased leukocyte migration into the brain are associated with tight junction destabilization. Although not part of the TJ, VE-cadherin destabilization in adherens junctions has been strongly connected with these hallmark features (Benn et al., 2016) (Engelhardt and Wolburg, 2004, Akers et al., 2010, Gavard, 2014). In contrast, stabilization of the VE-cadherin/catenin complex was shown to hinder permeability and leukocyte extravasation (Schulte et al., 2011).

Several compounds have been shown to alter the permeability of EC monolayers. Amongst these compounds, VEGF, thrombin and LPA, have been widely studied and reported to significantly increase permeability of vascular barriers (Ehringer et al., 1996). VEGF is a powerful permeability inducing agent also involved in EC migration, angiogenesis and regulation of pericytes and matrix metalloproteinases. Another agent, thrombin, disengages the cell-cell junctions by altering VE-cadherin distribution and destabilizing the VE-cadherin/catenin complex (Rabiet et al., 1996) (Bae et al., 2009). Another widely studied compound, LPA, has been shown to increase permeability in brain capillary ECs, showing a rapid, reversible and dose-dependent decrease in the TEER of these cells. LPA treatment of brain EC caused a surge in the flux of the tracer sucrose, suggesting that the decrease in barrier function due to increase in permeability in TJs (Schulze et al., 1997).

Chemokines, potent pro-inflammatory meditators have also been suggested to be involved in vascular permeability and leukocyte transendothelial migration (Speyer C., 2011). There are numerous reports in the literature of chemokine's involvement in leukocyte migration in the brain. CCL3, a chemokine closely related to CCL4, is involved in dendritic cell transmigration into the CNS through BBB microvessel endothelial cells (Zozulya et al., 2006). CCL2, from the same subfamily as CCL4, has also been strongly implicated in CNS inflammation and increased permeability, disrupting adherens junctions (Dimitrijevic et al., 2006, Vukic et al., 2009, Roberts et al., 2012). Similarly, another study demonstrated that CCL4 and CCL5 enhance adhesion of CD4+ T cells to activated brain ECs (Quandt and Dorovini-Zis, 2004). Additionally, the receptor CCR2, expressed in EC, is involved in leukocyte migration through the BBB (Dzenko et al., 2001).

In a non-CNS context, chemokine CXCL8 has been shown to induce permeability in endothelial cells, inducing gaps in F-actin and downregulation of tight junction proteins, including ZO-1 (Yu et al., 2013). CXCR2, a receptor for CXCL8 has also been implicated in acute and chronic vascular permeability (Gavard et al., 2009). CXCL8, has been shown to increase leukocyte recruitment to cerebrovascular endothelium, in a BBB model using hCMEC/D3 (Omatsu et al., 2014). In MS patients, CXCL8 and CXCL10 are upregulated in MS lesions, suggesting a potential involvement in other inflammatory responses in the CNS (Subileau et al., 2009). Another chemokine of interest, CXCL10, has been shown to be involved in natural-killer cell migration and increased permeability of the BBB in ischemia (Zhang et al., 2014). In rabies, the production of CXCL10 by neurons induces recruitment of CD4+ T cells into the CNS and leads to a reduction of TJ proteins and an enhancement of BBB permeability (Gnanadurai and Fu, 2016)

This evidence suggests that chemokine signalling in the BBB endothelium, specifically, CCL4, CXCL8 and CXCL10 could be involved in downstream effects in permeability to

macromolecules and immune cells and ultimately in the onset and progression of neuroinflammatory conditions.

Tight junctions also allow the existence of a high transendothelial electrical resistance (TEER) of 1500–2000 Ω.cm2 at the BBB when compared to other organs (human placenta endothelial cells present a TEER of 22–52 Ω.cm2) (Huber et al., 2001). The staggering difference in TEER correlates positively with tight junction strand number and complexity in different organs (Holman et al., 2011).

Measurement of EC barrier permeability

Several *in vitro* methods have been developed to study the EC barrier permeability to water, macromolecules and small inorganic ions. One of the most widely used methods is the measurement of flux of a fluorescent or radio-labelled tracer with known molecular weight, coupled with an organic molecule (usually a fluorescent labelled-dextran) (Srinivasan et al., 2015). A monolayer of ECs is cultured on a filter between two fluid compartments and the rate of transport of the tracer from the donor (upper) compartment to the acceptor (lower) compartment in response to a certain stimulus is calculated by sampling the second compartment over predetermined periods of time (**Figure 52**-A).

Transendothelial electric resistance (TEER) is another method of measuring the effect on permeability of a compound on cells grown on a matrix. This method detects changes in paracellular permeability, with disengagement of intercellular junctions of ECs. The barrier properties can be monitored in real-time and at high sensitivity. TEER establishes, under Ohm's law, that the resistance of the EC monolayer can be measured by its permeability to ions. This is valid providing that the resistance reading of a cell-free filter/well is subtracted and that the resistance is multiplied by area in cm^2 of the filter/well used (Srinivasan et al., 2015).

When using a constant current source and voltmeter (chopstick system), due to the lack of a consistent electric resistance throughout the monolayer, the TEER measurements can be overestimated and the cell polarity might be altered due to the direct current (DC) being applied to the cells. For this reason, TEER measurement with DC cannot be used for real-time monitoring (Wegener and Seebach, 2014).

Impedance spectroscopy measurements allow the real time measurement of the electrical properties of an endothelial monolayer using an alternating current (AC). The

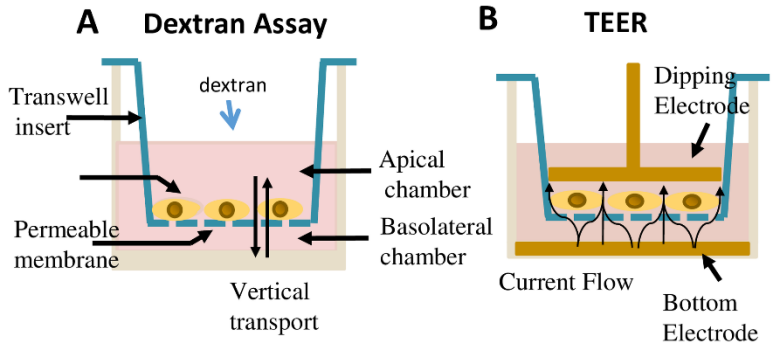

Figure 51 Dextran assay and TEER method for permeability changes assessment (adapted from (Ni, 2017 #2166)).

total impedance obtained using this method contains information about TEER and capacitance of the cell layer. The electrical current can take either a paracellular or transcellular pathway: in the paracellular pathway the junctional proteins represent the ohmic resistance (TEER) and in the transcellular pathway it is a composite of the resistance of the membrane and the electric capacitance of the cell layer. Resistance represents the function and integrity of the barrier (including the resistance to paracellular and transcellular flow) and capacitance provides a measurement of coverage of electrode by cells. Thus, resistance is a measure of barrier quality and excludes capacitance contributions from membrane, electrode and medium and translates into the ability of cells to resist to the electric flow (Benson et al., 2013) (Szulcek et al., 2014).

The electric cell-substrate impedance sensing (ECIS) system allows the growth of cells in transwells (where an upper and lower fluid compartment are created); or on coplanar gold-film electrodes (where only an upper fluid compartment exists), and measures impedance and a function of frequency (**Figure 53**-B). The gold-film electrodes present, in comparison to filters present two advantages: the cells can be visualised under a light microscope, and can be used to monitor single cell changes (instead of large populations of hundreds of cells which can be more heterogeneous) (Wegener and Seebach, 2014).

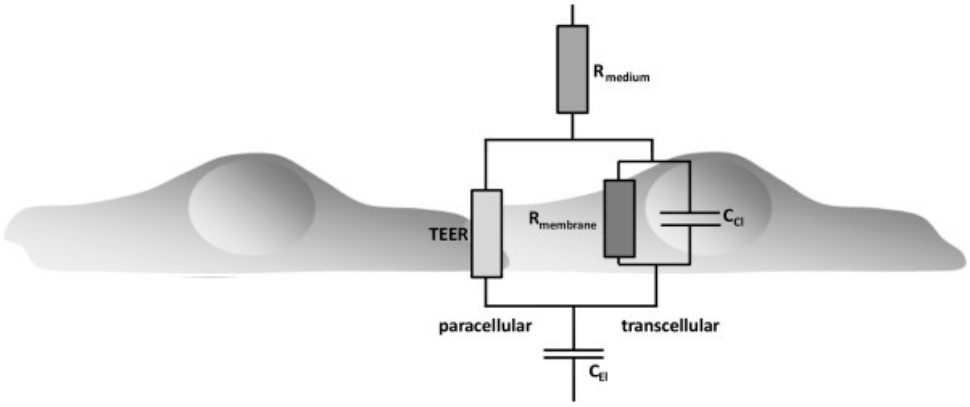

Figure 52 Contribution of the transcellular and paracellular pathways to total impedance in a monolayer. TEER – transendothelial resistance, C_E – capacitance of electrodes, C_{Ci} – capacitance of cell layer, R_{medium} – ohmic resistance of the medium, $R_{membrane}$ – ohmic resistance of the membranes (Benson et al., 2013).

5.2 Aims

In the previous chapter, we have shown that CCL4, CXCL8 and CXCL10, to different degrees, alter the distribution of VE-cadherin and ZO-1 in hCMEC/D3 and induce cytoskeleton changes (stress fibres induction). These effects were seen within 60 min of chemokine treatments. These results led us to draw our attention on two outcomes of junction destabilization: permeability to macromolecule and lymphocyte migration. To assess these outcomes, we focused on the passage of macromolecules and

lymphocytes across our BBB model. Finally, we studied the *in vivo* effect of CCL4 injections on the permeability of the BBB and BRB.

5.3 Results

5.3.1 Assessment of absolute permeability coefficient of hCMEC/D3

Macromolecules of various sizes, such as albumin or dextrans, conjugated to a fluorescent probe (e.g., FITC or TRITC), can be used to measure changes in microvascular leakage in cultured ECs (Siflinger-Birnboim et al., 1987). In order to perform permeability studies using our BBB model and compare our results to the existing literature on hCMEC/D3, it was necessary to establish a permeability coefficient (Pe) for the hCMEC/D3 in our lab. Despite the existence of several studies in the literature that report the Pe for hCMEC/D3, this coefficient can vary for the same cell line and depends of factors such as passage number and growth media used (Volpe, 2008, Oltra-Noguera et al., 2015).

The differences in the permeability values found for the slopes for hCMEC/D3 (Pe) and filters (Pf) to the dextrans tested were highly statistically different, meaning that a hCMEC/D3 barrier against the dextrans was formed (**Figure 54**-A). Upon analysis, the mean permeability coefficient of 4 kDa was $0.92x10^{-3}$ cm/min (SEM +/- 0.0057), 70 kDa was $0.12x10^{-3}$ cm/min (SEM +/- 0.0002) and 250 kDa was $0.02x10^{-3}$cm/min (SEM +/- 0.0013) (**Figure 54**-B). The permeability to 4 kDa dextran was considerably higher than to the other dextrans tested, suggesting that the barrier formed was rather weak (**Figure 54**-C and D).

5.3.2 Effect of chemokines on transendothelial flux of dextrans across hCMEC/D3

To test whether our specific chemokines CCL4, CXCL8 and CXCL10 altered barrier properties, resulting in changes in the paracellular permeability to dextrans, the flux of three different sized dextrans coupled to a fluorescent molecule was measured for at least 90 min.

A positive control, thrombin, was selected due to its acute effect on permeability. Accordingly, it has been shown that the transient effect (over 30 minutes) of thrombin-induced increase in EC permeability results in an increase of passage of a 40 kDa dextran and peroxidase, and a decrease of transendothelial electrical resistance (TEER) to around 80% of basal values (Amerongen et al., 1998). Thrombin treatment leads to the formation of intercellular gaps and release of inflammatory mediators, growth factors and other agents (Laposata et al., 1983, Thomas et al., 2017).

Treatment of hCMEC/D3 with thrombin and chemokines did not result in significant changes in the transendothelial passage of 4kDa FITC dextran. In contrast, thrombin, increased the transendothelial flux of 70 kDa RITC dextran across the hCMEC/D3 monolayer by 1.6-fold (**Figure 55**-A). The chemokines CCL4 and CXCL10 also induced a significant increase in the flux (1.4 and 1.3-fold, respectively) of 70 kDa dextran. CXCL8 resulted in a mean increase comparable to the effect of CCL4 but potentially due to higher SEM, it was not significant (**Figure 55**-B). The flux of 250 kDa FITC was affected by the addition of thrombin, resulting in an increase of 1.8-fold. The chemokines CCL4, CXCL8 and CXCL10 however, did not significantly change the transendothelial flux of the largest molecular weight dextran -250 kDa (**Figure 55**-C).

5.3.3 TEER measurement in chemokine treated hCMEC/D3

The measurement of barrier function using TEER in hCMEC/D3 was then performed. Initially, the establishment of a tight barrier was attempted using hCMEC/D3 in 8W1E wells. The development of a higher TEER was expected to develop over time as hCMEC/D3 grew to confluency.

The TEER of the hCMEC/D3 was only higher than the empty well control after 3 days (72h) of culture, reaching ~7 $\Omega.cm^2$. We expected that at this point EC junctions presumably would have been established. On day 4 TEER remained at comparable levels to the previous day 3 and then only dropped to ~2 $\Omega.cm^2$ at day 6 (120h) (**Figure 56**-A). The TEER of the wells with hCMEC/D3 on day 0 was lower than the reading of empty wells on the same day, resulting in the negative value seen in the graph at t=0h and t=24h (**Figure 56**-A).

A

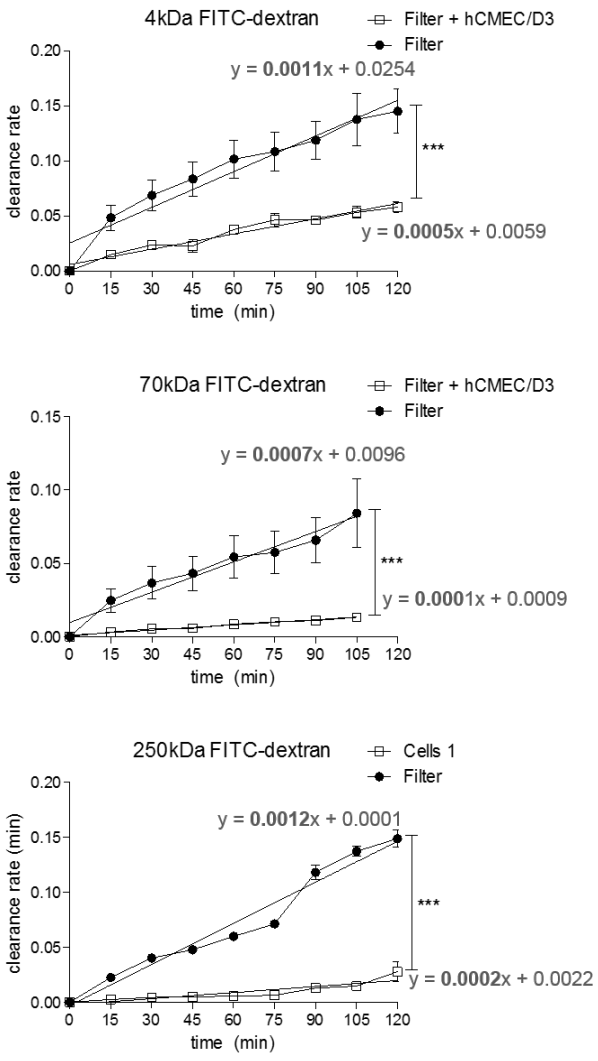

B

	Dextrans		
	4kDa	70kDa	250kDa
Mean (x 10^{-3} cm/min)	0.92	0.12	0.02
Std. Deviation	0.0057	0.0002	0.0013

C

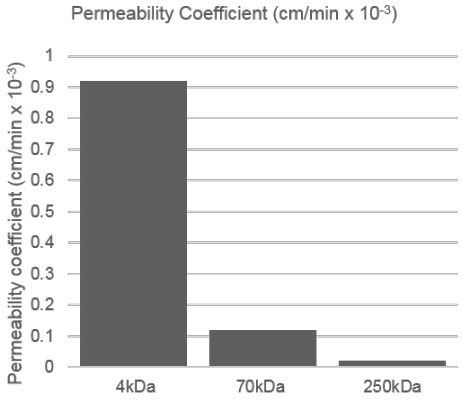

D

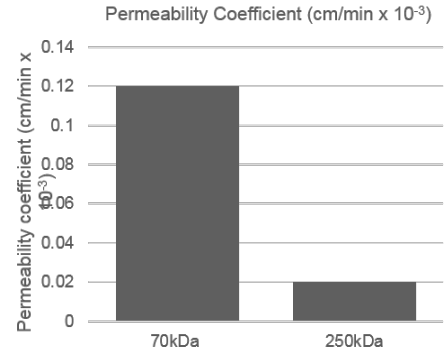

Figure 53 Permeability assessment of 4, 70 and 250 kDa dextrans in cm/min. A- Scatter plots representing the fluorescein of the fluorescent units measured in the bottom wells of collagen I coated transwells (filters) or hCMEC/D3 grown on collagen I coated transwells (filters + cells). Data obtained from at least three independent experiments. ***, P≤ 0.001linear regression. B- Mean permeability coefficient and standard deviation of 4, 70 and 250 kDa dextrans. C- Histogram of the permeability coefficient in cm/min of the dextrans tested. D- Histogram detailing the permeability coefficient of 70 and 250 kDa.

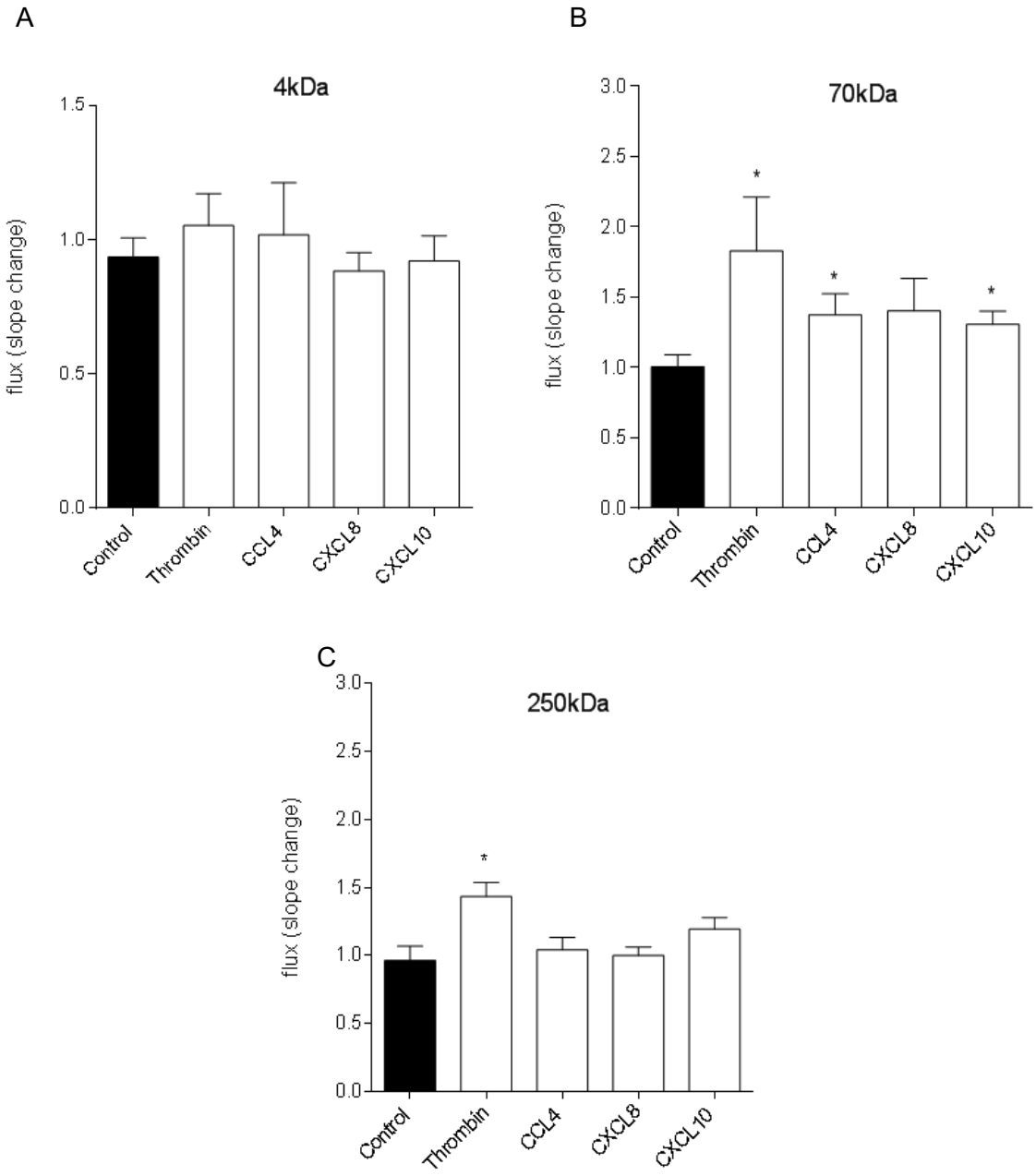

Figure 54 Transendothelial flux changes in response to chemokines in hCMEC/D3. Transendothelial flux was measured in confluent hCMEC/D3 grown in collagen coated transwells over a period of 180 min. Response to apical 0.1% PBSA (Control), Thrombin (1U/ml), CCL4 (100 ng/mL), CXCL8 (100 ng/ML) and CXCL10 (ng/mL). Data represents the mean slope change after addition of treatments for 4 kDa (A), 70 kDa (B) and 250 kDa (C). Means ± SEM of at least four independent experiments. ∗, $P < 0.05$.

The effect of chemokines on endothelial cell monolayer electrical barrier properties was also measured by ECIS. HCMEC/D3 were grown for 4 days and overnight serum-starved prior to additions. Impedance (and consequently the TEER) of hCMEC/D3 was not altered by the exposure to chemokines or LPA, presenting TEER levels compared to PBSA (negative control) addition to wells. There were minor increases in TEER in the order of 5-10% immediately after compound additions but these were merely artefactual (system recalibrating) and were not significant (**Figure 56**-B).

5.3.4 Permeability changes following intravitreal injection of CCL4

To examine the effects of CCL4 on BRB permeability, the chemokine was introduced to the abluminal side of the BBB by injection into the vitreous humour of adult C57BL/6 mice. Fundus images were obtained at 1.5 and 7 min following fluorescein dye injection and the difference in pixel count reflected the amount of dye leaked from the retinal vessels. PBSA 0.1%, the diluent of CCL4, was used as a negative control (**Figure 57**-A).

There was no significant difference in fluorescein leakage between control and CCL4 injected animals. The ratios obtained in the CCL4 injected animals are broadly distributed and despite suggesting a trend of an increase in leakage, are not significantly different from control (**Figure 57**-B).

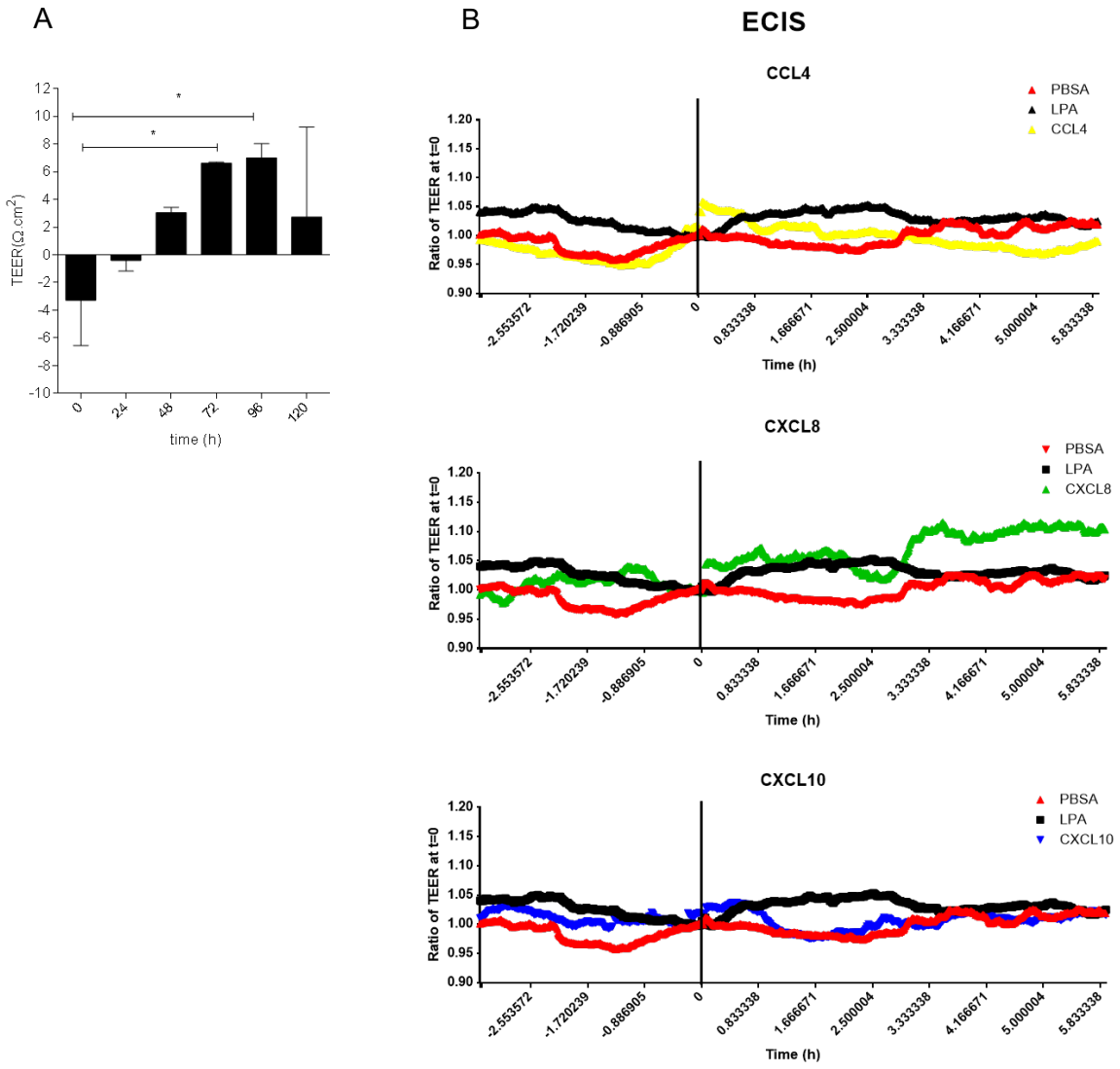

Figure 55 Development of TEER by hCMEC/D3 and chemokine additions to monolayer using ECIS. A- TEER measurement in hCMEC/D3 cells (cultured at $6x10^4$ cells/cm^2, reaching confluence on day 3). HCMEC/D3 cells developed a higher TEER when cultured up to 4 days on 8W1E grids (TEER≈7 Ω.cm^2, corrected for values of empty inserts). No statistically significant increase in TEER was observed when cells grow from non-confluent monolayers (day 2) to confluent monolayers (day 4). Repeated measures one-way ANOVA with Bonferroni's *post hoc* test was used to compare the mean TEER values: *, $P < 0.05$. Experiments were performed in duplicate wells. B- ECIS measurements of confluent hCMEC/D3 grown on 8W1E grids. Wells were subjected to apically 0.1% PBSA (control), LPA (10 µM), CCL4 (100 ng/ml), CXCL8 (100 ng/mL) or CXCL10 (50 ng/mL) and time-dependent changes in electrical resistance were monitored by ECIS. Data not significant.

5.3.5 *In vivo* measurements of permeability in pial microvessels following CCL4 addition

To measure alterations in permeability of brain microvessels following CCL4 addition, anesthetised Wistar rats were subject to cranial window formation and sulforhodamine B was introduced into the cerebral microcirculation. The signal was recorded and viewed under 540/25 nm illumination using a microscope with an image-intensifier camera through the cranial window. The chemokine was added either to the pial microvasculature (abluminal) or injected via the carotid vein (luminal) and the time-dependent loss of dye in an artificially occluded pial vessel was recorded as a measure of vessel permeability. For abluminal application, as a positive control, VEGF-A, was applied onto the brain surface (Hudson et al., 2014).

There was an increase in permeability following VEGF abluminal administration, increasing the microvessel permeability from 4.3 to $4.7x10^6$ cm/s, validating our positive control (**Figure 58**-A). Following abluminal administration of CCL4, there was significant increase in permeability in comparison to mean permeability change of control. The variation of permeability increased from $3.6x10^6$ cm/s to $5.2x10^6$ cm/s (**Figure 58**-C).In contrast, luminal administration of CCL4, via the carotid vein, did not result in a significant increase in permeability (**Figure 58**-B).

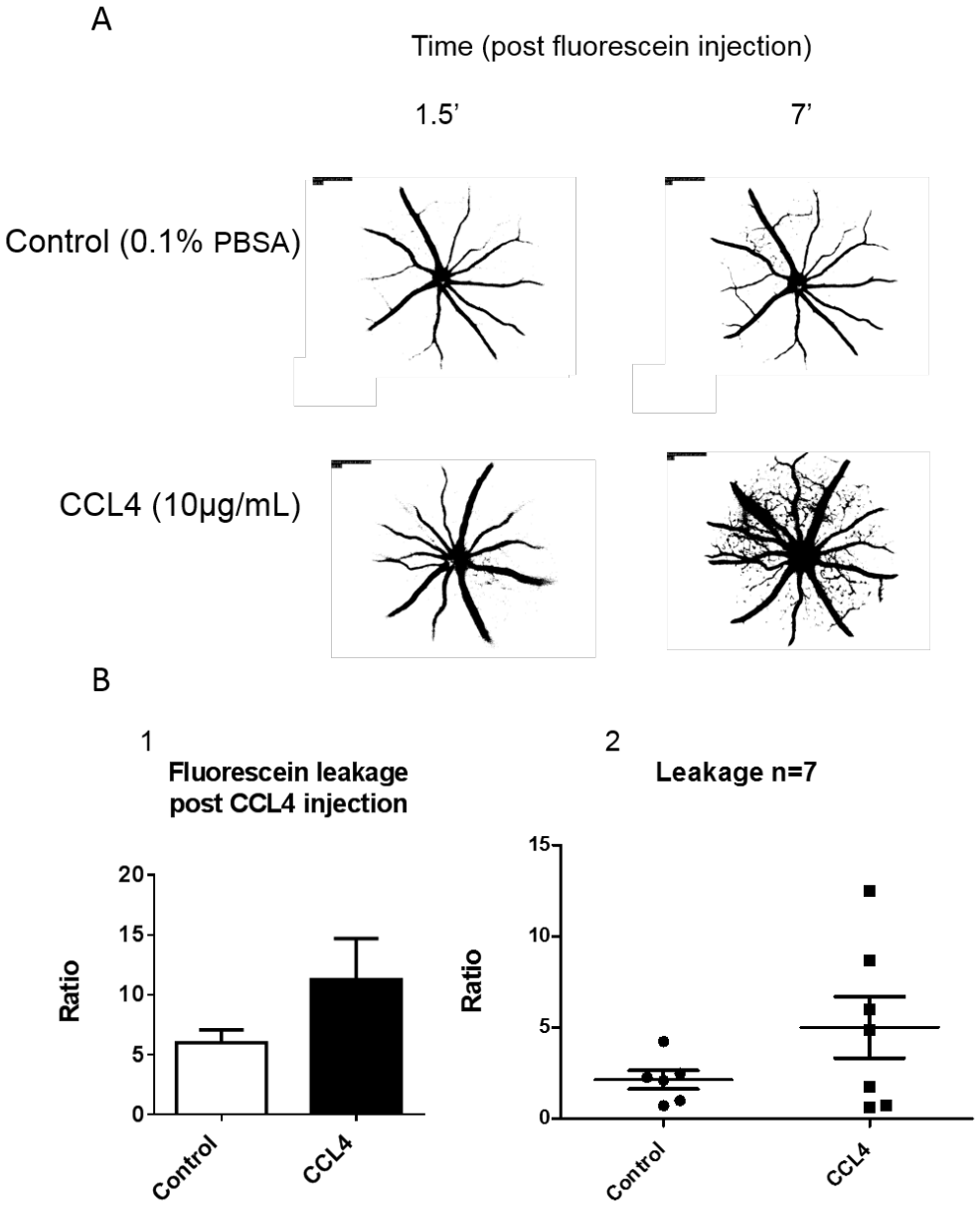

Figure 56 Fluorescein leakage following CCL4 intravitreal injection. A- Representative binary images of the fundus fluorescein angiography of retinas of adult mice injected with CCL4. Mice injected with CCL4 (10µg/mL, IVT injection) 15 min prior to imaging. B- Images obtained at 1.5 and 7 min post fluorescein injection were thresholded and converted to black and white. Pixel number was measured and a ratio 1.5 min/7 min was calculated. 1 and 2 - Shown are means +/- SEM of a least 3 animals. Statistical analysis carried out using student's t test for variance of mean values. Data statistically non-significant. 2- Graph on the right side shown distribution of data.

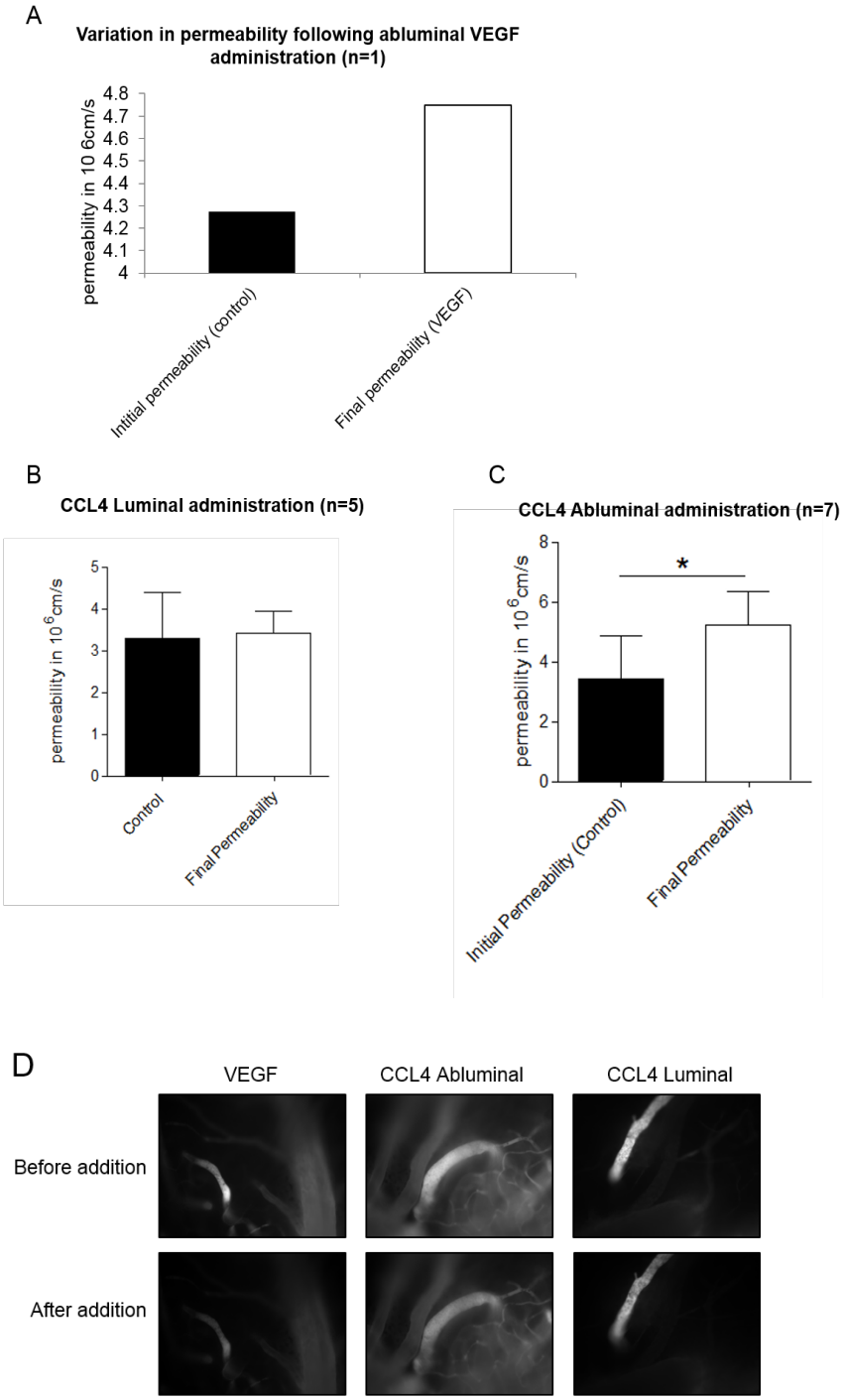

Figure 57 *In vivo* measurements of permeability in pial microvessels following CCL4 addition. A- Mean permeability change in response to VEGF-A (100 ng/ml). For VEGF-A, the positive control, only one vessel was tested. B- Mean permeability change in response to luminal administration of CCL4 (50 µg/mL). C- Mean permeability change in response to abluminal administration of CCL4 (100 ng/mL). B and C - Data are means ± SEM of at least 7 vessels. *, P<0.05. Statistical test carried out using a paired student t-test. Image analysis and densitometry was performed using ImageJ. Raw data generated by M Sarker.

5.3.6 Lymphocyte transendothelial migration

We next determined whether chemokines affected lymphocyte migration across the BBB in our model. HCMEC/D3 were grown to confluence, serum-starved overnight and then co-cultured with IL-2 activated T lymphocytes. Different experimental set ups were tested, with different chemokine incubation times.

Before any further testing of these could be done, and acknowledging the possible effect of the chemokines on the T lymphocytes, the expression of the classical chemokine receptors for CCL4, CXCL8 and CXCL10 was assessed on freshly isolated, IL-2 stimulated T cells, by immunoblot. T cells expressed the receptors CXCR1, CXCR2 and CXCR3 but not the receptor for CCL4, CCR5 (**Figure 59**). Nevertheless, CCL4 can bind to other chemokine receptors (Ben-Baruch et al., 1995).

In summary, prior to the addition of lymphocytes, chemokines (CCL4 and CXCL8 at 1 µg/mL or CXCL10 at 0.5 µg/mL) were added to the cells (either T cells set ups A and B, or hCMEC/D3 set ups C and D). Following incubations, 100 µL of T-lymphocytes (50,000 cells per well) were added to the ECs. Lymphocytes were left to adhere and migrate for 30 min in an incubator and non-adherent T lymphocytes were washed off using HBSS. Please refer to Page 75 for full protocol details.

In the first set up, T cells were pre-treated with chemokines for 30 min prior to their addition to hCMEC/D3 in order to test the effect of circulating chemokines on T cells (**Figure 60**-A). In the second set up, T cells and hCMEC/D3 were simultaneously incubated with chemokines for 30 min before the diapedesis assessment (**Figure 60**-B). Finally, two other conditions were employed to test 10 and 30 min of pre-incubation of hCMEC/D3 with chemokines prior to T cell additions (**Figure 60**-C-D).

Upon addition of T cells to hCMEC/D3, following incubation and prior to imaging, the wells were washed in HBSS to remove non-adherent T cells. Diapedesis was assessed by time-lapse video microscopy as described in Material and Methods. Adherent lymphocytes were counted and only probing lymphocytes that successfully migrated underneath the EC monolayer were considered transmigrated.

Chemokine pre-treatment of T cells with the chemokines CCL4, CXCL8 and CXCL10 for 30 min did not result in a significant change in the percentage of migration. There was a positive trend in the percentage of migration in response to CCL4 treatment but possibly due to high SEM, this result was not significant (**Figure 60**-A).

The simultaneous addition of T lymphocytes and chemokines to hCMEC/D3, where chemokines were in contact with both cells types for 30 min prior to imaging, resulted in a non-significant increase in lymphocyte transmigration in comparison to control (**Figure 60**- B).

Activation of hCMEC/D3 with our chemokines of interest, prior to the addition of T cells was then tested. The pre-incubation of hCMEC/D3 with chemokines for 10 min resulted in a significant increase in the percentage of migration of T lymphocytes in response to CXCL10. Upon 10 min pre-incubation with CCL4 and CXCL8, the percentage of migration remained comparable to control levels (**Figure 60**-C).

Finally, hCMEC/D3 were pre-incubated with chemokines for 30 min, prior to T cell addition. This length of pre-incubation resulted in a significant increase in the percentage of migrated T lymphocytes, when ECs were incubated with CCL4 and CXCL10 but not with CXCL8, (**Figure 60**-D).

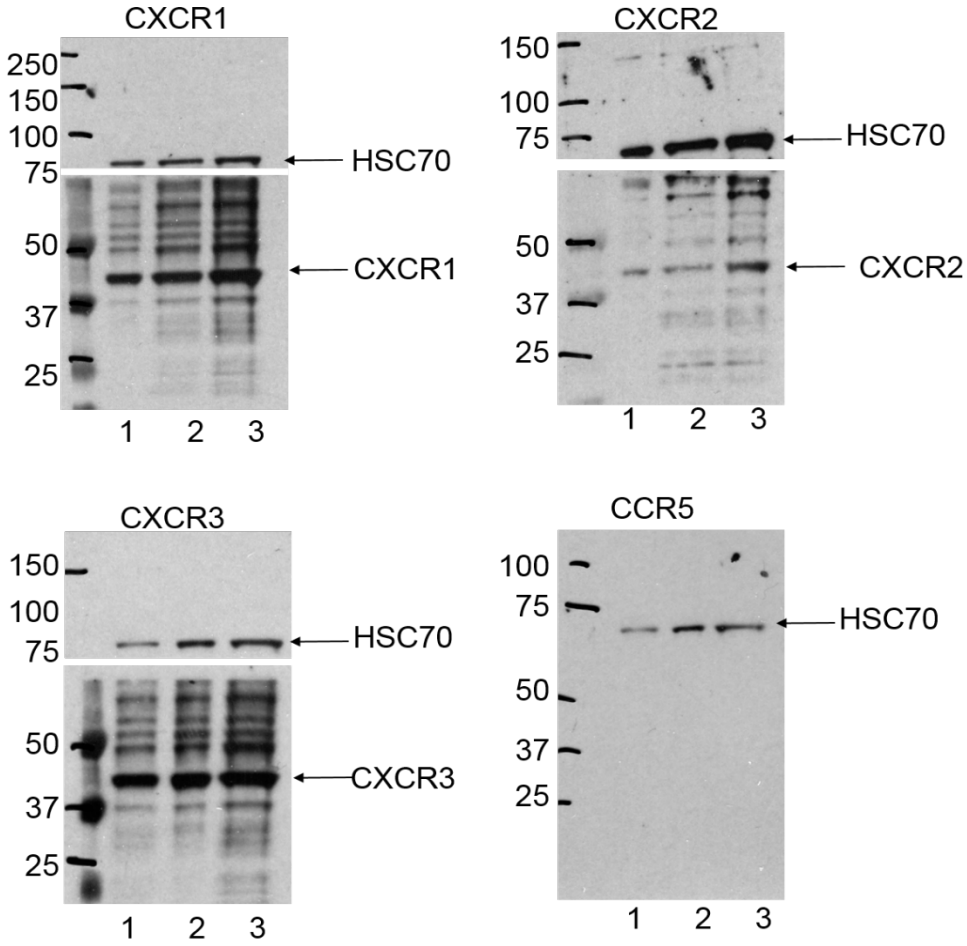

Figure 58 Expression of chemokine receptors by T cells. Freshly isolated IL-2 stimulated T cells were harvested, lysed and subjected to immunoblot. Expression of chemokine receptors for CCR1, CCR2 and CXCR3 was confirmed. The classical receptor for CCL4, CCR5 was not expressed by T cells analysed. The three lanes (1-3) for each blot are sequential dilutions, from left to right shows higher concentration, of the T cells lysate. These sequential dilutions were included to demonstrate that different amounts of protein were loaded onto the gel and so that there was a higher chance of detecting lower expressed receptors in the lysate.

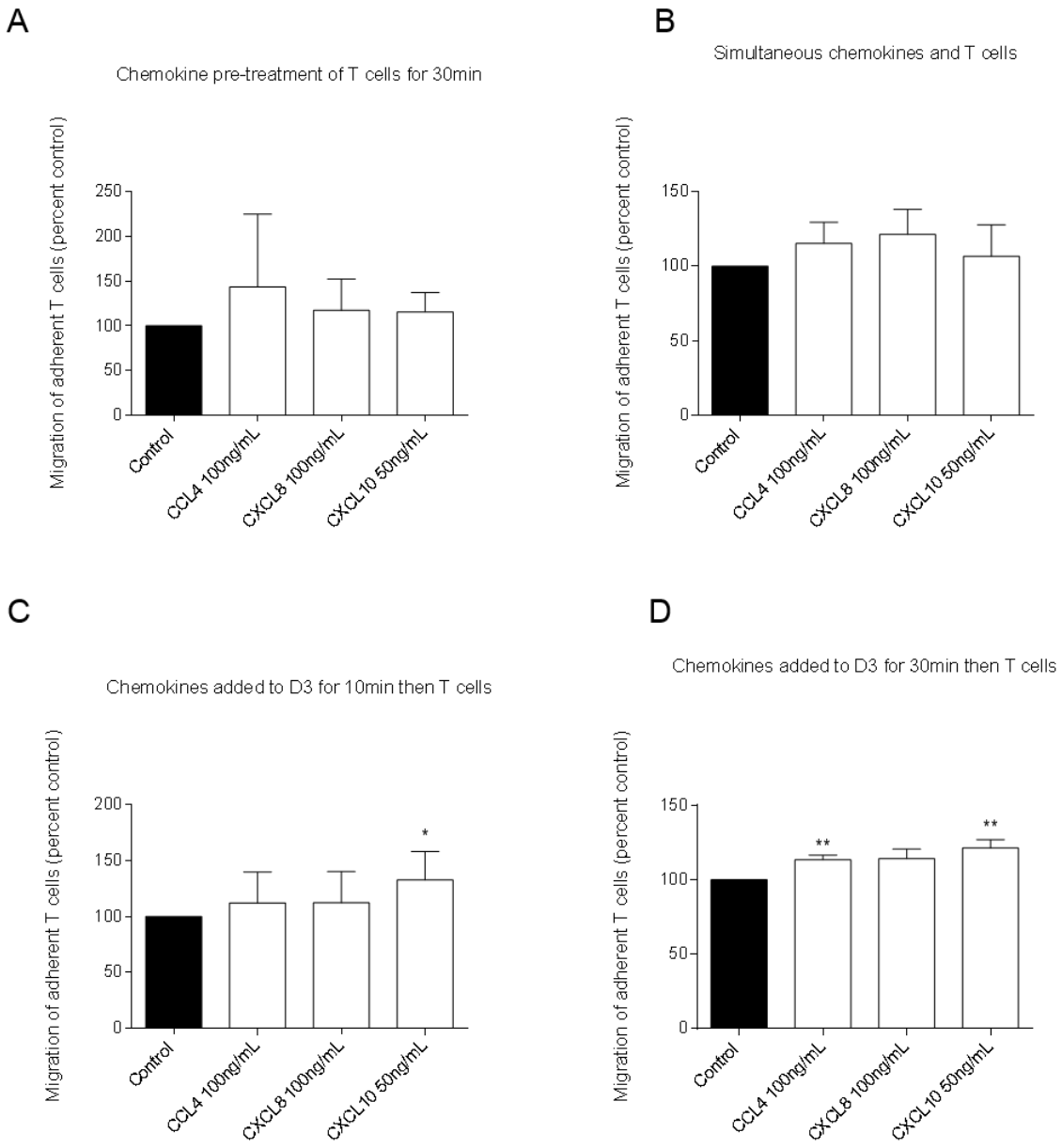

Figure 59 Effect on CCL4, CXCL8 and CXCL10 on lymphocyte transmigration. A- T cells pre-treated with chemokines for 30 min, added to hCMEC/D3 and incubated for 30 min before imaging. B- Chemokines and T cells added simultaneously to hCMEC/D3 and incubated for 30 min before imaging. C- Chemokines added to hCMEC/D3 for 10 min, T cells added to hCMEC/D3 and incubated for 30 min before imaging. D- Chemokines added to hCMEC/D3 for 30 min, T cells added to hCMEC/D3 and incubated for 30 min before imaging. Values of migration are expressed as mean percentages of control from at least 4 independent experiments +/- SEM. Variances of mean values were statistically analysed by the Student's t test. *, $P<0.05$; **, $0.001<P<0.01$.

We can also conclude that chemokines did not increase leukocyte adhesion, since the rates of adhesion of T cells added to chemokine treated hCMEC/D3 were comparable to adhesion figures (**Figure 61**).

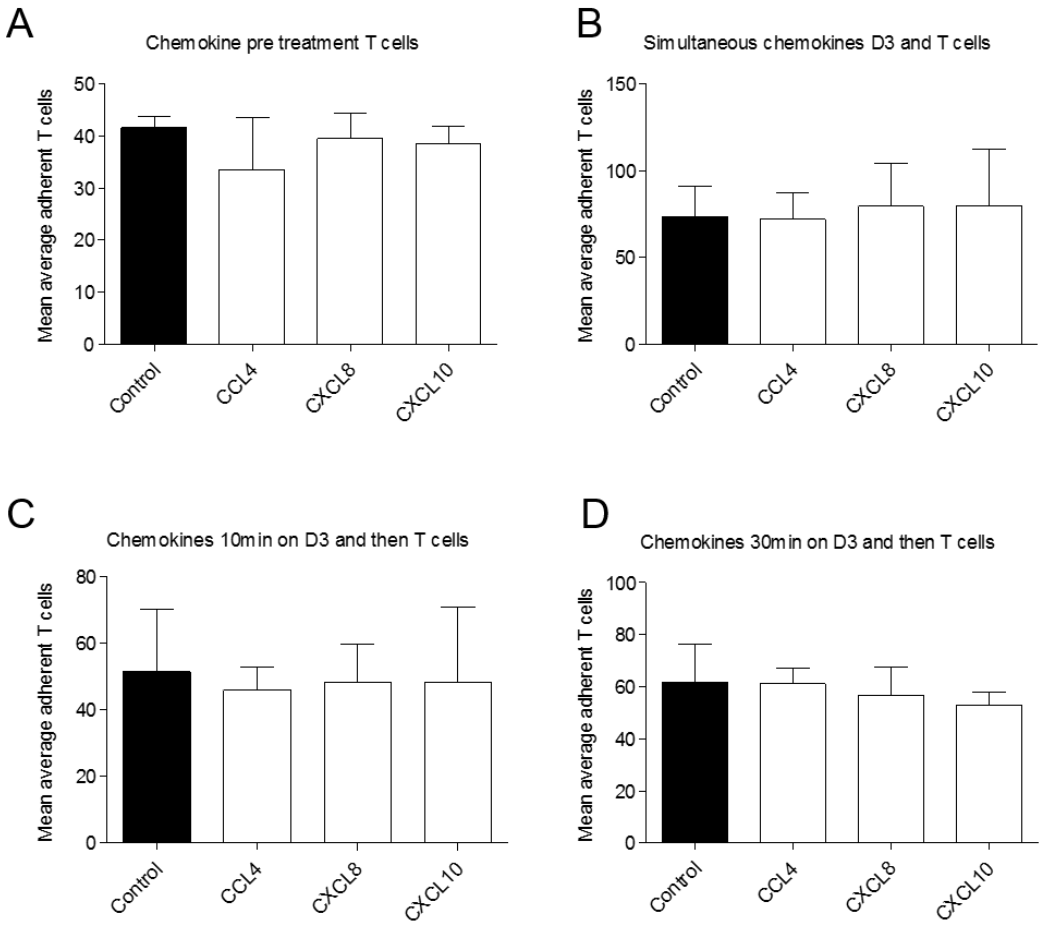

Figure 60 Effect on CCL4, CXCL8 and CXCL10 on lymphocyte adhesion to hCMEC/D3. A- T cells pre-treated with chemokines for 30 min, added to hCMEC/D3 and incubated for 30 min before imaging. B- Chemokines and T cells added simultaneously to hCMEC/D3 and incubated for 30 min before imaging. C- Chemokines added to hCMEC/D3 for 10 min, T cells added to hCMEC/D3 and incubated for 30 min before imaging. D- Chemokines added to hCMEC/D3 for 30 min, T cells added to hCMEC/D3 and incubated for 30 min before imaging. Values of adhered T cells are expressed as mean values per condition from at least 4 independent experiments +/- SEM. Variances of mean values were statistically analysed by the Student's t test. Data not significant.

5.4 Discussion

The immortalised cell line hCMEC/D3 displays two essential BBB characteristics: junctional-associated proteins and a subsequent restricted paracellular transport pathway (Reichel et al., 2003, Weksler et al., 2013). The hCMEC/D3 cell line, used here as a BBB model, has been reported to have restricted permeability to low and high molecular weight dextrans, particularly under flow conditions (Cucullo et al., 2008). There is, however, inconsistency in the permeability coefficients published for 4, 70 and 250 kDa dextrans (Weksler et al., 2005) (Biemans et al., 2017) (Forster et al., 2008). The permeability coefficients found in our experiments fall outside the range seen in the literature for all the dextrans tested, revealing that the hCMEC/D3 barrier formed in our experiments was more permeable than previous reports in the literature (**Figure 54**).

The 4 kDa dextran in our experiments, had a permeability coefficient of $6.75x10^{-2}$ cm/s, higher than the other dextrans tested (**Figure 54**-A). The fold change for the 70 kDa dextran was $7.50x10^{-3}$ cm/s and for 250 kDa was $3.27x10^{-3}$ cm/s which indicates that as the dextran nearly triples in size, the permeability coefficient halves, as expected with paracellular transport of the dextrans across the hCMEC/D3 monolayer (**Figure 54**-B and C).

We started by testing the permeability to the 4 kDa dextran before and after treatments. Since there were no statistically differences between control and treatments, including thrombin, our positive control, we concluded that the barrier formed is too permeable for this dextran (**Figure 55**-A). Our BBB model, in its normal state, is known to present a tighter barrier for larger than smaller molecules (Biemans et al., 2017). The rate of passage of the 70 and 250 kDa dextrans from the upper to the lower chamber was, accordingly, increased in a significant manner upon treatments (**Figure 55**- B and C).

Taken together, our results suggest that CCL4 and CXCL10 increase the permeability to macromolecules in our BBB model (**Figure 55**-B and C).

The TEER for this hCMEC/D3 has been reported to be 30-50 Ω·cm^2 but other studies suggest even lower TEERs, as low as 5 in a similar set up (Weksler et al., 2013) (Biemans et al., 2017) (Eigenmann et al., 2013). These low TEER values, that are consistent with our results, demonstrate that we were only able to establish a relatively leaky barrier, only allowing the quantification of permeability to larger molecules.

The TEER of the human blood-brain barrier has not been directly determined but extrapolating from mammal studies, it is believed to be in the order of 1,000-2,000Ω.cm^2 (Reichel et al., 2003). In a previous report in the literature, the cell line hCMEC/D3 has shown a TEER value of 30-50 Ω·cm^2 (Weksler et al., 2013). Culture of hCMEC/D3 with other cell types has shown little improvement in TEER, with values ranging from 40 to 60 Ω·cm^2 following 5 days of co-culture (Hatherell et al., 2011). The suitability of the cultured cell lines, including hCMEC/D3 for TEER analysis has been challenged before, since the level of TEER readings obtained with these cells are a fraction of the TEER that can be seen *in vivo* (Man et al., 2008) (Forster et al., 2008) (Weksler, 2005, Biemans et al., 2017). It is important to note that if absolute TEER is determined using direct current and chopstick electrodes which most studies have, TEER values are higher than if derived from impedance spectroscopy, a more accurate method to estimate TEER (Srinivasan et al., 2015).

Our results suggest the formation of very weak barrier as TEER values do not reach on average more than 7Ω·cm^2, considerably lower than the studies above mentioned. There are several factors that affect TEER measurements, including temperature, cell passage number, cell culture medium composition and growth period, as well as the existence/absence of shear stress that can account for differences found the TEER

readings in different set ups (Srinivasan et al., 2015). Our results show a statistically significance increase in TEER from day 3, suggesting the formation of a functional, albeit very weak, barrier (**Figure 56**-A). LPA has been reported to significantly decrease TEER in an ECIS setup similar to the one tested (Bernas et al., 2010). In this instance, LPA was used as a positive control to chemokine additions, but not even the positive control showed a response. Overall, this suggests our model did not work for TEER measurements. The effects of CCL4, CXCL8 and CXCL10 treatments were tested using ECIS but due to the very weak barrier to ions, no change was visible. Possibly due to the same reason, no effect was seen upon stimulation with LPA (**Figure 56**-B). We concluded that hCMEC/D3 are unable to form adequate junctions for TEER measurements under these conditions.

The two parameters we studied for barrier function, macromolecular flux and impedance are physically distinct, and often results are inconsistent as we saw in our experiments. Growth conditions, including substrate, permeability of the support can influence cell polarization, differentiation and nutrient supply, resulting in distinct outputs (Bischoff et al., 2016). When relating the results obtained with the dextrans and the ECIS method, the very low TEER values for hCMEC/D3 found in ECIS are comparable to the high Pe seen with 4kDa dextran, suggesting that these set ups were not sensitive enough to the barrier tightness of our model.

The 70 kDa dextran on the other hand offered physiologically compatible results, with a positive effect using thrombin and two of the chemokines tested. This supports a modest but measurable effect of CCL4 and CXCL10 in increasing the passage of macromolecules through brain EC. It may be, however, that using a more representative tight barrier model, a more significant leakage could be observed following the addition of these chemokines - as their effect on junctional proteins and the actin cytoskeleton observed in the previous chapter is consistent with such changes in barrier permeability.

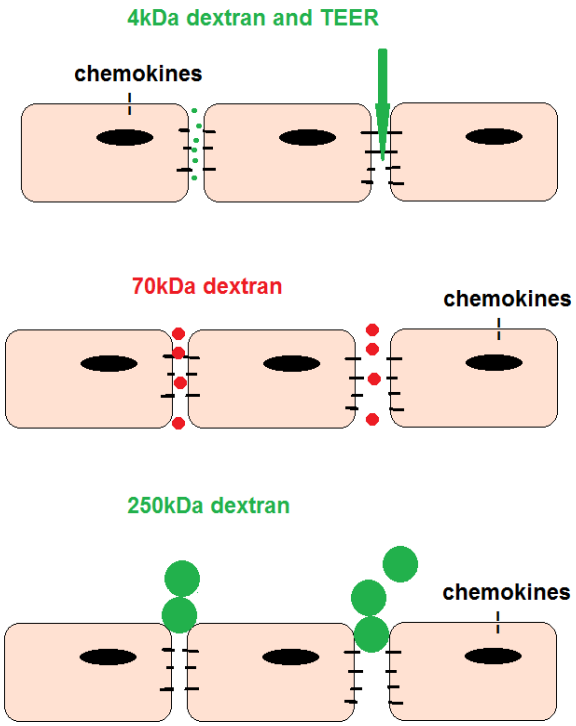

Figure 61 – Figure representing junction opening in hCMEC/D3 following chemokine treatments and methods used in this chapter to measure permeability to dextrans and TEER.

Lastly, we postulated that, despite the significant effect observed using thrombin, the effects of chemokines on the monolayer were not acute enough to allow the passage of 250kDa dextran (**Figure 62**).

Effects on T cell migration were then assessed. T cells in their resting status have little ability to enter the CNS via the BBB. *In vitro*, activated T cells and monocyte invasion of the CNS through the BBB has been demonstrated (Hawkins and Davis, 2005, Engelhardt, 2006). Numerous reports in the literature have ascertained the effect of cytokines in T cell migration across the BBB, but not of the effect of chemokines on ECs of the BBB (Quandt and Dorovini-Zis, 2004, Chui and Dorovini-Zis, 2010, Takeshita and Ransohoff, 2012, Masopust and Schenkel, 2013).

The T cells used for our experiments expressed receptors for CXCR1, CXCR2 and CXCR3 and the possibility of expressing a receptor for CCL4 other than CCR5 cannot be excluded. For this, we tested different set ups with variable incubation times of T cells and hCMEC/D3 to attempt to dissect the effect of chemokines in hCMEC/D3. To rule out an effect of chemokines on T cells affecting their migration capacity we pre-treated T cells with chemokines for 30 min. Interestingly, any differences seen in the percentage of migration of adherent cells between the control and the different chemokine treatments, were not statistically significant (**Figure 60**-A).

The simultaneous incubation of T cells and hCMEC/D3 with chemokines for 30 min did not result in significant differences in TEM. This set up was created to mimic a physiological situation, where chemokines would act on both cell types. There was a small increase in migration in response to all chemokines but this was not significant and can be attributed to variability between experimental repeats (**Figure 60**-B).

Since both ECs and T cells used in our experiments express chemokine receptors for the chemokines tested, the effect seen in TEM could be, strictly speaking, attributed to their effect on either, or both cell types. To try to dissect this effect, HCMEC/D3 were then pre-incubated with chemokines for 10 min to pre-activate the ECs and then washed, prior to T cell addition. The 10-min pre-incubation resulted in significant increase in migration in the wells with CXCL10 treated hCMEC/D3 (**Figure 60**-C). Interestingly, when the pre-incubation period was extended to 30 min, there was a high statistical significant increase in TEM in CCL4 and CXCL10 pre-treated hCMEC/D3 (**Figure 60**-D).

We concluded that the final set up tested, pre-incubation of hCMEC/D3 with chemokines for 30 min, followed by T cell addition for 30 min prior to assessment of migration, is an optimal set up for high transmigration rates. These results suggest that activation of hCMEC/D3 with chemokines prior to T cell addition results in higher TEM. Using this

simplistic model of leukocyte TEM, it is not possible to pinpoint whether the effect seen was a direct or indirect effect of chemokines on migration.

Chemokines attract not only leukocytes to sites of inflammation but also other immune cells, part of the innate immunity, such as neutrophils, monocytes, dendritic cells and natural killer cells (Esche et al., 2005). For example, neutrophils express chemokine receptors such as the CXCL8 receptors, CXCR1 and CXCR2, and respond to chemokines in acute inflammation (Sokol and Luster, 2015). CCL4 promotes recruitment of neutrophils and monocytes *in vivo* (Lee et al., 2000). Specifically in the CNS, the entry of innate immune cells has been correlated with chemokine expression (Holman et al., 2011). One must consider the possibility that these chemokines could also have an important role in promoting monocyte or neutrophil migration into the CNS.

At this stage, it was necessary to gather *in vivo* evidence to support the *in vitro* findings. From the three chemokines studied, CCL4 was selected due to its evident effect on junctional protein distribution, permeability and leukocyte migration. Therefore, the effect of CCL4 on BRB and BBB function *in vivo* was investigated.

The effect of chemokines on the BRB in the published literature are scarce and rather contradictory. The angiostatic chemokine PF-4var/CXCL4L1 has recently been shown to reduce VEGF induced retinal vascular permeability in diabetic retinopathy mice (Abu El-Asrar et al., 2015). In a different study, CCL2 (a highly-expressed chemokine in diabetic retinopathy) when added to human retinal microvascular endothelial cells, did not affect the integrity of the retinal endothelial barrier. Interestingly, in the same study, intraocular injection of CCL2 in diabetic mice, increased monocyte/macrophage infiltration in the retina (Rangasamy et al., 2014).

Our results obtained in CCL4 injected retinas were not conclusive, with a high variability of the data and the limited number of animals (**Figure 57**). The number of animals in this experiment was extremely low (n=3 control and n=4 CCL4 injected) and there was a high variability of results that will require an increase in the power of the study. Nevertheless, there was a greater variability in the CCL4 treated mice and there trend was towards greater permeability.

The recombinant human CCL4 used in these experiments is guaranteed endotoxin-free by the manufacturer (Peprotech) but the reconstitution, made with filtered (0.3µm) Mili-Q Water cannot be guaranteed to be entirely endotoxin free. The effect of endotoxin enhancing the permeability of the BRB has been described in the literature and so there is the possibility that the mild effect seen in our experiments could be due to endotoxin (Metrikin et al., 1995) (Rosenbaum et al., 2011). An endotoxin detection kit could have been employed to test for any traces of endotoxin and endotoxin-free water should have been used to prepare CCL4 for intravitreal injection. Alternatively, LPS could have been used as a positive control of endotoxin-induced retinal permeability.

Additionally, we stained mouse retinas for CD11b (a pan-macrophage marker) and EC junctional markers following 24h CCL4 intravitreal injections, but the results were also inconclusive (data not shown). Further experimental repeats would be necessary to identify the effects of CCL4 on BRB permeability.

Following the results obtained *in vitro* of the effects of CCL4 on permeability, the effects of this chemokine on the abluminal and luminal sides of rat brain microvessels were investigated. Interestingly, there was a significant result in permeability following abluminal but not luminal addition of CCL4 (**Figure 58**-B and C). Because of the similarity between the ECs of the BBB and the BRB our results suggest that with an increase in power, similar findings may also be observed in the retina.

Our *in vitro* set up on transwells intends to mimic a luminal addition of chemokines, and a significant effect of CCL4 was seen in this experimental condition. The establishment of a polarised monolayer and the absolute amount of chemokine reaching the ECs could be questioned and explored in future experiments. Some reports in the literature have shown that hCMEC/D3 retain polarity in transwell culture (Tai et al., 2009, Batista et al., 2010). However, most *in vitro* models of the BBB, including ours, lacks flow, astrocytic endfeet and pericytes, which are known to be determinants for EC polarity. In hCMEC/D3, polarity has been preserved to a degree and the transwell system created to study TEM aims to mimic apical and abluminal compartments (Worzfeld and Schwaninger, 2016). A degree of polarity loss must be considered, and we have to consider that chemokine receptors localisation could be compromised. Taking this into consideration, along with the high permeability of the *in vitro* junctions, the addition of chemokines to the apical side may also gain rapid access to the basal side and so conclusions regarding apical and basal compartment responses in our *in vitro* model may not be possible. Furthermore, it is also important to highlight that the absolute amount of chemokine that would have reached the brain endothelial cells via the blood is extremely difficult to assess in our *in vivo* set up, and this could be much lower than the concentration added *in vitro* or *in vivo* to the abluminal side of the microvasculature. This could explain the inconsistencies found between our *in vivo* and *in vitro* results.

In this body of research we have shown evidence that CCL4 and CXCL10 induce signalling responses in hCMEC/D3 that result in increased permeability and increased rates of T lymphocyte migration into the BBB. *In vivo* evidence also indicated a response to CCL4 by brain endothelial cells, resulting in increased permeability to macromolecules (Table 9).

Table 9 Summary of chapter 5 – Key findings in hCMEC/D3

	Experiment	CCL4	CXCL8	CXCL10	Observations
Chapter 5	Transendothelial flux to 4kDa FITC	-	-	-	Appropriate barrier not formed.
	Transendothelial flux to 70 kDa RITC	+	-	+	
	Transendothelial flux to 250kDa FITC	-	-	-	
	ECIS	-	-	-	Appropriate barrier not formed.
	IVT addition	-	N/A	N/A	
	Brain microvessel/ carotid addition	+ (abluminal)	N/A	N/A	
	Lymphocyte TEM (T cell pre-incubation)	-	-	-	
	Lymphocyte TEM (simultaneous CK to EC and T cells)	-	-	-	
	Lymphocyte TEM (10 min D3 pre-incubation)	-	-	+	
	Lymphocyte TEM (30 min D3 pre-incubation)	++	-	++	

6. Discussion and future work

Summary of results

In this body of work, the role of CCL4, CXCL8 and CXCL10 in brain EC signalling, permeability and leukocyte migration has been explored. Following initial testing of the response of HUVEC and hCMEC/D3 to the chemokines of interest, hCMEC/D3 were chosen to be used in our experiments as a BBB model. To explore our aims, molecular biology techniques were employed along with *in vivo* murine models. A summary of the results in hCMEC/D3 from Chapter 3 to 5 can be seen below - Table 10.

Upon analysis of the MAPK family, results indicated a response of the BBB microvasculature to these chemokines and an increase of nuclear P-ERK and P-P38 specifically following CCL4 treatments, suggesting an effect in gene expression and downstream signalling. Since the focus of this project was to ascertain the effects of these chemokines on the BBB microvasculature, we then investigated junctional proteins that are frequently altered in neuroinflammation. ZO-1 junctional expression decreased upon chemokine treatments leading us to conclude that chemokines can destabilise the TJs of the BBB. We then used the same experimental set up to test the effects of the chemokines on VE-cadherin, an adherens junction molecule frequently affected by pro-inflammatory stimuli and a hallmark of adherens junction destabilization. Consistent with our data on ZO-1, VE-cadherin also disappeared from the junctions upon chemokine treatment. The possibility of VE-cadherin internalisation was explored and we obtained strong evidence that VE-cadherin is internalised in response to all the chemokines studied. These results were supported by the constant total expression levels of ZO-1 and VE-cadherin protein observed throughout the timepoints tested. Knowing that when these two proteins are compromised in brain ECs, there are alterations in the barrier, we

looked at effect at the level of the cytoskeleton. Interestingly, ERK and P38, which were phosphorylated following chemokine treatments, have been shown to be involved in cytoskeleton activation and contraction, resulting in EC cell permeability (Borbiev et al., 2003, Borbiev et al., 2004). We then demonstrated that the chemokines induced stress fibre formation in our brain ECs, indicating cytoskeleton rearrangement, and further supporting the destabilising effect of chemokines on EC junctions in the BBB.

Once we gathered enough evidence that chemokines were affecting brain ECs junctions and cytoskeleton, we investigated functional outcomes: the effects of chemokines on macromolecule passage and TEM. We demonstrated that CCL4 and CXCL10 are involved in barrier disruption, resulting in increased passage of molecules through the barrier. Our model, however, did not form a tight enough barrier to allow ECIS measurements that could support the results seen using the dextrans.

Our *in vivo* experiments were pilot studies using only CCL4, with a low number of animals and for that we were unable to reach final conclusions. We can draw attention to CCL4 increasing permeability in brain microvascular cell permeability when added abluminally, mimicking effects of tissue derived chemokines on an EC barrier. This suggests that *in vivo*, chemokines from the brain side, could have a significant effect on BBB permeability. Finally, there was an obvious effect on TEM rates when brain ECs were treated with CCL4 and CXCL10, supporting the theory that chemokine signalling in brain ECs can increase leukocyte migration across the BBB.

The chemokines studied have been found in tissues in the CNS and associated with neuroinflammation. The presence of chemokines in the brain and retina, structures classically known to have limited immune activity and high barrier function in comparison to other tissues in the body, suggests that there may be is a physiological relevance for the responses of ECs to the chemokines.

Final discussion and conclusion

Throughout our experiments, CCL4 and CXCL10 showed consistently strong effects on junctional protein and barrier function modulation. Despite the extensive body of work on CXCL8 in the literature, our experiments showed that CCL4 and CXCL10 have stronger effects in signalling, junctional protein modulation and passage of macromolecules and leukocytes in brain ECs.

Our results fit with the current literature, where some evidence of chemokines, elevated in neuroinflammatory diseases have an effect, direct or indirect in disrupting adherens junctions in brain ECs and affecting BBB permeability. Our work is novel, showing these same effects with CCL4, CXCL8 and CXCL10.

In conclusion we have shown that CCL4, CXCL8 and CXCL10 have an effect in BBB permeability and leukocyte TEM.

Limitations

HCMEC/D3 have been widely used as a BBB model in recent years. This cell line is stable and easily maintained in culture, presenting many features of a normal BBB. hCMEC/D3 have been used in studies to assess the effect of inflammation and immune cell migration (Weksler et al., 2013). However, hCMEC/D3 have lower occludin and claudin 5 expression than *in vivo* and present low TEER compared to *in vivo* properties. Another limitation of this cell line is the high permeability to small macromolecules (He et al., 2014).

The loss of polarity in hCMEC/D3 also needs to be addressed when discussing the outlook of this project. Despite the expression of PGP by this cell line, it is accepted that only a certain degree of polarity has been maintained (Tai et al., 2009, Natalie Hudson,

2014). The effect of chemokines on a truly polarised tight EC was only fully tested in the *in vivo* studies where the pial microvasculature revealed significant changes in permeability in response to abluminal CCL4.

Future work

Regrettably, due to the lack of time, several experiments that would have been of great interest, were not performed.

To address the central limitation of this study, namely the poor barrier function of the hCMEC/D3 cells, the next step would be to use a primary source of ECs. Mouse and rat brain ECs isolation have been optimised and are widely used as they present higher TEER. A model using shear flow or a co-culture with other elements of the neurovascular unit could also be employed, such as astrocytes and/or pericytes to increase the functional barrier (Wilhelm et al., 2011, Helms et al., 2016).

Barrier tightness can be artificially increased by the addition of supplements or activation of the Wnt/ß-catenin pathway (Helms et al., 2016). These methods, that artificially alter the culture conditions and the signalling pathways, were not employed to avoid increasing the variables in our study.

The exact molecular mechanisms that governate these processes are still to be elucidated but our results suggest the potential involvement of ZO-1 and VE-cadherin. Future experiments could include the investigation of the phosphorylation of these junctional proteins and further investigation into VE-cadherin internalisation.

It would have been of great interest to test the effect of EC receptor knockdown on leukocyte TEM to dissect the absolute involvement of specific cell receptors in this

process. Furthermore, we could have inhibited MAPK to ascertain the effect on chemokine mediated effector processes (permeability/leukocyte migration).

Moreover, it would be informative to test an *ex-vivo* model delivery of chemokines into murine retina to obtain a real time effect of these chemokines on retinal permeability. Time permitting, we would have tested CXCL8 and CXCL10's effect on pial microvasculature permeability and on BRB permeability as was tested for CCL4. This technique has been used to evaluate leukocyte migration through the BBB (Villringer et al., 1991, Yata et al., 2014, Reichenbach et al., 2015).

One last question that should be answered is the source of CCL4, CXCL8 and CXCL10 acting on BBB ECs. Other chemokines have been shown in CNS inflamed tissues, for example, CCL2, CCL3 and CCL5 and their receptors are expressed by microglia, astrocytes or infiltrating lymphocytes and macrophages in MS lesions. The expression of chemokines by the ECs themselves has also been reported: CXCL10, CCL2, CCL5 and CXCL8 are secreted by activated ECs (Harkness et al., 2003, Subileau et al., 2009). This suggests that in MS, the origin of the chemokines could either be the ECs of the BBB, immune or glial cells within the brain. In other inflammatory conditions of the brain, chemokines could be produced locally and could be further amplifying recruitment of immune cells into the CNS. A final experiment that would be of great interest would be to identify cells responsible for producing these specific chemokines in other inflammatory CNS conditions.

Table 10 Summary of results in hCMEC/D3.

	Experiment	CCL4	CXCL8	CXCL10	Observations
Chapter 3	P-ERK expression	+++ (3', 5', 10')	+++ (5'), + (3')	-	
	P-P38 expression	-	+ (10', 30')	+ (1')	
	P-ERK nuclear localization	+ (30')	-	-	
	P-P38 nuclear localization	++ (5')	-	-	
Chapter 4	ZO-1 expression	-	-	-	No changes in ZO-1 expression in IF.
	ZO-1 distribution	+++ (10', 60')	+ (10')	+ (10', 60')	
	VE-cadherin distribution	+ (60')	+++ (5'), +/++ (10', 60')	+++ (5', 60')	
	VE-cadherin distribution (EGTA)	+ (5'), ++ (30', 60')	+ (5'), ++(60')	+++ (5', 30')	Expected to follow pattern above.
	VE-cadherin protein expression	-	-	-	No shedding or cleavage (>25 kDa).
	VE-cadherin membranar/total ratio	+ (30', 60')	+ (5', 60')	+ (5', 10', 30', 60')	

	VE-cadherin internalisation	++++ (5', 10', 30', 60')	++ (5', 30')	++ (30', 60')	
	F-actin - stress fibres induction	+++ (5', 30'), ++++ (10')	++ (10')	++++ (5'), +++(10')	
Chapter 5	Transendothelial flux to 4kDa FITC	-	-	-	Appropriate barrier not formed.
	Transendothelial flux to 70 kDa RITC	+	-	+	
	Transendothelial flux to 250kDa FITC	-	-	-	
	ECIS	-	-	-	Appropriate barrier not formed.
	IVT addition	-	N/A	N/A	
	Brain microvessel/ carotid addition	+ (abluminal)	N/A	N/A	
	Lymphocyte TEM (T cell pre-incubation)	-	-	-	
	Lymphocyte TEM (simultaneous CK to EC and T cells)	-	-	-	
	Lymphocyte TEM (10 min D3 pre-incubation)	-	-	+	
	Lymphocyte TEM (30 min D3 pre-incubation)	++	-	++	

Legend

-	No effect
+	Modest effect
++	Moderate effect
+++	Strong effect
++++	Very strong effect

7. Bibliography

Abbott, N. J., Patabendige, A. A., Dolman, D. E., Yusof, S. R. & Begley, D. J. 2010. Structure and function of the blood-brain barrier. *Neurobiology of Disease,* 37**,** 13-25.

Abbott, N. J., Ronnback, L. & Hansson, E. 2006. Astrocyte-endothelial interactions at the blood–brain barrier. *Nature Reviews: Neuroscience,* 7.

Abu El-Asrar, A. M., Mohammad, G., Nawaz, M. I., Abdelsaid, M., Siddiquei, M. M., Alam, K., Van Den Eynde, K., De Hertogh, G., Opdenakker, G., Al-Shabrawey, M., Van Damme, J. & Struyf, S. 2015. The Chemokine Platelet Factor-4 Variant (PF-4var)/CXCL4L1 Inhibits Diabetes-Induced Blood-Retinal Barrier Breakdown. *Investigative Ophthalmology and Visual Science,* 56**,** 1956-1964.

Adamson, P., Wilbourn, B., Etienne-Manneville, S., Calder, V., Beraud, E., Milligan, G., Couraud, P. O. & Greenwood, J. 2002. Lymphocyte trafficking through the blood-brain barrier is dependent on endothelial cell heterotrimeric G-protein signaling. *FASEB Journal,* 16**,** 1185-1194.

Ahn, N. G., Seger, R., Bratlien, R. L. & Krebs, E. G. 1992. Growth factor-stimulated phosphorylation cascades: activation of growth factor-stimulated MAP kinase. *Ciba Foundation Symposium,* 164**,** 113-126; discussion 126-131.

Akers, S. M., O'leary, H. A., Minnear, F. L., Craig, M. D., Vos, J. A., Coad, J. E. & Gibson, L. F. 2010. VE-cadherin and PECAM-1 enhance ALL migration across brain microvascular endothelial cell monolayers. *Experimental Hematology,* 38**,** 733-743.

Alberts, Bruce, Johnson, Alexander, Lewis, Julian, Raff, Martin, Roberts, Keith & Walter, Peter 2002. *Blood Vessels and Endothelial Cells,* New York, Garland Science.

Amerongen, Geerten P. Van Nieuw, Draijer, Richard, Vermeer, Mario A. & Van Hinsbergh, Victor W. M. 1998. Transient and Prolonged Increase in Endothelial Permeability Induced by Histamine and Thrombin. *Circulation Research,* 83**,** 1115-1123.

Anderson, J. M. & Van Itallie, C. M. 2009. Physiology and function of the tight junction. *Cold Spring Harbor Perspectives in Biology,* 1**,** a002584.

Aragon-Sanabria, V., Pohler, S. E., Eswar, V. J., Bierowski, M., Gomez, E. W. & Dong, C. 2017. VE-Cadherin Disassembly and Cell Contractility in the Endothelium are Necessary for Barrier Disruption Induced by Tumor Cells. *Scientific Reports,* 7**,** 45835.

Arbabi, S., Garcia, I., Bauer, G. J. & Maier, R. V. 1999. Alcohol (ethanol) inhibits IL-8 and TNF: role of the p38 pathway. *Journal of Immunology,* 162**,** 7441-7445.

Ardito, F., Giuliani, M., Perrone, D., Troiano, G. & Lo Muzio, L. 2017. The crucial role of protein phosphorylation in cell signaling and its use as targeted therapy (Review). *International Journal of Molecular Medicine,* 40**,** 271-280.

Armulik, A., Genove, G., Mae, M., Nisancioglu, M. H., Wallgard, E., Niaudet, C., He, L., Norlin, J., Lindblom, P., Strittmatter, K., Johansson, B. R. & Betsholtz, C. 2010. Pericytes regulate the blood-brain barrier. *Nature,* 468**,** 557-561.

Arthur, F. E., Shivers, R. R. & Bowman, P. D. 1987. Astrocyte-mediated induction of tight junctions in brain capillary endothelium: an efficient in vitro model. *Brain Research,* 433**,** 155-159.

Artursson, Per 1990. Epithelial Transport Of Drugs In Cell Culture. I: A Model For Studying The Passive Diffusion Of Drugs Over Intestinal Absorbtive (Caco-2) Cells. *Journal of Pharmaceutical Sciences,* 79**,** 476-482.

Bae, J. S., Kim, Y. U., Park, M. K. & Rezaie, A. R. 2009. Concentration dependent dual effect of thrombin in endothelial cells via Par-1 and Pi3 Kinase. *Journal of Cellular Physiology,* 219**,** 744-751.

Baekkevold, E. S., Yamanaka, T., Palframan, R. T., Carlsen, H. S., Reinholt, F. P., Von Andrian, U. H., Brandtzaeg, P. & Haraldsen, G. 2001. The CCR7 ligand elc (CCL19) is transcytosed in high endothelial venules and mediates T cell recruitment. *Journal of Experimental Medicine,* 193**,** 1105-1112.

Barberis, L., Pasquali, C., Bertschy-Meier, D., Cuccurullo, A., Costa, C., Ambrogio, C., Vilbois, F., Chiarle, R., Wymann, M., Altruda, F., Rommel, C. & Hirsch, E. 2009. Leukocyte transmigration is modulated by chemokine-mediated PI3Kgamma-

dependent phosphorylation of vimentin. *European Journal of Immunology,* 39**,** 1136-1146.

Barzo, P., Marmarou, A., Fatouros, P., Hayasaki, K. & Corwin, F. 1997. Contribution of vasogenic and cellular edema to traumatic brain swelling measured by diffusion-weighted imaging. *Journal of Neurosurgery,* 87**,** 900-907.

Batista, L., Miller, F., Clave, C., Arfi, A., Douillard-Guilloux, G., Couraud, P. O. & Caillaud, C. 2010. Induced secretion of beta-hexosaminidase by human brain endothelial cells: a novel approach in Sandhoff disease? *Neurobiology of Disease,* 37**,** 656-660.

Bell, R. D., Winkler, E. A., Sagare, A. P., Singh, I., Larue, B., Deane, R. & Zlokovic, B. V. 2010. Pericytes control key neurovascular functions and neuronal phenotype in the adult brain and during brain aging. *Neuron,* 68**,** 409-427.

Ben-Baruch, A., Xu, L., Young, P. R., Bengali, K., Oppenheim, J. J. & Wang, J. M. 1995. Monocyte chemotactic protein-3 (MCP3) interacts with multiple leukocyte receptors. C-C CKR1, a receptor for macrophage inflammatory protein-1 alpha/Rantes, is also a functional receptor for MCP3. *Journal of Biological Chemistry,* 270**,** 22123-22128.

Ben-Levy, R., Hooper, S., Wilson, R., Paterson, H. F. & Marshall, C. J. 1998. Nuclear export of the stress-activated protein kinase p38 mediated by its substrate MAPKAP kinase-2. *Current Biology,* 8**,** 1049-1057.

Benn, A., Bredow, C., Casanova, I., Vukicevic, S. & Knaus, P. 2016. VE-cadherin facilitates BMP-induced endothelial cell permeability and signaling. *Journal of Cell Science,* 129**,** 206-218.

Benson, K., Cramer, S. & Galla, H. J. 2013. Impedance-based cell monitoring: barrier properties and beyond. *Fluids Barriers CNS,* 10**,** 5.

Bernas, M. J., Cardoso, F. L., Daley, S. K., Weinand, M. E., Campos, A. R., Ferreira, A. J., Hoying, J. B., Witte, M. H., Brites, D., Persidsky, Y., Ramirez, S. H. & Brito, M. A. 2010. Establishment of primary cultures of human brain microvascular endothelial cells to provide an in vitro cellular model of the blood-brain barrier. *Nature Protocols,* 5**,** 1265-1272.

Biemans, Ealm, Jakel, L., De Waal, R. M. W., Kuiperij, H. B. & Verbeek, M. M. 2017. Limitations of the hCMEC/D3 cell line as a model for Abeta clearance by the human blood-brain barrier. *Journal of Neuroscience Research,* 95**,** 1513-1522.

Bischoff, I., Hornburger, M. C., Mayer, B. A., Beyerle, A., Wegener, J. & Furst, R. 2016. Pitfalls in assessing microvascular endothelial barrier function: impedance-based devices versus the classic macromolecular tracer assay. *Scientific Reports,* 6**,** 23671.

Borbiev, T., Birukova, A., Liu, F., Nurmukhambetova, S., Gerthoffer, W. T., Garcia, J. G. & Verin, A. D. 2004. p38 MAP kinase-dependent regulation of endothelial cell permeability. *American Journal of Physiology: Lung Cellular and Molecular Physiology,* 287**,** L911-918.

Borbiev, T., Verin, A. D., Birukova, A., Liu, F., Crow, M. T. & Garcia, J. G. 2003. Role of CaM kinase II and ERK activation in thrombin-induced endothelial cell barrier dysfunction. *American Journal of Physiology: Lung Cellular and Molecular Physiology,* 285**,** L43-54.

Bosisio, D., Salvi, V., Gagliostro, V. & Sozzani, S. 2014. Angiogenic and antiangiogenic chemokines. *Chemical Immunology and Allergy,* 99**,** 89-104.

Broom, O. J., Widjaya, B., Troelsen, J., Olsen, J. & Nielsen, O. H. 2009. Mitogen activated protein kinases: a role in inflammatory bowel disease? *Clinical and Experimental Immunology,* 158**,** 272-280.

Butcher, E. C. & Picker, L. J. 1996. Lymphocyte homing and homeostasis. *Science,* 272**,** 60-66.

Campbell, M. & Humphries, P. 2012. The blood-retina barrier: tight junctions and barrier modulation. *Advances in Experimental Medicine and Biology,* 763**,** 70-84.

Carman, C. V., Sage, P. T., Sciuto, T. E., De La Fuente, M. A., Geha, R. S., Ochs, H. D., Dvorak, H. F., Dvorak, A. M. & Springer, T. A. 2007. Transcellular diapedesis is initiated by invasive podosomes. *Immunity,* 26**,** 784-797.

Carman, C. V. & Springer, T. A. 2004. A transmigratory cup in leukocyte diapedesis both through individual vascular endothelial cells and between them. *Journal of Cell Biology,* 167**,** 377-388.

Chai, Q., She, R., Huang, Y. & Fu, Z. F. 2015. Expression of neuronal CXCL10 induced by rabies virus infection initiates infiltration of inflammatory cells, production of chemokines and cytokines, and enhancement of blood-brain barrier permeability. *Journal of Virology,* 89**,** 870-876.

Chaplin, D. D. 2010. Overview of the immune response. *Journal of Allergy and Clinical Immunology,* 125**,** S3-23.

Chapman, R. W., Minnicozzi, M., Celly, C. S., Phillips, J. E., Kung, T. T., Hipkin, R. W., Fan, X., Rindgen, D., Deno, G., Bond, R., Gonsiorek, W., Billah, M. M., Fine, J. S. & Hey, J. A. 2007. A novel, orally active CXCR1/2 receptor antagonist, Sch527123, inhibits neutrophil recruitment, mucus production, and goblet cell hyperplasia in animal models of pulmonary inflammation. *Journal of Pharmacology and Experimental Therapeutics,* 322**,** 486-493.

Chaudhary, P., Marracci, G. H. & Bourdette, D. N. 2006. Lipoic acid inhibits expression of ICAM-1 and VCAM-1 by CNS endothelial cells and T cell migration into the spinal cord in experimental autoimmune encephalomyelitis. *Journal of Neuroimmunology,* 175**,** 87-96.

Chen, R. H., Sarnecki, C. & Blenis, J. 1992. Nuclear localization and regulation of erk- and rsk-encoded protein kinases. *Molecular and Cellular Biology,* 12**,** 915-927.

Chen, S. U., Chou, C. H., Lin, C. W., Lee, H., Wu, J. C., Lu, H. F., Chen, C. D. & Yang, Y. S. 2009. Signal mechanisms of vascular endothelial growth factor and interleukin-8 in ovarian hyperstimulation syndrome: dopamine targets their common pathways. *Human Reproduction,* 25**,** 757-767.

Cheung, R., Malik, M., Ravyn, V., Tomkowicz, B., Ptasznik, A. & Collman, R. G. 2009. An arrestin-dependent multi-kinase signaling complex mediates MIP-1beta/CCL4 signaling and chemotaxis of primary human macrophages. *Journal of Leukocyte Biology,* 86**,** 833-845.

Chiba, H., Osanai, M., Murata, M., Kojima, T. & Sawada, N. 2008. Transmembrane proteins of tight junctions. *Biochimica et Biophysica Acta,* 1778**,** 588-600.

Chuderland, D. & Seger, R. 2005. Protein-protein interactions in the regulation of the extracellular signal-regulated kinase. *Molecular Biotechnology,* 29**,** 57-74.

Chui, R. & Dorovini-Zis, K. 2010. Regulation of CCL2 and CCL3 expression in human brain endothelial cells by cytokines and lipopolysaccharide. *Journal of Neuroinflammation,* 7**,** 1.

Cipolla, M. J., Crete, R., Vitullo, L. & Rix, R. D. 2004. Transcellular transport as a mechanism of blood-brain barrier disruption during stroke. *Frontiers in Bioscience,* 9**,** 777-785.

Clark, A. R., Dean, J. L. & Saklatvala, J. 2003. Post-transcriptional regulation of gene expression by mitogen-activated protein kinase p38. *Federation of European Biochemical Societies Letters,* 546**,** 37-44.

Cohen, P. 2000. The regulation of protein function by multisite phosphorylation – a 25 year update. *Trends in Biochemical Sciences,* 25**,** 596-601.

Cohen, P. 2002. The origins of protein phosphorylation. *Nature Cell Biology,* 4**,** E127-130.

Corada, M., Mariotti, M., Thurston, G., Smith, K., Kunkel, R., Brockhaus, M., Lampugnani, M. G., Martin-Padura, I., Stoppacciaro, A., Ruco, L., Mcdonald, D. M., Ward, P. A. & Dejana, E. 1999. Vascular endothelial-cadherin is an important determinant of microvascular integrity in vivo. *Proceedings of the National Academy of Sciences,* 96**,** 9815-9820.

Corada, Monica, Mariotti, Massimo, Thurston, Gavin, Smith, Kelly, Kunkel, Robin, Brockhaus, Manfred, Lampugnani, Maria Grazia, Martin-Padura, Ines, Stoppacciaro, Antonella, Ruco, Luigi, Mcdonald, Donald M., Ward, Peter A. & Dejana, Elisabetta 1999. Vascular endothelial–cadherin is an important determinant of microvascular integrity in vivo. *Proceedings of the National Academy of Sciences,* 96**,** 9815-9820.

Couty, J. P., Rampon, C., Leveque, M., Laran-Chich, M. P., Bourdoulous, S., Greenwood, J. & Couraud, P. O. 2007. PECAM-1 engagement counteracts ICAM-1-induced signaling in brain vascular endothelial cells. *Journal of Neurochemistry,* 103**,** 793-801.

Cramer, L. P., Siebert, M. & Mitchison, T. J. 1997. Identification of novel graded polarity actin filament bundles in locomoting heart fibroblasts: implications for the generation of motile force. *Journal of Cell Biology,* 136**,** 1287-1305.

Cramer, S. P., Modvig, S., Simonsen, H. J., Frederiksen, J. L. & Larsson, H. B. 2015. Permeability of the blood-brain barrier predicts conversion from optic neuritis to multiple sclerosis. *Brain,* 138**,** 2571-2583.

Cucullo, L., Couraud, P. O., Weksler, B., Romero, I. A., Hossain, M., Rapp, E. & Janigro, D. 2008. Immortalized human brain endothelial cells and flow-based vascular modeling: a marriage of convenience for rational neurovascular studies. *Journal of Cerebral Blood Flow and Metabolism,* 28**,** 312-328.

Cuenda, A. & Rousseau, S. 2007. p38 MAP-kinases pathway regulation, function and role in human diseases. *Biochimica et Biophysica Acta,* 1773**,** 1358-1375.

Cunha-Vaz, J., Bernardes, R. & Lobo, C. 2011. Blood-retinal barrier. *European Journal of Ophthalmology,* 21 Suppl 6**,** S3-9.

Daugaard, M., Rohde, M. & Jaattela, M. 2007. The heat shock protein 70 family: Highly homologous proteins with overlapping and distinct functions. *Federation of European Biochemical Societies Letters,* 581**,** 3702-3710.

Dimitrijevic, O. B., Stamatovic, S. M., Keep, R. F. & Andjelkovic, A. V. 2006. Effects of the chemokine CCL2 on blood-brain barrier permeability during ischemia-reperfusion injury. *Journal of Cerebral Blood Flow and Metabolism,* 26**,** 797-810.

Dragoni, S., Hudson, N., Kenny, B. A., Burgoyne, T., Mckenzie, J. A., Gill, Y., Blaber, R., Futter, C. E., Adamson, P., Greenwood, J. & Turowski, P. 2017. Endothelial MAPKs Direct ICAM-1 Signaling to Divergent Inflammatory Functions. *Journal of Immunology,* 198**,** 4074-4085.

Dufour, J. H., Dziejman, M., Liu, M. T., Leung, J. H., Lane, T. E. & Luster, A. D. 2002. IFN-gamma-inducible protein 10 (IP-10; CXCL10)-deficient mice reveal a role for IP-10 in effector T cell generation and trafficking. *Journal of Immunology,* 168**,** 3195-3204.

Dzenko, K. A., Andjelkovic, A. V., Kuziel, W. A. & Pachter, J. S. 2001. The chemokine receptor CCR2 mediates the binding and internalization of monocyte chemoattractant protein-1 along brain microvessels. *Journal of Neuroscience,* 21**,** 9214-9223.

Easton, A. S. & Fraser, P. A. 1994. Variable restriction of albumin diffusion across inflamed cerebral microvessels of the anaesthetized rat. *Journal of Physiology,* 475**,** 147-157.

Easton, A. S., Sarker, M. H. & Fraser, P. A. 1997. Two components of blood-brain barrier disruption in the rat. *Journal of Physiology,* 503 (Pt 3)**,** 613-623.

Ehringer, W. D., Edwards, M. J. & Miller, F. N. 1996. Mechanisms of alpha-thrombin, histamine, and bradykinin induced endothelial permeability. *Journal of Cellular Physiology,* 167**,** 562-569.

Eigenmann, D. E., Xue, G., Kim, K. S., Moses, A. V., Hamburger, M. & Oufir, M. 2013. Comparative study of four immortalized human brain capillary endothelial cell lines, hCMEC/D3, hBMEC, TY10, and BB19, and optimization of culture conditions, for an in vitro blood-brain barrier model for drug permeability studies. *Fluids Barriers CNS,* 10**,** 33.

Engelhardt, B. 2006. Molecular mechanisms involved in T cell migration across the blood–brain barrier. *Journal of Neural Transmission,* 113**,** 477-485.

Engelhardt, B. & Ransohoff, R. M. 2005. The ins and outs of T-lymphocyte trafficking to the CNS: anatomical sites and molecular mechanisms. *Trends in Immunology,* 26**,** 485-495.

Engelhardt, B. & Wolburg, H. 2004. Mini-review: Transendothelial migration of leukocytes: through the front door or around the side of the house? *European Journal of Immunology,* 34**,** 2955-2963.

Esche, C., Stellato, C. & Beck, L. A. 2005. Chemokines: key players in innate and adaptive immunity. *Journal of Investigative Dermatology,* 125**,** 615-628.

Esser, S., Lampugnani, M. G., Corada, M., Dejana, E. & Risau, W. 1998. Vascular endothelial growth factor induces VE-cadherin tyrosine phosphorylation in endothelial cells. *Journal of Cell Science,* 111 (Pt 13)**,** 1853-1865.

Etienne-Manneville, S. 2012. Adherens junctions during cell migration. *Sub-Cellular Biochemistry,* 60**,** 225-249.

Feghali, C. A. & Wright, T. M. 1997. Cytokines in acute and chronic inflammation. *Frontiers in Bioscience,* 2**,** d12-26.

Figueroa, X. F. & Duling, B. R. 2009. Gap junctions in the control of vascular function. *Antioxid Redox Signal,* 11**,** 251-266.

Flemming, S., Burkard, N., Renschler, M., Vielmuth, F., Meir, M., Schick, M. A., Wunder, C., Germer, C. T., Spindler, V., Waschke, J. & Schlegel, N. 2015. Soluble VE-cadherin is involved in endothelial barrier breakdown in systemic inflammation and sepsis. *Cardiovascular Research,* 107**,** 32-44.

Forster, C., Burek, M., Romero, I. A., Weksler, B., Couraud, P. O. & Drenckhahn, D. 2008. Differential effects of hydrocortisone and TNFalpha on tight junction proteins in an in vitro model of the human blood-brain barrier. *Journal of Physiology,* 586**,** 1937-1949.

Fox, J. M., Najarro, P., Smith, G. L., Struyf, S., Proost, P. & Pease, J. E. 2006. Structure/function relationships of CCR8 agonists and antagonists. Amino-terminal extension of CCL1 by a single amino acid generates a partial agonist. *Journal of Biological Chemistry,* 281**,** 36652-36661.

Freese, C., Reinhardt, S., Hefner, G., Unger, R. E., Kirkpatrick, C. J. & Endres, K. 2014. A novel blood-brain barrier co-culture system for drug targeting of Alzheimer's disease: establishment by using acitretin as a model drug. *PloS One,* 9**,** e91003.

Fukuhara, S., Sakurai, A., Sano, H., Yamagishi, A., Somekawa, S., Takakura, N., Saito, Y., Kangawa, K. & Mochizuki, N. 2005. Cyclic AMP potentiates vascular endothelial cadherin-mediated cell-cell contact to enhance endothelial barrier function through an Epac-Rap1 signaling pathway. *Molecular and Cellular Biology,* 25**,** 136-146.

Gardner, T. W., Antonetti, D. A., Barber, A. J., Lieth, E. & Tarbell, J. A. 1999. The molecular structure and function of the inner blood-retinal barrier. Penn State Retina Research Group. *Documenta Ophthalmologica,* 97**,** 229-237.

Gardner, T. W., Lesher, T., Khin, S., Vu, C., Barber, A. J. & Brennan, W. A., Jr. 1996. Histamine reduces ZO-1 tight-junction protein expression in cultured retinal microvascular endothelial cells. *Biochemical Journal,* 320 (Pt 3)**,** 717-721.

Gavard, J. 2009. Breaking the VE-cadherin bonds. *Federation of European Biochemical Societies Letters,* 583**,** 1-6.

Gavard, J. 2014. Endothelial permeability and VE-cadherin: a wacky comradeship. *Cell Adh Migr,* 8**,** 158-164.

Gavard, J. & Gutkind, J. S. 2006. VEGF controls endothelial-cell permeability by promoting the beta-arrestin-dependent endocytosis of VE-cadherin. *Nature Cell Biology,* 8**,** 1223-1234.

Gavard, J., Hou, X., Qu, Y., Masedunskas, A., Martin, D., Weigert, R., Li, X. & Gutkind, J. S. 2009. A role for a CXCR2/phosphatidylinositol 3-kinase gamma signaling axis in acute and chronic vascular permeability. *Molecular and Cellular Biology,* 29**,** 2469-2480.

Geeta, Ramesh, Mclean, Andrewg & Philipp, Mario T. 2013. Cytokines and Chemokines at the Crossroads of Neuroinflammation, Neurodegeneration, and Neuropathic Pain Geeta Ramesh,1 Andrew G. MacLean,2 and Mario T. Philipp1. *Mediators of Inflammation,* 2013.

Ginestier, C., Liu, S., Diebel, M. E., Korkaya, H., Luo, M., Brown, M., Wicinski, J., Cabaud, O., Charafe-Jauffret, E., Birnbaum, D., Guan, J. L., Dontu, G. & Wicha, M. S. 2010. CXCR1 blockade selectively targets human breast cancer stem cells in vitro and in xenografts. *Journal of Clinical Investigation,* 120**,** 485-497.

Gnanadurai, C. W. & Fu, Z. F. 2016. CXCL10 and blood-brain barrier modulation in rabies virus infection. *Oncotarget,* 7**,** 10694-10695.

Goczalik, I., Ulbricht, E., Hollborn, M., Raap, M., Uhlmann, S., Weick, M., Pannicke, T., Wiedemann, P., Bringmann, A., Reichenbach, A. & Francke, M. 2008. Expression of CXCL8, CXCR1, and CXCR2 in neurons and glial cells of the human and rabbit retina. *Investigative Ophthalmology and Visual Science,* 49**,** 4578-4589.

Gong, X., Ming, X., Deng, P. & Jiang, Y. 2010. Mechanisms regulating the nuclear translocation of p38 MAP kinase. *Journal of Cellular Biochemistry,* 110**,** 1420-1429.

Gonzalez-Mariscal, L., Tapia, R. & Chamorro, D. 2008. Crosstalk of tight junction components with signaling pathways. *Biochimica et Biophysica Acta,* 1778**,** 729-756.

Goodenough, D. A. & Paul, D. L. 2009. Gap junctions. *Cold Spring Harbor Perspectives in Biology,* 1**,** a002576.

Gotsch, U., Borges, E., Bosse, R., Boggemeyer, E., Simon, M., Mossmann, H. & Vestweber, D. 1997. VE-cadherin antibody accelerates neutrophil recruitment in vivo. *Journal of Cell Science,* 110 (Pt 5)**,** 583-588.

Granger, D. N. & Senchenkova, E. 2010. Inflammation and the Microcirculation. *Lancet (London, England),* 2**,** 910-911.

Greenwood, J., Etienne-Manneville, S., Adamson, P. & Couraud, P. O. 2002. Lymphocyte migration into the central nervous system: implication of ICAM-1 signalling at the blood-brain barrier. *Vascular Pharmacology,* 38**,** 315-322.

Greenwood, J., Howes, R. & Lightman, S. 1994. The blood-retinal barrier in experimental autoimmune uveoretinitis. Leukocyte interactions and functional damage. *Laboratory Investigation,* 70**,** 39-52.

Greenwood, John, Amos, Claire L., Walters, Claire E., Couraud, Pierre-Olivier, Lyck, Ruth, Engelhardt, Britta & Adamson, Peter 2003. Intracellular domain of brain endothelial ICAM-1 is essential for T-lymphocyte-mediated signalling and migration. *Journal of immunology (Baltimore, Md. : 1950),* 171**,** 2099-2108.

Gregersen, P. K. & Behrens, T. W. 2006. Genetics of autoimmune diseases--disorders of immune homeostasis. *Nat Rev Genet,* 7**,** 917-928.

Guay, J., Lambert, H., Gingras-Breton, G., Lavoie, J. N., Huot, J. & Landry, J. 1997. Regulation of actin filament dynamics by p38 map kinase-mediated phosphorylation of heat shock protein 27. *Journal of Cell Science,* 110 (Pt 3)**,** 357-368.

Gunzel, D. & Yu, A. S. 2013. Claudins and the modulation of tight junction permeability. *Physiological Reviews,* 93**,** 525-569.

Ha, H., Debnath, B. & Neamati, N. 2017. Role of the CXCL8-CXCR1/2 Axis in Cancer and Inflammatory Diseases. *Theranostics,* 7**,** 1543-1588.

Häggström, Mikael 2014. Medical gallery of Mikael Häggström 2014. *WikiJournal of Medicine,* 1.

Hare, D., Collins, S., Cuddington, B. & Mossman, K. 2016. The Importance of Physiologically Relevant Cell Lines for Studying Virus-Host Interactions. *Viruses,* 8**,** 297.

Harkness, K. A., Sussman, J. D., Davies-Jones, G. A., Greenwood, J. & Woodroofe, M. N. 2003. Cytokine regulation of MCP-1 expression in brain and retinal microvascular endothelial cells. *Journal of Neuroimmunology,* 142**,** 1-9.

Harris, E. S. & Nelson, W. J. 2010. VE-cadherin: at the front, center, and sides of endothelial cell organization and function. *Current Opinion in Cell Biology,* 22**,** 651-658.

Hartley, Gill. 2018. *UK Laser C-M* [Online]. Porton Down. Available: https://www.immunology.org/public-information/bitesized-immunology/experimental-techniques/laser-confocal-microscopy [Accessed 22/02/2018].

Hatherell, K., Couraud, P. O., Romero, I. A., Weksler, B. & Pilkington, G. J. 2011. Development of a three-dimensional, all-human in vitro model of the blood-brain barrier using mono-, co-, and tri-cultivation Transwell models. *Journal of Neuroscience Methods,* 199**,** 223-229.

Hawkins, B. T. & Davis, T. P. 2005. The blood-brain barrier/neurovascular unit in health and disease. *Pharmacological Reviews,* 57**,** 173-185.

Hayashi, A., Popovich, K. S., Kim, H. C. & De Juan, E., Jr. 1997. Role of protein tyrosine phosphorylation in rat corneal neovascularization. *Graefes Archive for Clinical and Experimental Ophthalmology,* 235**,** 460-467.

He, Y., Yao, Y., Tsirka, S. E. & Cao, Y. 2014. Cell-culture models of the blood-brain barrier. *Stroke,* 45**,** 2514-2526.

Heidland, August, Klassen, André, Rutkowski, Przemyslaw & Bahner, Udo 2006. The contribution of Rudolf Virchow to the concept of inflammation: what is still of importance? *Journal of Nephrology,* 19 Suppl 10**,** S102-109.

Helms, H. C., Abbott, N. J., Burek, M., Cecchelli, R., Couraud, P. O., Deli, M. A., Forster, C., Galla, H. J., Romero, I. A., Shusta, E. V., Stebbins, M. J., Vandenhaute, E., Weksler, B. & Brodin, B. 2016. In vitro models of the blood-brain barrier: An overview

of commonly used brain endothelial cell culture models and guidelines for their use. *Journal of Cerebral Blood Flow and Metabolism,* 36**,** 862-890.

Hewett, Peter W. 2016. Isolation and Culture of Human Endothelial Cells from Micro- and Macro-vessels. *In:* MARTIN, S. G. & HEWETT, P. W. (eds.) *Angiogenesis Protocols.* New York: Springer New York.

Hickey, W. F. 2001. Basic principles of immunological surveillance of the normal central nervous system. *Glia,* 36**,** 118-124.

Hickey, W. F., Hsu, B. L. & Kimura, H. 1991. T-lymphocyte entry into the central nervous system. *Journal of Neuroscience Research,* 28**,** 254-260.

Hillyer, P. & Male, D. 2005. Expression of chemokines on the surface of different human endothelia. *Immunology and Cell Biology,* 83**,** 375-382.

Hillyer P., Mordelet E., Flynn G., Male D. 2003. Chemokines, chemokine receptors and adhesion molecules on different human endothelia: discriminating the tissue-specific functions that affect leucocyte migration. *Clinical and Experimental Immunology*.

Hirase, T., Staddon, J. M., Saitou, M., Ando-Akatsuka, Y., Itoh, M., Furuse, M., Fujimoto, K., Tsukita, S. & Rubin, L. L. 1997. Occludin as a possible determinant of tight junction permeability in endothelial cells. *Journal of Cell Science,* 110**,** 1603-1613.

Hoefen, R. J. & Berk, B. C. 2002. The role of MAP kinases in endothelial activation. *Vascular Pharmacology,* 38**,** 271-273.

Holman, D. W., Klein, R. S. & Ransohoff, R. M. 2011. The blood-brain barrier, chemokines and multiple sclerosis. *Biochimica et Biophysica Acta,* 1812**,** 220-230.

Howland, S. W., Poh, C. M. & Renia, L. 2015. Activated Brain Endothelial Cells Cross-Present Malaria Antigen. *PLoS Pathogens,* 11**,** e1004963.

Huber, J. D., Egleton, R. D. & Davis, T. P. 2001. Molecular physiology and pathophysiology of tight junctions in the blood-brain barrier. *Trends in Neurosciences,* 24**,** 719-725.

Hudson, N., Powner, M. B., Sarker, M. H., Burgoyne, T., Campbell, M., Ockrim, Z. K., Martinelli, R., Futter, C. E., Grant, M. B., Fraser, P. A., Shima, D. T., Greenwood, J. & Turowski, P. 2014. Differential apicobasal VEGF signaling at vascular blood-neural barriers. *Developmental Cell,* 30**,** 541-552.

Hunter, Tony 2000a. Signaling—2000 and Beyond. *Cell,* 100**,** 113-127.

Hunter, Tony 2000b. Signaling - 2000 and beyond. *Cell,* 100**,** 113-127.

Huveneers, S., Oldenburg, J., Spanjaard, E., Van Der Krogt, G., Grigoriev, I., Akhmanova, A., Rehmann, H. & De Rooij, J. 2012. Vinculin associates with endothelial VE-cadherin junctions to control force-dependent remodeling. *Journal of Cell Biology,* 196**,** 641-652.

Iadecola, C. 2010. The overlap between neurodegenerative and vascular factors in the pathogenesis of dementia. *Acta Neuropathologica,* 120**,** 287-296.

Ingeborg, Klaassen, Cornelis, J. F., Van Noorden, Reiner & Schlingemann, O. 2013. Molecular basis of the inner blood-retinal barrier and its breakdown in diabetic macular edema and other pathological conditions. *Progress in Retinal and Eye Research.* Publisher: Elsevier.

Ivanov, A. I., Parkos, C. A. & Nusrat, A. 2010. Cytoskeletal regulation of epithelial barrier function during inflammation. *American Journal of Pathology,* 177**,** 512-524.

Jamieson, T., Clarke, M., Steele, C. W., Samuel, M. S., Neumann, J., Jung, A., Huels, D., Olson, M. F., Das, S., Nibbs, R. J. & Sansom, O. J. 2012. Inhibition of CXCR2 profoundly suppresses inflammation-driven and spontaneous tumorigenesis. *Journal of Clinical Investigation,* 122**,** 3127-3144.

Janeway, Charles A.;, Travers, Paul;, Walport, Mark; & Shlomchik, Mark J. 2001. Principles of innate and adaptive immunity.

Janeway, Charles A.; Travers, Paul; Walport, Mark; Shlomchik, Mark J. 2001. Principles of innate and adaptive immunity.

Jimenez, N., Krouwer, V. J. & Post, J. A. 2013. A new, rapid and reproducible method to obtain high quality endothelium in vitro. *Cytotechnology,* 65**,** 1-14.

Kaminska, B. 2005. MAPK signalling pathways as molecular targets for anti-inflammatory therapy--from molecular mechanisms to therapeutic benefits. *Biochimica et Biophysica Acta,* 1754**,** 253-262.

Kapitulnik, Jaime 2011. Drug transport and metabolism in the blood-brain barrier. *Frontiers in Pharmacology,* 2**,** 37-37.

Kaur, C., Foulds, W. S. & Ling, E. A. 2008. Blood-retinal barrier in hypoxic ischaemic conditions: basic concepts, clinical features and management. *Progress in Retinal and Eye Research,* 27**,** 622-647.

Kim, D. W., Zloza, A., Broucek, J., Schenkel, J. M., Ruby, C., Samaha, G. & Kaufman, H. L. 2014. Interleukin-2 alters distribution of CD144 (VE-cadherin) in endothelial cells. *Journal of Translational Medicine,* 12**,** 113.

Kim, E. K. & Choi, E. J. 2015. Compromised MAPK signaling in human diseases: an update. *Archives of Toxicology,* 89**,** 867-882.

Kitade, Hironori, Sawamoto, Kazuki, Nagashimada, Mayumi, Inoue, Hiroshi, Yamamoto, Yasuhiko, Sai, Yoshimichi, Takamura, Toshinari, Yamamoto, Hiroshi, Miyamoto, Ken-Ichi, Ginsberg, Henry N., Mukaida, Naofumi, Kaneko, Shuichi & Ota, Tsuguhito 2012. CCR5 Plays a Critical Role in Obesity-Induced Adipose Tissue Inflammation and Insulin Resistance by Regulating Both Macrophage Recruitment and M1/M2 Status. *Diabetes,* 61**,** 1680.

Kobilka, B. K. & Deupi, X. 2007. Conformational complexity of G-protein-coupled receptors. *Trends in Pharmacological Sciences,* 28**,** 397-406.

Koch Ae, Polverini Pj, Kunkel Sl, Harlow La, Dipietro La, Elner Vm, Elner Sg, Strieter Rm 1992. Interleukin-8 as a macrophage derived mediator of angiogenesis. *Science,* 11**,** 1798-1801.

Kohidai, L. & Csaba, G. 1998. Chemotaxis and chemotactic selection induced with cytokines (IL-8, RANTES and TNF-alpha) in the unicellular Tetrahymena pyriformis. *Cytokine,* 10**,** 481-486.

Kong, L. L., Wang, Z. Y., Hu, J. F., Yuan, Y. H., Li, H. & Chen, N. H. 2016. Inhibition of chemokine-like factor 1 improves blood-brain barrier dysfunction in rats following focal cerebral ischemia. *Neuroscience Letters,* 627**,** 192-198.

Kortekaas, R., Leenders, K. L., Van Oostrom, J. C., Vaalburg, W., Bart, J., Willemsen, A. T. & Hendrikse, N. H. 2005. Blood-brain barrier dysfunction in parkinsonian midbrain in vivo. *Annals of Neurology,* 57**,** 176-179.

Kumar, S., West, D. C. & Ager, A. 1987. Heterogeneity in endothelial cells from large vessels and microvessels. *Differentiation,* 36**,** 57-70.

Kyriakis, J. M. & Avruch, J. 2001. Mammalian mitogen-activated protein kinase signal transduction pathways activated by stress and inflammation. *Physiological Reviews,* 81**,** 807-869.

Kyriakis, J. M. & Avruch, J. 2012. Mammalian MAPK signal transduction pathways activated by stress and inflammation: a 10-year update. *Physiological Reviews,* 92**,** 689-737.

Lacotte, S., Brun, S., Muller, S. & Dumortier, H. 2009. CXCR3, inflammation, and autoimmune diseases. *Annals of the New York Academy of Sciences,* 1173**,** 310-317.

Lampe, P. D. & Lau, A. F. 2000. Regulation of gap junctions by phosphorylation of connexins. *Archives of Biochemistry and Biophysics,* 384**,** 205-215.

Lampugnani, M. G., Corada, M., Caveda, L., Breviario, F., Ayalon, O., Geiger, B. & Dejana, E. 1995. The molecular organization of endothelial cell to cell junctions: differential association of plakoglobin, beta-catenin, and alpha-catenin with vascular endothelial cadherin (VE-cadherin). *Journal of Cell Biology,* 129**,** 203-217.

Laposata, M., Dovnarsky, D. K. & Shin, H. S. 1983. Thrombin-induced gap formation in confluent endothelial cell monolayers in vitro. *Blood,* 62**,** 549-556.

Larochelle, C., Alvarez, J. I. & Prat, A. 2011. How do immune cells overcome the blood-brain barrier in multiple sclerosis? *Federation of European Biochemical Societies Letters,* 585**,** 3770-3780.

Lazennec, G. & Richmond, A. 2010. Chemokines and chemokine receptors: new insights into cancer-related inflammation. *Trends in Molecular Medicine,* 16**,** 133-144.

Lee, S. C., Brummet, M. E., Shahabuddin, S., Woodworth, T. G., Georas, S. N., Leiferman, K. M., Gilman, S. C., Stellato, C., Gladue, R. P., Schleimer, R. P. & Beck, L. A. 2000. Cutaneous injection of human subjects with macrophage inflammatory protein-1 alpha induces significant recruitment of neutrophils and monocytes. *Journal of Immunology,* 164**,** 3392-3401.

Lee, Y. R., Liu, M. T., Lei, H. Y., Liu, C. C., Wu, J. M., Tung, Y. C., Lin, Y. S., Yeh, T. M., Chen, S. H. & Liu, H. S. 2006. MCP-1, a highly expressed chemokine in dengue haemorrhagic fever/dengue shock syndrome patients, may cause permeability change, possibly through reduced tight junctions of vascular endothelium cells. *Journal of General Virology,* 87**,** 3623-3630.

Ley, K., Laudanna, C., Cybulsky, M. I. & Nourshargh, S. 2007. Getting to the site of inflammation: the leukocyte adhesion cascade updated. *Nature Reviews: Immunology,* 7**,** 678-689.

Li, A., Dubey, S., Varney, M. L., Dave, B. J. & Singh, R. K. 2003. IL-8 directly enhanced endothelial cell survival, proliferation, and matrix metalloproteinases production and regulated angiogenesis. *Journal of Immunology,* 170**,** 3369-3376.

Li, L., Hu, J., He, T., Zhang, Q., Yang, X., Lan, X., Zhang, D., Mei, H., Chen, B. & Huang, Y. 2015. P38/MAPK contributes to endothelial barrier dysfunction via MAP4 phosphorylation-dependent microtubule disassembly in inflammation-induced acute lung injury. *Scientific Reports,* 5**,** 8895.

Li, R., Luo, C., Mines, M., Zhang, J. & Fan, G. H. 2006. Chemokine CXCL12 induces binding of ferritin heavy chain to the chemokine receptor CXCR4, alters CXCR4 signaling, and induces phosphorylation and nuclear translocation of ferritin heavy chain. *Journal of Biological Chemistry,* 281**,** 37616-37627.

Lim, M. J., Chiang, E. T., Hechtman, H. B. & Shepro, D. 2001. Inflammation-induced subcellular redistribution of VE-cadherin, actin, and gamma-catenin in cultured human lung microvessel endothelial cells. *Microvascular Research,* 62**,** 366-382.

Lim, Mark J., Chiang, Eddie T., Hechtman, Herbert B. & Shepro, David 2001. Inflammation-Induced Subcellular Redistribution of VE-Cadherin, Actin, and γ-Catenin in Cultured Human Lung Microvessel Endothelial Cells. *Microvascular research,* 62**,** 366-382.

Liu, M., Guo, S., Hibbert, J. M., Jain, V., Singh, N., Wilson, N. O. & Stiles, J. K. 2011. CXCL10/IP-10 in infectious diseases pathogenesis and potential therapeutic implications. *Cytokine and Growth Factor Reviews,* 22**,** 121-130.

Liu, Q., Li, A., Tian, Y., Wu, J. D., Liu, Y., Li, T., Chen, Y., Han, X. & Wu, K. 2016. The CXCL8-CXCR1/2 pathways in cancer. *Cytokine and Growth Factor Reviews,* 31**,** 61-71.

Lokeshwar, V. B. & Selzer, M. G. 2000. Differences in hyaluronic acid-mediated functions and signaling in arterial, microvessel, and vein-derived human endothelial cells. *Journal of Biological Chemistry,* 275**,** 27641-27649.

Lu, Peirong, Nakamoto, Yasunari, Nemoto-Sasaki, Yoko, Fujii, Chifumi, Wang, Hui, Hashii, Minako, Ohmoto, Yasukazu, Kaneko, Shuichi, Kobayashi, Kenichi & Mukaida, Naofumi 2003. Potential Interaction between CCR1 and Its Ligand, CCL3, Induced by Endogenously Produced Interleukin-1 in Human Hepatomas. *The American Journal of Pathology,* 162**,** 1249-1258.

Lucas, S. M., Rothwell, N. J. & Gibson, R. M. 2006. The role of inflammation in CNS injury and disease. *British Journal of Pharmacology,* 147 Suppl 1**,** S232-240.

Luciano Ottonelloa, Fabrizio Montecuccoa, Maria Bertolottoa, Nicoletta Arduinoa, Marina Mancinia, Anna Corcioneb, Vito Pistoiab, Franco Dallegria 2005. CCL3 (MIP-1α) induces in vitro migration of GM-CSF-primed human neutrophils via CCR5-dependent activation of ERK 1/2. *Cellular Signalling,* 17**,** 335-363.

Ludwig, Andreas, Ehlert, Jan E., Flad, Hans-Dieter & Brandt, Ernst 2000. Identification of Distinct Surface-Expressed and Intracellular CXC-Chemokine Receptor 2 Glycoforms in Neutrophils: N-Glycosylation Is Essential for Maintenance of Receptor Surface Expression. *The Journal of Immunology,* 165**,** 1044.

Luissint, A. C., Artus, C., Glacial, F., Ganeshamoorthy, K. & Couraud, P. O. 2012. Tight junctions at the blood brain barrier: physiological architecture and disease-associated dysregulation. *Fluids Barriers CNS,* 9**,** 23.

Luscinskas, Francis W., Ma, Shuo, Nusrat, Asma, Parkos, Charles A. & Shaw, Sunil K. 2002. Leukocyte transendothelial migration: A junctional affair. *Elsevier,* 14**,** 105-113.

Luster, A. D., Unkeless, J. C. & Ravetch, J. V. 1985. Gamma-interferon transcriptionally regulates an early-response gene containing homology to platelet proteins. *Nature,* 315**,** 672-676.

Ma, S. C., Li, Q., Peng, J. Y., Zhouwen, J. L., Diao, J. F., Niu, J. X., Wang, X., Guan, X. D., Jia, W. & Jiang, W. G. 2017. Claudin-5 regulates blood-brain barrier permeability by modifying brain microvascular endothelial cell proliferation, migration, and adhesion to prevent lung cancer metastasis. *CNS Neuroscience & Therapeutics,* 23**,** 947-960.

Mahtani, K. R., Brook, M., Dean, J. L., Sully, G., Saklatvala, J. & Clark, A. R. 2001. Mitogen-activated protein kinase p38 controls the expression and posttranslational modification of tristetraprolin, a regulator of tumor necrosis factor alpha mRNA stability. *Molecular and Cellular Biology,* 21**,** 6461-6469.

Man, S., Ubogu, E. E., Williams, K. A., Tucky, B., Callahan, M. K. & Ransohoff, R. M. 2008. Human brain microvascular endothelial cells and umbilical vein endothelial cells differentially facilitate leukocyte recruitment and utilize chemokines for T cell migration. *Clinical & Developmental Immunology,* 2008**,** 384982.

Mancardi, S., Vecile, E., Dusetti, N., Calvo, E., Stanta, G., Burrone, O. R. & Dobrina, A. 2003. Evidence of CXC, CC and C chemokine production by lymphatic endothelial cells. *Immunology,* 108**,** 523-530.

Manes, T. D., Shiao, S. L., Dengler, T. J. & Pober, J. S. 2007. TCR signaling antagonizes rapid IP-10-mediated transendothelial migration of effector memory CD4+ T cells. *Journal of Immunology,* 178**,** 3237-3243.

Manning, G., Whyte, D. B., Martinez, R., Hunter, T. & Sudarsanam, S. 2002. The protein kinase complement of the human genome. *Science,* 298**,** 1912-1934.

Manousou, P., Kolios, G., Valatas, V., Drygiannakis, I., Bourikas, L., Pyrovolaki, K., Koutroubakis, I., Papadaki, H. A. & Kouroumalis, E. 2010. Increased expression of chemokine receptor CCR3 and its ligands in ulcerative colitis: the role of colonic epithelial cells in in vitro studies. *Clinical and Experimental Immunology,* 162**,** 337-347.

Mantovani, A. 1999. The chemokine system: redundancy for robust outputs. *Immunology Today,* 20**,** 254-257.

Mantovani, A., Bonecchi, R. & Locati, M. 2006. Tuning inflammation and immunity by chemokine sequestration: decoys and more. *Nature Reviews: Immunology,* 6**,** 907-918.

Marsh, D. R. & Flemming, J. M. 2011. Inhibition of CXCR1 and CXCR2 chemokine receptors attenuates acute inflammation, preserves gray matter and diminishes autonomic dysreflexia after spinal cord injury. *Spinal Cord,* 49**,** 337-344.

Martinelli, R., Zeiger, A. S., Whitfield, M., Sciuto, T. E., Dvorak, A., Van Vliet, K. J., Greenwood, J. & Carman, C. V. 2014. Probing the biomechanical contribution of the endothelium to lymphocyte migration: diapedesis by the path of least resistance. *Journal of Cell Science,* 127**,** 3720-3734.

Masopust, D. & Schenkel, J. M. 2013. The integration of T cell migration, differentiation and function. *Nature Reviews: Immunology,* 13**,** 309-320.

Massena, S. & Philipson, M. 2012. Intravascular Leukocyte Chemotaxis: The Rules of Attraction. *Hematology - Science and Practice***,** 229-242.

Maurer, M. & Von Stebut, E. 2004. Macrophage inflammatory protein-1. *International Journal of Biochemistry and Cell Biology,* 36**,** 1882-1886.

Mckimmie, Clive & Michlmayr, Daniela 2014. Role of CXCL10 in central nervous system inflammation. *International Journal of Interferon, Cytokine and Mediator Research,* 2014**,** 1.

Menten, P., Wuyts, A. & Van Damme, J. 2002. Macrophage inflammatory protein-1. *Cytokine and Growth Factor Reviews,* 13**,** 455-481.

Metrikin, D. C., Wilson, C. A., Berkowitz, B. A., Lam, M. K., Wood, G. K. & Peshock, R. M. 1995. Measurement of blood-retinal barrier breakdown in endotoxin-induced endophthalmitis. *Investigative Ophthalmology and Visual Science,* 36**,** 1361-1370.

Michiels, C. 2003. Endothelial cell functions. *Journal of Cellular Physiology,* 196**,** 430-443.

Middleton, J., Neil, S., Wintle, J., Clark-Lewis, I., Moore, H., Lam, C., Auer, M., Hub, E. & Rot, A. 1997. Transcytosis and surface presentation of IL-8 by venular endothelial cells. *Cell,* 91**,** 385-395.

Millan, J., Cain, R. J., Reglero-Real, N., Bigarella, C., Marcos-Ramiro, B., Fernandez-Martin, L., Correas, I. & Ridley, A. J. 2010. Adherens junctions connect stress fibres between adjacent endothelial cells. *BMC Biology,* 8**,** 11.

Millard, C. J., Ludeman, J. P., Canals, M., Bridgford, J. L., Hinds, M. G., Clayton, D. J., Christopoulos, A., Payne, R. J. & Stone, M. J. 2014. Structural basis of receptor sulfotyrosine recognition by a CC chemokine: the N-terminal region of CCR3 bound to CCL11/eotaxin-1. *Structure,* 22**,** 1571-1581.

Mittelstadt, P. R., Salvador, J. M., Fornace, A. J., Jr. & Ashwell, J. D. 2005. Activating p38 MAPK: new tricks for an old kinase. *Cell Cycle,* 4**,** 1189-1192.

Miyasaka, M. & Tanaka, T. 2004. Lymphocyte trafficking across high endothelial venules: dogmas and enigmas. *Nature Reviews: Immunology,* 4**,** 360-370.

Monahan-Earley, R., Dvorak, A. M. & Aird, W. C. 2013. Evolutionary origins of the blood vascular system and endothelium. *Journal of Thrombosis and Haemostasis,* 11 Suppl 1**,** 46-66.

Moses, A. V., Bloom, F. E., Pauza, C. D. & Nelson, J. A. 1993. Human immunodeficiency virus infection of human brain capillary endothelial cells occurs via a CD4/galactosylceramide-independent mechanism. *Proceedings of the National Academy of Sciences of the United States of America,* 90**,** 10474-10478.

Mueller, S. G., Schraw, W. P. & Richmond, A. 1995. Activation of protein kinase C enhances the phosphorylation of the type B interleukin-8 receptor and stimulates its degradation in non-hematopoietic cells. *Journal of Biological Chemistry,* 270**,** 10439-10448.

Muller, W. A. 2011. Mechanisms of leukocyte transendothelial migration. *Annual Review of Pathology,* 6**,** 323-344.

Murdoch, C. & Finn, A. 2000. Chemokine receptors and their role in inflammation and infectious diseases. *Blood,* 95**,** 3032-3043.

Nagar, B., Overduin, M., Ikura, M. & Rini, J. M. 1996. Structural basis of calcium-induced E-cadherin rigidification and dimerization. *Nature,* 380**,** 360-364.

Nagy, J. A., Benjamin, L., Zeng, H., Dvorak, A. M. & Dvorak, H. F. 2008. Vascular permeability, vascular hyperpermeability and angiogenesis. *Angiogenesis,* 11**,** 109-119.

Naor, Z., Benard, O. & Seger, R. 2000. Activation of MAPK cascades by G-protein-coupled receptors: the case of gonadotropin-releasing hormone receptor. *Trends in Endocrinology and Metabolism,* 11**,** 91-99.

Natalie Hudson, Michael B. Powner, Mosharraf H. Sarker, Thomas Burgoyne, Matthew Campbell, Zoe K. Ockrim, Roberta Martinelli, Clare E. Futter, Maria B. Grant, Paul A. Fraser, David T. Shima, John Greenwood and Patric Turowski 2014. Differential Apicobasal VEGF Signaling at Vascular Blood-Neural Barriers. *Developmental Cell,* 30**,** 541-522.

Nathan, C. 2002. Points of control in inflammation. *Nature,* 420**,** 846-852.

Navarro, P., Caveda, L., Breviario, F., Mandoteanu, I., Lampugnani, M. G. & Dejana, E. 1995. Catenin-dependent and -independent functions of vascular endothelial cadherin. *Journal of Biological Chemistry,* 270**,** 30965-30972.

Norman, M. U. & Hickey, M. J. 2005. Mechanisms of lymphocyte migration in autoimmune disease. *Tissue Antigens,* 66**,** 163-172.

Nourshargh, S., Hordijk, P. L. & Sixt, M. 2010. Breaching multiple barriers: leukocyte motility through venular walls and the interstitium. *Nature Reviews: Molecular Cell Biology,* 11**,** 366-378.

Numahata, K., Komagata, T., Hirasawa, N., Someya, K., Xiao, Y. Q. & Ohuchi, K. 2003. Analysis of the mechanism regulating the stability of rat macrophage inflammatory protein-2 mRNA in RBL-2H3 cells. *Journal of Cellular Biochemistry,* 90**,** 976-986.

Oltra-Noguera, D., Mangas-Sanjuan, V., Centelles-Sanguesa, A., Gonzalez-Garcia, I., Sanchez-Castano, G., Gonzalez-Alvarez, M., Casabo, V. G., Merino, V., Gonzalez-Alvarez, I. & Bermejo, M. 2015. Variability of permeability estimation from different

protocols of subculture and transport experiments in cell monolayers. *Journal of Pharmacological and Toxicological Methods,* 71**,** 21-32.

Omatsu, T., Cepinskas, G., Clarson, C., Patterson, E. K., Alharfi, I. M., Summers, K., Couraud, P. O., Romero, I. A., Weksler, B., Fraser, D. D. & Canadian Critical Care Translational Biology, Group 2014. CXCL1/CXCL8 (GROalpha/IL-8) in human diabetic ketoacidosis plasma facilitates leukocyte recruitment to cerebrovascular endothelium in vitro. *American Journal of Physiology: Endocrinology and Metabolism,* 306**,** E1077-1084.

Oppermann, M., Mack, M., Proudfoot, A. E. & Olbrich, H. 1999. Differential effects of CC chemokines on CC chemokine receptor 5 (CCR5) phosphorylation and identification of phosphorylation sites on the CCR5 carboxyl terminus. *Journal of Biological Chemistry,* 274**,** 8875-8885.

Page, S., Munsell, A. & Al-Ahmad, A. J. 2016. Cerebral hypoxia/ischemia selectively disrupts tight junctions complexes in stem cell-derived human brain microvascular endothelial cells. *Fluids Barriers CNS,* 13**,** 16.

Pasantes-Morales, H. & Franco, R. 2002. Influence of protein tyrosine kinases on cell volume change-induced taurine release. *Cerebellum,* 1**,** 103-109.

Pearson, Gray, Robinson, Fred, Beers Gibson, Tara, Xu, Bing-E, Karandikar, Mahesh, Berman, Kevin & Cobb, Melanie H. 2001. Mitogen-Activated Protein (MAP) Kinase Pathways: Regulation and Physiological Functions*. *Endocrine Reviews,* 22**,** 153-183.

Perriere, N., Yousif, S., Cazaubon, S., Chaverot, N., Bourasset, F., Cisternino, S., Decleves, X., Hori, S., Terasaki, T., Deli, M., Scherrmann, J. M., Temsamani, J., Roux, F. & Couraud, P. O. 2007. A functional in vitro model of rat blood-brain barrier for molecular analysis of efflux transporters. *Brain Research,* 1150**,** 1-13.

Petreaca, M. L., Yao, M., Liu, Y., Defea, K. & Martins-Green, M. 2007. Transactivation of vascular endothelial growth factor receptor-2 by interleukin-8 (IL-8/CXCL8) is required for IL-8/CXCL8-induced endothelial permeability. *Molecular Biology of the Cell,* 18**,** 5014-5023.

Petti, L. M., Marlatt, S. A., Luo, Y., Scheideman, E. H., Shelar, A. & Dimaio, D. 2018. Regulation of C-C chemokine receptor 5 (CCR5) stability by Lys(197) and by

transmembrane protein aptamers that target it for lysosomal degradation. *Journal of Biological Chemistry,* 293**,** 8787-8801.

Phillips, Marian J., Needham, Michelle & Weller, Roy O. 1999. Role of cervical lymph nodes in autoimmune encephalomyelitis in the Lewis rat. *The Journal of Pathology,* 182**,** 457-464.

Plenchette, S., Cathelin, S., Rebe, C., Launay, S., Ladoire, S., Sordet, O., Ponnelle, T., Debili, N., Phan, T. H., Padua, R. A., Dubrez-Daloz, L. & Solary, E. 2004. Translocation of the inhibitor of apoptosis protein c-IAP1 from the nucleus to the Golgi in hematopoietic cells undergoing differentiation: a nuclear export signal-mediated event. *Blood,* 104**,** 2035-2043.

Pober, J. S. & Sessa, W. C. 2007. Evolving functions of endothelial cells in inflammation. *Nature Reviews: Immunology,* 7**,** 803-815.

Prasain, N. & Stevens, T. 2009. The actin cytoskeleton in endothelial cell phenotypes. *Microvascular Research,* 77**,** 53-63.

Privratsky, J. R. & Newman, P. J. 2014. PECAM-1: regulator of endothelial junctional integrity. *Cell and Tissue Research,* 355**,** 607-619.

Quandt, J. & Dorovini-Zis, K. 2004. The beta chemokines CCL4 and CCL5 enhance adhesion of specific CD4+ T cell subsets to human brain endothelial cells. *Journal of Neuropathology and Experimental Neurology,* 63**,** 350-362.

Rabiet, M. J. P., Plantier, J. L., Rival, Y., Genoux, Y., Lampugnani, M. G. & Dejana, E. 1996. Thrombin-induced increase in endothelial permeability is associated with changes in cell-to-cell junction organization. *Arteriosclerosis Thrombosis and Vascular Biology,* 16**,** 488-496.

Raman, M., Chen, W. & Cobb, M. H. 2007. Differential regulation and properties of MAPKs. *Oncogene,* 26**,** 3100-3112.

Rangasamy, S., Mcguire, P. G., Franco Nitta, C., Monickaraj, F., Oruganti, S. R. & Das, A. 2014. Chemokine mediated monocyte trafficking into the retina: role of inflammation in alteration of the blood-retinal barrier in diabetic retinopathy. *PloS One,* 9**,** e108508.

Raper, Daniel, Louveau, Antoine & Kipnis, Jonathan 2016. How Do Meningeal Lymphatic Vessels Drain the CNS? *Trends in Neurosciences,* 39**,** 581-586.

Reichel, Andreas, Begley, David J. & Abbott, N. Joan 2003. An Overview of In Vitro Techniques for Blood-Brain Barrier Studies. *In:* NAG, S. (ed.) *The Blood-Brain Barrier: Biology and Research Protocols.* Totowa, NJ: Humana Press.

Reichenbach, Z. W., Li, H., Gaughan, J. P., Elliott, M. & Tuma, R. 2015. IV and IP administration of rhodamine in visualization of WBC-BBB interactions in cerebral vessels. *Microscopy Research and Technique,* 78**,** 894-899.

Reitsma, S., Slaaf, D. W., Vink, H., Van Zandvoort, M. A. & Oude Egbrink, M. G. 2007. The endothelial glycocalyx: composition, functions, and visualization. *Pflügers Archiv. European Journal of Physiology,* 454**,** 345-359.

Roberts, T. K., Eugenin, E. A., Lopez, L., Romero, I. A., Weksler, B. B., Couraud, P. O. & Berman, J. W. 2012. CCL2 disrupts the adherens junction: implications for neuroinflammation. *Laboratory Investigation,* 92**,** 1213-1233.

Rocha, S. F. & Adams, R. H. 2009. Molecular differentiation and specialization of vascular beds. *Angiogenesis,* 12**,** 139-147.

Rosenbaum, James T., Woods, April, Kezic, Jelena, Planck, Stephen R. & Rosenzweig, Holly L. 2011. Contrasting ocular effects of local versus systemic endotoxin. *Investigative Ophthalmology and Visual Science,* 52**,** 6472-6477.

Roskoski, R., Jr. 2012. ERK1/2 MAP kinases: structure, function, and regulation. *Pharmacological Research,* 66**,** 105-143.

Rousseau, S., Houle, F., Landry, J. & Huot, J. 1997. p38 MAP kinase activation by vascular endothelial growth factor mediates actin reorganization and cell migration in human endothelial cells. *Oncogene,* 15**,** 2169-2177.

Roux, P. P. & Blenis, J. 2004. ERK and p38 MAPK-activated protein kinases: a family of protein kinases with diverse biological functions. *Microbiology and Molecular Biology Reviews,* 68**,** 320-344.

Russo, R. C., Garcia, C. C., Teixeira, M. M. & Amaral, F. A. 2014. The CXCL8/IL-8 chemokine family and its receptors in inflammatory diseases. *Expert Review of Clinical Immunology,* 10**,** 593-619.

Salcedo R., Et Al. 2000. Differential expression and responsiveness of chemokine receptors (CXCR1–3) by human microvascular endothelial cells and umbilical vein endothelial cells. *FASEB,* 14**,** 2055-2064.

Sarker, M. H., Hu, D. E. & Fraser, P. A. 2000. Acute effects of bradykinin on cerebral microvascular permeability in the anaesthetized rat. *Journal of Physiology,* 528 Pt 1**,** 177-187.

Schenkel, A. R., Mamdouh, Z., Chen, X., Liebman, R. M. & Muller, W. A. 2002. CD99 plays a major role in the migration of monocytes through endothelial junctions. *Nature Immunology,* 3**,** 143-150.

Schraufstatter, I. U., Chung, J. & Burger, M. 2001. IL-8 activates endothelial cell CXCR1 and CXCR2 through Rho and Rac signaling pathways. *American Journal of Physiology-Lung Cellular and Molecular Physiology,* 280**,** L1094-L1103.

Schulte, D., Kuppers, V., Dartsch, N., Broermann, A., Li, H., Zarbock, A., Kamenyeva, O., Kiefer, F., Khandoga, A., Massberg, S. & Vestweber, D. 2011. Stabilizing the VE-cadherin-catenin complex blocks leukocyte extravasation and vascular permeability. *EMBO Journal,* 30**,** 4157-4170.

Schulze, C., Smales, C., Rubin, L. L. & Staddon, J. M. 1997. Lysophosphatidic acid increases tight junction permeability in cultured brain endothelial cells. *Journal of Neurochemistry,* 68**,** 991-1000.

Scott, A. 2004. What is "inflammation"? Are we ready to move beyond Celsus? *British Journal of Sports Medicine,* 38**,** 248-249.

Seger, R. & Krebs, E. G. 1995. The MAPK signaling cascade. *FASEB Journal,* 9**,** 726-735.

Semple, B. D., Kossmann, T. & Morganti-Kossmann, M. C. 2010. Role of chemokines in CNS health and pathology: a focus on the CCL2/CCR2 and CXCL8/CXCR2 networks. *Journal of Cerebral Blood Flow and Metabolism,* 30**,** 459-473.

Shahabuddin, S., Ji, R., Wang, P., Brailoiu, E., Dun, N., Yang, Y., Aksoy, M. O. & Kelsen, S. G. 2006. CXCR3 chemokine receptor-induced chemotaxis in human airway epithelial cells: role of p38 MAPK and PI3K signaling pathways. *American Journal of Physiology: Cell Physiology,* 291**,** C34-39.

Shechter, R., London, A. & Schwartz, M. 2013. Orchestrated leukocyte recruitment to immune-privileged sites: absolute barriers versus educational gates. *Nature Reviews: Immunology,* 13**,** 206-218.

Shiu, C., Barbier, E., Di Cello, F., Choi, H. J. & Stins, M. 2007. HIV-1 gp120 as well as alcohol affect blood-brain barrier permeability and stress fiber formation: involvement of reactive oxygen species. *Alcoholism, Clinical and Experimental Research,* 31**,** 130-137.

Siflinger-Birnboim, A., Del Vecchio, P. J., Cooper, J. A., Blumenstock, F. A., Shepard, J. M. & Malik, A. B. 1987. Molecular sieving characteristics of the cultured endothelial monolayer. *Journal of Cellular Physiology,* 132**,** 111-117.

Smith, K. A. 1988. Interleukin-2: inception, impact, and implications. *Science,* 240**,** 1169.

Smith, Michael L., Olson, Timothy S. & Ley, Klaus 2004. CXCR2- and E-Selectin–induced Neutrophil Arrest during Inflammation In Vivo. *The Journal of Experimental Medicine,* 200**,** 935.

Soejima, K. & Rollins, B. J. 2001. A functional IFN-gamma-inducible protein-10/CXCL10-specific receptor expressed by epithelial and endothelial cells that is neither CXCR3 nor glycosaminoglycan. *Journal of Immunology,* 167**,** 6576-6582.

Sokol, C. L. & Luster, A. D. 2015. The chemokine system in innate immunity. *Cold Spring Harbor Perspectives in Biology,* 7**,** a016303.

Speyer, C. L. & Ward, P. A. 2011. Role of endothelial chemokines and their receptors during inflammation. *Journal of Investigative Surgery,* 24**,** 18-27.

Speyer C., Ward P. 2011. Role of Endothelial Chemokines and TheirReceptors during Inflammation. *Journal of Investigative Surgery,* 24**,** 18-27.

Springer, T. A. 1994. Traffic signals for lymphocyte recirculation and leukocyte emigration: the multistep paradigm. *Cell,* 76**,** 301-314.

Srinivasan, B., Kolli, A. R., Esch, M. B., Abaci, H. E., Shuler, M. L. & Hickman, J. J. 2015. TEER measurement techniques for in vitro barrier model systems. *J Lab Autom,* 20**,** 107-126.

Staddon, J. M., Herrenknecht, K., Smales, C. & Rubin, L. L. 1995. Evidence that tyrosine phosphorylation may increase tight junction permeability. *J Cell Sci,* 108 (Pt 2)**,** 609-619.

Stamatovic, S. M., Dimitrijevic, O. B., Keep, R. F. & Andjelkovic, A. V. 2006. Inflammation and brain edema: new insights into the role of chemokines and their receptors. *In:* HOFF, J. T., KEEP, R. F., XI, G. & HUA, Y. (eds.) *Brain Edema XIII.* Vienna: Springer Vienna.

Stamatovic, S. M., Keep, R. F. & Andjelkovic, A. V. 2008. Brain endothelial cell-cell junctions: how to "open" the blood brain barrier. *Current Neuropharmacology,* 6**,** 179-192.

Stamatovic, S. M., Keep, R. F., Kunkel, S. L. & Andjelkovic, A. V. 2003. Potential role of MCP-1 in endothelial cell tight junction 'opening': signaling via Rho and Rho kinase. *Journal of Cell Science,* 116.

Stamatovic, S. M., Keep, R. F., Wang, M. M., Jankovic, I. & Andjelkovic, A. V. 2009. Caveolae-mediated internalization of occludin and claudin-5 during CCL2-induced tight junction remodeling in brain endothelial cells. *Journal of Biological Chemistry,* 284**,** 19053-19066.

Steffen, B. J., Breier, G., Butcher, E. C., Schulz, M. & Engelhardt, B. 1996. ICAM-1, VCAM-1, and MAdCAM-1 are expressed on choroid plexus epithelium but not endothelium and mediate binding of lymphocytes in vitro. *American Journal of Pathology,* 148**,** 1819-1838.

Strieter, R. M., Burdick, M. D., Gomperts, B. N., Belperio, J. A. & Keane, M. P. 2005. CXC chemokines in angiogenesis. *Cytokine and Growth Factor Reviews,* 16**,** 593-609.

Stuart, R. O., Sun, A., Panichas, M., Hebert, S. C., Brenner, B. M. & Nigam, S. K. 1994. Critical role for intracellular calcium in tight junction biogenesis. *Journal of Cellular Physiology,* 159**,** 423-433.

Subileau, E. A., Rezaie, P., Davies, H. A., Colyer, F. M., Greenwood, J., Male, D. K. & Romero, I. A. 2009. Expression of Chemokines and Their Receptors by Human Brain Endothelium: Implications for Multiple Sclerosis. *Journal of Neuropathology and Experimental Neurology,* 68**,** 227-240.

Suffredini, Anthony F., Fantuzzi, Giamila, Badolato, Raffaele, Oppenheim, Joost J. & O'grady, Naomi P. 1999. New insights into the biology of the acute phase response. *Journal of Clinical Immunology,* 19**,** 203-214.

Sugimoto, M., Nakayama, M., Goto, T. M., Amano, M., Komori, K. & Kaibuchi, K. 2007. Rho-kinase phosphorylates eNOS at threonine 495 in endothelial cells. *Biochemical and Biophysical Research Communications,* 361**,** 462-467.

Sumagin, R., Lomakina, E. & Sarelius, I. H. 2008. Leukocyte-endothelial cell interactions are linked to vascular permeability via ICAM-1-mediated signaling. *American Journal of Physiology: Heart and Circulatory Physiology,* 295**,** H969-H977.

Sun, Y., Li, N., Zhang, J., Liu, H., Liu, J., Xia, X., Sun, C., Feng, X., Gu, J., Du, C., Han, W. & Lei, L. 2016. Enolase of Streptococcus Suis Serotype 2 Enhances Blood-Brain Barrier Permeability by Inducing IL-8 Release. *Inflammation,* 39**,** 718-726.

Szulcek, R., Bogaard, H. J. & Van Nieuw Amerongen, G. P. 2014. Electric cell-substrate impedance sensing for the quantification of endothelial proliferation, barrier function, and motility. *J Vis Exp,* 10.3791/51300**,** 51300.

Tai, L. M., Holloway, K. A., Male, D. K., Loughlin, A. J. & Romero, I. A. 2010. Amyloid-beta-induced occludin down-regulation and increased permeability in human brain endothelial cells is mediated by MAPK activation. *Journal of Cellular and Molecular Medicine,* 14.

Tai, L. M., Reddy, P. S., Lopez-Ramirez, M. A., Davies, H. A., Male, D. K., Loughlin, A. J. & Romero, I. A. 2009. Polarized P-glycoprotein expression by the immortalised human brain endothelial cell line, hCMEC/D3, restricts apical-to-basolateral permeability to rhodamine 123. *Brain Research,* 1292**,** 14-24.

Takeshita, Y. & Ransohoff, R. M. 2012. Inflammatory cell trafficking across the blood-brain barrier: chemokine regulation and in vitro models. *Immunological Reviews,* 248**,** 228-239.

Tamura, K., Shan, W. S., Hendrickson, W. A., Colman, D. R. & Shapiro, L. 1998. Structure-function analysis of cell adhesion by neural (N-) cadherin. *Neuron,* 20**,** 1153-1163.

Tebo, J., Der, S., Frevel, M., Khabar, K. S., Williams, B. R. & Hamilton, T. A. 2003. Heterogeneity in control of mRNA stability by AU-rich elements. *Journal of Biological Chemistry,* 278**,** 12085-12093.

Thomas, A., Wang, S., Sohrabi, S., Orr, C., He, R., Shi, W. & Liu, Y. 2017. Characterization of vascular permeability using a biomimetic microfluidic blood vessel model. *Biomicrofluidics,* 11**,** 024102.

Tudor, C., Marchese, F. P., Hitti, E., Aubareda, A., Rawlinson, L., Gaestel, M., Blackshear, P. J., Clark, A. R., Saklatvala, J. & Dean, J. L. 2009. The p38 MAPK pathway inhibits tristetraprolin-directed decay of interleukin-10 and pro-inflammatory mediator mRNAs in murine macrophages. *Federation of European Biochemical Societies Letters,* 583**,** 1933-1938.

Turowski, P., Adamson, P. & Greenwood, J. 2005. Pharmacological targeting of ICAM-1 signaling in brain endothelial cells: potential for treating neuroinflammation. *Cellular and Molecular Neurobiology,* 25**,** 153-170.

Turowski, P., Martinelli, R., Crawford, R., Wateridge, D., Papageorgiou, A. P., Lampugnani, M. G., Gamp, A. C., Vestweber, D., Adamson, P., Dejana, E. & Greenwood, J. 2008. Phosphorylation of vascular endothelial cadherin controls lymphocyte emigration. *Journal of Cell Science,* 121**,** 29-37.

Ueno, M. 2009. Mechanisms of the penetration of blood-borne substances into the brain. *Current Neuropharmacology,* 7**,** 142-149.

Valentijn, K. M., Sadler, J. E., Valentijn, J. A., Voorberg, J. & Eikenboom, J. 2011. Functional architecture of Weibel-Palade bodies. *Blood,* 117**,** 5033-5043.

Van Buul, J. D. & Hordijk, P. L. 2004. Signaling in leukocyte transendothelial migration. *Arteriosclerosis, Thrombosis, and Vascular Biology,* 24**,** 824-833.

Van De Wetering, M., Oving, I., Muncan, V., Pon Fong, M. T., Brantjes, H., Van Leenen, D., Holstege, F. C., Brummelkamp, T. R., Agami, R. & Clevers, H. 2003. Specific inhibition of gene expression using a stably integrated, inducible small-interfering-RNA vector. *EMBO Rep,* 4**,** 609-615.

Villringer, A., Dirnagl, U., Them, A., Schurer, L., Krombach, F. & Einhaupl, K. M. 1991. Imaging of leukocytes within the rat brain cortex in vivo. *Microvascular Research,* 42**,** 305-315.

Volpe, D. A. 2008. Variability in Caco-2 and MDCK cell-based intestinal permeability assays. *Journal of Pharmaceutical Sciences,* 97**,** 712-725.

Vu, K., Weksler, B., Romero, I., Couraud, P. O. & Gelli, A. 2009. Immortalized human brain endothelial cell line HCMEC/D3 as a model of the blood-brain barrier facilitates in vitro studies of central nervous system infection by Cryptococcus neoformans. *Eukaryot Cell,* 8**,** 1803-1807.

Vukic, V., Callaghan, D., Walker, D., Lue, L. F., Liu, Q. Y., Couraud, P. O., Romero, I. A., Weksler, B., Stanimirovic, D. B. & Zhang, W. 2009. Expression of inflammatory genes induced by beta-amyloid peptides in human brain endothelial cells and in Alzheimer's brain is mediated by the JNK-AP1 signaling pathway. *Neurobiology of Disease,* 34**,** 95-106.

Wachtel, M., Frei, K., Ehler, E., Fontana, A., Winterhalter, K. & Gloor, S. M. 1999. Occludin proteolysis and increased permeability in endothelial cells through tyrosine phosphatase inhibition. *Journal of Cell Science,* 112 (Pt 23)**,** 4347-4356.

Wallez, Y. & Huber, P. 2008. Endothelial adherens and tight junctions in vascular homeostasis, inflammation and angiogenesis. *Biochimica et Biophysica Acta,* 1778**,** 794-809.

Wang, W., Dentler, W. L. & Borchardt, R. T. 2001. VEGF increases BMEC monolayer permeability by affecting occludin expression and tight junction assembly. *American Journal of Physiology: Heart and Circulatory Physiology,* 280**,** H434-440.

Wang, Y., Zhang, J., Yi, X. J. & Yu, F. S. 2004. Activation of ERK1/2 MAP kinase pathway induces tight junction disruption in human corneal epithelial cells. *Experimental Eye Research,* 78**,** 125-136.

Waugh, D. J. & Wilson, C. 2008. The interleukin-8 pathway in cancer. *Clinical Cancer Research,* 14**,** 6735-6741.

Weber, C., Fraemohs, L. & Dejana, E. 2007. The role of junctional adhesion molecules in vascular inflammation. *Nature Reviews: Immunology,* 7**,** 467-477.

Wegener, J. & Seebach, J. 2014. Experimental tools to monitor the dynamics of endothelial barrier function: a survey of in vitro approaches. *Cell and Tissue Research,* 355**,** 485-514.

Weksler, B. B. 2005. Blood-brain barrier-specific properties of a human adult brain endothelial cell line. *The FASEB Journal,* 10.1096/fj.04-3458fje.

Weksler, B. B., Subileau, E. A., Perriere, N., Charneau, P., Holloway, K., Leveque, M., Tricoire-Leignel, H., Nicotra, A., Bourdoulous, S., Turowski, P., Male, D. K., Roux, F., Greenwood, J., Romero, I. A. & Couraud, P. O. 2005. Blood-brain barrier-specific properties of a human adult brain endothelial cell line. *FASEB Journal,* 19**,** 1872-1874.

Weksler, B., Romero, I. A. & Couraud, P. O. 2013. The hCMEC/D3 cell line as a model of the human blood brain barrier. *Fluids Barriers CNS,* 10**,** 16.

Weller, R. O., Galea, I., Carare, R. O. & Minagar, A. 2010. Pathophysiology of the lymphatic drainage of the central nervous system: Implications for pathogenesis and therapy of multiple sclerosis. *Pathophysiology,* 17**,** 295-306.

Wewer, C., Seibt, A., Wolburg, H., Greune, L., Schmidt, M. A., Berger, J., Galla, H. J., Quitsch, U., Schwerk, C., Schroten, H. & Tenenbaum, T. 2011. Transcellular migration of neutrophil granulocytes through the blood-cerebrospinal fluid barrier after infection with Streptococcus suis. *Journal of Neuroinflammation,* 8**,** 51.

Wilhelm, I., Fazakas, C. & Krizbai, I. A. 2011. In vitro models of the blood-brain barrier. *Acta Neurobiologiae Experimentalis,* 71**,** 113-128.

Wolff, B., Burns, A. R., Middleton, J. & Rot, A. 1998. Endothelial cell "memory" of inflammatory stimulation: human venular endothelial cells store interleukin 8 in Weibel-Palade bodies. *Journal of Experimental Medicine,* 188**,** 1757-1762.

Wong, A. J., Pollard, T. D. & Herman, I. M. 1983. Actin filament stress fibers in vascular endothelial cells in vivo. *Science,* 219**,** 867-869.

Wong, Raymond K., Baldwin, Ann L. & Heimark, Ronald L. 1999. Cadherin-5 redistribution at sites of TNF-α and IFN-γ-induced permeability in mesenteric venules. *American Journal of Physiology - Heart and Circulatory Physiology,* 276**,** H736-H748.

Worzfeld, T. & Schwaninger, M. 2016. Apicobasal polarity of brain endothelial cells. *Journal of Cerebral Blood Flow and Metabolism,* 36**,** 340-362.

Xiao, L., Liu, Y. & Wang, N. 2014. New paradigms in inflammatory signaling in vascular endothelial cells. *American Journal of Physiology: Heart and Circulatory Physiology,* 306**,** H317-325.

Xie, Jenny H., Nomura, Naomi, Lu, Min, Chen, Shiow-Ling, Koch, Greg E., Weng, Youmin, Rosa, Raymond, Di Salvo, Jerry, Mudgett, John, Peterson, Laurence B., Wicker, Linda S. & Demartino, Julie A. 2003. Antibody-mediated blockade of the CXCR3 chemokine receptor results in diminished recruitment of T helper 1 cells into sites of inflammation. *Journal of Leukocyte Biology,* 73**,** 771-780.

Xu, H., Forrester, J. V., Liversidge, J. & Crane, I. J. 2003. Leukocyte trafficking in experimental autoimmune uveitis: breakdown of blood-retinal barrier and upregulation of cellular adhesion molecules. *Investigative Ophthalmology and Visual Science,* 44**,** 226-234.

Yang, Y., Kim, S. C., Yu, T., Yi, Y. S., Rhee, M. H., Sung, G. H., Yoo, B. C. & Cho, J. Y. 2014. Functional roles of p38 mitogen-activated protein kinase in macrophage-mediated inflammatory responses. *Mediators of Inflammation,* 2014**,** 352371.

Yata, K., Nishimura, Y., Unekawa, M., Tomita, Y., Suzuki, N., Tanaka, T., Mizoguchi, A. & Tomimoto, H. 2014. In vivo imaging of the mouse neurovascular unit under chronic cerebral hypoperfusion. *Stroke,* 45**,** 3698-3703.

Yeung, Y. G. & Stanley, E. R. 2009. A solution for stripping antibodies from polyvinylidene fluoride immunoblots for multiple reprobing. *Analytical Biochemistry,* 389**,** 89-91.

Yoon, S. & Seger, R. 2006. The extracellular signal-regulated kinase: multiple substrates regulate diverse cellular functions. *Growth Factors,* 24**,** 21-44.

Youakim, A. & Ahdieh, M. 1999. Interferon-gamma decreases barrier function in T84 cells by reducing ZO-1 levels and disrupting apical actin. *American Journal of Physiology,* 276**,** G1279-1288.

Yu, H., Huang, X., Ma, Y., Gao, M., Wang, O., Gao, T., Shen, Y. & Liu, X. 2013. Interleukin-8 regulates endothelial permeability by down-regulation of tight junction but not dependent on integrins induced focal adhesions. *International Journal of Biological Sciences,* 9**,** 23-09-2013.

Yuan, S. Y. & Rigor, R. R. 2010. Regulation of Endothelial Barrier Function, Chapter 2, Structure and Function of Exchange Microvessels. San Rafael (CA): Morgan & Claypool Life Sciences.

Zeremski, M., Petrovic, L. M., Chiriboga, L., Brown, Q. B., Yee, H. T., Kinkhabwala, M., Jacobson, I. M., Dimova, R., Markatou, M. & Talal, A. H. 2008. Intrahepatic levels of CXCR3-associated chemokines correlate with liver inflammation and fibrosis in chronic hepatitis C. *Hepatology,* 48**,** 1440-1450.

Zhang, Y., Gao, Z., Wang, D., Zhang, T., Sun, B., Mu, L., Wang, J., Liu, Y., Kong, Q., Liu, X., Zhang, Y., Zhang, H., He, J., Li, H. & Wang, G. 2014. Accumulation of natural killer cells in ischemic brain tissues and the chemotactic effect of IP-10. *Journal of Neuroinflammation,* 11**,** 79.

Zhao, M., Discipio, R. G., Wimmer, A. G. & Schraufstatter, I. U. 2006. Regulation of CXCR4-mediated nuclear translocation of extracellular signal-related kinases 1 and 2. *Molecular Pharmacology,* 69**,** 66-75.

Zhu, X., Zou, Y., Wang, B., Zhu, J., Chen, Y., Wang, L., Li, J. & Deng, X. 2016. Blockade of CXC chemokine receptor 3 on endothelial cells protects against sepsis-induced acute lung injury. *Journal of Surgical Research,* 204**,** 288-296.

Zhu, Z., Ramos, J., Kampa, K., Adimoolam, S., Sirisawad, M., Yu, Z., Chen, D., Naumovski, L. & Lopez, C. D. 2005. Control of ASPP2/(53BP2L) protein levels by proteasomal degradation modulates p53 apoptotic function. *Journal of Biological Chemistry,* 280**,** 34473-34480.

Zlokovic, B. V. 2005. Neurovascular mechanisms of Alzheimer's neurodegeneration. *Trends in Neurosciences,* 28**,** 202-208.

Zlotnik, A. & Yoshie, O. 2000. Chemokines: a new classification system and their role in immunity. *Immunity,* 12**,** 121-127.

Zozulya, A. L., Reinke, E., Baiu, D. C., Karman, J., Sandor, M. & Fabry, Z. 2006. Dendritic Cell Transmigration through Brain Microvessel Endothelium Is Regulated by MIP-1 Chemokine and Matrix Metalloproteinases. *The Journal of Immunology,* 178**,** 520-529.

8. Appendix I

The following equipment was used throughout the experimental procedures described in Materials and Methods (Table 11):

Table 11 Laboratory equipment, models and manufacturers.

Equipment	Model	Manufacturer
Centrifuge	Centrifuge 5415D, 5415R Function line Labofuge 400R	Eppendorf (Hamburg, Germany) Heraeus (Hanau, Germany)
Fume Cupboard	Enterprise DynamicFlow™ Fume Cupboard	Premier Laboratory Systems (Cambridge, UK)
Hood	Hera Safe	Kendro Laboratory Products (Asheville, USA)
Incubator	Hera Cell	Heraeus (Hanau, Germany)
Microscope (confocal)	LSM710/LSM700	Zeiss (Oberkochen, Germany)
Microscope (optical)	Leica DM IL	Leica (Milton Keynes, UK)
Nanodrop spectrophotometer	Nanodrop ND100™	Thermofisher (Wilmington, USA)
qPCR device	7900HT Fast Real-Time PCR system	Applied Biosystems (Foster City, USA)

Retinal imaging system for mice and rat	Micron III	Phoenix Research Labs (Pleasanton, USA)
RT-PCR/cDNA synthesis device	T100™ Thermal Cycler	Bio-Rad (Hemel Hempstead, UK)
Time Lapse phase contrast microscope	Zeiss 200M Axiovert	Zeiss (Oberkochen, Germany)
Waterbath	Shake Temp SW22	Julabo (Seelbach, Germany)

Reagents were purchased from Sigma Aldrich (Poole, UK), unless otherwise stated (Table 12).

Table 12 General Reagents

Product	Manufacturer
2-metacaptoethanol (50 mm)	Gibco® Life Technologies (Carlsbad, USA)
4% Paraformaldehyde (PFA)	Electron Microscopy Sciences (Pennsylvania, USA)
Phosphate-buffered saline (DPBS) (1X), no calcium, no magnesium	Gibco® Life Technologies (Carlsbad, USA)

The following reagents were used in tissue culture experimental procedures (Table 13):

Table 13 General tissue culture reagents

Product	Manufacturer
Foetal Calf Serum	Invitrogen (Paisley, UK)
BSA 22% w/v in PBS	First Link UK (Wolverhampton, UK)

Ascorbic Acid	Sigma Aldrich (Poole, UK)
DMEM/F-12	Life Technologies (Loughborough, UK)
DDPBS (1X), no calcium, no magnesium	Gibco® Life Technologies (Carlsbad, USA)
EGM™-2 Basal Medium	Lonza (Basel, Switzerland)
EGM™-2 BulletKit™	Lonza (Basel, Switzerland)
F-10 with Glutmax	Invitrogen (Paisley, UK)
HBSS (10X), no calcium, no magnesium	Gibco® Life Technologies (Carlsbad, USA)
HBSS (1X), calcium, magnesium	Gibco® Life Technologies (Carlsbad, USA)
RPMI 1640 Medium, GlutaMAX™	Gibco® Life Technologies (Carlsbad, USA)
Collagenase/Dispase	Lorne Laboratories (Reading, UK)
1M 4-(2-hydroxyethyl)-1-piperazineethanesulfonic acid) (HEPES)	Invitrogen (Paisley, UK)
Penicillin/Streptomycin	Invitrogen (Paisley, UK)
Puromycin	Sigma Aldrich (Poole, UK)
Basic fibroblast growth factor (bFGF)	Sigma Aldrich (Poole, UK)
Trypsin	Sigma Aldrich (Poole, UK)
Collagen type I	BD Biosciences (San Jose, USA)
Fibronectin	Sigma Aldrich (Poole, UK)
Transwell® Permeable Supports	Appleton Woods (Birmingham, UK)
TrypLE™ Cell Dissociation Reagent	Gibco® Life Technologies (Carlsbad, USA)
CD4 Microbeads, human	Miltenyi Biotec (Bisley, UK)